Plastin 3 rescues defective cell surface translocation and activation of TrkB in mouse models for spinal muscular atrophy

Plastin 3 kompensiert die defekte Zelloberflächen-Translokation und Aktivierung von TrkB in Mausmodellen für spinale Muskelatrophie

Doctoral thesis for a doctoral degree
at the Institute of Clinical Neurobiology,
University Hospital Würzburg
and
at the Graduate School of Life Sciences,
Julius-Maximilians-Universität Würzburg,
Section Neuroscience

submitted by

Luisa Hennlein

from

Hildburghausen, Germany

Würzburg, September 2022

Submitted on: …………………………………………………..……..

Members of the Thesis Committee

Chairperson: Prof. Dr. Matthias Gamer

Primary Supervisor: PD Dr. Sibylle Jablonka

Supervisor (Second): Prof. Dr. Michael Sendtner

Supervisor (Third): Prof. Dr. Georg Nagel

Supervisor (Fourth): Prof. Dr. Markus Sauer

Date of Public Defense: …………………………………………...

Date of Receipt of Certificates: ………………………………..

Table of Contents

Summary

Spinal muscular atrophy (SMA) is a genetic pediatric condition that affects lower motoneurons in the spinal cord leading to their degeneration and muscle weakness. This progressive lethal neuromuscular disease is caused by homozygous loss or mutations in the *Survival Motor Neuron 1* (*SMN1*) gene. Currently, available therapies based on SMN protein restoration are successfully applied to patients; however, the pathomechanism leading to motoneuron degeneration is not fully resolved yet. SMA mouse models and primary cell cultures are widely used to study disease manifestation *in vivo* and *in vitro,* respectively. Cultured embryonic murine SMA motoneurons display axon elongation and differentiation defects accompanied by collapsed growth cones with disturbed actin cytoskeleton and impaired clustering of calcium channels.

Intriguingly, motoneurons cultured from mice deficient for the Tropomyosin-kinase receptor B (TrkB), lacking the receptor for Brain-derived neurotrophic factor (BDNF), exhibit similar pathological features. Thus, the question arises whether SMA motoneurons suffer from defective BDNF/TrkB signaling and whether there is a link to the disturbed actin cytoskeleton.

In the recent years, a growing body of evidence suggests that modifier genes such as *Plastin 3* (*PLS3*) beneficially interfere with SMA pathology. PLS3 is an actin-bundling protein whose upregulation has shown to improve motoneuron and neuromuscular junction (NMJ) phenotype in SMA animal models. Nevertheless, the mechanism how PLS3 counteracts SMN deficiency and modulates F-actin dependent processes is not well understood.

In this study, we used an asset of imaging techniques and molecular biology methods to investigate TrkB localization and its activation in cultured SMA motoneurons and NMJs of *ex vivo* muscle explants. Our initial data revealed that while TrkB levels are only mildly affected locally in axon terminals, BDNF-mediated TrkB phosphorylation was massively disturbed in growth cones and NMJs of later symptomatic SMA mice. Moreover, the two processes of activity-dependent TrkB translocation to the plasma membrane and its activation via BDNF were shown to be Plastin 3 (Pls3) and actin-dependent processes, as they were abolished by disruption of the actin cytoskeleton or by knockdown of Pls3. In contrast to that, when human PLS3 was overexpressed in cultured SMA motoneurons, an impressive rescue effect could be observed on both morphological and functional level. As a consequence, axon length and growth cone size were normalized to wild type level and the activity-induced TrkB cell surface recruitment and its activation upon BDNF stimulation were significantly improved. Live-cell imaging techniques further revealed that the relocation of TrkB after BDNF-induced internalization is disturbed in SMA, which is based on an actin-dependent TrkB translocation defect from intracellular stores. In addition to Pls3, the cooperation with the actin-related protein 2/3 complex (Arp2/3) complex mediating actin branching is required for the surface recruitment of TrkB after BDNF stimulation. Lastly, adeno-associated virus (AAV9)-mediated PLS3 overexpression *in vivo* in neonatal SMA mice provided further evidence for the capacity of PLS3 to modulate actin dynamics necessary for accurate BDNF/TrkB signaling.

In conclusion, the results collected during my PhD thesis demonstrate a novel role for PLS3 in mediating proper alignment of transmembrane proteins as prerequisite for their appropriate functioning. Hence, PLS3 is required for a key process indispensable for the development and function of motoneurons even beyond the context of SMA.

Zusammenfassung

Die spinale Muskelatrophie (SMA) ist eine monogenetische Erkrankung der unteren spinalen Motoneurone, die zu einer Degeneration der Nervenzellen und anschließendem Muskelschwund führt. Ausgelöst wird diese fortschreitende neuromuskuläre Erkrankung durch Verlust oder Mutation des *Survival Motor Neuron 1* (*SMN1)* Gens. Aktuelle Behandlungsmöglichkeiten, die das Ziel haben den SMN Proteingehalt zu erhöhen, werden heutzutage schon erfolgreich bei SMA Patienten angewandt. Allerdings sind die Auswirkungen des SMN-Verlusts auf die Motoneurone bis heute nicht vollständig verstanden. Um die Krankheitsmechanismen zu entschlüsseln, werden sowohl Mausmodelle als auch Zellkulturmodelle genutzt. Kultivierte embryonale Motoneurone von SMA Mäusen zeigen eine veränderte zelluläre Differenzierung, die sich vor allem durch ein gestörtes axonales Wachstum auszeichnet. Die Axonterminalen weisen aufgrund eines veränderten Aktin Zytoskeletts vermehrt kollabierte Wachstumskegel mit beeinträchtigter Cluster-Formierung von Kalzium Kanälen auf. Interessanterweise bilden Motoneurone mit einem Verlust des Tropomyosinrezeptorkinase B (TrkB), dem hochaffinen Rezeptor des Brain-derived neurotrophic factor (BDNF), die gleichen zellulären Dysregulationen aus. Daher stellte sich die Frage, ob Smn-defiziente Motoneurone eine Störung der BDNF/TrkB Signalkaskade entwickeln, die auf einem gestörten Aktin Zytoskelett beruht.

Studien der letzten Jahre haben gezeigt, dass F-Aktin-assoziierte Proteine, wie zum Beispiel *Plastin 3* (*PLS3*), eine stark modifizierende und schützende Wirkung auf die Pathophysiologie von SMA Patienten haben. PLS3 ist ein Aktin-bindendes und –bündelndes Protein, dessen Hochregulierung bei Smn-Defizienz die Funktionalität der Motoneurone und der neuromuskulären Endplatten (NME) in SMA Tiermodellen verbessert. Allerdings ist der genaue Mechanismus, inwieweit PLS3 F-Aktin-gesteuerte Prozesse modifiziert nicht gut verstanden.

In dieser Studie wurde mit Hilfe von bildgebenden Verfahren und molekularbiologischen Methoden die Lokalisierung und Aktivierbarkeit von TrkB in den Axonterminalen und Endplatten von SMA Motoneurone untersucht. Die initialen Ergebnisse zeigten, dass die Lokalisierung von TrkB zwar nur wenig verändert ist, aber die Aktivierung von TrkB mittels BDNF Stimulation lokal in den Wachstumskegeln Smn-defizienter Motoneurone und der Endplatte spät-symptomatischer SMA Mäuse stark beeinträchtigt ist. Darüber hinaus konnte gezeigt werden, dass sowohl die aktivitätsabhängige Translokation von TrkB zur Plasmamembran, als auch dessen Liganden-induzierte Phosphorylierung Aktin-abhängige Prozesse sind, die durch eine Störung des Aktin Zytoskeletts oder einen Knockdown von Pls3 inhibiert werden können. Im Gegensatz dazu, bewirkt die Überexpression von humanem PLS3 in Smn-defizienten Motoneuronen eine Wiederherstellung der morphologischen und funktionellen Defekte. Axonenwachstum und Wachstumskegelgröße werden auf Wildtyp-Niveau normalisiert und die aktivitätsabhängige TrkB Membran-Translokation sowie die BDNF-induzierte TrkB Phosphorylierung werden signifikant verbessert. Lebendfärbungen an Smn-defizienten Axonterminalen konnten zeigen, dass die gestörte Re-Lokalisierung von TrkB an die Zellmembran nach BDNF Stimulation auf einen defekten TrkB Translokation aus intrazellulären Speichern basiert und diese durch Überexpression von humanen PLS3 signifikant verbessert wird. Darüber hinaus, ist das Zusammenspiel von Pls3 mit dem Arp2/3 Komplex, der für die Verzweigung von Aktin Filamenten verantwortlich ist, ebenfalls wichtig für die BDNF-vermittelte Rekrutierung von TrkB an die Zelloberfläche.

Final lieferten Experimente in denen humanes PLS3 in SMA Mäusen überexprimiert wurde weitere Beweise für die Fähigkeit von PLS3 die Dynamik des Aktin Zytoskeletts zu regulieren, was eine Grundvoraussetzung für eine akkurate BDNF/TrkB Signalübertragung darstellt.

Zusammenfassend zeigen die Daten aus meiner Doktorarbeit eine neue und wichtige Rolle von PLS3 für die korrekte Anordnung von Transmembranproteinen, als Grundvoraussetzung für deren Funktionalität. Somit wird PLS3 für einen Schlüsselprozess benötigt, der für die Entwicklung und Funktion von Motoneuronen, auch über den Kontext von SMA hinaus, unverzichtbar ist.

1. Introduction

1.1. Spinal muscular atrophy (SMA)

1.1.1. Clinical manifestations in SMA

SMA is an autosomal recessive neuromuscular disorder that manifests in proximal muscle weakness and atrophy caused by degeneration of lower motoneurons in the anterior horn of the spinal cord (Jablonka and Sendtner, 2017). With an approximately incidence of 1:6000 – 1:10000 births worldwide (Verhaart et al., 2017), SMA is the most common monogenetic cause of infant mortality (Crawford and Pardo, 1996). The prevalent form of SMA is caused by mutations in or homozygous deletions of the *survival motoneuron gene 1 (SMN1)* that is located at human chromosome 5q13.2 (Lefebvre et al., 1995). Only on rare occasions, spinal muscular atrophy variants (non-5q-SMA) can be caused by dysfunction of other genes (Darras, 2011; Russman, 2007). A large scale, pan-ethnic screening of the United States population revealed a carrier frequency of one out of 54 (Sugarman et al., 2012) that coincides with previously reports (Smith et al., 2007). As SMA is inherited in an autosomal recessive manner, both parents need to be heterozygous carriers for SMA-causing deletions and mutations, to inherit the disease (Verhaart et al., 2017). In general, the clinical appearance of SMA patients varies according to the disease type. Originally, Guido Werdnig and Johann Hoffmann gave the first descriptions of an early infantile clinical condition in the 1890s (Hoffmann, 1893; Werdnig, 1891). Later on, Victor Dubowitz described a slowly progressive intermediate form (Dubowitz, 1964), and Erik Kugelberg and Lisa Welander reported a juvenile, mild form of SMA (Kugelberg and Welander, 1956). According to this, three SMA types were initially classified (type I- severe, type II- intermediate, type III- mild) (Munsat and Davies, 1992). Subsequently, two additional forms were supplemented: type 0- congenital (Dubowitz, 1999) and type IV- adult onset (Zerres et al., 1995). However, this classification is mainly dependent on the onset of the disease and the achieved motor milestones that bears the disadvantage of overlaps and omits dynamic changes (Wirth et al., 2020). Therefore, a new functional classification was introduced comprising non-sitters, sitters and walkers (**Fig. 1**), to ensure a SMA phenotype consensus especially in terms of functional evaluation of the therapeutic feedback (Wirth et al., 2020).

Fig. 1: SMA Classification. *Clinical types of SMA according to the original descriptions and the new functional classification. Modified from (Eggermann et al., 2020)*

1.1.2. The genetic cause of spinal muscular atrophy

Deletions of or mutations in the *SMN1* are the genetic cause for spinal muscular atrophy. The *SMN* gene is located within a 500 kilobase pairs (kb) inverse duplicated region of the human chromosome five (5q13), resulting in two nearly homologous copies of the gene: *SMN1* (telomeric) and *SMN2* (centromeric) (Brzustowicz et al., 1990; Lefebvre et al., 1995; MacKenzie et al., 1993). Both genes are comprised of nine exons and eight introns, encode for the same protein and only differ in five base pairs (Burglen et al., 1996; Lefebvre et al., 1995). However, a great majority of patients suffering from SMA

display homologous deletions only in *SMN1*, primarily within exon seven and eight, or to lesser extend point mutations in exon one or three, missense mutations in exon two and six or frameshift mutations (Bussaglia et al., 1995; Campbell et al., 1997; Cobben et al., 1995; Coovert et al., 1997; Cusco et al., 2004; Gennarelli et al., 1995; Hahnen et al., 1997; Lefebvre et al., 1995; Parsons et al., 1998a; Parsons et al., 1996; Skordis et al., 2001; Sun et al., 2005; Talbot et al., 1997; Wirth et al., 1999). Studies by Lorson et al. 1999 and Monani et al. 1999 demonstrated that the silent cytosine (C) to thymine (T) (C → T) nucleotide transition within exon seven of *SMN2* is capable to induce exon seven skipping (Lorson et al., 1999; Monani et al., 1999). In the recent years, several factors regulating alternative splicing of *SMN2* leading to exon seven exclusion had been identified. The C → T transition was demonstrated to disrupt an exonic splicing enhancer (ESE) that usually interacts with splicing factors SF2/ASF (Cartegni and Krainer, 2002; Lorson et al., 1999). Furthermore, binding of the heterogeneous nuclear ribonucleoproteins (hnRNPs) play an important role in exon seven exclusion (Hua et al., 2008; Kashima and Manley, 2003; Kashima et al., 2007; Pagliarini et al., 2015; Pedrotti et al., 2010; Singh et al., 2006). Thus, *SMN2* produces primarily a transcript lacking exon seven (SMNΔ7) resulting in a great majority of truncated and unstable SMN protein and only approximately 10 – 20 % of full-length SMN protein (Cho and Dreyfuss, 2010; Hofmann and Wirth, 2002; Jodelka et al., 2010; Lorson and Androphy, 2000; Lorson et al., 1998). As a consequence, *SMN2* is not able to compensate the loss of full-length SMN protein deriving from *SMN1*, which is functionally disturbed in SMA patients (**Fig. 2**). Nevertheless, *SMN2* copy number seems to inversely correlate with disease severity and is therefore considered as the most prominent modifier of the disease. While the majority of patients with the severe type I SMA only have one or two *SMN2* copies, most of the intermediate SMA patients carry three and patients with milder SMA four *SMN2* copies (Coovert et al., 1997; Feldkotter et al., 2002; McAndrew et al., 1997; Parsons et al., 1998b; Vitali et al., 1999).
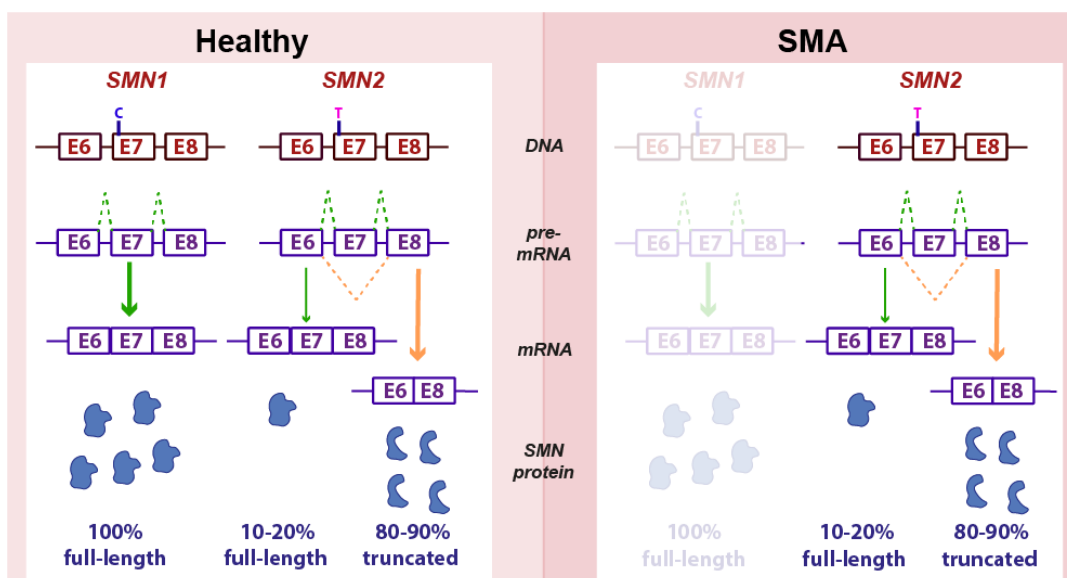
Fig. 2: Schematic overview about the genetic cause of SMA. *The disease causing survival of motoneuron genes SMN1 and SMN2 are located in an inverse duplicated region of human chromosome 5q13. A single nucleotide exchange within exon seven (C → T) functionally discriminates the two genes and results in exon seven skipping in SMN2. Hence, from SMN1 transcripts a full-length SMN protein is produced, while SMN2 transcripts mainly (80 – 90 %) lead to a non-functional truncated form of the protein. SMA patients lack SMN1 due to homozygous deletions or mutations, resulting in dramatically reduced protein levels. Modified from (Jablonka et al., 2022).*

More recently, examinations by Ruggiu et al. demonstrated that the Smn protein affects its own mRNA splicing and that Smn deficiency results in reduced exon seven inclusion in *Smn1* and *Smn2* independent from the C → T nucleotide transition. Strikingly, they used an *in vivo* SMA mouse model and showed that motoneurons express significantly lower amounts of full-length Smn deriving from *Smn2* than other neuronal cells in the spinal cord and that Smn deficiency particularly inhibits exon seven inclusion in spinal motoneurons (Ruggiu et al., 2012). Therefore, the loss of *SMN1* and hence dramatically reduced SMN proteins levels in SMA, might especially affect motoneurons first due to their lower expression of *SMN2*-derived protein and more pronounced downstream effects through a negative feedback loop.

For many years it was thought that the disease outcome of SMA is exclusively modified by the number of *SMN2* copies. However, in the past years further SMA modifiers have been identified due to the observation of phenotypic variabilities in patients with the same genotypic background. The initial examination of these discordant families revealed *Plastin 3* (*PLS3*) as gender-specific disease modifier in females (Oprea et al., 2008). Subsequently, reduced levels of Neurocalcin delta (NCALD), a neuronal Ca^{2+} sensor that negatively regulates endocytosis, were found to protect against SMA in five other asymptomatic homozygous *SMN1*-depleted patients (Riessland et al., 2017). For the latter one it has been demonstrated that the Ca^{2+}-dependent NCALD- clathrin- interaction is enhanced under low Ca^{2+} conditions in Smn-deficient cells, leading to an increased inhibition of its endocytosis. In turn, a suppression of NCALD was shown to improve the SMA phenotype in different animal model (Riessland et al., 2017). Collectively, these studies emphasize the strength of genetic modifiers as potential targets for non-SMN-dependent therapeutic approaches.

1.1.3. SMN structure & and complex formation

The full-length 38 kilodalton (kDa) SMN protein consists of 294 amino acids and is ubiquitously expressed in various tissues such as brain, spinal cord, muscles, heart, kidney, fibroblasts, etc. (Briese et al., 2006; Coovert et al., 1997; Lefebvre et al., 1995; Nash et al., 2016). It is conserved across species (Smn), besides humans (SMN), including macaque monkeys (Battaglia et al., 1997), rodents (DiDonato et al., 1997; La Bella et al., 1998; Schrank et al., 1997; Viollet et al., 1997), zebrafish (McWhorter et al., 2003), flies (Miguel-Aliaga et al., 2000), nematodes (Miguel-Aliaga et al., 1999; Talbot et al., 1997) and even yeast (Hannus et al., 2000; Owen et al., 2000; Paushkin et al., 2000). The expression of SMN/Smn protein is developmentally regulated with highest levels during the embryonic period, which progressively declines postnatally as seen in humans and rodents (Burlet et al., 1998; Fan and Simard, 2002; Jablonka et al., 2000; La Bella et al., 1998). SMN can be found in the cytoplasm as well as in the nucleus where it is located in dot-like structures termed gems (gemini of coiled bodies) because of their close proximity or association to coiled bodies (or Cajal bodies) (Giavazzi et al., 2006; Lefebvre et al., 1997; Liu and Dreyfuss, 1996). It was shown that the number of gems correlates with disease severity and is markedly reduced in type I SMA patients (Coovert et al., 1997). In addition to the nucleus and surrounding cytoplasm, SMN/Smn can be found within the axon, where it is associated with microtubules (Giavazzi et al., 2006; Pagliardini et al., 2000), and in growth cones of spinal neurons (Fan and Simard, 2002; Jablonka et al., 2001).

Although an overall progressively decrease in Smn protein amount is observed postnatally, the levels of SMN/Smn in human and rodent motoneurons seems to be very high and mostly stable even in adult stages, demonstrating a particularly high demand of SMN/Smn in motoneurons (Giavazzi et al., 2006; Pagliardini et al., 2000).

The SMN/Smn protein is comprised of eight domains which allow binding to several factors and formation of the SMN complex. Self-association and oligomerization of Smn is mediated via its domains two b and six (Lorson and Androphy, 1998; Young et al., 2000). Particularly, a highly conserved tyrosine-glycine motif (YG-box) within domain six is critical for Smn activity and mediates self-association via formation of helical oligomers (Lorson et al., 1998; Martin et al., 2012; Talbot et al., 1997; Wang and Dreyfuss, 2001). Typical polyproline stretches are located within domain four, five and six (DiDonato et al., 1997; Giesemann et al., 1999). Moreover, a tudor domain is located in the central section of the Smn protein allowing binding of snRNP Smith antigen (Sm) proteins (Buhler et al., 1999; Miguel-Aliaga et al., 1999; Selenko et al., 2001). Furthermore, the tudor domain, together with the YG-box and the lysine (K)-rich N-terminal domain, was shown to be important for Smn localization in coiled bodies (Renvoise et al., 2006). On the other hand, a cytoplasmic targeting signal is located within the exon seven-encoded domain (Zhang et al., 2003). In vertebrates, a macromolecular Smn complex is built that, besides Smn, comprises Gemin2, Gemin3 with Gemin4, Gemin5, the heterodimer Gemin6 - Gemin7, Gemin8 and the unr-interacting protein unrip (Kroiss et al., 2008; Pellizzoni, 2007) and functions as molecular chaperone that mediates small nuclear ribonucleoproteins (snRNP) biogenesis (Li et al., 2014; Pellizzoni, 2007).

1.1.4. SMA mouse models

To gain a better understanding of the function of SMN in disease mechanisms, multiple SMA animal models have been introduced. As stated above, Smn is conserved across various species and orthologues can even been found in fungi. However, humans are the only species that have a second *SMN* gene (*SMN2*) as a result of gene duplication that took place more than five million years ago (Rochette et al., 2001). Hence, as SMA is a result of massively reduced, but not completely abolished, SMN levels, it is difficult to mimic the human SMA pathology in model organisms that only possess one copy of the *Smn* gene. Advantages and disadvantages of different animal models are extensively reviewed in (Edens et al., 2015). The most common used SMA model organism to study ramifications upon Smn deficiency are mice. Mice carry only one copy of the Smn gene, which shares approximately 82 % similarity with the human Smn amino acid sequence (DiDonato et al., 1997; Viollet et al., 1997). A targeted disruption of murine *Smn* gene (*Smn$^{-/-}$*) via homologous recombination results in a massive cell death and lethality during early embryonic development (Schrank et al., 1997). Heterozygous deletion of *Smn* (*Smn$^{+/-}$*) does not cause any obvious alterations during embryonic or early postnatal development. However, during maturation the hemizygous loss of *Smn* results in extensive reduction of Smn protein levels (~46 %) in 6-month-old animals that is accompanied by loss of 40 % of the motoneurons in the lumbar spinal cord (Jablonka et al., 2000). Therefore, this model mimics the clinical characteristics seen in SMA type III patients.

To obtain a model that more closely resembles the genetic conditions in humans, several copies of the human *SMN2* were introduced onto a homozygous *Smn* knockout background. While Arthur Burghes and colleagues generated a *Smn⁻ᐟ⁻;SMN2* mouse line that expresses two transgenic copies of the full-length *SMN2* (Monani et al., 2000), the working group of Hung Li used a genomic DNA fragment that beyond the *SMN2* also includes the Small EDRK-Rich Factor 1A (*SERF1A*) gene and a portion of the neuronal apoptosis inhibitory protein (*NAIP*) gene to produce a *Smn⁻ᐟ⁻;SMN2*(Hung) mouse line (Hsieh-Li et al., 2000). Small amounts of full length Smn protein deriving from only two *SMN2* transgenes is capable for rescuing embryonic lethality upon Smn knockout, however, these animals die during early postnatal development. Interestingly, motoneuron loss from 50 % is only observed from in later disease stages when symptoms have already developed, demonstrating that SMA is a "dying-back-disease" and cell death of motoneurons is not the root cause (Monani et al., 2000). Given this phenotype, these mice resemble the SMA type I-like patients. This model is widely used for cell culture experiments of motoneurons isolated from embryonic day (E) 12.5-13.5 spinal cords (Jablonka et al., 2007; Rossoll et al., 2003; Rossoll et al., 2002). Interestingly, the survival rates up to seven *days in vitro* (DIV7) is indistinguishable from these seen in wild type motoneurons when cells are maintained in the presence of neurotropic factors (Rossoll et al., 2003). However, morphological differences become apparent from DIV4, when Smn-deficient motoneurons start to show differentiation defects such as abnormal axon length and smaller growth cones (Jablonka et al., 2007; Rossoll et al., 2003). Therefore, this mouse model is well suitable for examinations of early defects caused by Smn loss.

A further attenuation of the phenotype was obtained by introducing another human cDNA fragment lacking exon seven (SMNΔ7) onto the *Smn⁻ᐟ⁻;SMN2* background (*Smn⁻ᐟ⁻;SMN2;SMNΔ7*, hereafter shortened named *SMNΔ7* mice) (Le et al., 2005). Homozygous insertions of both transgenes were shown to increase the mean survival rate up to 13.3 ± 0.3 days. Obvious phenotypic abnormalities start from postnatal day (P) 5, when the *SMNΔ7* mice have less body weight and start to have troubles righting themselves which worsen over time. These pathological hallmarks correspond to the waste of spinal motoneurons and severe NMJ defects including reduced NMJ diameter and only partially innervation or completely denervation seen in later disease stages (Le et al., 2005). Therefore, it mirrors the clinical picture seen in SMA type II patients and is widely used for examinations of neuromuscular synapses in progressed disease stages.

1.1.5. SMN functions and contribution to the pathophysiology of SMA

1.1.5.1. SMN complex functions in snRNP assembly and pre-mRNA processing

As previously stated, the macromolecular SMN complex has important functions in snRNP biogenesis and therefore plays a crucial role in pre-mRNA splicing (Fischer et al., 1997; Li et al., 2014; Liu et al., 1997; Pellizzoni, 2007; Pellizzoni et al., 1998). In line with this, several studies revealed that Smn depletion dramatically affects snRNP assembly and splicing *in vitro* and *in vivo* (**Fig. 3, *left panel***) (Feng et al., 2005; Fischer et al., 1997; Gabanella et al., 2007; Lotti et al., 2012; Meister et al., 2000; Pellizzoni et al., 1998; See et al., 2014; Wan et al., 2005; Winkler et al., 2005; Wishart et al., 2014; Zhang et al., 2008). Similarly, SMA patient-derived fibroblasts display reduced capacity of snRNP assembly (Wan et al., 2005) and a lack of snRNPs in cajal bodies (Renvoise et al., 2006). For Smn-depleted zebrafish it

was shown that axonal degeneration and arrest of the development could be prevented by co-injection of U snRNPs (McWhorter et al., 2003; Winkler et al., 2005). A knockdown of other components important for snRNP assembly, like pICln or Tgs1, was also shown to lead to a similar phenotype in zebrafish and fruit fly as seen upon Smn deficiency (Borg et al., 2016; Chan et al., 2003; Winkler et al., 2005). These results, and the fact that the SMA causing mutation (D44V) (Sun et al., 2005) was reported to prevent Smn - Gemin2 binding and result in reduced snRNP assembly (Ogawa et al., 2007; Zhang et al., 2011), are demonstrating a direct link between disturbed snRNP assembly and the pathophysiology of SMA. Moreover, via RNA-sequencing of microdissected motoneuron somas from a SMA type II mouse model, Zhang and colleagues revealed cell-specific alterations in the expression of selective mRNAs at P1. However, affected genes correspond only to approximately 3 % of the total genes in motoneurons (Zhang et al., 2013). In line with this, RNA-sequencing and microarray analysis of the spinal cord and other tissues collected from different SMA mouse models showed only a small number of genes with altered expression at P1, before most of the symptoms appear. Strikingly, changes in the transcriptome progressively increased over the developmental time. At later symptomatic stages, a great number of transcripts were altered, including down-regulation of genes involved in cell division, axon guidance, growth factor signaling or up-regulation of stress-related genes (Doktor et al., 2017; Murray et al., 2010). Furthermore, alternative splicing events were observed to be increased in a time-dependent manner in Smn-deficient tissues (Baumer et al., 2009; Doktor et al., 2017). In contrast to that, microarray analysis of embryonic murine motoneurons cultured in compartmentalized microfluidic chambers revealed that Smn knockdown results in a large scale of transcriptome changes in both compartments. Interestingly, comparable amounts of transcripts were either down- or upregulated in the somatodendritic compartment, while axonal transcripts were mostly downregulated (Saal et al., 2014).

Even though there are several lines of evidence pointing SMN functions in pre-mRNA splicing, there is still an ongoing debate whether this is the primary cause for SMA. Firstly, SMN is ubiquitously expressed and a correct splicing machinery is inalienable in every cell type and not only motoneurons. Secondly, alterations in gene expression and splicing occur relatively late when the disease had already progressed, and therefore are not plausible to explain early disease symptoms (Baumer et al., 2009). Thirdly, several studies were able to demonstrate that Smn functions independently from snRNPs. For instance, in Smn-deficient zebrafish embryos, expression of a mutated SMN was able to prevent axonal outgrowth defects while SMN self-association or binding to Sm proteins as prerequisite for snRNP assembly was not rescued by this injection (Carrel et al., 2006). Analogue observations were made upon Smn re-expression in Smn-deficient Drosophila larvae that was only partially able to restore expression of minor class U small nuclear RNAs (snRNAs) while lethality and locomotor defects were completely rescued (Praveen et al., 2012). Thus, both studies disconnect snRNP assembly from the SMA-like pathology, suggesting that impaired snRNP biogenesis is not primarily causative for SMA (Praveen et al., 2012). Moreover, RNA sequencing revealed that Smn-deficient Drosophila larvae are developmental delayed and changes in mRNA levels or alternative splicing could be attributed to this developmental arrest (Garcia et al., 2013).

1.1.5.2. SMN and its role in axonal mRNA transport, local protein translation and cytoskeleton regulation

As stated above, Smn functions in snRNP assembly and therefore is often localized in the nucleus and peri-nuclear cytoplasm. However, in the human nervous system a redistribution of SMN from a mainly nuclear localization to a more cytoplasmic/axonal localization is observed during the maturation, which is especially prominent in motoneurons (Giavazzi et al., 2006). Moreover, Smn and Gemins comprising granules, that are associated with microtubules and microfilaments enabling an active and bidirectional transport, can be found in dendrites, axons and growth cones of cultured human neuroblastoma cells, primary mouse motoneurons as well as mouse NMJ (Dombert et al., 2014; Todd et al., 2010a; Todd et al., 2010b; Zhang et al., 2006; Zhang et al., 2003). Interestingly, Sm proteins are not found in Smn granules and a large amount of Smn protein does not co-localize with Gemin2 or Gemin3 in the axons and growth cones of motoneurons (Jablonka et al., 2001; Zhang et al., 2006). Taken together, these data support another role for Smn within the axon and terminals of motoneurons independent from that in snRNP assembly that may be relevant for SMA pathophysiology.

In the recent years, it became evident that SMN inherits further regulatory functions. Extensive studies have been performed which support the hypothesis that SMN is involved in the translocation of mRNA along the axon and local protein translation, as well as modulation of actin dynamics and endocytosis in the axon terminals (**Fig. 3, *middle - right panel***) (Jablonka and Sendtner, 2017). Besides the SMN complex members, several further interaction partners have been identified. Among them various RNA binding proteins (RBPs) such as hnRNP R (Rossoll et al., 2003), Transactive response DNA Binding protein 43 kDa (TDP-43) (Turner et al., 2008), HuD (Akten et al., 2011; Fallini et al., 2011; Hubers et al., 2011) or insulin-like growth factor II -mRNA binding protein 1 (IMP1) (Fallini et al., 2014). Especially in neurons, RBP attach great importance, as they are indispensable for the transportation of mRNA along the axons, which are needed for local translation of proteins at the axon terminals to induce and maintain neurite outgrowth or synapse formation (Tolino et al., 2012). Interestingly, both hnRNP R and IMP1 were shown to bind to the 3′untranslated region (3′UTR) of *β-actin* mRNA to mediate axonal transport into the growth cones (Glinka et al., 2010; Ross et al., 1997; Rossoll et al., 2003). Under Smn-deficient conditions, a significant reduction of hnRNP R and IMP-1 protein levels is observed within the axonal compartment (Fallini et al., 2014; Rossoll et al., 2003), that correlates with reduced β-actin mRNA and protein levels (Donlin-Asp et al., 2017; Moradi et al., 2017; Rathod et al., 2012; Rossoll et al., 2003). Upon axonal transport of mRNAs, local protein translation is necessary for the supply of synaptic proteins. Upon Smn deficiency, less inactive ribosomes can be found at the plasma membrane resulting in a decreased formation of polyribosomes and impaired local translation of proteins (Gabanella et al., 2016). Moreover, the local translation of *β-actin*, was found to be deregulated in motoneurons derived from a severe SMA mouse model (Rathod et al., 2012). Not only local translation of *β-actin*, but also local translation of the two other actin isoforms (α- and γ-actin) is reduced in terminals of Smn-deficient motoneurons. Consequently, this reduction counteracts the compensatory mechanism in which reduction of one isoform leads to the upregulation of the two other isoforms (Moradi et al., 2017) leading to a more pronounced phenotype. As a result, the balanced ratio of globular (G) to filamentous (F) actin, important for organization and functionality of the presynapse, is disrupted (Jablonka and Sendtner, 2017).

This effect is even more fortified by a disturbed regulation of the actin dynamics. Early functional studies on SMN have demonstrated that the proline-rich stretches act as binding site for profilins (Giesemann et al., 1999; Nolle et al., 2011). These small 12 – 15 kDa proteins are from major importance for actin organization as they are known to inherit various regulatory functions (Hensel and Claus, 2018). Primarily, profilins bind to monomeric G-actin and catalyze adenosine diphosphate (ADP) to adenosine triphosphate (ATP) exchange, leading to the binding of G-actin to the barbed end of F-actin promoting the directed polymerization of the actin filament (Hensel and Claus, 2018; Witke, 2004). Thereby, the activity of profilins is regulated via phosphorylation at distinct sites (Fan et al., 2012; Hensel and Claus, 2018). Besides SMN, a variety of interacting partners have been described such as actin related protein 2 (Arp2), a subunit of the actin-related protein 2/3 (Arp2/3) complex (Mullins et al., 1998), gephyrin (Giesemann et al., 2003), further actin-related proteins like formins or Wiskott–Aldrich Syndrome protein (WASP) and many others (Davey and Moens, 2020; Murk et al., 2021; Romero et al., 2004). Consequently, profilins are involved in a plethora of biological activities that, besides regulation of actin dynamics, include signaling pathways, membrane trafficking or even mRNA splicing and transcription (Murk et al., 2021). Due to this fact, dysregulation of profilins and the resulting alterations in actin cytoskeleton dynamics were shown to be linked to various diseases such as Fragile X syndrome (Michaelsen-Preusse et al., 2016) or the familial form of amyotrophic lateral sclerosis (ALS) (Smith et al., 2015; Tanaka et al., 2016).

With regard to SMA, especially the ubiquitously expressed isoform profilin I and with even stronger affinity the mainly in the CNS expressed isoform profilin II are known to interact with SMN (Birbach, 2008; Giesemann et al., 1999; Nolle et al., 2011). For pheochromocytoma 12 (PC12) cells as well as murine spinal cords of an intermediate SMA mouse model, it has been demonstrated that deficiency of Smn results in increased levels of the neuronal profilin IIa (Bowerman et al., 2009; Bowerman et al., 2007). In terms of SMA it is thought that loss of SMN-profilin binding could result in a more accessible phosphorylation site leading to a hyper-phosphorylation and inactivation on the one hand. Simultaneously on the other hand, this promotes a stronger binding to Rho-associated protein kinase (ROCK) on the other hand, which in turn is not able to phosphorylate and modulate downstream targets like cofilin anymore, another actin-regulatory protein, resulting in diminished stability of the actin cytoskeleton (Bowerman et al., 2007; Hensel and Claus, 2018; Nolle et al., 2011). In addition, it has been found out recently that yeast Smn mutants display splicing defects in the profilin gene, leading to less dynamic actin filaments interfering with processes like endocytosis (Antoine et al., 2020).

In the recent years, another actin-regulator had been identified to play a role in the pathomechanism of SMA. As stated before, investigations of six discordant families revealed PLS3 as a fully protective SMA modifier (Oprea et al., 2008). Various set of experiments provide evidence for its beneficial role in SMA, which will be further discussed in a separate chapter. Noteworthy, various overexpression studies that rescue axonal-defects in SMA animal models (Ackermann et al., 2013; Alrafiah et al., 2018; Hosseinibarkooie et al., 2016; Oprea et al., 2008) have demonstrated the importance of the actin cytoskeleton in the disease mechanism and strength of actin-modulating proteins for therapeutic strategies.
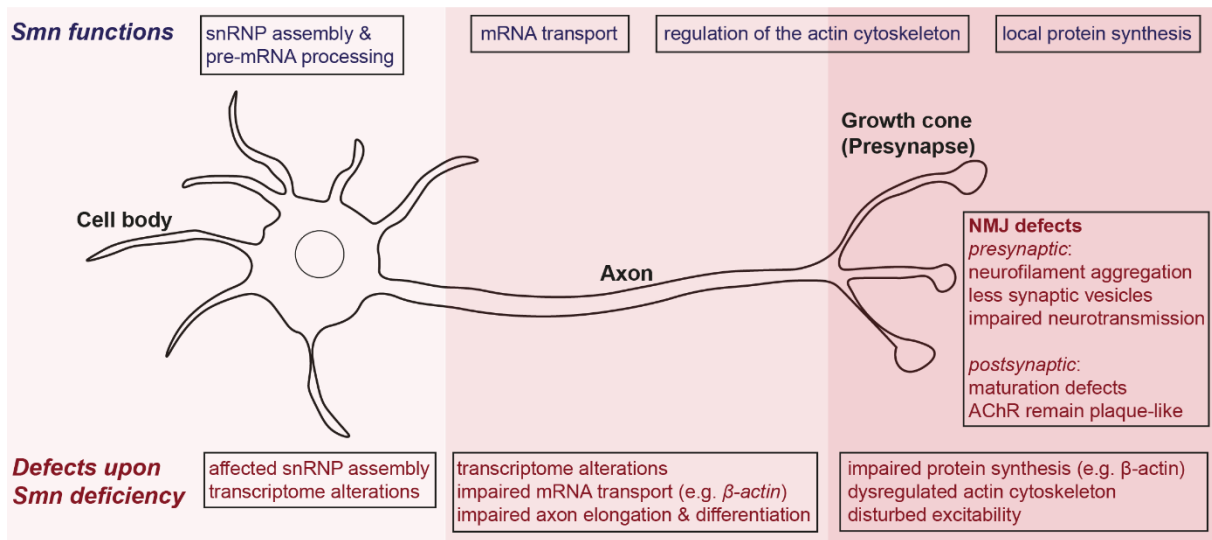
Fig. 3: Schematic illustration of Smn functions in distinct cellular compartments of motoneurons. *While Smn acts in a macromolecular complex to participate in the assembly of snRNPs and therefore is involved in pre-mRNA processing and splicing especially in the soma, it was also shown to interact with RNA-binding proteins to realize the transport of mRNAs along the axon. Moreover, Smn is involved in the local protein translation in the presynaptic compartment and regulation of the actin cytoskeleton via interaction with various modulatory proteins. Thus, Smn deficiency leads to dysregulation of various processes including snRNP assembly leading to transcriptome alterations and the one hand, and impaired mRNA transport as well as local translation, and a defective actin cytoskeleton that are one the other hand thought to be causative for further prominent structural and functional defects of motoneurons and neuromuscular endplates such as impaired axon elongation, disturbed excitability due to affected clustering of VGCCs or impaired neurotransmission (see references in the main text).*

1.1.5.3. SMN's role in axonal terminals and maintenance of the NMJs

According to the previous descriptions, reduction of Smn results in defective actin cytoskeleton attributable to impaired axonal mRNA transport, disturbed local translation and dysfunctional network of regulatory proteins. Given the fact that functional and well-coordinated actin dynamics are master-regulator of processes including neurite outgrowth, growth cone tuning and composition of the presynaptic compartment including trafficking of synaptic vesicles and membrane proteins, it is reasonable that the disturbed cytoskeleton provides the link to the clinical picture seen in SMA patients and animal models (Hensel and Claus, 2018).

Especially in terms of motoneurons, which build highly specialized synapses in the peripheral nervous system to initiate muscle contraction, this is of major importance (Sanes and Lichtman, 1999). Hence, the loss of SMN manifests in an axonal phenotype and neuromuscular junction defects. *In vitro*, these defects become morphological apparent in cultured embryonic motoneurons from *Smn$^{-/-}$;SMN2* mice that show impaired axon elongation together with smaller or collapsed growth cones (Jablonka et al., 2007; Rossoll et al., 2003). Further functional abnormalities comprise reduced β-actin mRNA and protein level as well as disturbed accumulation of voltage-gated calcium channels (VGCC) in the axonal terminals (**Fig. 3, *right panel***) (Jablonka et al., 2007; Moradi et al., 2017; Rathod et al., 2012; Rossoll et al., 2003). These clustering defects correspond to a reduced frequency of spontaneous Ca^{2+} transients locally at the growth cone, while the global excitability is unaffected (Jablonka et al., 2007). A rescue effect can be observed when the properties of the VGCCs are modified by R-Roscovitine.

Treatment with this drug over the entire culture period resulted in significant morphological and functional improvements in Smn-deficient motoneurons like properly differentiated growth cones with increased $Ca_v2.2$ accumulation and enhanced frequencies of spontaneous Ca^{2+} transients (Tejero et al., 2020).

In vivo, an abnormal motor behavior and muscle atrophy are observed in human SMA patients as well as SMA animal models such as drosophila (Chan et al., 2003; Rajendra et al., 2007), zebrafish (Carrel et al., 2006; McWhorter et al., 2003; Winkler et al., 2005), and mice (Kariya et al., 2008; Le et al., 2005). As mentioned before, the expression of SMN is highly regulated with highest levels peaking during the embryonic development (Burlet et al., 1998; Jablonka et al., 2000), the time where motor axons emerge to their target muscles and build synapses called neuromuscular junction (NMJ). Morphological and functional examinations of human patients as well as SMA animal models revealed substantial abnormalities in Smn-deficient NMJs, in both the pre- and the postsynaptic compartment (**Fig. 3, *right panel***). Smn-deficient postsynpases are smaller and show maturation defects like persistent expression of the fetal acetylcholine receptor (AChR) isoform and retention of the plaque-like shape (Harding et al., 2015; Kariya et al., 2008; Kong et al., 2009; Murray et al., 2008; Ruiz et al., 2010). Moreover, pathological features in the presynapse comprise neurofilament (NF) accumulation and loss of synaptic occupation or denervation (Cifuentes-Diaz et al., 2002; Kong et al., 2009; Ling et al., 2012; Murray et al., 2008; Ruiz et al., 2010). In contrast to the *in vivo* data obtained from fly or zebra fish SMA models describing motoneuron routing and axonal outgrowth defects (McWhorter et al., 2003; Rajendra et al., 2007; Winkler et al., 2005), no axonal outgrowth defects could be detected *in vivo* in embryonic or neonatal mice (McGovern et al., 2008). Thus, it is postulated that the observed denervation is resulting from insufficient preservation of the presynaptic compartment leading to the loss of synaptic occupation and not by failure of the initial synapse formation (Ling et al., 2012; McGovern et al., 2008). Indeed, electrophysiological examinations in early and later disease stages of *SMNΔ7* mice revealed that the initial multi-innervated terminals function normally, but the presynaptic neurotransmission seems to be highly impaired (Ruiz et al., 2010).

One of the most severely affected muscles is the *Transversus abdominis* (*TVA*), a slow-twitch muscle located in the abdominal wall (Murray et al., 2008; Ruiz et al., 2010; Torres-Benito et al., 2011). Intracellular recordings even in early disease stages revealed that the *TVA* muscle-evoked neurotransmission is functionally disturbed and the amount of vesicles released during an action potential is reduced by more than 50 % (Ruiz et al., 2010; Torres-Benito et al., 2011). These transmission defects are accompanied by morphological abnormalities like a reduced amount of synaptic vesicles that stay immaturely clustered, smaller size of the readily releasable pool (RRP) and less active zones (Torres-Benito et al., 2011). Analogous observations were made in the *Tibialis anterior* (*TA*) (Kong et al., 2009), nonetheless the fact that in other low-affected muscles like the fast-twitch muscle *Levator auris longus* (*LAL*) or the diaphragm, the defects are unincisive or only mild (Ruiz et al., 2010; Tejero et al., 2016; Torres-Benito et al., 2012). Further investigation of the *TVA* demonstrated that neurotransmission defects are at least partially result of 1) reduced levels of regulatory proteins important for synchronous neurotransmitter release such as synaptotagmin-2 and synaptic vesicle protein 2 (SV2) B and 2) greatly diminished presence of P/Q-type VGCCs required for neurotransmission (Tejero et al., 2016). Thus, re-balancing the Ca^{2+} homeostasis by using R-

Roscovitine beneficially improved motor endplate morphology and function as well as survival *of SMNΔ7* mice (Tejero et al., 2020).

Taken together, the defects observed at the motor endplate, especially at the presynapse, are one of the earliest events in SMA pathogenesis that anticipate motoneuron degeneration, wherefore SMA is commonly characterized as a "dying back" disease (Jablonka and Sendtner, 2017).

<u>1.1.6. Therapeutics in SMA</u>

The extensive examinations in SMA cell culture and animal models and the substantial progress that has been made in understanding the genetic cause and pathomechanism of SMA were prerequisite for the development of suitable SMA treatments. Nowadays three different therapies are approved in the US by the Food and Drug Administration (FDA) as well as in Europe by the European Medicines Agency (EMA) that are all designed to increase the level of functional SMN protein on the basis of 1) inhibition of exon seven skipping (Nusinersen/Spinraza[TM] and Risdiplam/Evrysdi[TM]) or 2) gene delivery (Onasemnogene abeparvovec/Zolgensma[TM]). The functional mechanisms and major results from the clinical trials are briefly stated hereinafter, but a detailed description with the most important clinical studies was reviewed recently (Jablonka et al., 2022).

The first approved drug for SMA in 2016/2017 was Nusinersen/Spinraza[TM] (Biogen), an antisense oligonucleotide (ASO) that prevents hnRNP A1 binding to the ISS in *SMN2* intron 7 and thus interrupts splice inhibitor site favoring the inclusion of exon seven in the pre-mRNA (Hua et al., 2008; Singh et al., 2006). As these ASOs are too huge in size to cross the blood-brain barrier (BBB) they have to be administered by intrathecal injections (Nicklin et al., 1998). Results from more than 30 clinical phase 1-3 studies confirmed that Nusinersen is safe and well-tolerated by the patients from SMA type I-III patients and significantly improves survival and motor functions (Jablonka et al., 2022). However, more clinical data is required to evaluate the response of type 0 SMA infants, the reason why some patients do not respond to the ASO treatment (non-responders) or the fact that the systemic application particularly restores the expression of full-length SMN in the central nervous system (CNS) while peripheral expression is neglected (Gidaro and Servais, 2019).

A further recently FDA-approved splicing modifier that supports the inclusion of exon seven is the small molecule Risdiplam/Evrysdi[TM] (Roche). In contrast to the ASOs, it can cross the BBB and hence, when applied orally, increases full-length SMN levels in the CNS as well as in the periphery (Poirier et al., 2018). In the initial phases of the first two (still ongoing) clinical trials the well-tolerability and efficacy of the drug was shown in SMA type I-III patients with significant improvement of the over-all motor functions and survival with only minor adverse effects (Jablonka et al., 2022). Two further ongoing clinical trials aim to evaluate the efficacy, safety and tolerability of Risdiplam even in infants that are diagnosed with SMA but do not show any symptoms yet (Dhillon, 2020).

The third FDA- and EMA-approved SMA treatment is Onasemnogene abeparvovec/Zolgensma[TM] (Novartis) which is a single intravenous injection of non-replicating, self-complementary adeno-associated virus 9 (scAAV9) delivering a functional copy of *SMN1* cDNA. Clinical phase 1 and phase 3 trails (partial ongoing) proofed the beneficial effects of Onasemnogene abeparvovec injection in SMA type I and type II patients (Jablonka et al., 2022). In the initial open-label study START (NCT02122952), in total 15 SMA type I infants received either low dose (6.7 × 10^{13} vector genomes per kilogram (vg/kg),

3 patients) or high dose (1.1×10^{14} vg/kg, 12 patients) of the viral vector. Surprisingly, the evaluation revealed that all of the 15 patients that received the intravenous injection were alive at the age of 20 months- while untreated patients with the same condition only had an 8 % chance of survival up to this age. Moreover, the motor functions of the patients did improve significantly, so that 11 out of 12 infants of the high dose cohort become able to sit unassisted (Mendell et al., 2017). Subsequent monitoring of the patients participated in this study is monitored in the long-term follow-up (LTFU) study 001 (NCT03421977). Additionally, in four ongoing phase 3 studies that include pre-symptomatic infants as well, the safety, efficacy and tolerability of Onasemnogene abeparvovec is going to be further analyzed in detail. Likewise, a second LTFU study will enroll participants from the currently ongoing phase 1 and phase 3 clinical trials (Hoy, 2019; Jablonka et al., 2022).

As SMN expression is highly regulated over development, with highest level during the embryonic stage and early postnatal life (Burlet et al., 1998; Fan and Simard, 2002; Jablonka et al., 2000; La Bella et al., 1998), the temporal requirements for SMN-elevating therapies are crucial. Therefore, the results obtained from SMA mouse models that were injected with scAAV9-*SMN* at different time points are not surprising; an early even pre-symptomatic therapy starting at P1/P2 had the highest beneficial effects, which are markedly decreased by drug application at P5 when the first symptoms have already occurred. At P10, when the disease had already progressed, no beneficial effects were observed upon scAAV9-*SMN* application (Foust et al., 2010). In contrast, a permanent elevation of the SMN protein level could have severe adverse effects as recent observations in mice revealed (Van Alstyne et al., 2021). Upon intracerebroventricular delivery of sc-AAV9-*SMN* in newborn *SMNΔ7* mice, the pups showed indeed ameliorated motoric functions and survival, however at 4 months of age the treated SMA mice developed a neurological condition. The authors of the publication found out, that long-term SMN overexpression results in a dose-dependent loss of proprioceptive neurons and decrease in motoneuron soma size and survival in later development in SMA-mice (P190) as well as wild type mice (P300). These defects are caused by cytoplasmic aggregation of the overexpressed SMN protein (Van Alstyne et al., 2021). Therefore, the continuous elevation of SMN via viral vectors bears the risk of toxic gain-of-function mechanisms, which needs to be considered for the long-term evaluation and monitored by the LTFU described before. In addition to the already approved SMA therapeutics, combinatorial SMN-independent therapies could have beneficial effects for many SMA patients, especially when the symptoms already occurred and persist the treatment (Jablonka et al., 2022; Wirth et al., 2020).

1.2. The protective modifier Plastin 3

1.2.1. Plastin 3 expression and structure

Plastin 3 (PLS3) belongs to a family of highly conserved actin-binding proteins. This plastin (PLS) protein family (originally termed fimbrins, according to the first descriptions (Bretscher and Weber, 1980)), counts three homologous members: PLS1 (I-plastin), PLS2 (L-plastin) and PLS3 (T-plastin) which show different tissue-specific expression patterns and functions (Shinomiya, 2012). The human *PLS3* gene was initially identified in the laboratory of John Leavitt in 1988 (Lin et al., 1988). The ~90 kb gene consists of 16 exons and maps to chromosome Xq23 (Lin et al., 1988; Lin et al., 1993). The genes encoding PLS1 and PLS2 are located on chromosome 3 and 13, respectively; and display a highly conserved exon sequence indicating divergence of all three genes from one ancestral gene (Lin et al., 1993; Lin et al., 1994). The human PLS3 (hPLS3) protein consist of 630 amino acids and is widely expressed in various cell types of solid tissues including brain, spinal cord and muscles (Lin et al., 1988; Lin et al., 1993; Oprea et al., 2008). Comparison of the amino acid sequence shows 79 % similarity between PLS3 and PLS2 and 75 % similarity between PLS3 and PLS1, however their structure is highly conserved. The murine PLS3 isoform is 99 % identical to the human one (Shinomiya, 2012). As the most prominent function of PLS is actin-binding and -bundling, PLS comprise two tandem actin binding domains (ABD1 and ABD2) of which every domain is composed of two alpha-helical calponin homology sub-domains (Banuelos et al., 1998; de Arruda et al., 1990; Goldsmith et al., 1997; Klein et al., 2004). High-resolution cryo-electron microscopy allowed the generation of a 12-Å-resolution map of F-actin alone in comparison to F-actin decorated with human PLS2 (Galkin et al., 2008). In their study, the authors propose a mechanism in which initially the ABD2 binds and stabilizes a nascent actin filament and subsequently activates ABD1 to bind another actin filament in a more ordered fashion. N-terminally, two alpha-helical-rich Ca^{2+} binding EF-hand motifs are located (de Arruda et al., 1990). It was shown that these EF-motifs change their structural confirmation upon Ca^{2+} binding with lower sensitivity in PLS3 compared to PLS1 and PLS2 (Miyakawa et al., 2012; Schwebach et al., 2017). For the latter one it has been demonstrated that the actin-bundling function is dependent, but negatively regulated by increased Ca^{2+} levels (Namba et al., 1992). Based on electron cryomicroscopy and helical reconstruction it was similarly proposed for PLS3 that the N-terminal Ca^{2+}-binding domains inhibit PLS3-actin binding in the presence of Ca^{2+} and therefore negatively regulate PLS function (Hanein et al., 1998). However, another group reported that PLS3-actin binding was unaffected by Ca^{2+} concentrations up to 2.2 µM (Giganti et al., 2005), which is consistent with the observation that PLS3, in contrast to PLS2, is incapable of changing confirmation upon Ca^{2+} spikes in activated cells, but only responds to higher Ca^{2+} concentrations (Miyakawa et al., 2012). More recently, it was proven that all three PLS isoforms were capable of binding actin in a Ca^{2+}-independent manner and that this binding is thought to be mediated by ABD1, while in contrast the interaction of ABD2 with actin was shown to be inhibited by Ca^{2+} (Schwebach et al., 2017). Hence in contrast to the ABDs, the rather small homology within in Ca^{2+}-binding domains of the PLS isoforms may indicate the reason for their differential regulated actin-binding capacities (Delanote et al., 2005). Nevertheless, the presented studies strongly suggest a dependency on well-balanced Ca^{2+} homeostasis for proper PLS function (Wolff et al., 2021).

1.2.2. Functions of Plastin 3

The most prominent functions of PLS3 is actin binding and cross-linking resulting in formation of bundled actin filaments with the same polarity (Arpin et al., 1994; Delanote et al., 2005; Shinomiya, 2012). Furthermore, it has been demonstrated that PLS3 can modulate actin filament stability (Giganti et al., 2005; Karpova et al., 1995) and regulate the access of other actin-binding proteins to the actin filaments (Skau and Kovar, 2010). PLS3-induced cytoskeletal organization was early demonstrated by Arpin and colleagues. Here, the authors have shown that PLS3 overexpression resulted in rounding-up of fibroblast-like CV-1 cells and reorganization of their actin bundles. Moreover, PLS3, in contrast to PLS2, was tightly associated with microvilli at the cell surface and responsible for elongation of these microvilli composed of polarized actin bundles (Arpin et al., 1994). Similarly, PLS3 was observed to be located at the leading edge of filopodia in mouse melanoma cells and therefore suggested to be involved in filopodia formation and movement (Xue et al., 2010). More recently, Garbett and colleagues have brought further evidence for PLS3's function in the protrusive network. In their study, they investigated the role of PLS3 enriched at the leading edge of filopodia and lamellipodia of human endothelial cells. Interestingly, they show that PLS3 knockdown results in a defective protrusive network including reduced amounts of the actin nucleator Arp2/3 complex (Rouiller et al., 2008; Welch et al., 1997) and F-actin amount within lamellipodia. By using a fibronectin micropattern assay, they observed a reduced capacity of gap bridging in the PLS3 knockdown cells (Garbett et al., 2020). Collectively, PLS3 was shown to be involved in actin-dependent processes like motility and cell migration (Brun et al., 2014; Garbett et al., 2020; Serio et al., 2010; Xue et al., 2010), membrane assembly in the epidermis (Dor-On et al., 2017), membrane trafficking under hyopoxic conditions (Wottawa et al., 2017) and endocytic processes (Hagiwara et al., 2011; Jorde et al., 2011; Kubler and Riezman, 1993). Therefore, it is not surprising that imbalances in the PLS3 levels are tightly associated with diverse disease conditions such as bone disorders, cancer subtypes or neurodegenerative diseases like SMA (Wolff et al., 2021). For instance, mutations in *PLS3* are linked to X-linked osteoporosis and osteoporotic fractures (van Dijk et al., 2013; Wolff et al., 2021). Recent investigation revealed PLS3 as regulator of osteclastegnesis through interaction with NFκB repressing factor (NKRF) and thus altering its signalling. The authors of this study provide evidence that on the one hand PLS3 knockout leads to osteoporosis in mice, PLS3 overexpression on the other hand results in thicker cortical bones and increased strength (Neugebauer et al., 2018). Furthermore, aberrant PLS3 expression is associated with various cancer subtypes (Wolff et al., 2021). With this regard, it has been shown that elevated PLS3 levels result in an increased invasiveness by induction of epithelial–mesenchymal transition in colorectal cancer cells (Sugimachi et al., 2014). Similarly, it was demonstrated in pancreatic cancer cells that PLS3 promotes proliferation and invasion of these cells by interaction with the phosphoinositide 3-kinase (PI3K)/protein kinase B (Akt) pathway (Xin et al., 2020).

1.2.3. Plastin 3 – a fully protective modifier of SMA

The discovery of PLS3 as protective modifier of SMA was driven by investigations of rare families with children harbouring the same genotype with a homozygous loss of *SMN1* but develop distinct phenotypes. Although the loss of *SMN1* and three to four copy numbers of *SMN2* would emerge in an intermediate type of SMA as seen in the symptomatic children, their siblings with identical *SMN1* and

SMN2 alleles were completely asymptomatic. Using native blood samples and Epstein-Barr-virus-transformed lymphoblastoid (LB) cell lines of these asymptomatic patients, Oprea and colleagues deciphered PLS3 as first SMA modifier apart from *SMN2* copy number (Oprea et al., 2008). The results obtained from differential gene expression analysis as well as RT-PCR and protein examinations clearly showed that *PLS3*/PLS3 levels were highly upregulated in the asymptomatic individuals compared to their sickened siblings. Later on, the same group confirmed the findings by showing highly elevated PLS3 levels in motoneurons differentiated from induced pluripotent stem cell (iPSCs) derived from skin fibroblasts of the asymptomatic SMA patients (Heesen et al., 2016). However, PLS3 seems to act as a gender specific SMA modifier, since the results revealed that three out of six highly *PLS3*-expressing female patients have only mild SMA while carrying two *SMN2* copies; and on the other hand in all of the 10 male patients having high *PLS3* levels the SMA type tightly correlated with the *SMN2* copy number (Oprea et al., 2008). Similar conclusions were obtained from two other groups who additionally found out that *PLS3*- besides acting in a gender-specific manner- also has an age-specific association with the disease outcome and strongly acts as a modifier selectively in post-pubertal females, suggesting the influence of female hormones (Stratigopoulos et al., 2010; Yanyan et al., 2014).

In the recent years, several studies were undertaken to elucidate the mechanism underlying the protective effect of PLS3. For humans and mice, it has been shown that PLS3/Pls3 is highly expressed in the spinal cord. Furthermore, an association between Pls3 and Smn was discovered in mouse spinal cord extracts, which were shown to act in a ~500 kDa complex together with actin and in a second ~200 kDa large complex. Immunohistochemical examinations of murine motoneurons confirmed the co-localization of Pls3 and Smn and their accumulation in F-actin rich axonal terminals (Oprea et al., 2008). Although a similar developmental regulation was observed between SMN and PLS3 in iPSC-derived motoneurons and the expression of both proteins declined during motoneuron maturation (Boza-Moran et al., 2015), the expression of Smn or its localization seems to be independent from Pls3 (Hao le et al., 2012; Oprea et al., 2008). However, focussing on the cell morphology, Pls3 had tremendous effects: analogous to Smn, a depletion of Pls3 resulted in significantly shortened neurites and smaller growth cones; while upregulation of PLS3 in Smn-deficient embryonic motoneurons rescued the impaired axon length (Alrafiah et al., 2018; Oprea et al., 2008). Besides SMN, PLS3 was additionally shown to interact with Coronin 1C (CORO1C), another actin-binding protein (Hosseinibarkooie et al., 2016). Similar to Pls3, knockdown of CORO1C resulted in decreased F-actin levels and impaired endocytosis, while overexpression of CORO1C was able to improve the phenotype in Smn-deficient cells (Hosseinibarkooie et al., 2016). The *in vitro* findings are immensely supported by extensive *in vivo* examinations, primarily in zebrafish and mouse models. Nevertheless, even the invertebrate homologues of *PLS3* in Drosophila and nematodes were shown to modify the phenotypic outcome upon Smn deficiency, indicating *PLS3/Pls3* as conserved, cross-species acting modifier gene (Dimitriadi et al., 2010; Walsh et al., 2020). In the original publication from 2008, Oprea et al., initially showed the beneficial effect of PLS3 overexpression in Smn-deficient zebrafish embryo that, together with a slight morpholino-induced upregulation of Smn, was able to rescue axonal outgrowth defects (Oprea et al., 2008). A specific PLS3 up-regulation in motoneurons was sufficient to rescue NMJ defects and improve the movement deficits in Smn mutants (Hao le et al., 2012). On the other hand, decreasing Pls3 levels results in detrimental effects like axonal branching defects and, when Pls3 levels were greatly reduced,

to lethality (Hao le et al., 2012; Oprea et al., 2008). Subsequent studies using SMA mouse models further confirmed these findings. Initially, the Cre/loxP system was used to generate conditional PLS3 overexpressing mice that were crossed onto the $Smn^{-/-};SMN2$(Hung) background (SMA$_{PLS3V5}$) (Ackermann et al., 2013). Analysis of these mice revealed significant improvements of NMJ phenotype including increased muscle fiber and endplate size as wells as ameliorated neuromuscular connectivity compared to the affected SMA mice. Moreover, the motoneuron soma size and the number of proprioceptive inputs was fully restored to normal levels in the SMA$_{PLS3V5}$ mice (Ackermann et al., 2013). Even when PLS3 was exclusively overexpressed in motoneurons, equal effects were observed demonstrating that appropriate PLS3 levels specifically in the presynaptic compartment are important und sufficient to improve the neuromuscular phenotype (Ackermann et al., 2013). On a milder SMA background, obtained by either a mixed genetic background (Ackermann et al., 2013) or by slight ASO-induced upregulation of Smn (Hosseinibarkooie et al., 2016), the effect of elevated PLS3 levels was even more pronounced. In detail, these milder SMA mice overexpressing PLS3 showed restoration of synaptic vesicles amount and their organization within the readily releasable pool, as well as reconstitution of the active zones and F-actin amount within the axonal terminals (Ackermann et al., 2013). Furthermore, the impaired endocytosis and synaptic vesicle recycling in Smn-deficient NMJs were restored to control levels (Hosseinibarkooie et al., 2016). Additionally, the survival and body weight of the milder SMA mice expressing PLS3 was significantly, albeit only moderately, increased compared to the control SMA mice. In contrast, severely affected SMA mice ubiquitously overexpressing PLS3 (SMA$_{PLS3V5}$) did not show any improvement of the mean survival nor body weight (Ackermann et al., 2013). These results support the idea that a certain amount of SMN is needed for the protective effects of PLS3, which is in line with the human data of asymptomatic patients harboring three to four copies of SMN2 that benefit from higher PLS3 levels (Oprea et al., 2008). Using AAV9–mediated approaches it was shown that delivery of *PLS3* alone did not improve the life span of *SMNΔ7* mice when applied via intravenous injection into the superficial facial vein (Kaifer et al., 2017). However, a combined therapeutic strategy using AAV9-*PLS3* and simultaneously administration of a low, suboptimal dose of *Smn* ASOs significantly ameliorated the life span of these mice, accompanied by improved NMJ phenotype and motor function (Kaifer et al., 2017). More recently, another group provided evidence that indeed AAV9-*PLS3* alone is indeed sufficient to extend the survival of *SMNΔ7* mice significantly, if only moderately, when administrated via cisterna magna at P1 (Alrafiah et al., 2018).

Taken together, these data collectively demonstrate the enormous potential of PLS3 in rescuing the SMA motoneuron phenotype and its capability as an additive, combinatorial therapeutic for SMA.

However, the underlying mechanism how SMN and PLS3 interact and how PLS3 on the cellular level is able to counteract the SMA manifestation is still not well understood. In zebrafish, it was shown that Smn neither influences Pls3 transcription nor its RNA stability, but rather the translation is affected leading to reduced Pls3 levels upon Smn deficiency (Hao le et al., 2012). Furthermore, deletion constructs of PLS3 surprisingly revealed that the Ca^{2+}-binding EF-hand motif is from major importance for PLS3 ability to rescue the SMA phenotype. In contrast, PLS3 constructs lacking the ABD2 or even constructs lacking both ABDs were still able to rescue axonal defects in Smn morphants (Lyon et al., 2014). Hence, further research is required to decipher the exact role of PLS3 in the SMA pathomechanism.

1.3. BDNF/TrkB signaling

During early development, a multiplicity of motoneurons is generated that grow out to their target muscles- however, a large portion undergoes physiological cell death (Oppenheim, 1991; Sanes and Lichtman, 1999; Sendtner et al., 2000). Extensive research focussing on this critical time period led to the discovery of neurotrophic factors that support survival and maturation of these motoneurons and thus maintain their functionality (Sendtner, 2014; Sendtner et al., 2000). Among these, the best studied are neurotrophins that comprise the structurally related nerve growth factor (NGF), BDNF, neurotrophin-3 (NT-3), NT-4/5, NT-6, and NT-7 in lower vertebrates (Barde, 1990; Chevrel et al., 2006; Huang and Reichardt, 2001). Further families include transforming growth factor β superfamily, glial cell–derived neurotrophic factor (GDNF) family, the ciliary neurotrophic factor (CNTF)/ leukemia inhibitory factor family and further factors including insulin-like growth-factors or hepatocyte growth factor (Chevrel et al., 2006; Kalinowska-Lyszczarz and Losy, 2012). Neurotrophin signaling is mediated via Tropomyosin-kinase receptors (Trks) and via pan neurotrophin p75 receptor (p75^{NTR}) to induce various of signaling pathways associated with a variety of cellular processes (Reichardt, 2006).

1.3.1. Brain-derived neurotrophic factor

1.3.1.1. BDNF gene

Initially, BDNF was isolated from pig brain extracts in 1982 and described as factor that supports survival of and outgrowth from cultured sensory neurons (Barde et al., 1982), before the entire primary structure of BDNF was revealed in 1989 (Leibrock et al., 1989). Since then, a vast array of BDNF actions have been reported demonstrating its involvement in a wide range of neurophysiological functions. The ~ 70 kb human *BDNF* gene maps to chromosome 11p13-14 (Hanson et al., 1992) and consist of 11 exons and nine promotors, leading to the emergence of 17 alternative transcripts (Pruunsild et al., 2007). These transcripts are expressed in a developmental-regulated and tissue-specific manner, with highest levels in the CNS but also in the non-neuronal tissue including heart, muscles, lung and placenta (Pruunsild et al., 2007). Similar distributions were observed in rodents, in which the *Bdnf* gene displays 9 exons and 11 alternative transcripts (Aid et al., 2007; Ernfors et al., 1990; Hofer et al., 1990; Leibrock et al., 1989; Maisonpierre et al., 1990; Rosenthal et al., 1991; Schecterson and Bothwell, 1992; Timmusk et al., 1993). *BDNF* expression was shown to be regulated in an activity-dependent manner, which is dependent on Ca^{2+} influx via L-type VGCCs- and N-methyl-d-aspartate (NMDA) receptors (Lu, 2003; Tabuchi et al., 2000; Tao et al., 1998). Especially rodent promotor IV (previously reported as promoter III) comprises the regulatory elements leading to activity-dependent *Bdnf* transcription (Hong et al., 2008; Sakata et al., 2009; Tao et al., 1998; Tao et al., 2002). Moreover, different alternative *Bdnf* transcripts are spatially segregated into distinct cellular compartments (Baj et al., 2011; Chiaruttini et al., 2009). Thus, the complex structure of the *BDNF* gene explains the various functions BDNF exerts in diverse brain regions, cell types and subcellular locations via differential activation of the distinct promotors leading to the production of specific transcripts during determined developmental periods (Hong et al., 2008; Park and Poo, 2013).

1.3.1.2. BDNF protein production and release

Similar to *BDNF* mRNA expression, BDNF protein in rodents, humans or monkeys can be detected in neuronal cells throughout the CNS including cortex, substantia nigra, hippocampus and brainstem structures and spinal cord (Conner et al., 1997; Yan et al., 1997a; Zhang et al., 2007) as well as in the enteric nervous system (Hoehner et al., 1996) and in non-neuronal cells such as megakaryocytes (Tamura et al., 2012), immune cells (Kerschensteiner et al., 1999), skeletal muscle cells (Matthews et al., 2009), spleen and liver (Katoh-Semba et al., 1997). The *BDNF* mRNA is translated in the endoplasmic reticulum (ER) to a precursor form (pre-pro-BDNF), from which pro-BDNF (32 kDa) is generated (Foltran and Diaz, 2016; Park and Poo, 2013). Pro-BDNF is converted into mature BDNF (~13-14 kDa) upon N-terminal cleavage and proper folding (Foltran and Diaz, 2016; Lu et al., 2005; Mowla et al., 2001). This cleavage is either mediated within the Golgi network by furin, intracellularly by protein convertases (Lu et al., 2005) or pro-BDNF is secreted extracellularly where it is cleaved by plasmin (Pang et al., 2004). Interestingly, sorting into the regulated secretory pathway for activity-triggered release is mediated on the one hand via pro-domain binding to sortilin in the Golgi network (Chen et al., 2005) and on the other hand, by a motif in the mature domain that binds to carboxypeptidase E (CPE) (Lou et al., 2005).

The transport of BDNF-containing vesicles within neurons and their primary releasing site has been under long debate. Several lines of evidence suggested a postsynaptic or target-cell mediated releasing mechanism that includes the transport of either *BDNF* transcripts (Baj et al., 2011; Chiaruttini et al., 2009) or protein to postsynaptic releasing sites, which then retrogradely acts on the presynaptic side (DiStefano et al., 1992; Sobreviela et al., 1996; Yan et al., 1992). However, anterograde transport of BDNF along the axon and release from the presynaptic compartment, where the mature form as well as pro-BDNF are stored in large dense-core vesicles (Dieni et al., 2012), has also been demonstrated in various studies (Andreska et al., 2014; Conner et al., 1997; Dieni et al., 2012; Fawcett et al., 2000; Smith et al., 1997; Yan et al., 1997b; Zhou and Rush, 1996). Nowadays it is widely accepted that BDNF is released from both postsynaptic structures as well as presynaptic structures (Notaras and van den Buuse, 2019; Sasi et al., 2017). Tagged-BDNF expression studies in cultured cortical and hippocampal neurons showed dense signal within the soma and dendrites but also within axons, where it mainly moved into the anterograde but also in the retrograde direction (Adachi et al., 2005; Kohara et al., 2001; Matsuda et al., 2009).

In neurons, BDNF release is triggered upon membrane depolarization during activity and is dependent on Ca^{2+} influx, and high-frequency stimulation was shown to efficiently trigger the release of BDNF in cultured neurons (Balkowiec and Katz, 2000; Brigadski and Lessmann, 2020; Gartner and Staiger, 2002; Hartmann et al., 2001). However, detailed analysis using the reporter BDNF-pHluorin revealed distinct releasing mechanisms in the two cellular compartments. While BDNF vesicle fusion and release in dendrites was observed under various stimulation conditions, the BDNF vesicle fusion and its release within axons were only evoked by high-frequency stimulation in cultured hippocampal neurons (Matsuda et al., 2009). In general, the pattern of stimulation and electrical activity which is needed for efficient induction of BDNF release highly differs between mature and developing neurons in various brain regions (Brigadski and Lessmann, 2020). Moreover, the increase in intracellular Ca^{2+} levels to trigger membrane fusion of BDNF-containing vesicles is tightly regulated in different cell types and achieved

via Ca^{2+} influx through VGCCs (Balkowiec and Katz, 2002; Kolarow et al., 2007), NMDA or α-amino-3-hydroxy-5-methyl-4-isoxazolepropionic acid (AMPA) receptors (Hartmann et al., 2001; Harward et al., 2016; Kolarow et al., 2007) or transient receptor potential cation channels as shown for smooth muscle cells (Vohra et al., 2013). Additionally, BDNF release can be induced by Ca^{2+} release from intracellular stores (Balkowiec and Katz, 2002; Canossa et al., 2001; Kolarow et al., 2007) and by BDNF itself via elevation of intracellular cyclic adenosine monophosphate (cAMP) levels (Cheng et al., 2011). Hence, as BDNF is important for neuronal development and synaptic plasticity for establishing neuronal networks and complex brain circuits it is not surprising that a highly regulated temporal and spatial BDNF release is required for such processes (Brigadski and Lessmann, 2020).

Upon release, BDNF can act via two receptors: p75^{NTR} (Dechant and Barde, 2002; Rodriguez-Tebar et al., 1990) and via its high-affinity receptor TrkB (Klein et al., 1991; Squinto et al., 1991). It is believed that these two receptors play important roles in the opposing effects of BDNF signaling which is prerequisite for the bilateral regulation of neuronal activity and synaptic plasticity (Gibon et al., 2015; Je et al., 2012; Sasi et al., 2017; Woo et al., 2005). While BDNF/TrkB signaling is associated with induction of long-term potentiation (LTP) and pro-survival effects (Huang and Reichardt, 2001; Korte et al., 1995; Lai et al., 2012; Minichiello, 2009), activation of p75^{NTR} preferentially by pro-BDNF is connected to the induction of long-term depression (LTD) (Rosch et al., 2005; Woo et al., 2005; Yang et al., 2014), negative regulation of dendritic complexity (Yang et al., 2014; Zagrebelsky et al., 2005), and neuronal apoptosis (Bamji et al., 1998; Teng et al., 2005).

1.3.2. Tropomyosin-kinase receptor B

1.3.2.1. TrkB expression

TrkB as a part of the tyrosine protein kinase family of cell surface receptors is referred to as the high-affinity receptor for BDNF (Glass et al., 1991; Klein et al., 1991; Klein et al., 1989), even though less potent activation of TrkB was also shown by NT-3 and NT-4 (Glass et al., 1991; Klein et al., 1991; Windisch et al., 1995). Besides TrkB, the family comprises TrkA (receptor for NGF) and TrkC (preferentially activated by NT-3), that share homology in protein structure and functions (Huang and Reichardt, 2001; Nakagawara et al., 1995; Reichardt, 2006). The Human *NTRK2* gene maps to chromosome 9q22 (Nakagawara et al., 1995; Slaugenhaupt et al., 1995; Valent et al., 1997) and exhibits a highly complex structure harbouring 24 exons from which at least 36 possible TrkB isoforms could be generated via alternative splicing (Luberg et al., 2010; Stoilov et al., 2002). Besides the 822 amino acid full-length TrkB protein, two major variants are produced: a TrkB isoform lacking the tyrosine kinase domain (TrkB-T1) and a one that lacks the kinase domain as well but harbours the Shc-binding domain (TrkB-T-Shc) (Nakagawara et al., 1995; Stoilov et al., 2002). Similar to humans, multiple mRNA variants are expressed in rodents leading to the production of the full-length protein and truncated isoforms (Baxter et al., 1997; Klein et al., 1990; Middlemas et al., 1991). Expression studies in humans and rodents have demonstrated that *TrkB* mRNA is highly expressed during embryonic development up to adulthood especially in the CNS (brain, spinal cord, motoneurons), as well as the peripheral nervous system (PNS) and peripheral tissues such as lung, heart, muscles or liver (Barbacid, 1994; Griesbeck et al., 1995; Klein et al., 1989; Koliatsos et al., 1993; Luberg et al., 2010; Middlemas et al., 1991; Stoilov

et al., 2002). Similar to the expression of *BDNF*, *TrkB* expression was also shown to be increased upon depolarization and Ca^{2+} influx in cortical neurons (Kingsbury et al., 2003). However, not only the expression of *TrkB*, but also the recruitment and accumulation of its mRNA to dendritic structures is induced by neuronal activity in hippocampal neurons. For these cells its was shown that neuronal activity induced by KCl-mediated depolarization and BDNF application are able to efficiently promote the translocation of *BDNF* mRNA and *TrkB* mRNA into dendrites leading to increased BDNF and TrkB protein levels by local translation independent from mRNA synthesis (Righi et al., 2000; Tongiorgi et al., 1997). In neurons, TrkB protein is localized intracellularly and on the cell surface within the somatodendritic and the axonal compartment throughout the development (Aoki et al., 2000; Drake et al., 1999; Gomes et al., 2006; Kryl et al., 1999; Yan et al., 1997a). Furthermore, it has been demonstrated in axons that TrkB can move in both anterograde and retrograde direction (similar for dendrites) and colocalizes with proteins important for synaptic vesicles (Gomes et al., 2006). The full-length TrkB protein comprises a complex structure: in the extracellular domain after an N-terminal signal sequence, there are three leucine-rich motifs framed between two cysteine-rich domains and two immunoglobulin-like domains for BDNF binding. Following a single transmembrane domain, the intracellular C-terminal part of TrkB consists of a Shc-docking side, the tyrosine kinase domain and a phospholipase C γ (PLCγ) binding site (Huang and Reichardt, 2003; Luberg et al., 2010; Windisch et al., 1995).

1.3.2.2. Receptor activation and induction of signaling pathways

Upon ligand binding, TrkB dimerizes and undergoes autophosphorylation of the tyrosine residues within the intracellular kinase domain. This in turn initiates phosphorylation of further tyrosine residues of the receptor leading to the induction of three main signaling pathways (Chao, 2003; Cunningham and Greene, 1998; Minichiello, 2009; Sasi et al., 2017). Phosphorylation of tyrosine residue 515 leads to docking of the Shc adaptor protein. Phosphorylated Shc in turn recruits further adaptor proteins like receptor-bound protein 2 (GRB2) that links two signaling pathways to the activated TrkB: the PI3K–Akt pathway on the one hand and the Ras- mitogen-activated protein kinase (MAPK) pathway on the other (Huang and Reichardt, 2003; Kaplan and Miller, 2000; Minichiello, 2009).

Via the PI3K/Akt signaling cascade, a variety of transcription-dependent and transcription-independent processes are triggered that are associated with the mediation of neuronal survival (Atwal et al., 2000; Brunet et al., 2001; Crowder and Freeman, 1998; Dolcet et al., 1999; Hetman et al., 1999; Vaillant et al., 1999), axonal outgrowth (Atwal et al., 2000), control of dendritic complexity and dendritic filopodia motility (Dijkhuizen and Ghosh, 2005; Kumar et al., 2005; Luikart et al., 2008) as well as synaptic function (Schratt et al., 2004). Furthermore, the PI3K/Akt/mTOR pathways was associated with translational regulation of proteins important for dendritic arborization and cytoskeleton dynamics (Gonzalez et al., 2016; Jaworski et al., 2005; Kowianski et al., 2018; Kumar et al., 2005; Schratt et al., 2004).

Induction of the Ras/MAPK pathway leads to regulation of protein synthesis that is further associated with dendritic branching via activation of the transcription factor cAMP responsive element binding protein (CREB) (Finkbeiner et al., 1997; Finsterwald et al., 2010; Kwon et al., 2011). Moreover,

increased expression of serum-inducible kinase (SNK) via transcriptional regulation was also shown to have a promoting effect on dendritic arborization (Guo et al., 2012).

Additionally, a further tyrosine on position 816 is phosphorylated leading to the binding and activation of the PLCγ pathway. PLCγ cleaves phosphatidylinositol 4,5-bisphosphate (PIP_2) to produce inositol 1,4,5-trisphosphate (IP_3) and diacyl glycerol (DAG). Subsequently, Ca^{2+} is released from intracellular stores leading to the activation of Ca^{2+}-dependent enzymes such as Ca^{2+}/calmodulin dependent protein kinase (CaMK) (Minichiello, 2009; Numakawa et al., 2001). CaMK activation in turn can mediate the phosphorylation of transcription factors such as CREB resulting in regulation of gene expression linked to induction of hippocampal LTP (Finkbeiner et al., 1997; Minichiello et al., 2002). DAG production on the other hand can activate protein kinase C (PKC), which was shown to induce neurite outgrowth and MAPK activation upon NGF stimulation, (Corbit et al., 1999; Minichiello, 2009; Pradhan et al., 2019). Besides the three main pathways, phosphorylation of the serine residue at position 478 by the cyclin-dependent kinase 5 (Cdk5) was shown to link TrkB to the TIAM1/Rac1 pathway that mediates dendritic growth and activity-dependent spine remodeling necessary for LTP and memory formation (Cheung et al., 2007; Lai et al., 2012). Furthermore, BDNF-induced dimerization of TrkB was demonstrated to trigger the interaction with LIM kinase 1 (LIMK1) (Dong et al., 2012). BDNF-induced LIMK1 activation finally promotes de-activation of cofilin, leading to actin cytoskeleton remodeling and promotion of neurite formation and axon elongation (Dong et al., 2012; Saito et al., 2013). This pathway together with the activation of profilin upon BDNF stimulation was shown to be an important mediator of the dynamic F-actin assembly in growth cones of cultured embryonic motoneurons (Dombert et al., 2017). Moreover, BDNF influences levels of β-actin by regulation of its local protein synthesis via phosphorylation of the mRNA zipcode binding protein to control growth cone formation and tuning (Sasaki et al., 2010). In turn, modulation of the actin cytoskeleton by BDNF within growth cones can affect various actin-dependent processes, as demonstrated for the cluster formation of VGCCs leading to the induction of spontaneous Ca^{2+} transients (Dombert et al., 2017).

In addition to the classical BDNF-induced TrkB activation, several studies have shown that TrkB activation can occur in the absence of neurotrophins, which may be from major importance especially during early development, when high TrkB activation is observed in the CNS, while BDNF levels simultaneously are very low and raise postnatally (Maisonpierre et al., 1990; Puehringer et al., 2013). For instance, it has been demonstrated that adenosine, or adenosine agonists, can stimulate TrkB phosphorylation via the adenosine 2A (A_{2A}) receptor. In contrast to the BDNF-induced receptor activation, transactivation of TrkB via adenosine appears slower and seems to selectively activate the PI3K/Akt signaling pathway to promote cell survival (Lee and Chao, 2001; Lee et al., 2002a; Wiese et al., 2007). Furthermore, G protein-coupled receptors (GPCR), activated by pituitary adenylate cyclase-activating polypeptide, or dopamine, could effectively trigger TrkB transactivation and its surface expression (Iwakura et al., 2008; Lee et al., 2002b; Rajagopal et al., 2004). Similarly, the epidermal growth factor (EGF), via its receptor EGFR, is able to induce TrkB activation in cortical precursor cells to control their migration within the cortex (Puehringer et al., 2013). Moreover, it was reported that synaptic vesicular zinc can induce TrkB transactivation via elevated Scr-activity (Huang et al., 2008), although more recent studies contravene these findings (Helgager et al., 2014).

1.3.2.3. BDNF/TrkB signaling endosomes

Upon ligand-induced receptor activation, the BDNF-TrkB complex undergoes endocytosis. Early work especially on NGF/TrkA showed that the ligand/Trk complex is rapidly internalized in a clathrin-mediated way to form signaling endosomes that contain the phosphorylated ligand/receptor-complex including associated signaling molecules such as PLCγ or the proteins of the Ras/MAPK pathway (Beattie et al., 2000; Grimes et al., 1997; Grimes et al., 1996; Howe et al., 2001). Later on, a Pincher-mediated, clathrin-independent macropinocytosis pathway was demonstrated to efficiently promote ligand/Trk signaling (Valdez et al., 2005). In axons, signaling endosomes are then retrogradely transported to the cell body to promote the induced signaling pathways especially in terms of transcriptional regulation and pro-survival effects (Heerssen et al., 2004; Valdez et al., 2005; Watson et al., 1999). Extended research during the last decades revealed further mediators involved in regulating endocytic trafficking of BDNF/TrkB signaling endosomes, such as proteins involved in internalization and sorting (Ayloo et al., 2017; Burk et al., 2017; Fu et al., 2011; Liu et al., 2015), various Rab GTPases (Burk et al., 2017; Gonzalez-Gutierrez et al., 2020; Moya-Alvarado et al., 2018; Song et al., 2015), as well as dynein isoforms or interactors (Ha et al., 2008; Olenick et al., 2019; Zhou et al., 2012). However, the complex mechanism of Trk trafficking is still not fully resolved. The established conceptual framework implies the following mechanism: 1) Ligand-induced TrkB activation and recruitment of singling molecules. 2) Ligand/Trk complex internalization via either a clathrin-dependent mechanism or Pincher-mediated micropinocytosis. 3) Endosomal trafficking via early endosomes (Rab5) and late endosomes (Rab7) that could either lead to Trk recycling (Rab11), lysosomal degradation or 4) retrograde trafficking to the soma via dynein along microtubules (Barford et al., 2017; Cosker and Segal, 2014; Harrington and Ginty, 2013). Thus, endocytic trafficking was shown to be required for induction of specific signaling cascades by BDNF, as blockade of clathrin or dynamin efficiently inhibited BDNF-induced activation of Akt (Zahavi et al., 2018; Zheng et al., 2008). Additionally, sustained MAPK activation and nuclear CREB phosphorylation by BDNF were disturbed upon disruption of Rab5 or Rab11 (Gonzalez-Gutierrez et al., 2020). Moreover, a recently published study claimed that TrkB, in contrast to the common understanding, is activated as a monomer on the cell membrane (Zahavi et al., 2018). Using high resolution imaging techniques, the authors have demonstrated that monomeric TrkB can induce MAPK signaling, whereas dimerization and clustering occurs within signaling endosomes, which is needed for a sustained P13K/Akt activation. Therefore, they postulate a mechanism in which these endosomes function as a cellular gate that regulates BDNF/TrkB signaling in a spatial and temporal manner (Zahavi et al., 2018).

1.3.2.4. Regulation of TrkB cell surface expression

The neuronal responsiveness to BDNF seems to be highly regulated process, which is dependent on several factors (Andreska et al., 2020). One major mechanism to modulate the neuronal ability to respond to BDNF is the expression of its receptor on the cell surface (**Fig. 4**). Early studies showed that CNS neurons such as retinal ganglion cells and motoneurons are less responsive to BDNF stimulation *in vitro* compared to neurons derived from the PNS (Meyer-Franke et al., 1995). However, a simultaneous increase of cAMP within the cells was shown to efficiently potentiate the response to BDNF stimulation

in these neurons (Meyer-Franke et al., 1998). The authors of this publication further found out, that the majority of TrkB is localized intracellularly and that this potentiation effects is due to the increase of TrkB cell surface translocation induced by cAMP elevation (Meyer-Franke et al., 1998). Furthermore, TrkB surface recruitment was shown to be induced by K^+- depolarization (Meyer-Franke et al., 1998), chemical LTP induction via glycine (Zhao et al., 2009) and high frequency tetanic stimulation (Du et al., 2000). The fact that blockade of protein synthesis does not influence the induced TrkB surface insertion (Cheng et al., 2011; Du et al., 2003; Meyer-Franke et al., 1998; Zhao et al., 2009), together with the rapid occurring insertion of TrkB (Zhao et al., 2009) argue for recruitment of TrkB from an existing pool of receptors, rather than being based on the synthesis of new receptors. Importantly, a Ca^{2+} influx through VGCCs or NMDA receptors (Du et al., 2000; Zhao et al., 2009) and the subsequent activation of Ca^{2+}/calmodulin-dependent protein kinase II (CamKII) (Du et al., 2000) is needed for TrkB membrane translocation. Surface recruitment also requires an intact cytoskeleton where both microtubules and
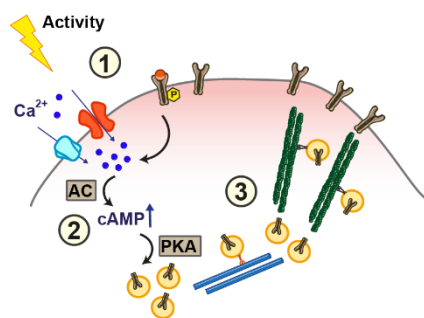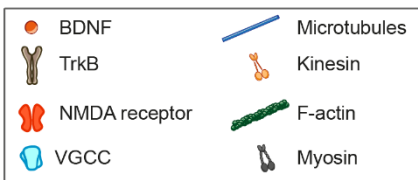
Fig. 4: Regulation of TrkB surface translocation. *Neuronal activity, e.g. induced by depolarization, or BDNF/TrkB signaling itself induce Ca^{2+} influx via VGCCs or NMDA receptors that in turn activates adenylate cyclase (AC). Subsequent elevation of cAMP levels and protein kinase A (PKA) activation trigger mobilization of the intracellular available TrkB pool promoting the cell surface transport of the receptors along microtubules and actin (see references in the main text and (Andreska et al., 2020)).*

actin filaments with their specific motor proteins are inevitably for proper TrkB membrane translocation (Zhao et al., 2009). Furthermore, activity-dependent BDNF release could be an important trigger for TrkB cell surface recruitment, as demonstrated by the acute BDNF exposure for 15 seconds that resulted in increased TrkB cell surface levels in hippocampal neurons (Haapasalo et al., 2002). This was later confirmed by Cheng and colleagues, who showed that BDNF acts in an autocrine manner in developing hippocampal neurons to promote its own secretion via protein kinase A (PKA)/cAMP elevation on one hand, and furthermore promotes cell surface recruitment of TrkB on the other hand (Cheng et al., 2011). In their study, they propose a mechanism for polarized cells, in which diverse extrinsic or intrinsic signals induce cAMP elevation leading to a positive feedback mechanism of BDNF/TrkB signaling. First, cAMP elevation results in local secretion of BDNF, which in turn activates TrkB and further promotes PKA activity and cAMP production. Secondly, increased cAMP levels trigger TrkB surface insertion, which further enhances BDNF/TrkB signaling that also mediates anterograde TrkB transport in a PI3K-dependent pathway (Cheng et al., 2011).

1.3.3. BDNF/TrkB-mediated actions

The variety of signaling cascades that are triggered upon BDNF-induced TrkB activation explains the multiplicity of BDNF/TrkB-mediated actions. Strongest effects of BDNF were reported on neuronal survival and regeneration after damage (Boyd and Gordon, 2003; Clatterbuck et al., 1994; Friedman et al., 1995; Henderson et al., 1993; Johnson et al., 1986; Kowianski et al., 2018; Li et al., 1994; Lindholm

et al., 1993; Linnarsson et al., 2000; Novikov et al., 1997; Oppenheim et al., 1992; Sendtner et al., 1992; Yan et al., 1992), as well as neuronal growth, morphology and complexity (Atwal et al., 2000; Dijkhuizen and Ghosh, 2005; Gonzalez et al., 2016; Kumar et al., 2005; Minichiello, 2009; Rauskolb et al., 2010; Sanchez et al., 2006). Furthermore, it regulates synaptic plasticity, function and neurotransmission (Blum and Konnerth, 2005; Dombert et al., 2017; Kowianski et al., 2018; Kwon and Gurney, 1996; Liou et al., 1997; Lohof et al., 1993; Numakawa et al., 2002; Schratt et al., 2004) and is involved in LTP induction and formation of memory (Korte et al., 1995; Korte et al., 1996; Lin et al., 2018; Minichiello, 2009; Patterson et al., 1996; Sasi et al., 2017; Yamada et al., 2002).

In line with this, the importance of BDNF/TrkB signaling was further confirmed by studies using mice with targeted disruption of either BDNF or TrkB, respectively. Knockout of *Bdnf* in mice is not embryonic lethal and the neonatal homozygous *Bdnf*-depleted mice initially do not differ from their healthy littermates. However, during early postnatal development they display growth defects, impaired movements and reduced breathing rates, and eventually die during the first weeks (Erickson et al., 1996; Jones et al., 1994; Rauskolb et al., 2010). Investigations of these mice revealed that the CNS does not show marked abnormalities, survival of sympathetic and midbrain dopaminergic neurons is normal and motoneuron number and function seem to be unimpaired, while sensory neurons are highly affected (Ernfors et al., 1994; Jones et al., 1994; Liu et al., 1995). Similarly, the anatomical and morphological aspects of the hippocampus appear to be normal in BDNF knockout mice, although highly impaired LTP induction was observed (Korte et al., 1995; Korte et al., 1996). These results were confirmed by studies using a conditional BDNF knockout within the CNS, where only minor alterations were found in CA1 pyramidal neurons (Rauskolb et al., 2010). Furthermore, this study revealed marked area specific and cell-intrinsic differences of BDNF responsiveness: while hippocampal neurons are relatively less affected by BDNF depletion, medium spiny neurons in the striatum showed reduced size and complexity *in vivo. In vitro* experiments demonstrating growth-promoting effects of BDNF in striatal, but not hippocampal neurons further proofed the findings (Rauskolb et al., 2010). Other deficits that occur upon BDNF deprivation include impairments of spatial learning (Linnarsson et al., 1997), reduced mechanosensitivity (Carroll et al., 1998), and behavioural abnormalities (Li et al., 2012; Rauskolb et al., 2010). Similarly, transgenic mice that either completely lack TrkB (*Ntrk2-/-*) (Rohrer et al., 1999) or harbour a TrkB with disabled kinase domain (*trkBTK-/-*) (Klein et al., 1993) develop to birth but display severe abnormalities including reduced body weight, behavioural anomalies, problems to right themselves and irregular breathing, finally leading to death during the early postnatal period (Klein et al., 1993; Rohrer et al., 1999). Moreover, TrkB-deficient mice have severe neuronal deficiencies in the CNS and the PNS (Klein et al., 1993; Lush et al., 2005; Perez-Pinera et al., 2008), In addition, TrkB deficiency is associated with impaired development of the striatum (Li et al., 2012), decreased embryonic precursor cell proliferation (Bartkowska et al., 2007), and disturbed structure and function of NMJs (Kulakowski et al., 2011). Interestingly, primary cultured motoneurons from *trkBTK-/-* E13 mouse embryos that were cultured on laminin-221/211 show marked differentiation defects including smaller growth cones and disturbed axon elongation, accompanied by reduced *β-actin* mRNA and impaired $Ca_v2.2$ accumulation in axon terminals leading to reduced frequency of spontaneous Ca^{2+} transients (Dombert et al., 2017). Therefore, TrkB-deficient motoneurons resemble the *in vitro* phenotype of *Smn-/-; SMN2* motoneurons (Jablonka et al., 2007; Rossoll et al., 2003).

Given the fact that BDNF/TrkB signaling regulates important cellular processes and brain circuits it is not surprising that imbalances in BDNF homeostasis are associated with neurodegenerative diseases such as Alzheimer´s disease (AD), Parkinson´s disease (PD) or epilepsy; and psychiatric disorders like depression or schizophrenia (Lima Giacobbo et al., 2019). Early evidence for implications of BDNF in AD comes from studies in the 1990s that reported reduced BDNF levels in the hippocampus and temporal cortex of patient-derived *post mortem* tissue (Connor et al., 1997; Hock et al., 2000; Phillips et al., 1991). Furthermore, serum BDNF levels were found to be significantly reduced in patients with early-onset and late-onset AD (Gezen-Ak et al., 2013). More recently, it has been shown that amyloid-β oligomers, that play a central role in the pathology of AD, interfere with the axonal transport of BDNF (Gan and Silverman, 2015; Ramser et al., 2013) and that higher BDNF levels are associated with slower progression of cognitive decline in AD patients (Buchman et al., 2016; Laske et al., 2011). Similarly, reduced BDNF expression was observed in the substantia nigra (Howells et al., 2000), the relevant brain structure for PD; however animal studies during the last decades reported controversial results on the beneficial effects of BDNF treatment in rodent PD models (Palasz et al., 2020). In contrast to that, several lines of evidence connected an increased BDNF/TrkB signaling with detrimental effects to neurodegenerative diseases such as ALS as recently reviewed in (Pradhan et al., 2019). Hence, further research on BDNF/TrkB signaling and its implications in diseases is inevitable required to understand the mechanism by which BDNF participates in the pathophysiological events and how that can be successfully applied for therapeutic strategies.

1.4. Aim of the study

Although current available SMA therapies focus efficiently on SMN restoration, the cellular mechanisms underlying the pathological features and motoneurons degeneration are still not fully understood. Moreover, as stated before, SMN-independent therapeutic targets offer the possibility for additional, combinatorial therapies especially for patients with persistent symptoms. Therefore, Smn-modifying genes such as *PLS3* are from major interest, since their protective functions have been reported in SMA patients as well as in various SMA animal and cell culture models.

Recently, it has been shown that TrkB-deficient motoneurons display similar morphological and functional alterations as Smn-deficient motoneurons (Dombert et al., 2017; Jablonka et al., 2007; Rossoll et al., 2003). Given the fact that BDNF/TrkB signaling is one of the most important signaling pathways for survival, maturation and differentiation of neurons, the goal of my project was to investigate whether a disturbed BDNF/TrkB signaling could play a central role in the pathomechanism of SMA. Thus, I studied the localization and activation of TrkB in Smn-deficient motoneurons and neuromuscular endplates. As my initial results revealed that the BDNF-induced TrkB activation is massively impaired in Smn-deficient axon terminals albeit TrkB cell surface presentation and BDNF-induced internalization are not affected in motoneuron growth cones by Smn deficiency, my studies focused on the role of the disturbed actin cytoskeleton in this scenario. In more detail, I decided to focus on the role of Pls3 in the dynamic cell surface presentation of TrkB and determine its potential in rescuing the observed TrkB translocation and activation defects in SMA.

2. Material and methods

2.1. Materials

2.1.1. Chemicals, solutions and buffers

Table 1: List of chemicals used for this study

Chemicals	Manufacturer
Aceton	Sigma-Aldrich
Acrylamid 40 %	Biorad
Agarose	Biozym Scientific
Ammonium Persulfate (APS)	Sigma-Aldrich
Betaine monohydrate	Sigma-Aldrich
Boric acid	Sigma-Aldrich
Bromophenol blue	Sigma-Aldrich
Calcium chloride (CaCl$_2$)	Merck
Chelex	Bio-Rad
Ethylenediaminetetraacetic acid (EDTA)	Sigma-Aldrich
Ethanol	Sigma-Aldrich
Glucose	Merck
Glycerin	Carl Roth
HEPES (4-(2-hydroxyethyl)-1-piperazineethanesulfonic acid)	Sigma-Aldrich
Lysogeny Broth (LB medium)	Sigma-Aldrich
Magnesium chloride (MgCl$_2$)	Sigma-Aldrich
Methanol	Th. Geyer
Potassium chloride (KCl)	Sigma-Aldrich
Powdered Milk	Carl Roth
Sarkosyl (N-Lauroylsarcosine)	Sigma-Aldrich
Selective Agar	Invitrogen (Thermo)
Sodium acetate (C$_2$H$_3$NaO$_2$)	Sigma-Aldrich
Sodium bicarbonate (NaHCO$_3$)	Sigma-Aldrich
Sodium chloride (NaCl)	Sigma-Aldrich
Sodium dodecyl sulfate (SDS)	AppliChem
TEMED	Carl Roth
Tris / Tris-HCl	Carl Roth
Triton X-100	Sigma-Aldrich
Tween 20	Sigma-Aldrich
Xylene cyanol	Sigma-Aldrich
β-Mercaptoethanol	Carl Roth

Table 2: List of additional enzymes, media and supplements used in this study

Ezymes, media and supplements	Manufacturer
8-(4-Chlorophenylthio)adenosine3′,5′-cAMP (8-CPT-cAMP)	Calbiochem
Amersham ECL™ Western Blotting Detection Reagent	Cytiva Sciences
Ampicillin	Sigma-Aldrich
Aqua Poly/Mount	Polysciences
B-27 supplement	Life Technologies (Thermo)
BamII	Thermo Fisher Scientific
Bovine serum albumin (BSA)	Sigma-Aldrich
Brain-derived neurotrophic factor (BDNF)	Prof. Sendtner
Cal-590™ AM	Biomol
Ciliary neurotrophic factor (CNTF)	Prof. Sendtner
CK-666	Sigma-Aldrich

Cycloheximide (CHX)	Sigma-Aldrich
Cytochalasin D (CytoD)	Sigma-Aldrich
Dimethyl sulfoxide (DMSO)	Sigma-Aldrich
DNA ladder (100 bp, GeneRuler)	Thermo Fisher Scientific
Deoxyribonucleotides (dNTPs, 100mM)	GeneOne
Dulbecco´s Modified Eagle Medium (DMEM)	Life Technologies
Dulbecco's Phosphate Buffered Saline (PBS)	Life Technologies
EcoRI	Thermo Fisher Scientific
FastDigest Green Puffer (10x)	Thermo Fisher Scientific
Fast Green	Sigma-Aldrich
Fetal Calf Serum (FCS)	Thermo Fisher Scientific
Glutamax (100x)	Life Technologies (Thermo)
Hank's Balanced Salt Solution (HBSS)	Life Technologies (Thermo)
HDGreen® Plus Safe DNA Dye	Intas
Horse serum	Linaris
KAPA HiFi HotStart ReadyMix (2x)	Thermo Fisher Scientific
Key buffer (10x)	VWR
Laminin-111	Invitrogen (Thermo)
Laminin-221/211 (human)	Merck
Luminaris HiGreen qPCR Master Mix	Thermo Fisher Scientific
Methanol-free formaldehyde 16 % (Pierce™)	Thermo Fisher Scientific
Neurobasal medium (NB)	Life Technologies (Thermo)
Nhe1 HF	New England Biolabs
Nocodazole	Merck
Opti-MEM	Invitrogen (Thermo)
Oregon Green 488 BAPTA-1, AM	Thermo Fisher
P75^{NTR}	MLR2, Biosensis M-009-100
Poly-D-L-ornithine hydrobromide (PORN)	Sigma-Aldrich
Protein Ladder	Thermo Fisher Scientific
Proteinase K	Roche
Sal1 HF	New England Biolabs
SiR-actin	Tebu-bio
T4 ligase	Thermo Fisher Scientific
Tango Buffer Yellow (10x)	Thermo Fisher Scientific
Thermus aquaticus (Taq) polymerase	VWR
Tris buffered saline with Tween-20 (TBS-T) Tablets	Gebaxxon Bioscience
TOP10 E.coli cells	Thermo Fisher Scientific
TransIT	Mirus
Trypsin	Worthington
Trypsin inhibitor	Sigma-Aldrich
Vitamin D-binding protein (DBP)	Millipore (Merck)

Table 3: Composition of buffers and media used for cell culture

Cell culture buffer and media	Composition
100x poly-D/L-ornithine hydrobromide (PORN)	500 mg powder 10 ml Borate Buffer
1x PORN	500 µl PORN (100x) in 50 ml Borate buffer
1 % Trypsin	1 % Trypsin in HEPES (pH 7.4)
1 % Trypsin inhibitor	500 mg Trypsin inhibitor 1 ml 1 M HEPES (pH 7.4) 49 ml HBSS

1 M HEPES pH 7.4	23.83 g HEPES powder 100 ml H_2O
Borate Buffer pH 8.3	150 mM boric acid (9.27 g) Ad 1 l H_2O
Complete medium	Neurobasal medium 2 % B27 2 % Horse serum (heat-inactivated at 56°C, 45 min.)
Depolarization medium	0.8 % NaCl (4 g) 30 mM KCl (1.1184 g) Ad 500 ml H_2O
Laminin-111 Laminin-221/211	2.5 µg/ml laminin-111 in HBSS 2.5 µg/ml laminin-221/211 in HBSS
Neurobasal (NB) medium	Neurobasal 1 % Glutamax (100x)
P75^{NTR} solution	0.5 µg/ml p75^{NTR} in 10 mM Tris buffer
Tris Buffer 10 mM pH 9.5	121.14 g Tris Ad 1 l H_2O

Table 4: Composition of solutions used for immunocyto and -histochemistry

Solutions for immunocyto/-histochemistry	Composition
0.1 M Glycine	0.37535 g Glycine Ad 50 ml PBS
0.3 % Triton X-100	20 % Triton X-100 → 1:66.667 in TBS-T
1 % Triton X-100	20 % Triton X-100 → 1:20 in TBS-T
4 % Methanol-free formaldehyde	16 % methanol-free formaldehyde → 1:4 in PBS
20 % Triton X-100	1 ml Triton X-100 4 ml TBS-T
Antibody solution	10 % BSA → 1:10 in TBS-T for 1 % BSA 1:4 in TBS-T for 2.5 % BSA
Blocking solution (10 % BSA)	1 g BSA Ad 10 ml H_2O
Physiological solution (NMJ Buffer)	135 mM NaCl 12 mM NaHCO$_3$ 5 mM KCl 1 mM MgCl$_2$ 20 mM Glucose (freshly added) ± 2 mM CaCl$_2$ (freshly added) Ad H_2O
TBS-T pH 7.6	0.15 M NaCl 0.05 M Tris-HCl 0.05 % Tween-20 Ad H_2O

Table 5: Composition of solutions used for Western Blots

Solutions for Western Blots	Composition
1x Transfer buffer	200 ml Methanol 100 ml 10x Towbin Buffer Ad 1 l H_2O
4x Stacking gel buffer	0.5 M Tris, pH 6.8 0.4 % SDS
4x Separating gel buffer	1.5 M Tris, pH 8.8 0.4 % SDS
5x Laemmli (diluted in water for 2x Laemmli)	250 mM Tris-HCl (pH 6.8) 25 % β-Mercaptoethanol 10 % SDS 50 % glycerol 0.2 % bromophenol blue
10x Transfer buffer	250 mM Tris (60.6 g) 2M Glycine (288 g) Ad 2 l H_2O
4 % Separating gel	4 % Acrylamide 1x separating gel buffer 10 % APS1 1 % TEMED in H_2O
4 % Stacking gel	4 % Acrylamide 1x stacking gel buffer 10 % APS1 1 % TEMED in H_2O
5 % Milk solution	5 % milk powder in TBS-T
12 % Separating gel	12 % Acrylamide 1x stacking gel buffer 10 % APS1 1 % TEMED in H_2O
TBS-T pH 7.6	0.15 M NaCl 0.05 M Tris-HCl 0.05 % Tween-20 Ad H_2O

Table 6: Composition of additional solutions used in this study

Other solutions	Composition
2 % Agarose gel	100 ml 1x TAE buffer 2 g Agarose 5 µl HDGreen® Plus Safe DNA Dye
6x Loading buffer	30 % glycerin solution in TAE 0.15 % bromophenol blue 0.15 % xylene cyanol Ad 50 ml 1× TAE
50x Tris-acetate-EDTA-buffer (TAE buffer)	2 M Tris 25 mM Sodium acetate 50 mM EDTA Ad H_2O

Agar plates	7.5 g selective Agar 10 g LB Ad 500 ml H_2O
Betaine (5 M)	20.28 g Betaine monohydrate Ad 30 ml H_2O
LB medium	20 g LB in 1 l H_2O
TBS-5 Buffer	50 mM Tris-HCl 130 mM NaCl 10 mM KCl 5 mM $MgCl_2$ Ad H_2O
Tyrode solution pH 7.4	125 mM NaCl 2 mM KCl 2 mM $CaCl_2$ 2 mM $MgCl_2$ 20 mM glucose 25 mM HEPES Ad H_2O
Calcium imaging buffer pH 7.4	135 mM NaCl 6 mM KCl 1 mM $CaCl_2$ 1 mM $MgCl_2$ 5.5 mM glucose 10 mM HEPES Ad H_2O
"Quick and Dirty" Lysisbuffer	2.5 ml 10 % Sarcosyl 1 ml 5 M NaCl 2.5 g Chelex Ad 50 ml H_2O

2.1.2. Primer and plasmids

Table 7: List of primer and the corresponding sequence used for genotyping

Genotyping primer	Sequence (5' → 3')
Smn WT/KO	
Smn 201f	CTGGAATTCAATATGCTAGACTGGCCTG
Smn 1049r2	CAATCTATCACCTGTTTCAAGGGAGTTGTGG
Smn KO	GATGTGCTGCAAGGCGATTAAGTTG
SMN2tg	
Tw3	CATACCTTAAAGGAAGCCAC
Tw7	AGGTTCTGAGGTCAGAACAGC
SMNΔ7	
oMIR3679	TCCATTTCCTCCTGGACCAC
oMIR3680	ACCCATTCCACTTCC TTT
TrkB WT/KO	
TrkB-c8	ACTGACATCCGTAAGCCAGT
TrkB-n2	ATGTCGCCCTGGCTGAAGTG
pgk3-1	GGTTCTAAGTACTGTGGTTTCC
Primer for Colony PCR	
Primer a	AATGTCTTTGGATTTGGGAATCTTAT
Primer b	TGGTCTAACCAGAGAGACCCAGTA

Table 8: List of primer and the corresponding sequence used for RT-PCR

Primer RT-PCR	Sequence (5' → 3')
GAPDH (murine)	
GAPDH forward	GCAAATTCAACGGCACA
GAPDH reverse	CACCAGTAGACTCCACGAC
TrkB (murine)	
TrkB forward	CGGGAGCATCTCTCGGTCTAT
TrkB reverse	CTGGCAGAGTCATCGTCGTTG
PLS3 (murine)	
mPLS3 forward	CAAGCCTCCATACCCAAAGC
mPLS3 reverse	CCATCGTTCAGGTCTTGTCC
PLS3 (human)	
hPLS3 forward	GAACGTTGAGTGAAGCTGGA
hPLS3 reverse	TTGCCACTCTTCACAAGGTC

Table 9: List of primer and the corresponding sequence used for clonings

Cloning primer	Sequence (5' → 3')
shPLS3	
shPLS3.1 sense	GATCCCTCATGGTGGATGGTGACAGCTTCCTGTCAGACTGTCACCATCCACCATGAGTTTTTG
shPLS3.1 antisense	AATTCAAAAACTCATGGTGGATGGTGACAGTCTGACAGGAAGCTGTCACCATCCACCATGAGG
hPLS3	
hPLS3-P1_fwd	TTAGTGAACCGTCAGATCCGCTAGCGCTACCGGTCGCCACCATGGATGAGATGGCTACCAC
hPLS3-P1_rev	CCTATCGCCGTCGAGCATCAGTTTCTGAATAATTTCTC
hPLS3-P2_fwd	ATTCAGAAACTGATGCTCGACGGCGATAGGAATAAAGATGGG
hPLS3-P2_rev	TGTAATCCAGAGGTTGATTGTCGACAGCGTAATCTGGAACATCGTATGGGTACACTCTCTTCATTCCCCTGC

Table 10: List of plasmid vectors used in this study

Plasmid vectors	Manufacturer
pCMV-VSVG (helper plasmids for virus production)	(Rehberg et al., 2008)
pCMVΔR8.91(helper plasmids for virus production)	(Rehberg et al., 2008)
pLV-mCherry-UBC>hPLS3 (ID: VB200130-1089naj)	Vectorbuilder
pLV-mCherry/Neo-EF1A>Stuffer300 (ID: VB181226-1081ctz)	Vectorbuilder
pscAAV-CMV>EGFP (ID: VB191101-2319suw)	Vectorbuilder
pscAAV-CMV>hPLS3/HA (ID: VB201021-1415qev)	Vectorbuilder
pSIH-H1 vector	System Bioscience

2.1.3. Antibodies

Table 11: List of primary antibodies used for immunohistochemistry

First antibodies (Immunohistochemistry)	Host	Dilution	Manufacturer and catalogue number
Ca2+ channel P/Q-type alpha-1A	rabbit	1:250	Synaptic systems, 152 203
Choline acetyltransferase (ChAT)	goat	1:500	Merck, AB144P
Green fluorescent protein (GFP)	chicken	1:2000	Abcam, ab13970
Human influenza hemagglutinin (HA)	rat	1:500	Roche, 11867423001
Neurofilament H (NF)	chicken	1:1000	Sigma Aldrich, AB5539
p-TrkB	rabbit	1:250	Cell signaling, 4621
Synaptophysin-1 (SYP)	guinea pig	1:500	Synaptic systems, 101 004
TrkB	goat	1:300	R&D systems, AF1494

Table 12: List of primary antibodies used for immunocytochemistry

First antibodies (Immunocytochemistry)	Host	Dilution	Manufacturer and catalogue number
Arp3	mouse	1:200	Sigma Aldrich, A5979
Ca^{2+} channel N-type alpha-1B ($Ca_v2.2$)	guinea pig	1:500	Synaptic systems, 152 305
DBP (GC)	rabbit	1:500	Thermo Fisher Scientific, PA5-19802
HA	rat	1:1000	Roche, 11867423001
mCherry (mCh)	rat	1:1000	Thermo Fisher Scientific, M11217
Myosin VI	mouse	1:250	GeneTex, GTX11095
p-Akt	rabbit	1:500	Cell signaling, 4060
Plastin 3 middle region	rabbit	1:100	Aviva systems biology, ARP56623
Profilin (a.a. 126-137)	rabbit	1:700	ECM biosciences, PP4801
p-Profilin (Tyr-129)	rabbit	1:400	ECM biosciences, PP4751
p-TrkB	rabbit	1:500	Cell signaling, 4621
Synaptophysin-1 (SYP)	guinea pig	1:1000	Synaptic systems, 101 004
TrkB	rabbit	1:1000 1:200 (live)	Merck, 07-225
	goat	1:500	R&D systems, AF1494
TrkC	rabbit	1:1000	Cell signaling, 3376

Table 13: List of primary antibodies used for Western Blots

First antibodies (Western Blots)	Host	Dilution	Manufacturer and catalogue number
Beta actin	mouse	1:3000	GeneTex, GTX26276
p-TrkB	rabbit	1:1000	Cell signaling, 4621
TrkB	rabbit	1:1000	Merck, 07-225

Table 14: List of secondary antibodies and labeling toxins

Secondary antibodies and labeling agents	Application	Dilution	Manufacturer and catalogue number
Alexa Fluor® 488			
Donkey anti-chicken	IHC (SC)	1:1000	JIR, 703-545-155
Donkey anti-guinea pig	ICC	1:500	JIR, 706-545-148
Donkey anti- rabbit	ICC	1:600	JIR, 711-545-152
	ICC (live)	1:300	
Cy™3			
Donkey anti-chicken	IHC (NMJ)	1:500	JIR, 703-165-155
Donkey anti-goat	IHC (NMJ)	1:500	JIR, 705-165-003
Donkey anti-guinea pig	ICC	1:500	JIR, 706-165-148
	IHC (NMJ)	1:1000	
Donkey anti-mouse	ICC	1:500	JIR, 715-165-151
Donkey anti-rabbit	ICC	1:500	JIR, 711-165-152
Donkey anti-rat	ICC	1:500	JIR, 712-165-150
	IHC (SC)	1:1000	
Cy™5			
Donkey anti-goat	IHC (NMJ)	1:500	JIR, 705-175-003
Donkey anti-guinea pig	ICC	1:500	JIR, 706-175-148
	IHC (NMJ)	1:500	
Goat anti-mouse	ICC	1:500	JIR, 115-175-146
Alexa Fluor® 647			
Donkey anti-goat	IHC (SC)	1:1000	JIR, 705-605-003
Donkey anti-rabbit	ICC	1:800	Thermo Fisher Scientific, A-31573
	ICC (live)	1:400	
	IHC (NMJ)	1:600	
Horseradish peroxidase (HRP)			
Goat anti-mouse	WB	1:10000	JIR, 115-035-003
Goat anti-rabbit	WB	1:10000	JIR, 111-035-144
Alexa Fluor™ 488 α-Bungarotoxin (BTX)	IHC (NMJ)	1:500	Invitrogen (Thermo), B13422
ActinGreen™ 488 / ActinRed™ 555 ReadyProbe™	ICC	1:50	Thermo Fisher Scientific, R37110 / R37112
Alexa Fluor™ 546 Phalloidin	ICC	1:50	Invitrogen (Thermo), A22283

2.1.4. Consumables

Table 15: List of essential consumables used in this study

Consumables	Manufacturer
Cellstar 4-Wells	Greiner BioOne
Glass coverslips (Ø 10 mm)	Hartenstein
LightCycler 8-Tubes Stripes (white)	Roche
Nunc™ cell Culture Well Plates (24 Well)	Thermo Fisher Scientific
Parafilm	Bemis
Polyvinylidene fluoride (PVDF) membrane	Bio-Rad
X-ray films (Fujifilm Super RX)	Hartenstein
µ-dish35mm, high glass bottom	Ibidi

Table 16: List of kits used in this study

Kits	Manufacturer
NEBuilder® HiFi DNA Assembly Cloning Kit	New England Biolabs
NucleoBond® Xtra Mini/Midi/Maxi plasmid purification kit	Machery Nagel
NucleoSpin® Gel and PCR Clean-up kit	Machery Nagel
NucleoSpin® RNA Kit	Machery Nagel
RevertAid™ First Strand cDNA Synthesis Kit	Thermo Fisher Scientific

2.1.5. Instruments and software

Table 17: List of essential instruments and used in this study

Instruments	Manufacturer
Curix 60 developer	AGFA
LightCycler® 96	Roche
Nanodrop 1000 Spectrophotometer	Peqlab Biotech. GmbH
Nikon's Eclipse TE2000 inverted epifluorescence microscope	Nikon
Olympus Fluoview 1000 confocal system	Olympus
PCR Cycler Mastercycler Nexus X2 flexlid	Eppendorf AG
Zeiss ELYRA S.1 system	Carl Zeiss AG

Table 18: List of software and used in this study

Software	Manufacturer
Adobe Illustrator CS6	Adobe
Endnote X9	Endnote
FIJI	Wayne Rasband (NIH)
Graphpad Prism 6	GraphPad Software, Inc.
LightCycler®96 Application Software	Roche
MS Office	Microsoft
NIS-Elements AR 4.40.00 software	Nikon
Olympus Fluoview 1000	Olympus
Zeiss software	Carl Zeiss AG

2.2. Methods

2.2.1. Animals and AAV9 injections

2.2.1.1. Experimental animals

For all experimental setups, laboratory mice were bred in the animal facility of the Institute for Clinical Neurobiology, University Hospital of Würzburg. For AAV9-injections, mice were housed in the animal facility of the Faculty of Medicine, Leipzig University. The mice were maintained in a temperature and humidity-controlled room with a 12-hour light/dark cycle in groups of two-to-four animals with access to food and water *ad libitum*. All procedures and experiments were performed by trained personal in accordance with the regulations on animal protection of the German federal law as well as the Association for Assessment and Accreditation of Laboratory Animal Care and of the University of Würzburg / Leipzig University, approved by the local veterinary authority and Committee on the Ethics of Animal Experiments.

In this study diverse laboratory mouse lines were used. Wild type CD-1 or FVB/N mice were purchased from Charles River, Sulzfeld, Germany. For embryonic cell culture experiments SMA type I *Smn$^{-/-}$;SMN2* mice (Monani et al., 2000) were bred from *Smn$^{+/-}$;SMN2* mice initially obtained from Jackson Laboratory, Bar Harbor, USA. SMA type II *Smn$^{-/-}$;SMN2;SMNΔ7* mice (Le et al., 2005) used for postnatal experiments (hereafter named *SMNΔ7*) were bred from *Smn$^{+/-}$;SMN2;SMNΔ7* mice initial purchased from Jackson Laboratory, Bar Harbor, USA. As corresponding controls *Smn$^{+/+}$;SMN2 / Smn$^{+/-}$;SMN2* and *Smn$^{+/+}$;SMN2;SMNΔ7* and TrkB-deficient *Ntrk2$^{-/-}$* mice (Rohrer et al., 1999) were used.

2.2.1.2. AAV9-treatment in neonatal mice

These experiments were performed by Florian Gerstner and Dr. Christian Simon at the Carl-Ludwig-Institute for Physiology, Leipzig University. For hPLS3 overexpression in neonatal mice, pubs were anesthetized by isoflurane inhalation at P1/P2 and injected in the right lateral ventricle of the brain with ~5 x 10^{10} genome copies of AAV9 vectors in a PBS solution containing a vital dye (Fast Green) as previously described (Simon et al., 2017). The open reading frame (ORF) of human PLS3 (hPLS3) was HA-tagged and inserted into a scAAV9 under a Cytomegalovirus (CMV) promotor (Vector ID: VB201021-1415qev). An enhanced green fluorescent protein (EGFP)-containing scAAV9 (Vector ID: VB191101-2319suw) was used as control.

Furthermore, spinal cord immunohistochemistry was performed by Florian Gerstner and Dr. Christian Simon to check AAV9 expression in lumbar spinal motoneurons. Therefore, mice were perfused and the spinal cord was dissected and embedded in 5 % agar. Serial transverse 75 μm sections were cut and a standard immunofluorescence protocol was performed using primary antibody incubation over night at room temperature (RT). Details for this procedure can be found in (Buettner et al., 2021).

2.2.2. Tissue preparation and immunohistochemistry

2.2.2.1 Muscle preparation

Mice (P5-P10) were sacrificed by decapitation, opened along the midline and the abdominal wall was dissected. For further dissections, the tissue was pinned and spread out onto a well coated with silicone

rubber and the pre-warmed physiological solution containing $CaCl_2$. Afterwards, the superjacent muscles were removed to uncover the *Transversus abdominis anterior* (*TVA*) and the *obliquus internus abdominis* (*OIA*) muscle. Upon removal of the connective tissue with forceps, the preparations were maintained in fresh physiological solution containing $CaCl_2$ for 30 minutes (min.) at RT on a shaker, before it was replaced by physiological solution without $CaCl_2$ and incubated for 10 min. For BDNF-stimulation, 500 ng/ml BDNF was added to the physiological solution containing $CaCl_2$ for 30 min. Afterwards, the muscles were fixed with cold methanol-free 4 % formaldehyde for 90 min. at 4°C. Following three washing steps with PBS, the encompassing tissue was cut off and the *TVA*/*OIA* was placed into a 24-well plate for immunohistochemical staining.

2.2.2.2 Immunohistochemistry of whole mount muscle tissue

For immunofluorescence investigation of neuromuscular junctions a protocol adapted from Tejero et al., 2016 was used. The following steps were performed on an orbital shaker at RT and TBS-T was used as buffer, if not stated otherwise. Whole mount muscle preparations were first incubated with 0.1M glycine (in PBS) for 30 min., followed by permeabilization steps with 1 % Triton X-100 for 2x 5 min., 2x 10 min. and 2x 30 min. Blocking of unspecific binding sites was realized with 10 % BSA for three hours, before the first antibodies diluted in 2.5 % BSA and 1 % Triton X-100 were added and incubated at 4°C, shaking for three days. Subsequently, the tissue was washed with TBS-T three times for 15 min. and 2.5 % BSA containing secondary antibodies together with Alexa Fluor 488-conjugated Bungarotoxin was added for one hour. After washing with TBS-T for 1x 30 min. and 6x 10 min., the muscles were mounted on microscope slides using Aqua-Poly/Mount. For analysis, only superficial neuromuscular junctions were imaged.

2.2.3. Motoneuron cell culture and BDNF stimulation

2.2.3.1. Primary embryonic motoneuron cell culture

Isolation and cultivation of primary murine motoneurons was performed as described previously (Wiese et al., 2010). All procedures were realized under sterile conditions. In preparation for motoneuron cultures, glass coverslips placed into 4-well dishes for single cell immunofluorescence experiments or 24-well plates for dense motoneuron cultures were incubated over night at 4°C with 0.5 mg/ml poly-D/L-ornithine hydrobromide (PORN). PORN was washed off on the next day three times with HBSS and coverslips/plates were incubated with 2.5 µg/ml laminin-111 or laminin-221/211 for at least one hour. Furthermore, 24-well plates coated with p75^{NTR} antibody at a final concentration of 0.1 µg/ml diluted in Tris buffer were prepared for enrichment of p75^{NTR}-expressing cells and stored for short time periods at 4°C. Prior to the cultures, these p75^{NTR}-panning plates were washed three times with NB medium and covered with 900 µl NB medium.

For embryonic spinal cord dissection, pregnant mice were sacrificed by cervical dislocation and the embryos were detached from the uterus. With the help of forceps, the head and tail were cut-off and skin was opened to lift-up the spinal cord. After opening the spinal cord along the central channel and removal of the meninges including the dorsal root ganglia the lumbar part of the spinal cord was placed into a 1.5 ml tube filled with 90 µl HBSS. The following steps were performed under sterile conditions

with pre-warmed media. For digestion of the tissue, 10 µl 1 % Trypsin was added, and spinal cords were incubated at 37°C for 15 min. Afterwards trypsin was neutralized by 10 µl 1 % Trypsin inhibitor and tissue was dissolved by mechanical trituration. The suspension containing single cells was added to the washed $p75^{NTR}$-panning plate and incubated vibration-free for 45 - 60 min. at RT. For removal of unattached cells not expressing the $p75^{NTR}$ the wells were washed with NB medium three times. The remaining cells, which are mainly motoneurons that highly express the $p75^{NTR}$ at this age (Wiese et al., 1999), were separated from the coated wells by adding 250 µl depolarization medium. Upon addition of 750 µl complete medium, the cell suspension was pipette up-and-down, collected into a 15 ml tube and centrifuged at 400 g for 5 min. Following aspiration of the supernatant, the cells were re-suspended in 500 µl complete medium and directly plated onto laminin-coated 24-well plate for dense cultures. For single cell cultures, the amount of cells in the suspension was determined in a Neubauer chamber and only ~7.000 cells diluted in complete medium were plated onto a laminin-coated 10 mm^2 glass coverslip. For live cell imaging ~10.000 motoneurons were plated onto PORN/laminin-221/211 coated 35 mm high µ-dishes. The cells were allowed to settle down before the wells were filled up with complete medium supplied with 5 ng/ml CNTF and 2 ng/ml BDNF. Motoneurons were cultured for five (DIV5) to seven (DIV7) days at 37°C in a 5 % CO_2 supplying incubator. The medium was first exchanged at DIV1 and then every two to three days. For viral transduction, an appropriate number of cells was diluted in 50 µl complete medium and 5 - 10 µl of the virus suspension was added and incubated for 15 min. After that, the cells were plated onto 24-wells or glass coverslips as previously described.

2.2.3.2. BDNF pulse experiment

For BDNF pulse experiments, motoneurons were maintained with complete medium supplied with 5 ng/ml CNTF and 2 ng/ml BDNF. One day prior to the experiments, cells were deprived for BDNF for 16 - 24 hours. Therefore, cells were washed three times with pre-warmed NB medium and then complete medium only containing 5 ng/ml CNTF was added. On the next day, pulse experiments were performed by incubating the motoneurons with complete medium supplied with 100 ng/ml BDNF for 5 - 15 min. at 37°C. Finally, the cells were washed with NB medium and fixed with methanol-free 4 % formaldehyde for 5 - 10 min.

2.2.4. Immunocytochemistry of motoneurons

2.2.4.1. Live-cell immunocytochemistry for TrkB surface presentation

Live-cell staining technique was used to exclusively visualize TrkB receptors that are presented at the cell surface. Therefore, motoneurons were cultured on laminin-coated glass until DIV5/DIV7. For BDNF stimulation experiments, motoneurons were deprived for BDNF overnight prior to the day of experiments. In general, on DIV5/DIV7 the glass coverslips were placed on parafilm and covered with pre-warmed complete medium. Afterwards, the motoneurons were washed with cold complete medium and pre-incubated on ice for 2 min. to inhibit activity of the cells. The primary antibody was diluted in cold complete medium and incubated for 45 min. on ice. Following three washing steps with cold PBS, the secondary antibody diluted in cold complete medium was incubated for 30 min. on ice. After three washing steps with PBS at RT, cells were fixed with methanol-free 4 % formaldehyde for six min. and

washed again with PBS. After live-cell staining for TrkB, standard immunofluorescence method was performed to visualize intracellular proteins. Live-cell immunocytochemistry was conducted under various conditions. According to the experimental setup, motoneurons were pre-treated with the following toxins at 37°C: Cytochalasin D (Cyto D, 0.5 µM for 30 min.), Nocodazole (10 µM for two hours), Cycloheximide (CHX, 20 µM for one hour) or CK-666 (50 µM, 30 min. pre-incubated and during the BDNF stimulation and recovery). For *TrkB endocytosis assay*, motoneurons were exposed to BDNF to stimulate TrkB internalization. Therefore, motoneurons were stimulated with 100 ng/ml BDNF diluted in complete medium for defined time periods at 37°C. Afterwards they were washed with cold complete medium and directly placed on ice for staining. For *TrkB recruitment assay*, motoneurons were stimulated with 100 µM 8-(4-chlorophenylthio)–3′,5′ cAMP (8-CPT-cAMP) diluted in complete medium for 20 min. at 37°C. Directly after washing with cold complete medium, motoneurons were placed on ice to proceed with the staining. For *TrkB recovery assay*, motoneurons were stimulated with 100 ng/ml BDNF for 5 min. at 37°C before the medium was washed out the cells were covered with pre-warmed medium for 10 min. After recovery, motoneurons were placed on ice for staining. As additional control, a BDNF-stimulated condition without recovery was used. For all setups, an untreated control condition was implemented.

2.2.4.2. TrkB recycling assay

For TrkB recycling assay, double live-cell labeling experiments were performed on DIV5/DIV7 motoneurons. Therefore, the cells were placed on parafilm and immediately covered with cold complete medium before they were placed on ice. The 1st antibody (TrkB rb, 1:200) diluted in cold complete medium was incubated for 30 min., followed by three washing steps with cold PBS and incubation with the secondary antibody for 25 min. (donkey anti-rabbit Alexa Fluor® 488 AffiniPure, 1:300) diluted in cold complete medium. Afterwards, cells were washed with complete medium, removed from ice and stimulated with 100 ng/ml BDNF for 5 min. as previously described. Subsequently, remaining antibodies were washed-off twice with 1 mM EDTA in complete medium and cells were covered for 10 min. with warm complete medium. Next, motoneurons were placed back on ice and incubated again with a 1st antibody (TrkB, 1:200) diluted in cold complete medium for 30 min., washed trice with cold PBS and then incubated with the secondary antibody for 25 min. (donkey anti-rabbit Alexa Fluor® 647, 1:400) diluted in cold complete medium. Following three washing steps with cold PBS, cells were fixed with methanol-free 4 % formaldehyde for six min. and standard immunofluorescence protocol omitting permeabilization was used to visualize intracellular proteins. For analysis, the total number of individual TrkB-A488 and TrkB-A647 immunosignals were counted after linear brightness and contrast adjustments. According to the experimental setup, TrkB-A488 are endocytosed receptors that that have been at the cell surface prior to BDNF stimulation, and TrkB-A647 are recovered receptors at the cell surface after BDNF stimulation. Co-localization analysis was performed with the help of JaCoP Plugin, using "Objects based methods" and "Geometrical centre" (Bolte and Cordelieres, 2006). The quantity of recovered receptor (TrkB-A647 as percentage of TrkB-A488) and the quantity of recycled TrkB that have previously been at the cell surface (co-localizing receptors as percentage of TrkB-A647) was determined and illustrated as bar graphs.

2.2.4.3. Immunocytochemistry of fixed motoneurons

Immunofluorescence examination of cultured embryonic motoneurons was performed as previously described (Dombert et al., 2017). Depending on the experimental design, motoneurons were grown on laminin-coated glass coverslips for 5 - 7 days. Cells were washed with pre-warmed NB medium to remove serum components of the medium and fixed for 5 - 10 min. with methanol-free 4 % formaldehyde. Upon fixation, coverslips were washed three times with PBS. Afterwards, glass coverslips were placed on parafilm in a light-protected chamber and TBS-T was used as buffer. Except for TrkB stainings, motoneurons were treated with 0.3 % Triton X-100 for 20 min. to permeabilize the cell membrane. Upon three washing steps with TBS-T, unspecific binding sites were blocked using 10 % BSA for one hour. For labeling G-actin using Vitamin D-binding protein (DBP) (Lee et al., 2013), motoneurons were treated with ice-cold acetone for 5 min. before they were exposed to 5 µg/ml DBP for one hour at RT. After three washed with TBS-T, blocking with 10 % BSA was performed for one hour. Primary antibodies, diluted in 1 % BSA were incubated over night at 4°C. On the next day, coverslips were washed thrice with TBS-T and incubated for one hour with secondary antibodies diluted in 1 % BSA at RT. Finally, the coverslips were washed again three times with TBS-T and mounted on microscope slides using Aqua-Poly/Mount.

2.2.5. Imaging

2.2.5.1. Confocal imaging

For image acquisition an Olympus Fluoview 1000 confocal system equipped with a UPLSAPO 60x/ 1.35 NA oil objective was used. For NMJs, 0.5 µm z-stack images (16-bit, 1024x1024 pixel), and for motoneurons single stack images (16-bit, 512x512 pixel) were acquired. For every set of experiments, identical imaging settings (laser intensities, digital zoom, HV and background adjustments, pinhole) were applied. Unprocessed images were analyzed with Fiji. For z-stack images, the "Sum slices" projection was used. The ROIs were identified using the free-hand tool and the mean gray value of the immunosignal was quantified. For ratiometric images the "image calculator" function of Fiji and the pseudocolor "Rainbow RGB" was used. Outline of NMJs was done using the "Dotted Line" Plugin. Background mean gray intensity was subtracted and all values originated from one experiment were divided by the mean of the untreated control group for normalization. For F/G-actin ratio the mean gray values (background subtracted) of F-actin (Phalloidin) were divided by the mean gray value of G-actin (DBP) and normalized within individual experiments as described before. Statistical analysis and graph illustration were performed with GraphPad Prism 6.

2.2.5.2 Structured illumination microscopy (SIM)

SIM was performed on a Zeiss ELYRA S.1 or with the help of Dr. Teresa Klein and Prof. Markus Sauer on a Zeiss ELYRA 7 system, both equipped with a plan APO 63×/1.4 NA oil objective to obtain high resolution images. Fiji was used to generate Maximum intensity projections and Brightness/Contrast were adjusted for better visibility. For improved depiction of high density cluster-like $Ca_v2.2$ structures the pseudocolor "Cyan Hot" was used.

<u>2.2.6. Genotyping</u>

2.2.6.1. DNA extraction

To isolate genomic DNA from mouse tissues, e.g. tails from embryos for genotyping, the tissue samples were collected in 200 µl "Quick and Dirty" lysis buffer and digested by 20 µl proteinase K (100 µg/ml) that was incubated at 56°C, shaking at 850 rpm until the tissue is dissolved (for at least 12 min.). Upon digestion of the tissue, the samples were heated to 99°C for 8 min. under permanent shaking to inactivate proteinase K. To obtain proper amounts for analysis, the DNA was diluted in a 1:10 ration in distilled water and stored at 4°C.

2.2.6.2. Polymerase chain reaction for genotyping

For genotyping of transgenic mice, polymerase chain reaction (PCR) was performed with DNA extracts obtained from the tail biopsies. Isolated DNA, specific primers, 10x key buffer, betaine for further optimization, dNTPs and the Taq polymerase were prepared and subjected to 20 - 40 thermal cycles. To determine the genotypes of the different transgenic mice used in this study, primers specifically designed for the desired DNA target were used. Presence of *Smn* after breading *Smn$^{+/-}$;SMN2* or *Smn$^{+/-}$;SMN2;SMNΔ7* mice was tested by a tandem PCR using three primers to identify wild type, heterozygous or homozygous knockout. The presence of corresponding transgenes was tested regularly. Primers can be found in **Table 7**. The respective PCR protocols can be found in **Table 19**.

2.2.6.3. Gel electrophoresis

Separation of amplified PCR products according to their size was performed by gel electrophoresis that is based on an electrical field forcing negatively charged DNA fragments to migrate through an agarose gel. Therefore, 2 % agarose gels were prepared in 1x TAE buffer containing 5 µl HDGreen® Plus Safe DNA Dye per 100 ml agarose solution. PCR products were mixed with 10 µl 6x loading dye and loaded onto the agarose gel and ran in 1x TAE buffer at 120 V for 30 min. The HDGreen® Plus present in the agarose gel intercalates with the DNA fragments, making it visible under ultraviolet (UV) trans-illumination for analysis. For comparison, a 100 bp DNA ladder was used as size standard.

<u>2.2.7. RNA isolation, cDNA synthesis and reverse transcriptase PCR</u>

2.2.7.1. Isolation of RNA and cDNA synthesis

For examination of RNA expression in motoneurons, dense cultures plated on laminin-coated 24-wells were used. On DIV7, motoneurons were washed with HBSS and lysed in 350 µl RNA lysis buffer (RA1) comprising 3,5 µl β-Mercaptoethanol. Extraction of RNA was performed with the help of NucleoSpin® RNA Kit according to the manufacturer's protocol. RNA was eluted in 40 µl RNAse-free water and the amount of RNA quantified in Nanodrop™ 1000 spectrophotometer. The extracted RNA served as template for synthesizing cDNA using the RevertAid™ First Strand cDNA Synthesis Kit. Therefore, 0.5 – 1 µg total RNA was used for the reverse transcriptase reaction and subjected to amplification in the thermocycler as instructed by the manufacturer.

Table 19: Composition and thermocycling protocols for genotyping PCRs

Component	Concentration (Stock)	Concentration (Final)	Volume (µl)	Cycle conditions
Smn WT/KO PCR				
DNA	x	20-100 ng	1	Initial:
Key buffer	10x	1x	2.5	3 min.; 94°C
Betaine	5 M	1 M	5	30 cycles:
dNTPs	10 mM	0.2 mM	0.5	30 sec.; 94°C
Primer 1 (**Smn 201f**)	100 µM	0.3 µM	0.075	30 sec.; 56°C
Primer 2 (**Smn 1049r**)	100 µM	0.3 µM	0.075	60 sec.; 72°C
Primer 3 (**Smn KO**)	100 µM	0.3 µM	0.075	Final:
Taq polymerase	5 U/µl	0.03 U/µl	0.15	5 min.; 72°C
H_2O			15.625	Hold:
				∞; 4°C
Total volume			25 µl	
SMN2tg PCR				
DNA	x	20-100 ng	1	Initial:
Key buffer	10x	1x	2.5	3 min.; 94°C
Betaine	5 M	1 M	5	30 cycles:
dNTPs	10 mM	0.2 mM	0.5	30 sec.; 94°C
Primer 1 (**Tw3**)	100 µM	0.3 µM	0.075	30 sec.; 56°C
Primer 2 (**Tw7**)	100 µM	0.3 µM	0.075	30 sec.; 72°C
Taq polymerase	5 U/µl	0.03 U/µl	0.15	Final:
H_2O			15.7	5 min.; 72°C
				Hold:
Total volume			25 µl	∞; 4°C
SMNΔ7 PCR				
DNA	x	20-100 ng	1	Initial:
Key buffer	10x	1x	2.5	3 min.; 94°C
Betaine	5 M	1 M	5	28 cycles:
dNTPs	10 mM	0.2 mM	0.5	30 sec.; 94°C
Primer 1 (**oMIR3679**)	100 µM	0.3 µM	0.075	30 sec.; 54°C
Primer 2 (**oMIR3680**)	100 µM	0.3 µM	0.075	80 sec.; 72°C
Taq polymerase	5 U/µl	0.03 U/µl	0.15	Final:
H_2O			15.7	5 min.; 72°C
				Hold:
Total volume			25 µl	∞; 4°C
TrkB WT/KO PCR				
DNA	x	20-100 ng	1	Initial:
Key buffer	10x	1x	2.5	3 min.; 94°C
Betaine	5 M	1 M	5	30 cycles:
dNTPs	10 mM	0.2 mM	0.5	30 sec.; 94°C
Primer 1 (**TrkB-c8**)	100 µM	0.3 µM	0.075	30 sec.; 59°C
Primer 2 (**TrkB-n2**)	100 µM	0.3 µM	0.075	30 sec.; 68°C
Primer 3 (**pgk3-1**)	100 µM	0.3 µM	0.075	Final:
Taq polymerase	5 U/µl	0.03 U/µl	0.15	5 min.; 68°C
H_2O			15.625	Hold:
				∞; 4°C
Total volume			25 µl	

2.2.7.2. Reverse transcriptase PCR (RT-PCR)

To determine the amount of specific mRNAs in embryonic motoneuron cultures, RT-PCR was performed using LightCycler® 96. RT-PCR is a method based on standard PCR combined with DNA-intercalating dyes that emit a fluorescent signal which increases proportionally to the amplified DNA fragments and hence allow to visualize DNA concentrations in real time. Therefore, the synthesized cDNA was diluted in a 1:5 ratio. Specifically designed primers and the diluted cDNA were mixed with Luminaris HiGreen® qPCR Master Mix according to the following protocol:

Table 20: Composition of RT-PCR reactions

Component	Concentration (Stock)	Concentration (Final)	Volume (µl)
cDNA (1:5)	x	<1,000 ng	2
Luminaris Mastermix	2x	1x	10
Primer 1 (forward)	10 µM	0.5 µM	1
Primer 2 (reverse)	10 µM	0.5 µM	1
H$_2$O			6
Total volume			20 µl

As reference, the expression of *Glyceraldehyde-3-phosphate dehydrogenase* (*Gapdh)* was used. Primer specificity was determined by melting curve analysis and control samples that were treated without reverse transcriptase. The reaction mixtures were applied to the following program in the LightCycler® 96 instrument. Analysis was performed using the cycle quantification values (C_q) indicated by the LightCycler®96 Application Software. Relative changes in mRNA expression were calculated using the $2^{-\Delta\Delta CT}$ method previously described in (Livak and Schmittgen, 2001).

Table 21: Thermocycling conditions for RT-PCRs

Step	Temperature	Duration
UDG pre-treatment	50 °C	2 min.
Initial denaturation	95 °C	10 min.
40 cycles:		
Denaturation	95 °C	15 sec.
Annealing	60 °C	30 sec.
Extension	72 °C	30 sec.
Melting	95 °C	10 sec.
	65 °C	1 min.
	97 °C	1 sec.

2.2.8. Western Blot analysis

For determination of protein expression in motoneurons, dense cultures plated on laminin-coated 24-wells were used. For BDNF stimulation experiments, motoneurons were deprived on DIV6 and stimulated with 100 ng/ml BDNF in DIV7 for 15 min. On DIV7, motoneurons were washed with HBSS and lysed in 20 µl 2x Laemmli buffer. Samples were heated to 99°C for 5 min. and loaded onto a 4 – 12 % gradient SDS-polyacrylamide gel. Separation of the proteins by size was obtained by gel-electrophoresis in 1x running buffer at 8 mA for 30 min. followed by 25 mA for 120 min. The proteins were transferred onto a polyvinylidene fluoride (PVDF) membrane that was previously activated in

methanol. Therefore, the gel and the PVDF membrane embedded in blotting paper and sponges were placed in the blotting apparatus filled with 1x transfer buffer and ran at 150V for one hour at 4°C. Afterwards, the membrane was blocked with 5 % milk in TBS-T for one hour and probed with the primary antibodies in TBS-T over night at 4°C. Following three washing steps with TBS-T for 15 min., secondary HRP-conjugated antibodies diluted in TBS-T were incubated for one hour. Again, the membrane was washed three times with TBS-T for 15 min. before immunodetection was performed using Amersham ECL™ Western Blotting Detection Reagent according to the manufacturers protocol. Development of the X-ray films was done in Curix 60 developer after various exposure times.

2.2.9. Cloning and lentivirus production

2.2.9.1. Cloning of shRNA-containing knockdown construct targeting endogenous Pls3

To study the effects of Pls3 downregulation in wild type motoneurons we constructed short hairpin RNA (shRNA) against the murine *Pls3* which was introduced into a pSIH-H1 vector. This vector system is suitable for lentivirus (LV) production that contains a CMV promotor that drives the expression of a GFP while the H1 expression cassette drives the expression of the respective shRNA. 1 µg of the pSIH-H1 vector was digested using the enzymes ECOR1 and BamH1 and 10x Tango Yellow Buffer. The following reaction mixture was incubated at 37°C for 60 min. before it was submitted to gel electrophoresis at 120 V for 30 min. on a 2 % agarose gel. As negative control the undigested vector was used.

Table 22: Composition of the reaction for vector digestion

Component	Concentration (Stock)	Concentration (Final)	Volume (µl)
pSIH	1 µg/µl	0.02 µg/µl	1
Tango Yellow buffer	10x	1x	10
EcoR1	10 U/µl	0.4 U/µl	2
BamH1	10 U/µl	0.6 U/µl	3
H_2O			34
Total volume			50 µl

The vector was purified from the gel with the help of the NucleoSpin® Gel and PCR Clean-up kit following the manufacturer's instructions and concentration was determined with the Nanodrop 1000 spectrophotometer. Meanwhile, the sense and antisense oligonucleotides (**Table 9**) were annealed using the same buffer system as used for vector digestion. Therefore, the reaction mixture was first incubated at 95°C for 5 min. and then for 60 min. at 37°C.

Table 23: Composition of the reaction for oligonucleotide annealing

Component	Concentration (Stock)	Concentration (Final)	Volume (µl)
Tango Yellow buffer	10x	1x	5
shPl3.1 sense	10 µM	0.2 µM	1
shPL3.1 antisense	10 µM	0.2 µM	1
H_2O			43
Total volume			50 µl

Following a cooling period on ice and 1:10 dilution with water, the annealed oligonucleotides were ligated into the linearized pSIH-H1 vector for 60 min. at RT according to the following protocol. As negative control reaction mixtures without the oligonucleotides was used.

Table 24: Composition of the reaction for vector – oligonucleotide ligation

Component	Concentration (Stock)	Concentration (Final)	Volume (µl)
Digested pSIH (50 ng)	X	2.5 ng/µl	0.5
T4 ligase buffer	10x	1x	2
Annealed oligonucleotides	10 µM	0.5 µM	1
T4 ligase	5 U/µl	0.5 U/µl	2
H_2O			14.5
Total volume			20 µl

For transformation via heat shock competent TOP10 *Escherichia coli* (E.coli) cells were thaw on ice. 10 µl of the ligation reactions was added to competent TOP10 E.coli and incubated on ice for 30 min. before cells were placed in the 42°C water bath for 30 - 50 seconds (sec.) Afterwards, cells were immediately incubated on ice for 10 min. Upon addition of 250 µl pre-warmed LB medium cells were put in the thermocycler at 750 rpm and 37°C for 60 min. The transformation mixture was plated onto an agar plate containing 1 mg/ml ampicillin and incubated over night at 37°C. On the next day, single colonies were picked and checked via colony PCR using the standard PCR protocol. Therefore, the picked colonies were plates on another agar plate and the remaining colony was added into a tube containing 10 µl distilled water and incubated on the thermomixer for 10 min. at 99 °C and 800 rpm.

Table 25: Composition and thermocycling conditions for colony PCRs

Component	Concentration (Stock)	Concentration (Final)	Volume (µl)	Cycle conditions
Colony DNA	x	x	3	Initial:
Key buffer	10x	1x	2.5	30 sec.; 95°C
dNTPs	10 mM	0.2 mM	0.4	25 cycles:
Primer a	10 µM	0.16 µM	0.4	30 sec.; 94°C
Primer b	10 µM	0.16 µM	0.4	30 sec.; 60°C
Taq polymerase	5 U/µl	0.06 U/µl	0.3	60 sec.; 72°C
H_2O			18	Hold:
Total volume			25 µl	∞; 4°C

Using 2 % agarose gels the PCR products were separated by gel electrophoresis at 120V for 30 min. Colonies that contained the insert were picked again and transferred into 5 ml LB Medium containing 100 µg/ml ampicillin and incubated overnight, shaking at 37°C. Plasmid preparation was performed with the help of NucleoSpin® Plasmid Mini kit according to the manufacturer's protocol. Plasmid sequencing was performed by LGC Genomics GmbH to check for the right insertion of the shRNA into the vector. To obtain a high quantity of plasmid for lentivirus production, plasmid preparation was performed using the NucleoBond® Xtra Midi plasmid purification kit.

2.2.9.2. Cloning of hPLS3-overexpression construct

To investigate beneficial effects of PLS3 upregulation in Smn-deficient motoneurons we used the lentiviral system to overexpress the human PLS3 (hPLS3). For that, the plasmids were obtained from VectorBuilder (www.vectorbuilder.com). The hPLS3 [NM_001136025.4] ORF under the ubiquitin promotor was inserted into a mammalian gene expression lentiviral vector that additionally contains a mCherry (mCh) fluorescent protein under the CMV promotor (Vector ID: VB200130-1089naj). As corresponding control we used a similar vector harboring mCh/Neomycin under CMV promotor (Vector ID: VB181226-1081ctz). Virus packaging was performed in the Institute of Clinical Neurobiology as explained later.

2.2.9.3. Cloning of a HA-tagged, shRNA-resistant hPLS3-overexpression construct into the shPLS3 knockdown plasmid

To obtain a rescue construct harboring the shRNA against murine PLS3 and simultaneously overexpressing hPLS3-HA, the hPLS3 ORF needed to be modified. Therefore, specific primers introducing base pairs changes that result in silent mutations were designed (**Table 9**). The shRNA-resistant hPLS3 ORF was amplified by PCR from 10 ng/µl overexpression vector purchased from VectorBuilder (Vector ID: VB200130-1089naj) according to the following protocol. Here, the first primer pair was used to introduce the silent mutations leading to shRNA resistance, while the second primer pair was used to amplify the remaining part of the ORF and the HA-tag.

Table 26: Composition and thermocycling conditions for cloning PCRs

Component	Concentration (Stock)	Concentration (Final)	Volume (µl)	Cycle conditions
Template DNA	1-10 ng	0.04 – 0.4 ng	1	Initial:
KAPA HiFi HotStart ReadyMix	2x	1x	12.5	3 min.; 95°C
				5 cycles:
1) PLS3-P1_fwd	10 µM	0.3 µM	0.75	20 sec.; 98°C
PLS3-P1_rev	10 µM	0.3 µM	0.75	15 sec.; 60°C
or:				2 min.; 72°C
2) PLS3-P2_fwd	10 µM	0.3 µM	0.75	25 cycles:
PLS3-P2_rev	10 µM	0.3 µM	0.75	20 sec.; 98°C
H$_2$O			10	15 sec.; 65°C
				2 min.; 72°C
Total volume			25 µl	Final:
				2 min.; 72°C
				Hold:
				∞; 4°C

PCR products were loaded on a 2 % agarose gel and the expected 239 base pairs and 1774 base pairs fragments were purified after gel electrophoreses at 120 V for 30 min. with the NucleoSpin® Gel and PCR Clean-up kit. The shPLS3 containing pSIH vector was linearized using the steps described for the empty pSIH vector using the restriction enzymes NheI/SalI and FastDigest Green Puffer (10x).

Table 27: Composition of the reaction for vector digestion

Component	Concentration (Stock)	Concentration (Final)	Volume (µl)
pSIH-shPLS3.1	1 µg/ml	0.04 µg/ml	2
FastDigest Green buffer	10x	1x	5
Nhe1 HF	10 U/µl	1 U/µl	5
Sal1 HF	10 U/µl	1 U/µl	5
H_2O			33
Total volume			50 µl

After digestion, it was loaded on a 2 % agarose gel, separated via gel electrophoresis (120 V, 30 min.) and purified with the help of the Macherey-Nagel NucleoSpin® Gel and PCR Clean-up. The purified fragments were assembled into the opened sh*Pls3*-pSIH vector with the NEBuilder® HiFi DNA Assembly Cloning Kit according to the manufactures protocol (2-3 fragment assembly; 1:2 vector:insert).

Table 28: Calculation of the volume for fragment assembly

Amplified fragment	Lenght (bp)	PCR Product (ng/µl)	Mass (pmol)	Mass (ng)	Calculated volume (µl)
hPLS3 P1	239	119.05	0.2	29.54	0.25
hPLS2 P2	1774	237.11	0.2	219.3	0.92
Digested pSIH-shPLS3.1	6671	63.14	0.1	412.2	6.53

Table 29: Composition of the reaction for vector – PCR product assembly

Component	Concentration (Stock)	Concentration (Final)	Volume (µl)
hPLS3-P1	119.05 ng/µl	0.2 pmol	0.25
hPLS3-P2	237.11 ng/µl	0.2 pmol	0.92
Digested pSIH-shPLS3.1	63.14 ng/µl	0.1 pmol	6.53
NEBuilder HiFi DNA Assembly Master Mix	2x	1x	10
H_2O			2.3
Total volume			20 µl

Afterwards, 10 µl of the ligated construct was transformed into chemically competent TOP10 E. coli cells via heat shock as previously described. Colonies harboring the constructs were cultured overnight shaking at 37°C before they were harvested for plasmid preparation using NucleoSpin® Plasmid Mini kit. After sequencing, overnight cultures with positive colonies in 200ml LB medium and 100 µg/ml ampicillin were used for plasmid preparation with the NucleoBond® Xtra Midi plasmid purification kit.

2.2.9.4. Lentivirus production

Packaging of lentiviral particles was done by my colleague Hildegard Troll using human embryonic kidney 293TN cells (HEK293TN) cells and the two helper plasmid system reported previously (Rehberg et al., 2008). Transfection of the corresponding plasmids, together with the packaging vector

pCMVΔ8.91 and the pseudo typing vector pCMV-VSVG into HEK293TN cells was conducted using TransIT®-293 Transfection Reagent and Opti-MEM. Transfected HEK293TN cells were maintained in Opti-MEM supplied with 10 % FCS overnight. Upon medium exchange on the next day, the cells were supplied with NB medium supplied with 2 % B27 and maintained for two days. 72h after transfection, the supernatant of the transfected HEK293TN was collected and viruses were harvested via ultracentrifugation at 25000 rpm for two hours at 4°C. Virus pellets were re-suspended in ice-cold TBS-5-buffer, aliquoted on the next day and stored at -80°C.

2.2.10. Live-cell imaging of actin dynamics

For monitoring actin dynamics, DIV7 motoneurons grown on PORN/laminin-221/211 coated 35 mm high µ-dishes were incubated with 100 nM SiR-actin for two hours. Next, cells were washed with PBS, covered with pre-warmed Tyrode solution and placed into Tokai Hit stage incubator (37°C, constant 5 % CO_2 supply). Imaging was performed using the Nikon's Eclipse TE2000 inverted epifluorescence microscope that is equipped with a plan APO VC 60x/1.4 NA objective, a perfect focus system and NIS-Elements AR 4.40.00 software. For excitation at 635 nm a fluorescent LED light was used and 16-bit, 1024x1022 pixel images (2x2 binning) were taken every 15 sec. over 20 min. (exposure time 200 ms) with the ORCA Flash 4.0 V2 C11440-22C camera (Hamamatsu Photonics).

Fiji was used for analysis of the 81 frame videos. First, Maximum intensity projections were generated and single filopodia were defined (using the line tool starting from the growth cone center). The ROI was transferred to the time-lapse video and a kymograph was generated (Multi Kymograph function in Fiji). For calculation of the velocity (µm/min), the moved distance of single filopodia (y axis, length in µm) was divided by the individual time of movements (x axis, time in minutes). The velocity of single filopodia (moved distance over time) and the total distance of filopodia movements (amplitude) was visualized as scatter dot plots with bars.

2.2.11 Live-cell calcium imaging

For analysis of spontaneous calcium transients, DIV7 motoneurons grown on PORN/laminin-221/211 coated 35 mm high µ-dishes were incubated with 5 µM Oregon Green™ 488 BAPTA-1, AM or Cal-590™ AM in pre-warmed calcium imaging buffer for 15 minutes at 37°C. Afterwards, cells were washed trice and covered with pre-warmed calcium imaging buffer. For imaging, motoneurons were placed into Tokai Hit stage incubator (37°C, constant 5 % CO2 supply) and monitored using the Nikon's Eclipse TE2000 inverted epifluorescence microscope equipped with a plan APO VC 60x/1.4 NA objective, a perfect focus system and the NIS-Elements AR 4.40.00 software. For excitation, a fluorescence LED light source was used at 470 nm or 525 nm respectively, and 16-bit, 1024x1022 pixels pictures (2x2 binning) were taken at a frequency of 2 Hz over 5 minutes (exposure time 100 ms) at the ORCA Flash 4.0 V2 C11440-22C camera (Hamamatsu Photonics).

Analysis of the 601 frame videos was done with Fiji. Therefore, growth cones were defined as region of interest and a dynamic Z-axis profile was plotted (normalized against the average of the first 20 frames (F/F0)). Subsequently single calcium spikes were counted using the BAR Plugin and visualized as spikes per minute in scatter dot plots with bars.

2.2.12. Data analysis and statistics

GraphPad Prism 6 was used for statistical analysis and graph illustration. At least three independent experiments were performed for every data set. "n" represents the set of experiments while "N" indicates the total amount of collected objects. For N > 40 the results are shown as mean ± standard error of the mean (SEM), while for smaller N numbers the data is shown as mean ± standard deviation (SD). Mann-Whitney test was used for analysis of two groups, while more groups were analyzed by one-way analysis of variance (ANOVA) Kruskal-Wallis test and Dunn's Multiple Comparison post-hoc test.

Significance is indicated as * if p < 0.05, ** if p < 0.01, *** if p < 0.001 and **** if p < 0.0001 and n.s. (not significant) if p > 0.05. Data is shown as scatter dot plots with bars or bar plots and the final figure processing was performed with Adobe Illustrator v 25.2.2 software.

2.2.13. RNA sequencing

RNA Sequencing and analysis of compartmentalized Smn knockdown motoneurons was performed by Dr. Michael Briese, Dr. Lena Saal-Bauernschubert and Prof. Sendtner as previously described (Briese et al., 2016). The corresponding GFP control samples were previously published in (Briese et al., 2018) and processed in parallel to the Smn knockdown samples described here. Bioinformatics were performed by Dr. Michael Briese and Dr. Silke Appenzeller. Cuffdiff analysis was performed to analyse differential gene expression (Briese et al., 2016) and the Database for Annotation, Visualization and Integrated Discovery (DAVID) was used for Gene Ontology (GO) term analysis (Huang da et al., 2009). Fragments per kilobase of transcript per million 42 mapped reads (FPKM) were tested in GraphPad Prism6 via multiple t-test. The RNA sequencing data from Smn knockdown motoneurons is accessible in NCBI's Gene Expression Omnibus through GEO Series accession number GSE197638.

3. Results

The majority of the following results are published in Hennlein et al., 2023. Plastin 3 rescues cell surface translocation and activation of TrkB in spinal muscular atrophy. *J. Cell Biol.*, *in press.* DOI: 10.1083/jcb.202204113.

3.1. TrkB protein levels are reduced and BDNF-induced TrkB activation is impaired upon Smn deficiency

3.1.1. Smn-deficient motoneurons display reduced TrkB levels and impaired TrkB activation within their axonal terminals

Since previous reports showed that TrkB-deficient motoneurons exhibit similar pathological features similar to Smn-deficient motoneurons, we aimed to investigate whether cultured SMA motoneurons display defects in BDNF/TrkB signaling and whether this is connected to the observed pathophysiological events. Therefore, motoneurons were isolated from *Smn⁻/⁻;SMN2* and control embryos on E12.5 and cultured on the β2-chain-containing laminin isoform laminin-221/211 for 5 days. In the first place, we wanted to check whether TrkB expression and localization are altered upon Smn deficiency. The specificity of the TrkB antibody was tested on cultured TrkB-deficient motoneurons prior to the experiments. Slight background staining could be observed upon TrkB staining in *Ntrk2⁻/⁻* motoneurons, however no specific TrkB immunofluorescence signal could be detected in contrast to the control neurons, confirming the specificity of the antibody (**Fig. 5 a**).
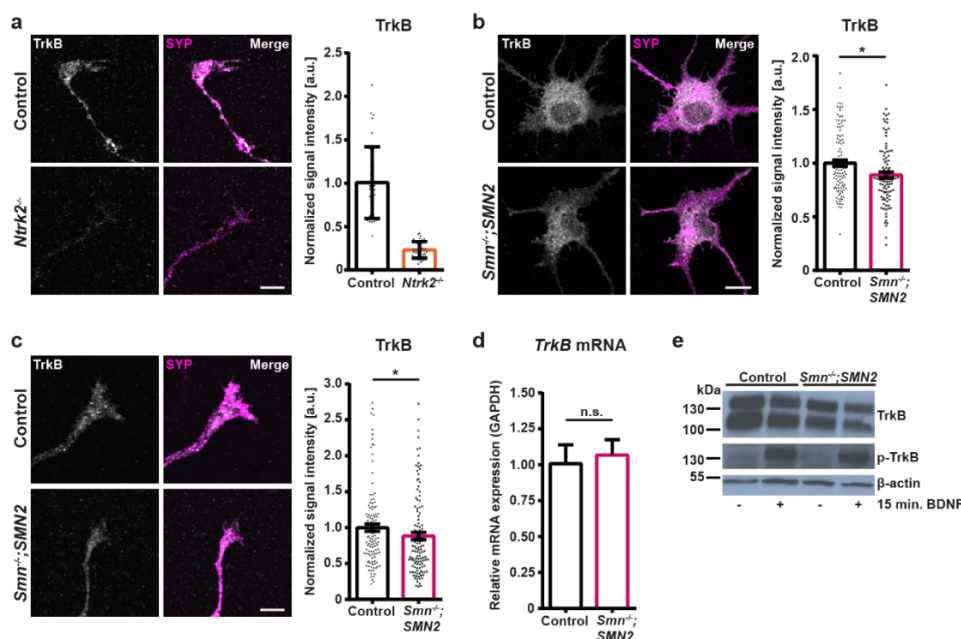
Fig. 5: TrkB localization shows only minor impairments in SMA motoneurons. *a) Growth cones from control and Ntrk2⁻/⁻ DIV5 motoneurons for antibody verification stained against TrkB (gray) and Synaptophysin-1 (SYP, magenta), scale bar: 5 µm. Normalized mean gray values of TrkB (n=1, N=40). Bar represents the mean ± SD.* ***b)*** *Control and Smn⁻/⁻;SMN2 soma stained against TrkB (gray) and SYP (magenta), scale bar: 10 µm. Normalized mean gray values of TrkB (n=3, N=102; Mann-Whitney test, * p = 0.0127). c) Control and Smn⁻/⁻;SMN2 growth cones stained against TrkB (gray) and SYP (magenta), scale bar: 5 µm. Normalized mean gray values of TrkB (n=6, N=120; Mann-Whitney test, * p = 0.0204). d) Relative expression of TrkB in whole cell lysates from control and Smn⁻/⁻;SMN2 DIV7 motoneurons. Quantification of TrkB relative to GAPDH (n=3, N=7; Mann-Whitney test, n.s. not significant). Data are presented as mean ± SD. e) Western blot analysis of TrkB and p-TrkB levels in whole cell lysates of control and Smn⁻/⁻;SMN2 motoneurons that were unstimulated or 15 min. BDNF stimulated. β-actin was used as loading control. Data are presented as scatter dot plot with bar / bar. Bar represent the mean ± SEM (except for a) and d)).*

Next, *Smn^-/-;SMN2* and control motoneurons were stained against TrkB. Confocal analysis revealed only minor alterations in TrkB expression within the cell bodies of Smn-deficient motoneurons (**Fig. 5 b**). Similar to that, a slight decrease in total TrkB levels was detected within growth cones of Smn-deficient motoneurons (**Fig. 5 c**). To further examine the TrkB expression, RNA was extracted from whole-cell lysates of motoneurons cultured until DIV7 and the expression of *TrkB* mRNA was quantified via RT-PCR. No changes in *TrkB* quantities were detected upon Smn deficiency (**Fig. 5 d**). Similarly, whole-cell protein analysis using Western blots did not reveal any significant altered TrkB levels in these cells (**Fig. 5 e**). Hence, Smn-deficient motoneurons seem to have only minor alterations in TrkB levels, but overall no great reduction could be seen. Since no gross abnormalities could be observed in TrkB expression, we wanted to test whether the activation of the receptor via its ligand BDNF is functional in in Smn-deficient cells.

Therefore, motoneurons were cultured in the presence of BDNF until DIV4 (or DIV6 for western Blot analysis) before they were deprived of BDNF overnight. On the next day, the neurons were stimulated with 100 ng/ml BDNF for 15 min. and immediately fixed. Again, p-TrkB antibody specificity was tested using TrkB-deficient neurons. The applied p-TrkB antibody recognizes phosphorylated tyrosine resides within the kinase domain of TrkB at position Tyr706/707. In control motoneurons, a significant increase in p-TrkB immunoreactivity could be detected upon BDNF stimulation for 15 min. (**Fig. 6 a**). *Ntrk2^-/-* motoneurons also displayed a slight, but less intense immunosignal, which is probably attributable to the expression of other Trk receptors with highly homologous kinase domain such as TrkC (**Fig. 6 b**). However, in these neurons no specific increase in p-TrkB immunosignal could be observed upon BDNF stimulation indicating a specificity of the antibody for activated TrkB (**Fig. 6 a**).
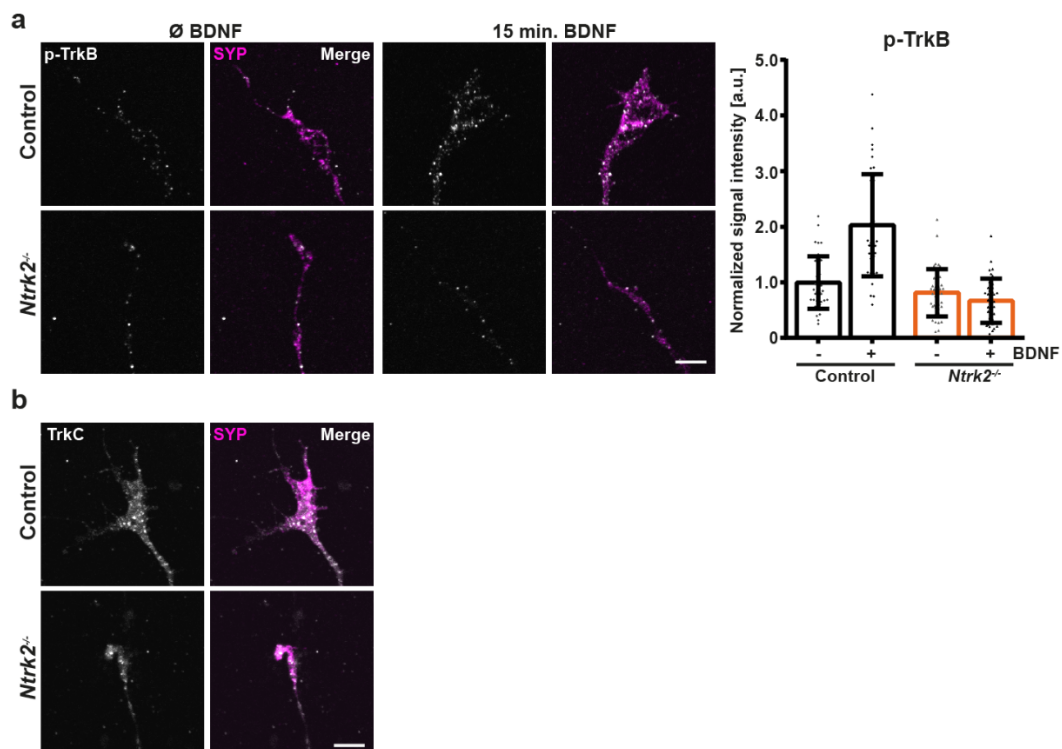
Fig. 6: Verification of the p-TrkB antibody in TrkB-deficient motoneurons. a) *Growth cones from control and Ntrk2^-/- DIV 5 motoneurons unstimulated and 15 min. BDNF stimulated stained against p-TrkB (gray) and Synaptophysin-1 (SYP, magenta). Normalized mean gray values of p-TrkB (n=2, N=40). Data are presented as scatter dot plot with bar. Bar represent the mean ± SD.* **b)** *Growth cones from control and Ntrk2^-/- DIV 5 motoneurons stained against TrkC (gray) and SYP (magenta). Scale bars: 5 µm.*

Next, we performed p-TrkB immunostainings on BDNF-stimulated motoneurons isolated from *Smn⁻/⁻; SMN2* embryos. Although these neurons display only marginal reduced TrkB levels within their growth cones (**Fig. 5 c**), the raise in p-TrkB signal that is seen in control motoneurons was absent in Smn-deficient axon terminals (**Fig. 7 a**). In contrast to that, phosphorylation of the receptor after BDNF stimulation worked properly in the soma of Smn-deficient cells (**Fig. 7 b**) and is similarly detectable in whole-cell lysates detected by Western Blot (**Fig. 5 e**). Thus, Smn-deficient motoneurons exhibit only minor TrkB deficiency but highly impaired BDNF-induced TrkB activation, which is exclusively restricted to the axon terminals.
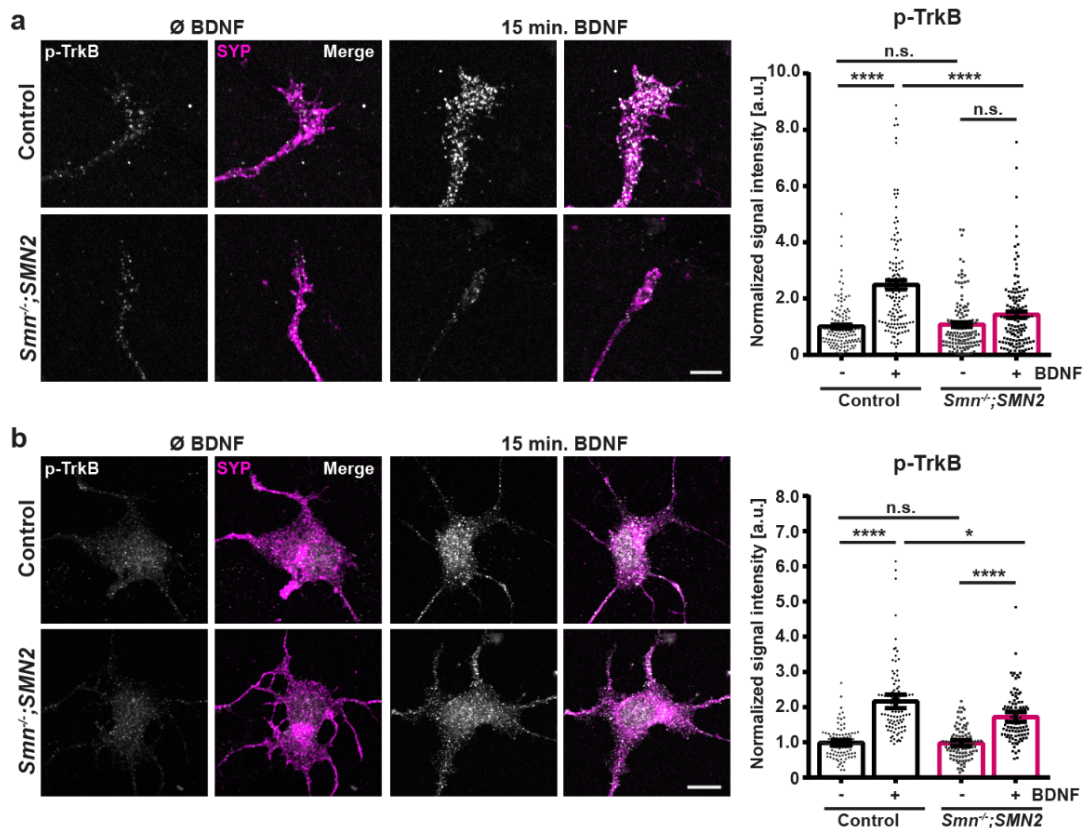
Fig. 7: SMA motoneurons display a TrkB activation defect locally at their axon terminals. *a) – b) Control and Smn⁻/⁻;SMN2 **a)** growth cones and **b)** cell bodies unstimulated and 15 min. BDNF stimulated stained against p-TrkB (gray) and Synaptophysin-1 (SYP, magenta). **a)** Normalized mean gray values of p-TrkB within growth cones (n=6, N=130; ANOVA Kruskal-Wallis test, **** p ≤ 0.0001; n.s. not significant). **b)** Normalized mean gray values of p-TrkB within cell bodies (n=3, N=100; ANOVA Kruskal-Wallis test, * p ≤ 0.05; **** p ≤ 0.0001; n.s. not significant). Data are presented as scatter dot plot with bar. Bar represent the mean ± SEM. Scale bars: 5 µm.*

One central pathophysiological hallmark of SMA motoneurons are collapsed growth cones with a defective actin cytoskeleton. In order to investigate whether the actin cytoskeleton is involved in the observed defects in TrkB localization and activation we used the mycotoxin CytoD to inhibit actin polymerization. A 30 min. CytoD pre-treatment of motoneurons cultured until DIV5 resulted in collapsing of axonal terminals (**Fig. 8 a**) and prevented the BDNF-induced phosphorylation of TrkB in control motoneurons (**Fig. 8 b**). Therefore, disruption of the actin cytoskeleton by CytoD results in SMA-like motoneuron phenotype indicating that it might be causative for the impaired TrkB activation in Smn-deficient axonal terminals.
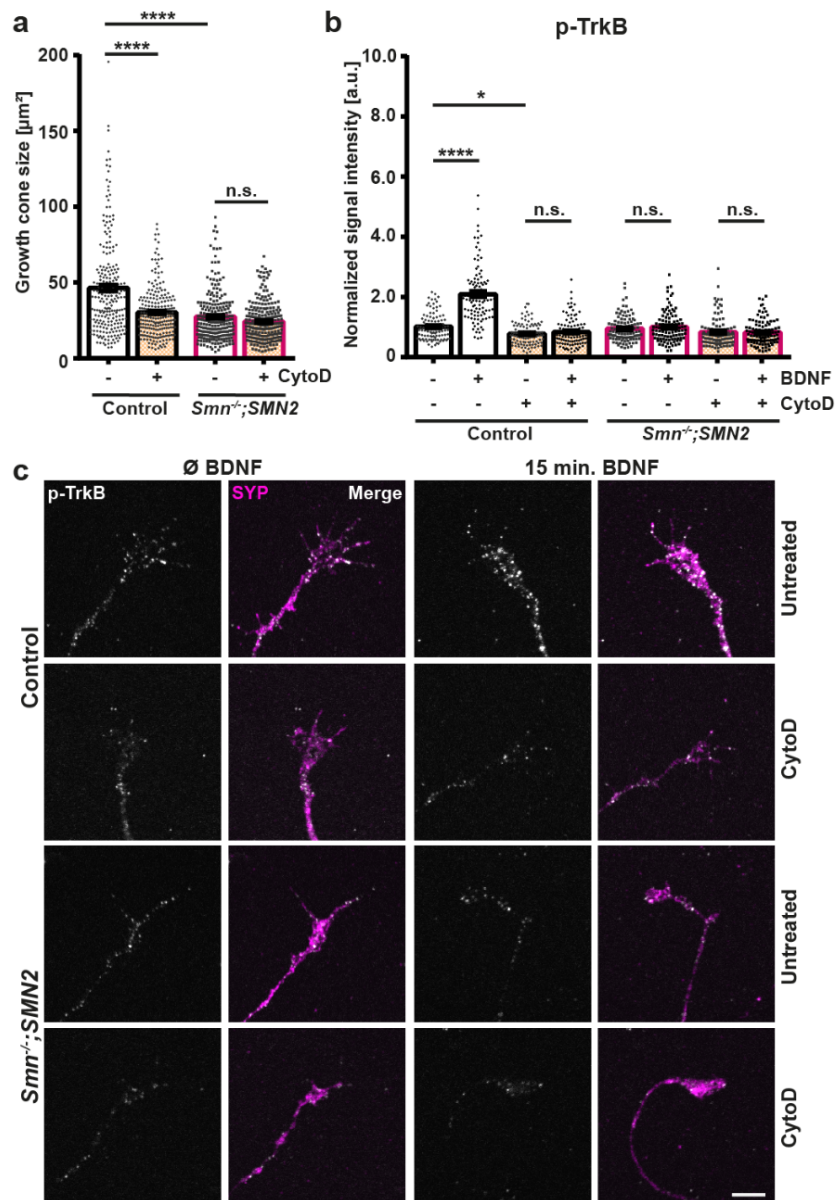
Fig. 8: Disrupting the actin polymerization interferes with TrkB activation in axon terminals*. a) Cytochalasin D (CytoD) treatment leads to collapsing of axon terminals in control cells (n=6; N=230; Control untreated: 46.36 ± 2.09 µm2, Control CytoD treated: 30.02 ± 1.07 µm2, Smn⁻/⁻;SMN2 untreated: 27.39 ± 1.09 µm2, Smn⁻/⁻;SMN2 CytoD treated: 24.26 ± 0.84 µm2; ANOVA Kruskal-Wallis test, **** p ≤ 0.0001; n.s. not significant).* ***b) – c)*** *Untreated or CytoD pre-treated control and Smn⁻/⁻;SMN2 growth cones unstimulated and 15 min. BDNF stimulated stained against p-TrkB (gray) and Synaptophysin-1 (SYP, magenta), scale bar: 5 µm. Normalized mean gray values of p-TrkB (n=3, N=105; ANOVA Kruskal-Wallis test, * p ≤ 0.05; **** p ≤ 0.0001; n.s. not significant). Data are presented as scatter dot plot with bar. Bar represent the mean ± SEM.*

3.1.2. NMJs of SMNΔ7 mice display reduced TrkB levels and impaired TrkB activation

Since we observed reduced TrkB levels and disturbed TrkB phosphorylation after BDNF stimulation within axon terminals of cultured Smn-deficient motoneurons, we wanted to test whether these defects are also present in NMJs of the severely affected *TVA* muscle in postnatal *SMNΔ7* mice.

Initially, TrkB and p-TrkB antibodies were tested in *TVA* muscles isolated from *Ntrk2⁻/⁻* mice at P5. For immunohistochemistry another TrkB antibody (TrkB goat, R&D Systems, AF1494) was used which showed highly specific staining within NMJs of control animals, but no signal within NMJs of TrkB-deficient animals (**Fig. 9 a**). Moreover, p-TrkB antibody that recognizes its epitope within the kinase domain of TrkB was tested in *Ntrk2⁻/⁻* muscle tissue. Similar to the immunocytochemistry in motoneurons, a p-TrkB immunosignal could be detected in the *Ntrk2⁻/⁻* muscle tissue, but no specific elevation was observed after BDNF stimulation in contrast to the controls (**Fig. 9 b**).
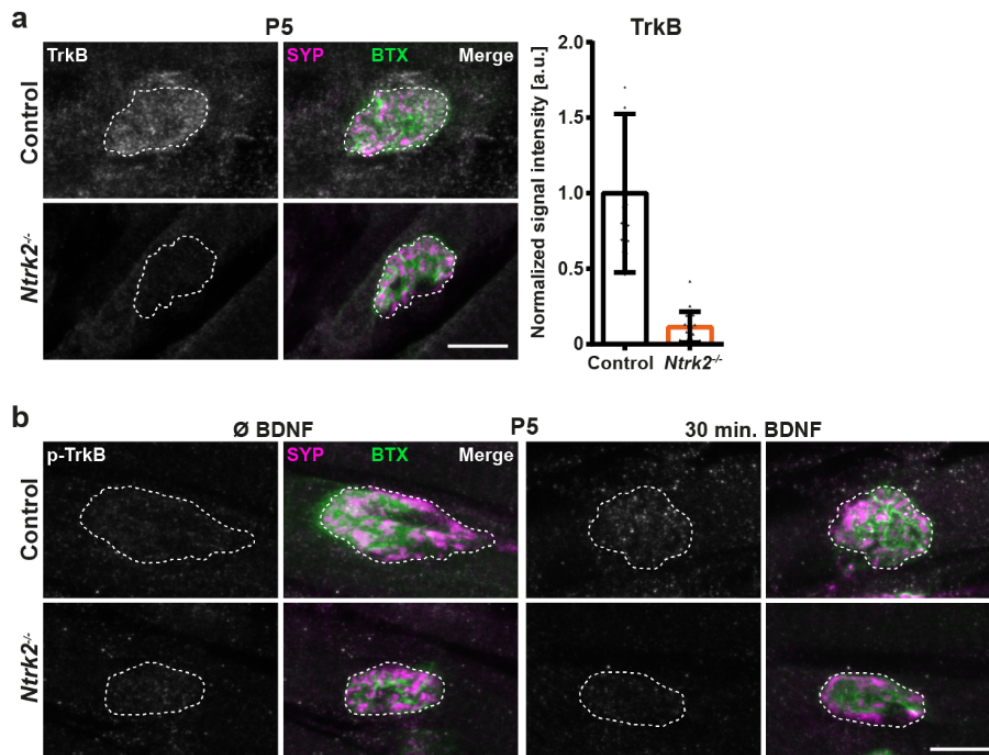
***Fig. 9: Test for TrkB and p-TrkB antibody specificity in TrkB-deficient NMJs. a)** NMJs from the Transversus abdominis anterior (TVA) muscle in control and Ntrk2⁻/⁻ P5 animals stained against TrkB (gray), Synaptophysin-1 (SYP, magenta) and postsynaptic ACh receptors (BTX, green). Normalized mean gray values of TrkB (n=2, N=24). Data are presented as scatter dot plot with bar. Bar represent the mean ± SD. **b)** NMJs from TVA in control and Ntrk2⁻/⁻ P5 animals unstimulated and 30 min. BDNF stimulated stained against p-TrkB (gray), Synaptophysin-1 (SYP, magenta) and postsynaptic ACh receptors (BTX, green). Dotted line depicts outline of the presynapse (SYP). Scale bars: 10 µm.*

For investigation of BDNF/TrkB signaling in axonal terminals of *ex vivo TVA* muscle tissue, *SMNΔ7* mice were analyzed at an early symptomatic stage at P5 and when the disease had progressed at a later symptomatic stage at P10-P11.

NMJs were identified using Synaptophysin-1 as presynaptic marker and Bungarotoxin to visualize postsynaptic AChR. In accordance with previous reports, the size of the NMJs and the ratio of the area of the presynapse vs. postsynapse (**Fig. 10 a**) was significantly reduced already at P5 in *SMNΔ7* mice. Immunostainings against TrkB revealed markedly reduced TrkB expression in these animals (**Fig. 10 b**). However, BDNF stimulation could still evoke a significant increase in p-TrkB levels in Smn-deficient mice, although to a lesser extend when compared to control mice (**Fig. 10 c**).
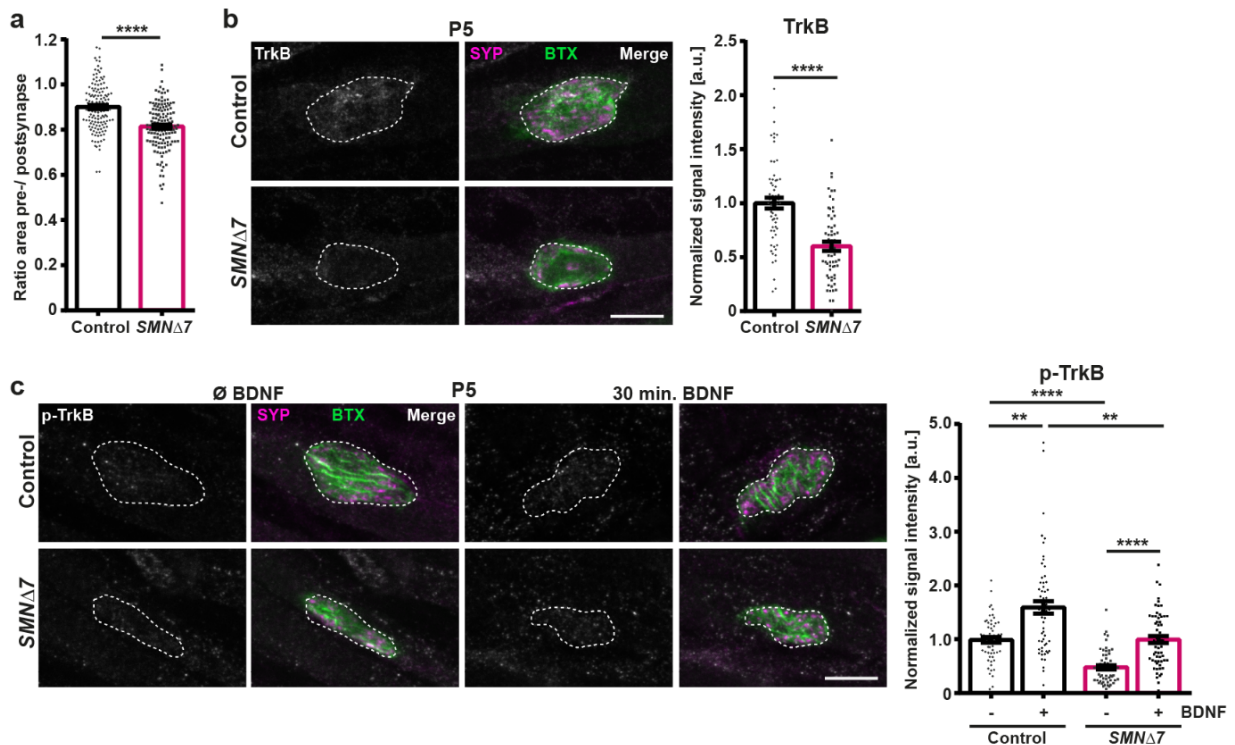
Fig. 10: Impaired TrkB localization NMJs of early-disease stage SMA mice. a) Ratio of the area of the presynapse (Synaptophysin-1, (SYP)) vs. postsynapse (BTX) in NMJs from Transversus abdominis anterior (TVA) muscle in control and SMNΔ7 P5 (n=4, N=140; Mann-Whitney test, **** p ≤ 0.0001). *b)* NMJs in the TVA muscle in control and SMNΔ7 P5 animals stained against TrkB (gray), SYP (magenta) and postsynaptic ACh receptors (BTX, green), scale bar: 10 µm. Normalized mean gray values of TrkB (n=4, N=62; Mann-Whitney test, **** p ≤ 0.0001). *c)* Unstimulated and 30 min. BDNF stimulated NMJs in the TVA muscle of control and SMNΔ7 P5 animals stained against p-TrkB (gray), SYP (magenta) and BTX (green), scale bar: 10 µm. Normalized mean gray values of p-TrkB (n=3, N=60; ANOVA Kruskal-Wallis test, ** p ≤ 0.01; **** p ≤ 0.0001). Data are presented as scatter dot plot with bar. Bar represent the mean ± SEM. Dotted line depicts outline of the presynapse (SYP).

Examinations of the *TVA* at the later symptomatic stage revealed an even more pronounced phenotype with reduced area ratio of the pre- vs. postsynapse (**Fig. 11 a**) and tremendous reduced TrkB levels (**Fig. 11 b**). In contrast to the early symptomatic stage at P5, BDNF stimulation could not evoke an increase in TrkB phosphorylation in P10-P11 *SMNΔ7* animals, while a marked raise could be observed in control animals upon BDNF stimulation. (**Fig. 11 c**). Hence, from the first set of experiments we conclude that Smn deficiency interferes with TrkB localization as well as its activation within axon terminals and neuromuscular endplates. Moreover, the data argues that the disturbed actin cytoskeleton could play a role in the observed abnormalities leading to defective BDNF/TrkB signaling.
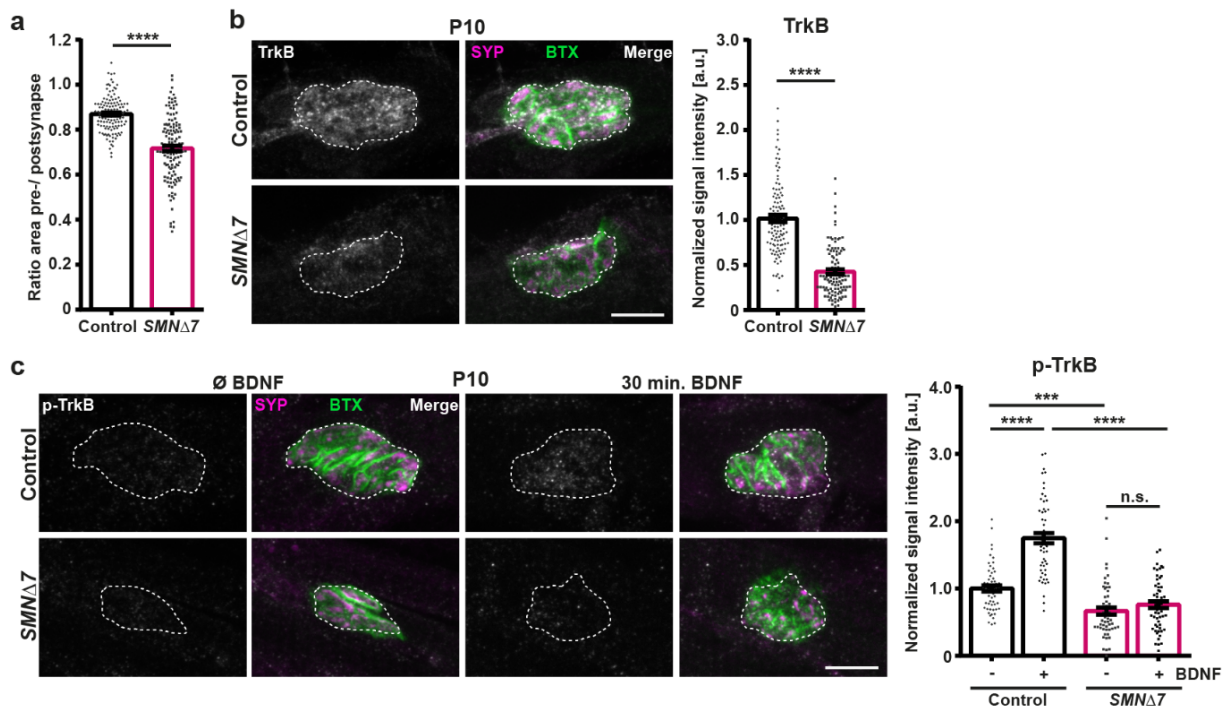
Fig. 11: Defective TrkB localization and activation NMJs of later-disease stage SMA mice. a) *Ratio of the area of the presynapse (Synaptophysin-1, (SYP)) vs. postsynapse (BTX) in NMJs from Transversus abdominis anterior (TVA) muscle in control and SMNΔ7 P10 (n=4, N=130; Mann-Whitney test, **** p ≤ 0.0001).* **b)** *NMJs in the TVA muscle in control and SMNΔ7 P10 animals stained against TrkB (gray), SYP (magenta) and postsynaptic ACh receptors (BTX, green), scale bar: 10 μm. Normalized mean gray values of TrkB (n=5, N=109; Mann-Whitney test, **** p ≤ 0.0001).* **c)** *Unstimulated and 30 min. BDNF stimulated NMJs in the TVA muscle of control and SMNΔ7 P10 animals stained against p-TrkB (gray), SYP (magenta) and BTX (green), scale bar: 10 μm. Normalized mean gray values of p-TrkB (n=4, N=56; ANOVA Kruskal-Wallis test, *** p ≤ 0.001; **** p ≤ 0.0001; n.s. not significant). Data are presented as scatter dot plot with bar. Bar represent the mean ± SEM. Dotted line depicts outline of the presynapse (SYP).*

3.2. cAMP-induced surface recruitment of TrkB mediated by actin filaments is disturbed in Smn-deficient growth cones

Since axon terminals of Smn-deficient motoneurons display only minor reductions of total TrkB but simultenously highly impaired BDNF-induced TrkB activation, we asked whether the surface presentation of the receptor is altered. To examine the localization of TrkB on the plasma membrane, we established a live-cell staning protocol to exclusively label receptors at the cell surface. For that, living motoneurons were placed on ice in order to inhibit activity of the cells and prevent permeation of the antibody into the cell. Afterwards, motoneurons were incubated with the TrkB antibody followed by incubation with the secondary antibody on ice prior to fixation. First, antibody specificity was tested again using TrkB-deficient motoneurons (**Fig. 12 a**). Furthermore, comparison of control motoneurons stained for total TrkB after fixation and live-stained motoneurons confirmed the efficiency of the protocol as shown for the cell body and the axon terminals (**Fig. 12 b – c**). Importantly, the comparison of the total pool of TrkB vs. cell surface TrkB revealed that the majority of the receptor seems to be localized intracellularly, while only a small portion was localized at the cell surface (**Fig. 12 c**).
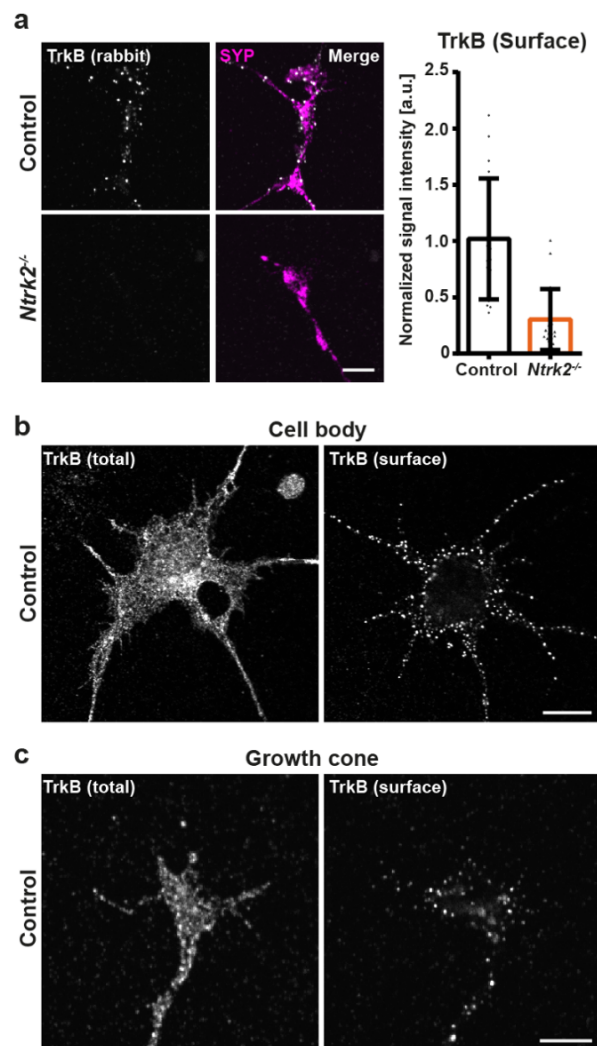
Fig. 12: Verification of TrkB cell surface staining. *a) Growth cones from control and Ntrk2⁻/⁻ DIV5 motoneurons stained against surface TrkB (gray) and Synaptophysin-1 (SYP, magenta). Normalized mean gray values of surface TrkB (n=1, N=20). Data are presented as scatter dot plot with bar. Bar represent the mean ± SD. b) – c) Representative images of a) cell bodies and b) growth cones of control DIV5 motoneurons stained against total TrkB (left panel) or surface TrkB (right panel). Scale bars: 5 µm.*

Initally, quantification of the baseline surface TrkB levels did not reveal any significant difference between control and Smn-deficient growth cones (**Fig. 13 a, first lane**). Next, motoneurons were stimulated with BDNF to follow TrkB endocytosis. Therefore, motoneurons were cultured in presence of BDNF until DIV4, before they were BDNF deprived over night. On DIV5, they were BDNF stimulated for 5 or 15 min. prior to the live-cell staning assay. Following ligand exposure, TrkB is rapidly endocytosed and disappered from the cell surface in a time-dependent manner (**Fig. 13 a**). In Smn-deficient cells, TrkB internalization seemed to be slighly delayed, however no significant differences were observed when compared to controls (**Fig. 13 a**). Moreover, the anterograde as well as the retrograde transport of cargos along actin filaments is mediated via myosin motor proteins (Hirokawa et al., 2010). Since an interaction of myosin VI and TrkB was demonstrated in hippocampal neurons for retrograde transport of BDN/TrkB signaling endosomes (Yano et al., 2006), we stained control and *Smn⁻/⁻;SMN2* motoneurons with an antibody directed against myosin VI to check whether the retrograde transport after internalization of the BDNF/TrkB complex is disturbed in axon terminals of SMA motoneurons. Confocal microscopy revealed that myosin VI is distributed all over the growth cones and no significant difference was found in Smn-deficient terminals in comparison to controls (**Fig. 13 b**). Thus, impaired TrkB activation in Smn-deficient axon terminals cannot be attributable to baseline cell surface TrkB presentation or its ligand-induced internalization.
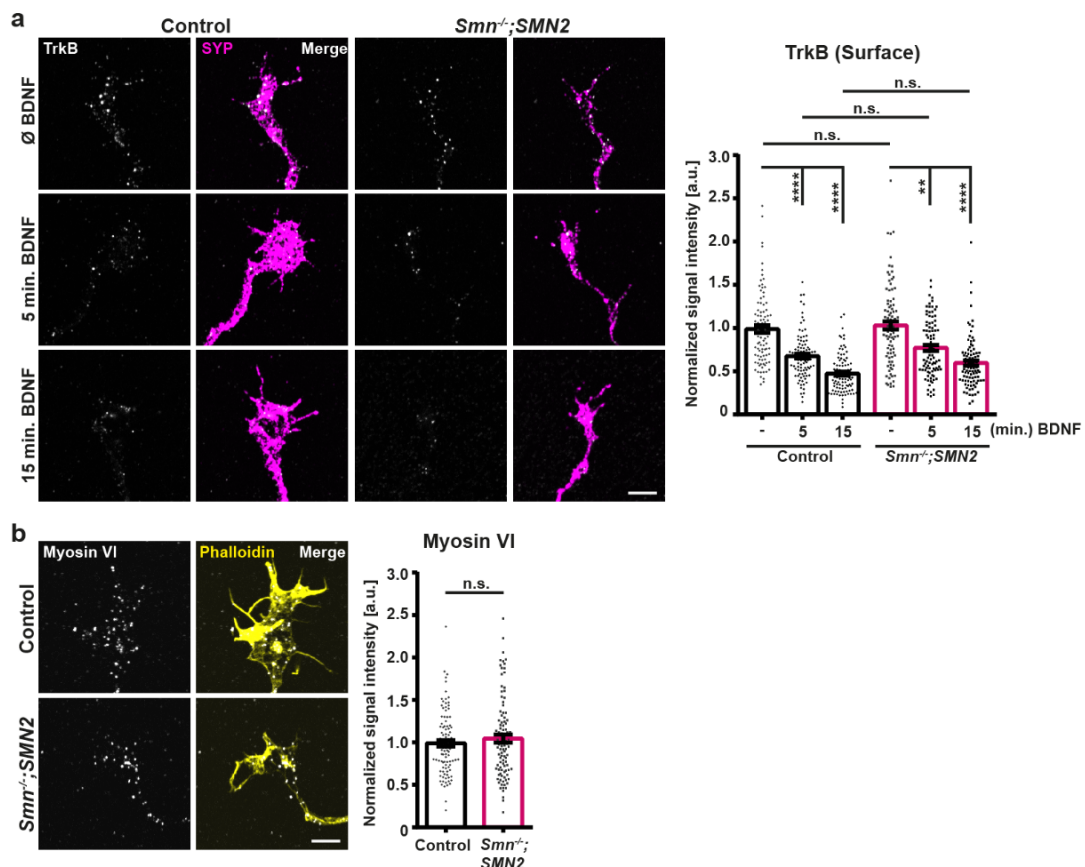
Fig. 13: BDNF-induced TrkB endocytosis is functional in SMA axon terminals. a) *Growth cones from control and Smn⁻/⁻;SMN2 motoneurons unstimulated, 5min. and 15 min. BDNF stimulated stained against surface TrkB (gray) and Synaptophysin-1 (SYP, magenta). Normalized mean gray values of surface TrkB (n=3, N=93; ANOVA Kruskal-Wallis test, ** p ≤ 0.01; **** p ≤ 0.0001; n.s. not significant).* ***b)*** *Control and Smn⁻/⁻;SMN2 growth cones stained against Myosin VI (gray) and F-actin (Phalloidin, yellow). Normalized mean gray values of Myosin VI (n=3, N=100; Mann-Whitney test, n.s. not significant). Data are presented as scatter dot plot with bar. Bar represent the mean ± SEM. Scale bars: 5 µm.*

Important regulator of TrkB cell surface localization and by association mediator of BDNF responsiveness is cAMP, that has been shown to promote TrkB cell surface translocation (Meyer-Franke et al., 1998). To examine stimulus-induced TrkB cell surface recruitment in *Smn⁻/⁻;SMN2* axon terminals, motoneurons were exposed to 8-CPT-cAMP for 20 min. prior to the live-cell staining assay. In control neurons, cAMP stimulation induced an elevation of TrkB on the plasma membrane, while no increased cell surface TrkB levels were detected at the surface of Smn-deficient growth cones (**Fig. 14 a**). In addition to neuronal activity, an intact cytoskeleton is required for proper TrkB cell surface translocation (Zhao et al., 2009). To test the possibility that the defective actin cytoskeleton is responsible for the impaired TrkB surface translocation in Smn-deficient motoneurons, the cells were pre-treated with CytoD to mimic the SMA phenotype prior to 8-CPT-cAMP stimulation. Analysis of the surface TrkB signals showed that inhibition of actin polymerization prevented the cAMP-induced TrkB recruitment in control motoneurons (**Fig. 14 b**). Thus, these experiments revealed that neither basal TrkB cell surface presentation, nor its BDNF-induced internalization are disturbed in SMA, but its activity-induced cell surface translocation via actin filaments is greatly diminished upon Smn deficiency.
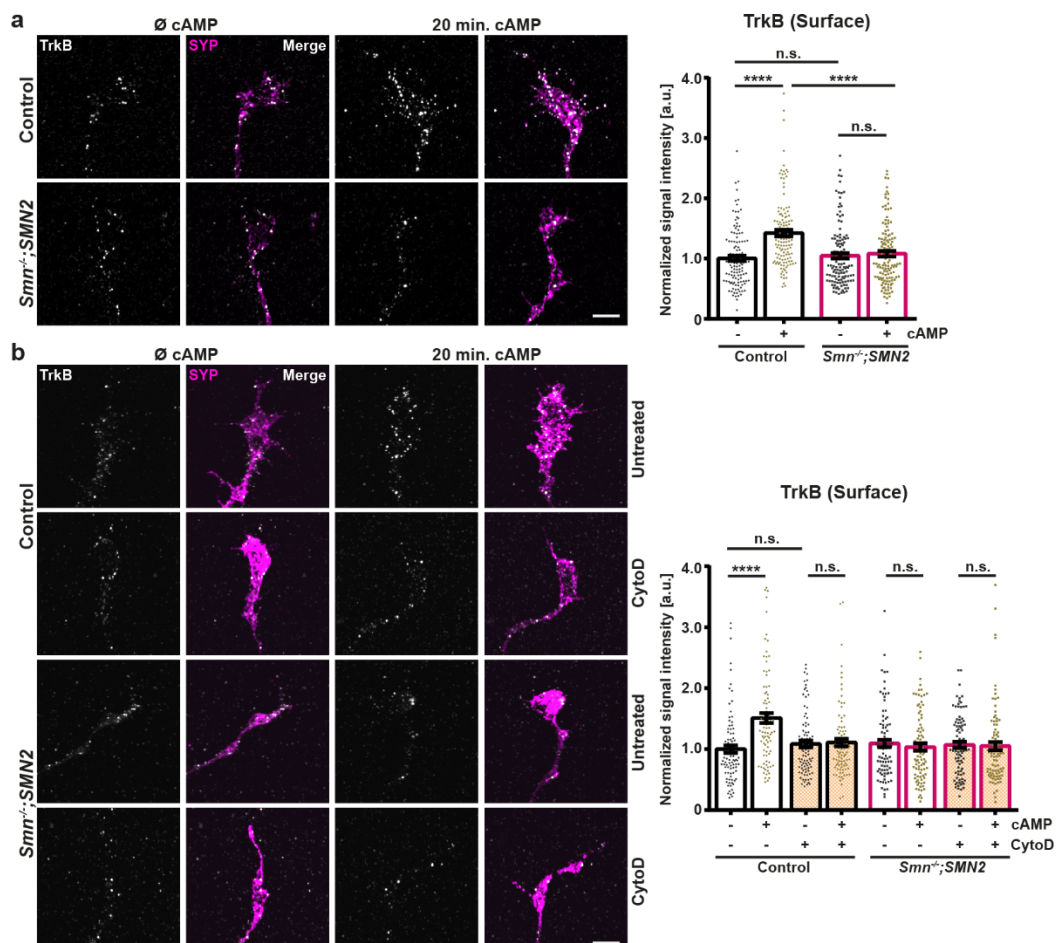
Fig. 14: The actin-dependent activity-induced TrkB cell surface translocation is impaired in SMA axon terminals. a) – b) *Growth cones from control and Smn⁻/⁻;SMN2 motoneurons stained against surface TrkB (gray) and Synaptophysin-1 (SYP, magenta).* **a)** *Normalized mean gray values of surface TrkB in control and Smn⁻/⁻;SMN2 terminals unstimulated and 20' 8-CPT-cAMP stimulated (n=4, N=125; ANOVA Kruskal-Wallis test, **** p ≤ 0.0001; n.s. not significant).* **b)** *Normalized mean gray values of surface TrkB in control and Smn⁻/⁻;SMN2 terminals treated with 0.5 µM CytoD prior to 20' 8-CPT-cAMP stimulation (n=3, N=90; ANOVA Kruskal-Wallis test, **** p ≤ 0.0001; n.s. not significant). Data are presented as scatter dot plot with bar. Bar represent the mean ± SEM. Scale bars: 5 µm.*

3.3. Pls3 deficiency causes a SMA-like phenotype in motoneurons

3.3.1. RNA sequencing reveals axonal compartment specific downregulation of actin-related transcripts

Since our data provides evidence that the disturbed actin cytoskeleton could be the key event preceding defective BDNF/TrkB signaling we wanted to investigate the underlying mechanism in more detail. Therefore, transcriptome analysis of Smn-knockdown motoneurons (**Fig. 15 a**) in comparison to GFP-expressing control motoneurons cultured in compartmentalized microfluidic chambers was performed by my colleagues Dr. Michael Briese, Dr. Lena Saal-Bauernschubert, Dr. Silke Appenzeller and Prof. Michael Sendtner [*unpublished data, personal communication Dr. Michael Briese*]. RNA sequencing revealed compartment-specific alterations in SMA motoneurons as demonstrated in **Fig. 15 b – c**. Gene Ontology (GO) term analysis was performed for identification of pathway that are potentially altered within the axonal compartment (**Fig. 15 d**).
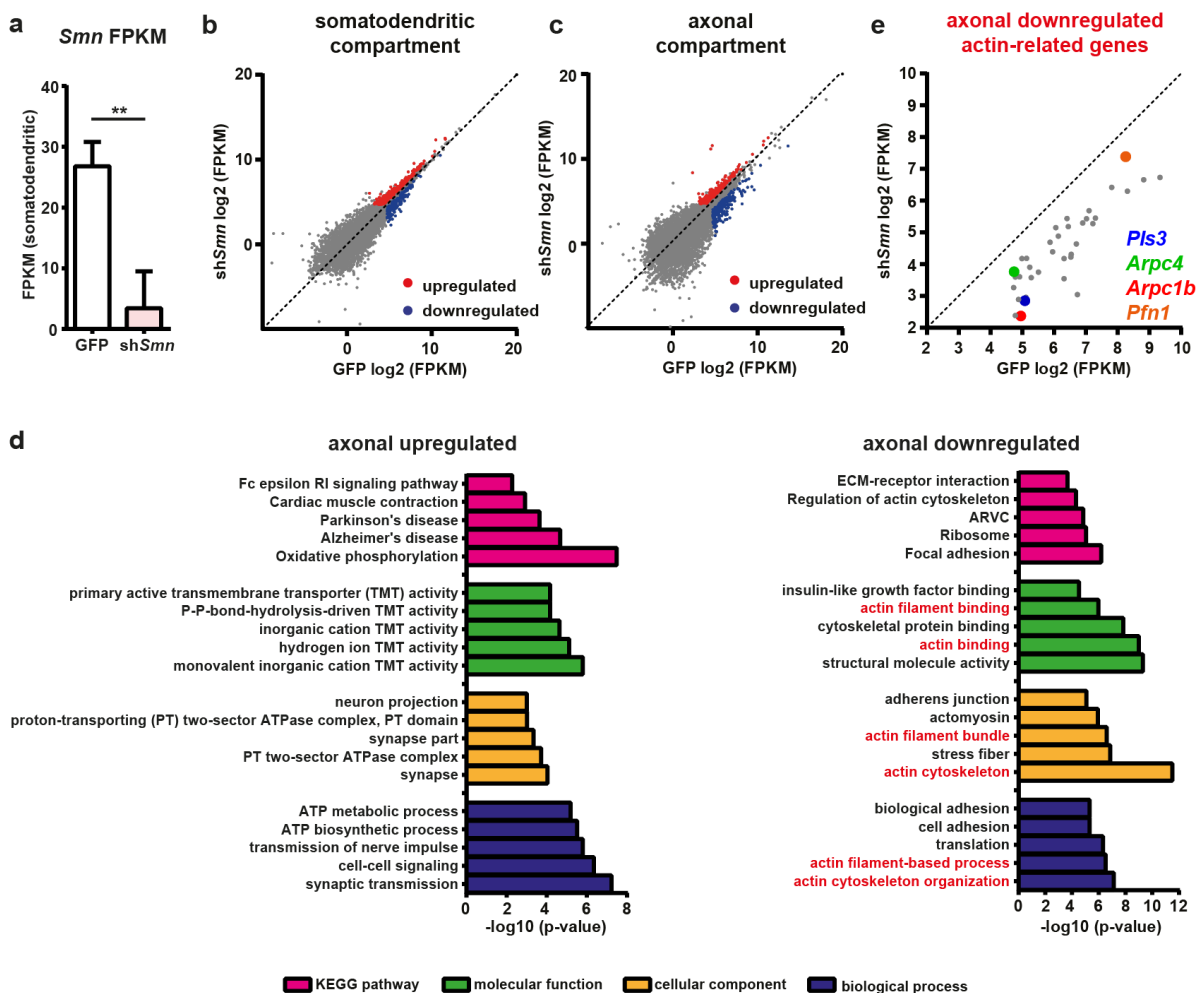
Fig. 15: Transcriptome alterations in Smn knockdown motoneurons. a) *FPKM of Smn measured by RNA sequencing within the somatodendritic compartment of Smn knockdown versus GFP control motoneurons (n=4/6 Multiple t-test, ** p ≤ 0.01). Data are presented as mean ± SD. b) - c) Scatter plots of logarithmized FPKM values derived from cuffdiff analysis of Smn knockdown versus GFP-expressing control motoneurons within the **b)** somatodendritic and **c)** axonal compartment. Genes marked in blue are significantly (p ≤ 0.05) downregulated, while genes marked in red are significantly (p ≤ 0.05) upregulated transcripts. **d)** Gene Ontology (GO) term analysis of transcripts up- or downregulated in the axonal compartment of Smn knockdown motoneurons. In red all actin-related GO groups are marked. **e)** Scatter plots of logarithmized FPKM values derived from cuffdiff analysis of all actin-related transcripts of Smn knockdown versus GFP-expressing control motoneurons that are significantly downregulated in the axonal compartment.*

Especially transcripts that encode for actin-regulatory proteins were downregulated in the axonal compartment of SMA motoneurons. Thus, the FPKMs of the relevant actin-related transcripts were examined in detail (**Fig. 15 e**). Among others, the transcripts encoding for the actin-bundling protein Pls3, subunits of the Arp2/3 complex such as Actin-related protein 2/3 complex subunit 4 (Arpc4) and Actin-related protein 2/3 complex subunit 1B (Arpc1b) or profilin I (Pfn1) were affected by Smn knockdown (**Fig. 15 e**). Interestingly, reduced quantities of the Pls3 transcript were found upon Smn deficiency in both compartments (**Fig. 16 a**). Since Pls3 attracted attention as a protective SMA modifier, we aimed to examine whether the lack of this actin-regulatory protein is involved in the impaired TrkB translocation and activation. First, immunostainings using an antibody directed against the middle region of Pls3 were used to detect protein levels within growth cones. Similar to the RNA sequencing, $Smn^{-/-}$; $SMN2$ motoneurons display significantly reduced Pls3 levels within their growth cones (**Fig. 16 b**).
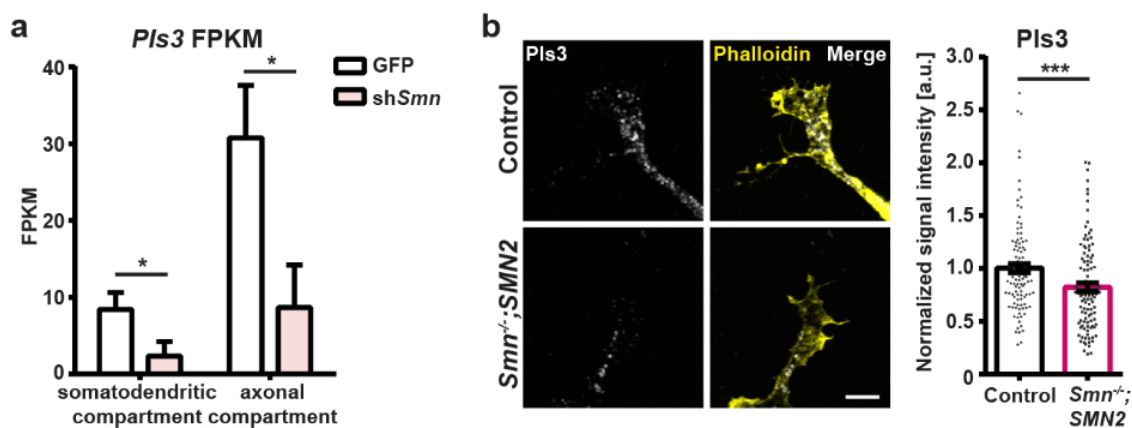
Fig. 16: SMA motoneurons display reduced Pls3 level. a) *FPKM of Pls3 measured by RNA sequencing within the somatodendritic and the axonal compartment of Smn knockdown versus GFP control motoneurons (n=4/6 Multiple t-test, * p ≤ 0.05). Data are presented as mean ± SD.* **b)** *Control and Smn$^{-/-}$;SMN2 growth cones stained against Pls3 (gray) and F-actin (Phalloidin, yellow), scale bar: 5 µm. Normalized mean gray values of Pls3 (n=3, N=106; Mann-Whitney test, *** p = 0.001). Data are presented as scatter dot plot with bar / bar. Bar represent the mean ± SEM.*

3.3.2. Knockdown of Pls3 induces significant morphological and functional alterations within the axon terminals

To further investigate Pls3's role in actin-mediated processes such as TrkB recruitment to the plasma membrane, we used a shRNA-mediated knockdown approach to target endogenous *Pls3* in motoneurons. Therefore, control motoneurons were transduced with a lentivirus harboring shRNA directed against *Pls3* or a control lentivirus harboring shRNA targeting *Luciferase* (*Luci*). A knockdown efficiency of ~60 % was confirmed via RT-PCR (**Fig. 17 a**). For confocal analysis, only transduced, GFP-expressing cells were used. Interestingly, examination of motoneurons lacking Pls3 revealed marked morphological abnormalities. Similar to Smn-deficient motoneurons (Jablonka et al., 2007), Pls3 knockdown motoneurons grew longer axons on the β2-chain containing laminin isoform (**Fig. 17 b**) and had significantly smaller growth cones (**Fig. 17 c**).

Functional analysis was performed using the fluorescently labeled F-actin binding probe SiR-actin for visualization of F-actin movements. Therefore, motoneurons were incubated with SiR-actin and growth cone movements were monitored over a time period of 20 min. (**Fig. 17 d**).

Quantification of the amplitude of single filopodia movements (**Fig. 17 e**) and the velocity of the movements (moved distance over time) (**Fig. 17 f**) revealed that filopodia from Pls3 knockdown growth cones display significantly impaired actin dynamics when compared to the control *shLuci* growth cones.
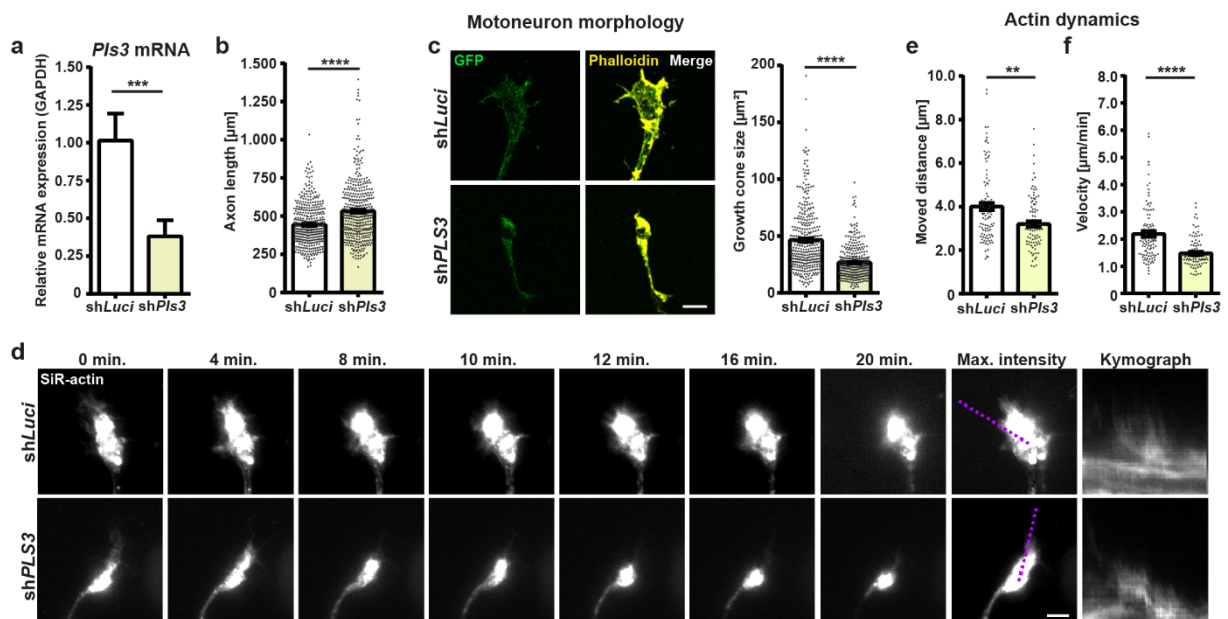
Fig. 17: Knockdown of Pls3 results in morphological changes and disturbed actin dynamics. a) *Relative expression of Pls3 in whole cell lysates of shLuci and shPls3 motoneurons. Quantification of Pls3 relative to GAPDH (n=5, N=8; Mann-Whitney test, *** p ≤ 0.001). Bars represent the mean ± SD.* **b) – c)** *Pls3 knockdown results in* **b)** *increased axon length (µm) (n=3; N=400; shLuci: 443.1 ± 6.7 µm, shPls3: 532.9 ± 9.8 µm; Mann-Whitney test, **** p ≤ 0.0001) and* **c)** *decreased growth cone size (µm2) (n=8; N=350; shLuci: 46.48 ± 1.52 µm2, shPls3: 26.63 ± 0.77 µm2; Mann-Whitney test, **** p ≤ 0.0001). **c)** Representative images of shLuci and shPls3 lentivirus-infected, GFP-expressing (green) motoneurons stained against F-actin (Phalloidin, yellow). **d) – f)** shLuci and shPls3 growth cones with SiR-actin were monitored for 20 min. ROI (purple dotted line) of a single filopodia with the corresponding kymograph. Quantification of **e)** moved distance (µm) of single filopodia (n=5; N=100; Mann-Whitney test, ** p = 0.0016) and **f)** the velocity (distance (µm) over time (min)) of single filopodia (n=5; N=100; Mann-Whitney test, **** p ≤ 0.0001) in shLuci and shPls3 lentivirus-infected growth cones. Data are presented as scatter dot plot with bar / bar. Bar represent the mean ± SEM (except for **a)**). Scale bars: 5 µm*

3.3.3. TrkB localization and activation is impaired upon Pls3 knockdown

In order to investigate the effect of Pls3 knockdown on TrkB localization and activation we performed immunocytochemical analysis of *shPls3* motoneurons. Decreasing endogenous Pls3 level resulted in significantly reduced total TrkB levels (**Fig. 18 a**) and impaired BDNF-induced TrkB phosphorylation within axon terminals (**Fig. 18 b**) which is comparable to the results obtained from Smn-deficient motoneurons.
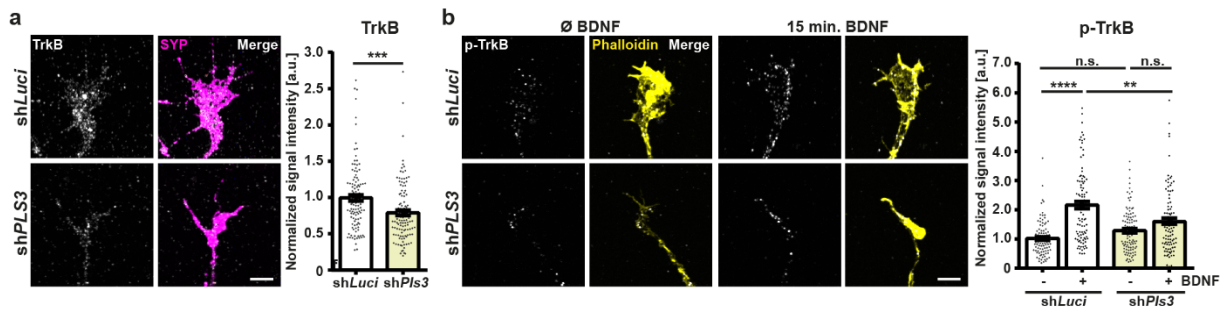
Fig. 18: Knockdown of Pls3 results in aberrant TrkB localization and activation. a) *shLuci and shPls3 growth cones stained against TrkB (gray) and Synaptophysin-1 (SYP, magenta). Normalized mean gray values of TrkB (n=5, N=115; Mann-Whitney test, *** p = 0.0002).* ***b)*** *shLuci and shPls3 growth cones unstimulated and 15 min. BDNF stimulated stained against p-TrkB (gray) and F-actin (Phalloidin, yellow). Normalized mean gray values of p-TrkB (n=3, N=100; ANOVA Kruskal-Wallis test, ** p ≤ 0.01; **** p ≤ 0.0001; n.s. not significant). Data are presented as scatter dot plot with bar / bar. Bar represent the mean ± SEM. Scale bars: 5 µm.*

Moreover, live-cell stainings showed that baseline surface TrkB levels and ligand-induced TrkB internalization are unaltered upon Pls3 knockdown (**Fig. 19 a**), however recruitment of TrkB to the cell surface by 8-CPT-cAMP stimulation was not detected in these cells (**Fig. 19 b**).
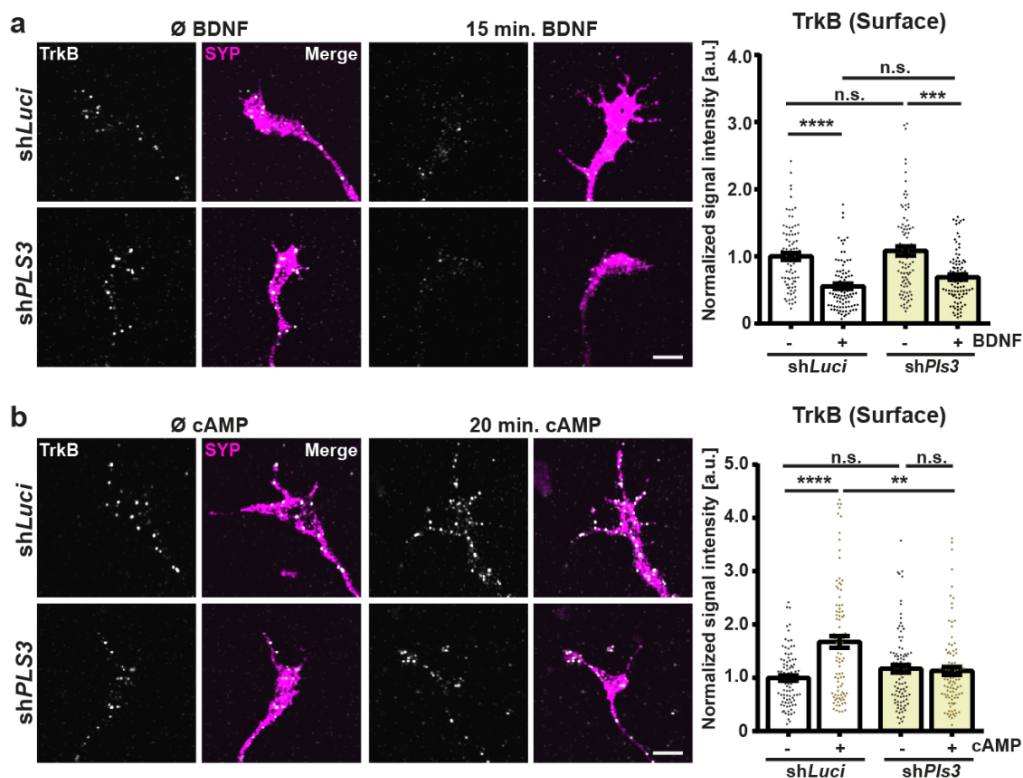
Fig. 19: Knockdown of Pls3 interferes with cAMP-mediated TrkB cell surface translocation. a) – b) *shLuci and shPls3 growth cones stained against surface TrkB (gray) and Synaptophysin-1 (SYP, magenta). Normalized mean gray values of surface TrkB upon* ***a)*** *15 min. BDNF stimulation (n=4, N=90; ANOVA Kruskal-Wallis test, *** p ≤ 0.001; **** p ≤ 0.0001; n.s. not significant) and* ***b)*** *20 min. 8-CPT-cAMP stimulation within axon terminals from shLuci and shPls3 motoneurons (n=4, N=95; ANOVA Kruskal-Wallis test, ** p ≤ 0.01; **** p ≤ 0.0001; n.s. not significant). Data are presented as scatter dot plot with bar. Bar represent the mean ± SEM. Scale bars: 5 µm.*

3.3.4. Pls3 knockdown affects Ca$_v$2.2 localization and functionality

In addition to BDNF/TrkB signaling, we wanted to check whether additional transmembrane proteins within the growth cones are affected similarly by Pls3 knockdown. Therefore, we decided to examine the localization and functionality of VGCCs as they were shown to be affected in SMA (Jablonka et al., 2007). Immunostainings of *shPls3* motoneurons revealed significantly reduced levels of Ca$_v$2.2 within axon terminals (**Fig. 20 a**). Moreover, using high-resolution SIM images we could observe high-density cluster-like accumulations of Ca$_v$2.2 in growth cones and especially filopodia of control motoneurons, which were greatly diminished in *shPLS3* growth cones (**Fig. 20 b**). Lastly, investigations of the spontaneous Ca^{2+} influx showed that Pls3 knockdown motoneurons suffer from significantly reduced frequencies of spontaneous Ca^{2+} transients within their axon terminals in contrast to the control *shLuci* motoneurons (**Fig. 20 c**).

Altogether we conclude that knocking down Pls3 in motoneurons phenocopies the SMA phenotype of cultured motoneurons indicating its involvement in the dynamic presentation and activation of TrkB.
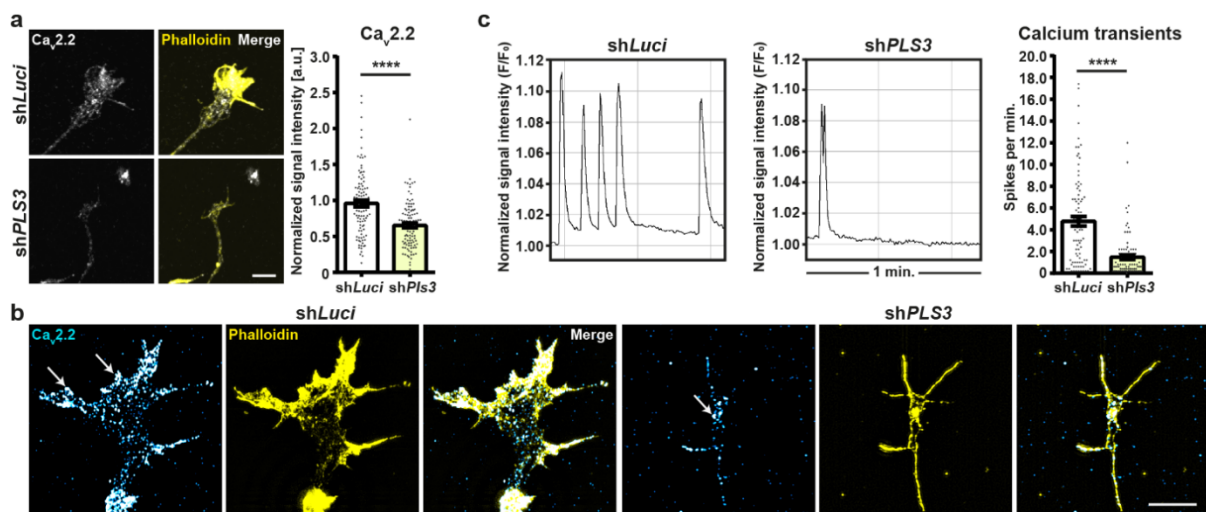
***Fig. 20: Knockdown of Pls3 interferes with Ca$_v$2.2 localization, cluster-like formation and function. a)** shLuci and shPls3 growth cones stained against Ca$_v$2.2 (gray) and F-actin (Phalloidin, yellow). Normalized mean gray values of Ca$_v$2.2 (n=4, N=100; Mann-Whitney test; **** p ≤ 0.0001). **b)** Maximum intensity projections of SIM images of shLuci and shPls3 growth cones stained against Ca$_v$2.2 (cyan) and F-actin (Phalloidin, yellow). Arrows indicate high-density, cluster-like formations of Ca$_v$2.2. **c)** Representative plots of Cal-900™ AM fluorescent changes over 5 min. indicating spontaneous Ca^{2+} spikes per min. of shLuci and shPls3 growth motoneurons. Quantification of spontaneous Ca^{2+} spikes per min. (n=5; N=89; Mann-Whitney test; **** p ≤ 0.0001). Data are presented as scatter dot plot with bar. Bar represent the mean ± SEM. Scale bars: 5 µm.*

To confirm that the observed defects after Pls3 knockdown are indeed attributable to the lack of Pls3 and not caused by unspecific off-target effects, a "Rescue" plasmid was constructed harboring a shRNA-resistant, HA-tagged version of hPLS3 that was cloned into the shPLS3-contaning plasmid. Control motoneurons transduced with a lentivirus delivering this plasmid showed lower levels of endogenous murine *Pls3* and simultaneously overexpressed *hPLS3* (**Fig. 21 a**). Although these alterations in mRNA expression were not significant (probably due to the low number of experiments), it can be assumed that HA-positive neurons are expressing the tagged hPLS3 that counteracts the shRNA-mediated Pls3 knockdown. Indeed, cells transduced with this virus neither show disturbed axon elongation (**Fig. 21 b**), nor altered growth cone size (**Fig. 21 c**).

Furthermore, no changes in total TrkB or its BDNF-mediated phosphorylation were observed in these cells (**Fig. 21 d – e**), confirming that the morphological abnormalities and affected TrkB localization and activation that are present upon Pls3 knockdown are specific effects due to the lack of the protein.
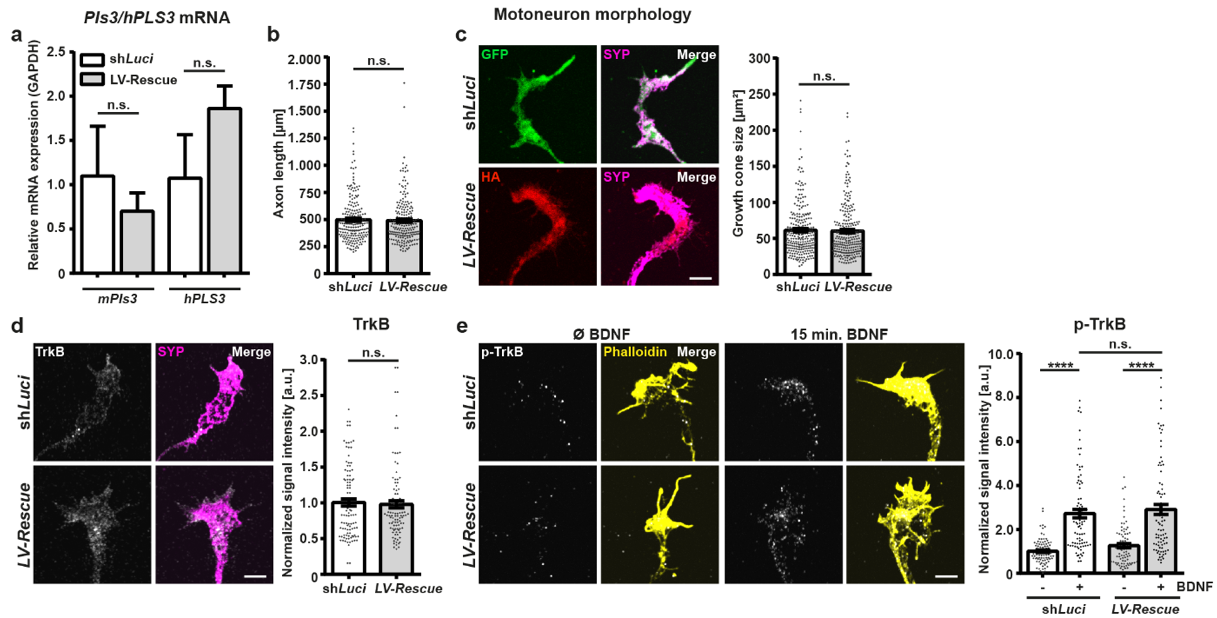

Fig. 21: Verification for Pls3 knockdown-specific effects*. **a)** Relative expression of murine Pls3 and human PLS3 in whole cell lysates of shLuci and LV-Rescue motoneurons. Quantification of mPls3/hPLS3 relative to GAPDH (N=3; ANOVA Kruskal-Wallis test, n.s. not significant). Bars represent the mean ± SD. **b) – c)** LV-Rescue transduction for hPLS3-HA-mediated overexpression that rescues shRNA-mediated Pls3 knockdown does not influence **b)** axon length (µm) (n=3; N=210; shLuci: 496.4 ± 14.4 µm, LV-Rescue: 489.2 ± 14.8 µm; Mann-Whitney test, n.s. not significant) and **c)** growth cone size (µm2) (n=4; N=255; shLuci: 61.37 ± 2.32 µm2, LV-Rescue: 60.46 ± 2.37 µm2; Mann-Whitney test). **c)** Representative images of shLuci and LV-Rescue lentivirus-infected, GFP- (green) or HA- (red) expressing DIV7 motoneurons stained against Synaptophysin-1 (SYP, magenta). **d)** shLuci and LV-Rescue growth cones stained against TrkB (gray) and Synaptophysin-1 (SYP, magenta). Normalized mean gray values of TrkB (n=3, N=100; Mann-Whitney test, n.s. not significant). **e)** shLuci and LV-Rescue growth cones unstimulated and 15 min. BDNF stimulated stained against p-TrkB (gray) and F-actin (Phalloidin, yellow). Normalized mean gray values of p-TrkB (n=3, N=85; ANOVA Kruskal-Wallis test, **** p ≤ 0.0001; n.s. not significant). Data are presented as scatter dot plot with bar / bar. Bar represent the mean ± SEM (except for a)). Scale bars: 5 µm.*

3.4. Overexpression of hPLS3 improves the phenotype of Smn-deficient motoneurons

3.4.1. Overexpression of hPLS3 rescues the morphological abnormalities and improves actin dynamics in SMA motoneurons

Given the fact that a lack of Pls3 causes pathological features that resemble those observed upon Smn deficiency, we hypothesized that increasing the levels of Pls3 would rescue the phenotype of SMA motoneurons. Therefore, $Smn^{-/-};SMN2$ and control motoneurons were transduced with a lentivirus delivering $hPLS3$ together with mCh (LV-$hPLS3$) or a control virus containing mCh only (LV-mCh) and cultured until DIV7. A robust overexpression of hPLS3 was confirmed via RT-PCR analysis of RNA extracts obtained from whole cell lysates of control motoneurons (**Fig. 22 a**). To see whether an overexpression of hPLS3 has a beneficial effect on cultured SMA motoneurons, we performed morphological analysis of the transduced, mCh positive cells. Interestingly, expression of hPLS3 in SMA motoneurons rescued the impaired axon length (**Fig. 22 b**) and markedly improved the growth cone size and morphology (**Fig. 22 c**). In contrast to SMA motoneurons, the overexpression of hPLS3 in control motoneurons did not influence their axon elongation or differentiation.
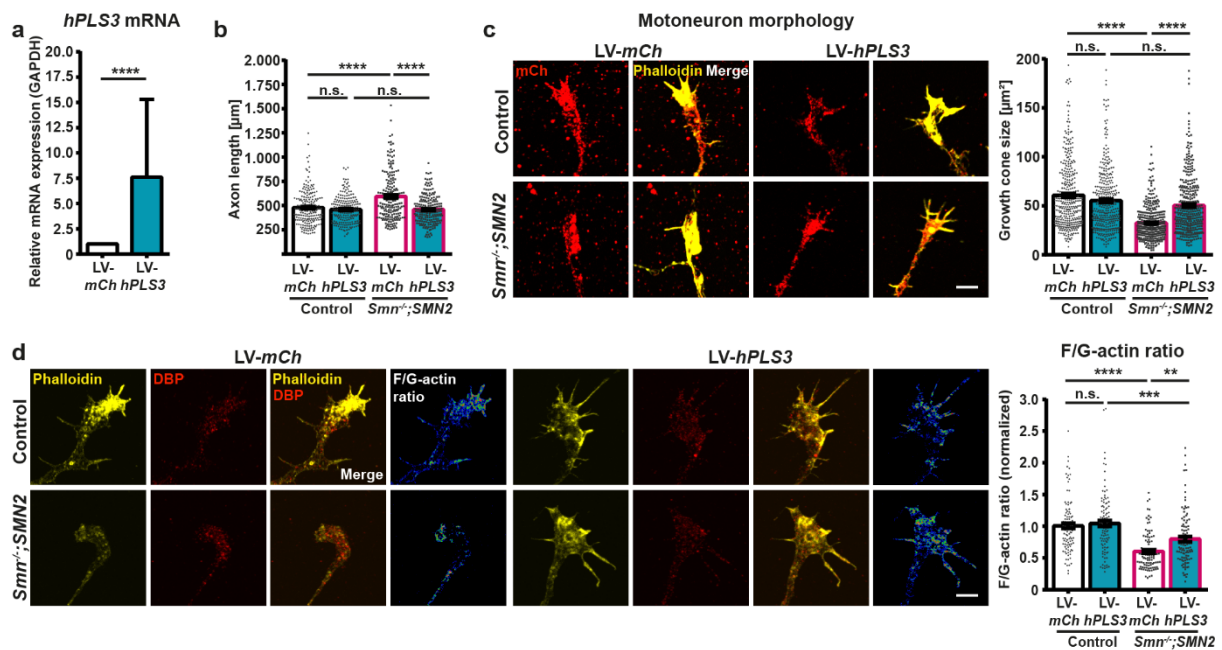
Fig. 22: Overexpression of hPLS3 ameliorates motoneuron differentiation and growth cone morphology.
*a) Relative expression of hPLS3 in whole cell lysates of LV-mCh and LV-hPLS3 transduced control motoneurons. Quantification of hPLS3 relative to GAPDH (n=6, N=10; Mann-Whitney test, **** p ≤ 0.0001). Data are presented as mean ± SD. b) – c) hPLS3 overexpression in Smn$^{-/-}$;SMN2 motoneurons results in b) rescued axon length (n=3; N=200; 478.8 ± 12.5 µm / 460.1 ± 9.8 µm / 593.7 ± 17.1 µm / 459.1 ± 10.2 µm; ANOVA Kruskal-Wallis test, **** p ≤ 0.0001; n.s. not significant) and c) increased growth cone size (n=6; N=350; 60.74 ± 1.85 µm2 / 55.24 ± 1.73 µm2 / 32.38 ± 0.91 µm2 / 50.30 ± 1.58 µm2; ANOVA Kruskal-Wallis test, **** p ≤ 0.0001; n.s. not significant). c) Representative images of LV-mCh and LV-hPLS3 transduced control and Smn$^{-/-}$;SMN2 DIV7 mCh-expressing stained against F-actin (Phalloidin, yellow). d) LV-mCh and LV-hPLS3 transduced control and Smn$^{-/-}$;SMN2 growth cones stained against F-actin (Phalloidin, yellow) and G-actin (Vitamin D-binding protein (DBP), red). Ratiometric images demonstrating the F/G-actin ratio. Quantification of the normalized F/G-actin ratio (n=3, N=102; ANOVA Kruskal-Wallis test, ** p ≤ 0.01; *** p ≤ 0.001; **** p ≤ 0.0001; n.s. not significant). Data are presented as scatter dot plot with bar / bar. Bar represent the mean ± SEM (except for a)). Scale bars: 5 µm.*

To investigate whether the upregulation of Pls3 impacts the actin cytoskeleton we aimed to analyze the ratio of F/G-actin within the axon terminals of motoneurons. Therefore, F-actin was visualized with fluorescently probed Phalloidin, while G-actin was labeled by Vitamin D-binding proteins (DBP) and the respective antibodies (Lee et al., 2013). Quantification of the amount of F-actin revealed diminished levels in *Smn^{−/−};SMN2* motoneurons which was reflected by a significantly rescued F/G-actin ratio (**Fig. 22 d**). In contrast to that, SMA motoneurons overexpressing hPLS3 displayed higher levels of F-actin leading to a markedly improved F/G-actin ratio in these motoneurons (**Fig. 22 d**).

Furthermore, to test whether Pls3 is functionally participating in the dynamic remodeling of the actin cytoskeleton within axon terminals, we used a live-cell imaging of SiR-actin incubated DIV7 motoneurons. Monitoring axon terminals over a time period of 20 min. revealed that filopodia from Smn-deficient neurons transduced with LV-*mCh* displayed markedly decreased actin movements (**Fig. 23 a**). However, overexpressing hPLS3 in *Smn^{−/−};SMN2* significantly improved the amplitude of actin movements within filopodia (**Fig. 23 b**) and the velocity (moved distance over time) of filopodia movements (**Fig. 23 c**).

In conclusion, upregulation of Pls3 in SMA motoneurons impressively rescues their morphological abnormalities and improves the dynamic actin movements within their axon terminals.
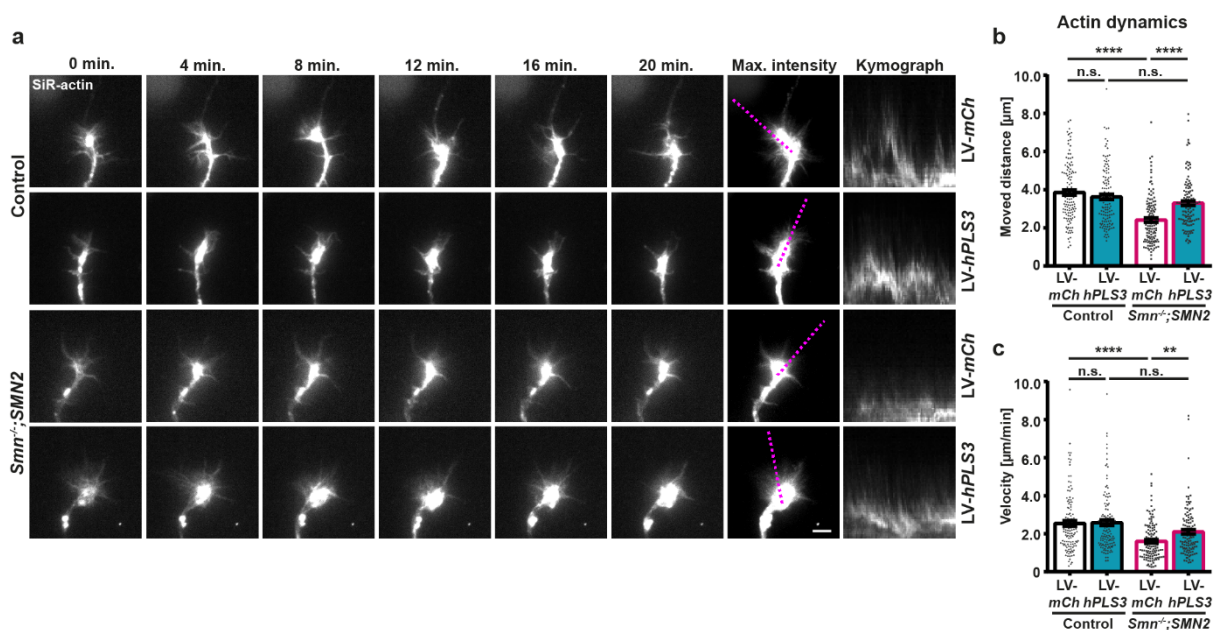
Fig. 23: Overexpression of hPLS3 functionally improves actin dynamics. a) *LV-mCh and LV-hPLS3 transduced control and Smn^{−/−};SMN2 growth cones with SiR-actin were monitored for 20 min. ROI (purple dotted line) of a single filopodia with the corresponding kymograph. Quantification of the **b)** moved distance (µm) of single filopodia (n=3; N=122; ANOVA Kruskal-Wallis test, **** p ≤ 0.0001; n.s. not significant) and **c)** the velocity (distance (µm) over time (min)) of single filopodia (n=3; N=122; ANOVA Kruskal-Wallis test, ** p ≤ 0.01; **** p ≤ 0.0001; n.s. not significant) in LV-mCh and LV-hPLS3 transduced control and Smn^{−/−};SMN2 growth cones. Data are presented as scatter dot plot with bar. Bar represent the mean ± SEM (except for **a)**). Scale bar: 5 µm.*

3.4.2. Overexpression of hPLS3 counteracts the impaired TrkB localization and activation in SMA motoneurons

In order to assess the effects of hPLS3 overexpression on the presence and surface translocation of TrkB, we performed immunostainings on transduced SMA motoneurons cultured until DIV7. Quantification of the TrkB signal intensity revealed that total TrkB levels were slightly increased in hPLS3-expressing *Smn^{-/-};SMN2* motoneurons (**Fig. 24 a**).

High-resolution SIM images were generated to further confirm these results (**Fig. 24 b**). Moreover, the higher spatial resolution obtained by SIM revealed that cluster-like TrkB structures are present in control motoneurons (independent from virus transduction) and Smn-deficient motoneurons overexpressing hPLS3, but are greatly lacking in SMA motoneurons transduced with the LV-*mCh* (**Fig. 24 b**).
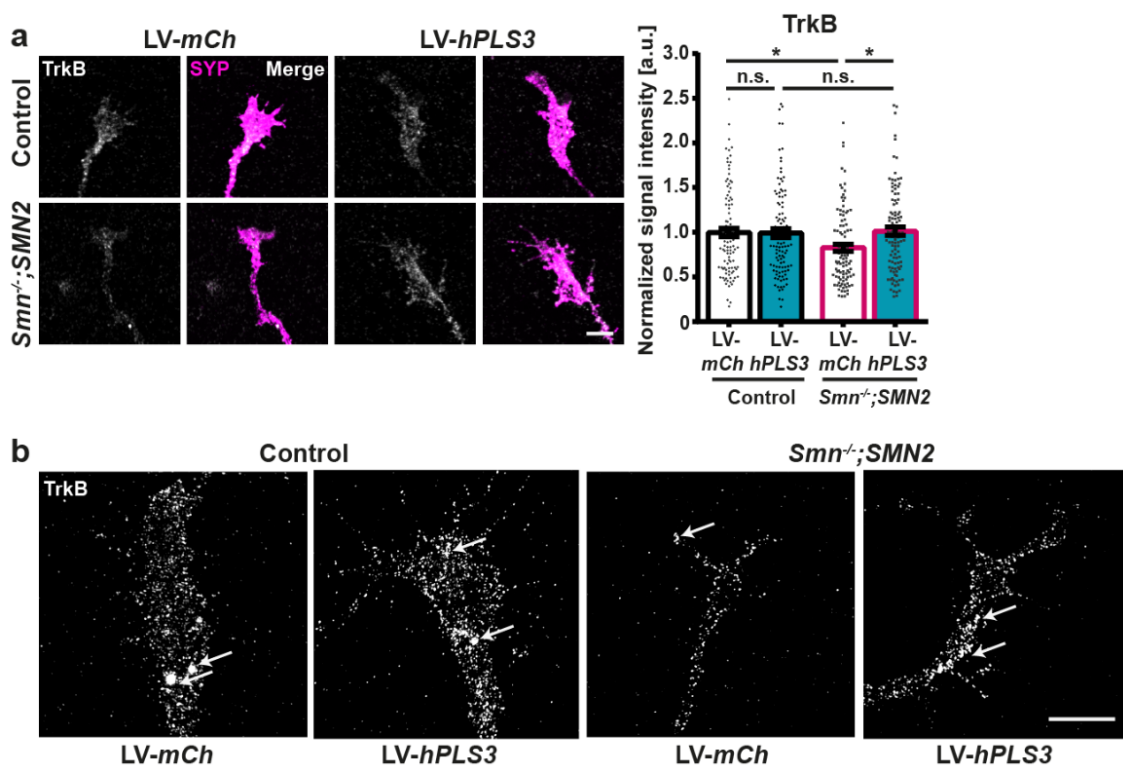
Fig. 24: Overexpression of hPLS3 improves TrkB localization in SMA axon terminals. a) *LV-mCh and LV-hPLS3 transduced control and Smn^{-/-};SMN2 growth cones stained against TrkB (gray) and Synaptophysin-1 (SYP, magenta), Normalized mean gray values of TrkB (n=4, N=105; ANOVA Kruskal-Wallis test, * p ≤ 0.05; n.s. not significant). Data are presented as scatter dot plot with bar. Bar represent the mean ± SEM. Scale bar: 5 µm.* ***b)*** *Maximum intensity projections of SIM images of control and Smn^{-/-};SMN2 growth cones transduced with LV-mCh and LV-hPLS3 stained against TrkB (gray). Arrows indicate TrkB cluster-like formations. Scale bar: 5 µm.*

Given the high resolution of about 100 nm obtained by SIM, we aimed to further investigate the spatial relation of Pls3, TrkB and the actin cytoskeleton. As impressively shown in **Fig. 25 (first lane, a' - a'')** in control motoneurons, Pls3 is tightly associated along actin filaments, validating its role as actin-bundler. Moreover, TrkB is highly associated along these actin filaments pointing to a possible mechanistic scenario in which TrkB is transported along these Pls3-bundles actin filaments. In comparison to control motoneurons, Smn-deficient motoneurons transduced with LV-*mCh* displayed highly diminished levels of F-actin, Pls3 and TrkB (**Fig. 25, third lane**).

However, by hPLS3 overexpression which was reflected by higher Pls3 signal intensities (**Fig. 25, fourth lane**), SMA motoneurons showed increased levels F-actin, more Pls3-bundled actin filaments and higher TrkB quantities, which further highlight the beneficial effects of hPLS3 overexpression on Smn-deficient cells.
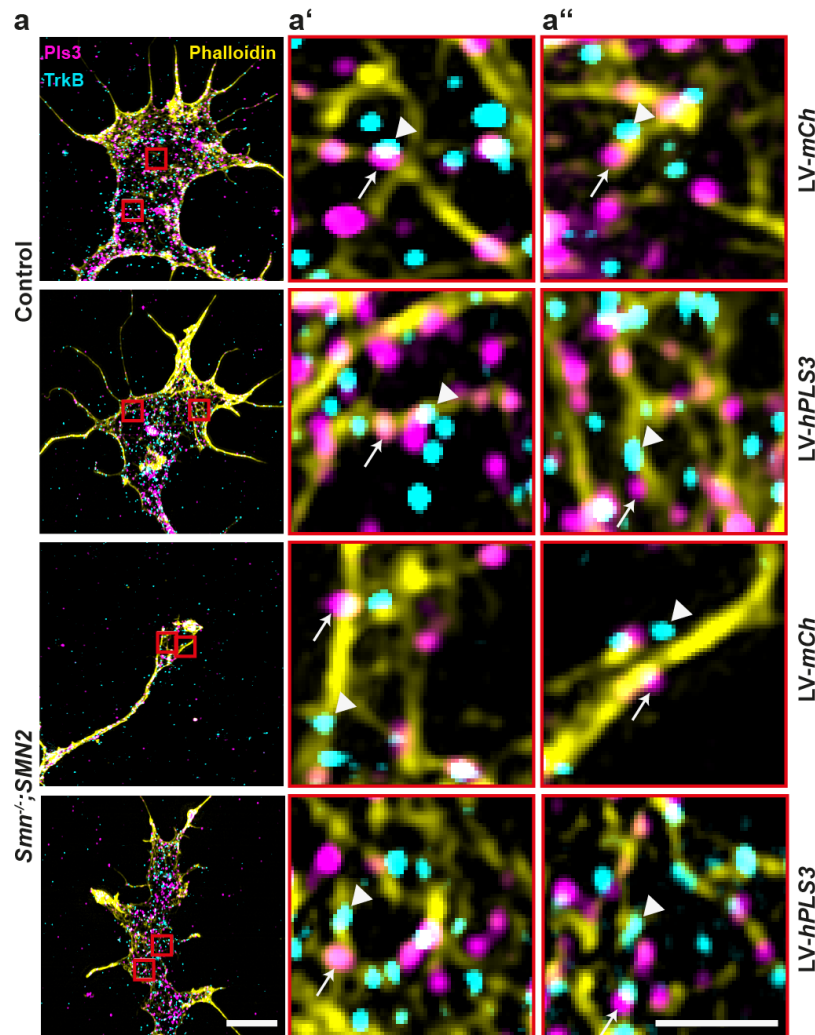

Fig. 25: Spatial relation of Pls3-bundled actin filaments and TrkB. a) Maximum intensity projections of SIM images of control and Smn⁻/⁻;SMN2 growth cones transduced with LV-mCh and LV-hPLS3 stained against Pls3 (magenta), TrkB (cyan) and F-actin (Phalloidin, yellow), scale bar: 5 µm. a') and a'') Zoomed in detail images of a). Arrows indicate Pls3, and arrowheads indicate TrkB along actin filaments. Scale bar: 1 µm.

Next, live-cell staining was performed to see the localization of TrkB at the plasma membrane and whether Pls3 functionally participates in the transport of TrkB along actin filaments as indicated by the previous SIM images (**Fig. 25**).

As endocytosis of the receptor after BDNF stimulation was not altered (**Fig. 13**), but the activity-induced increase in TrkB membrane translocation was absent in Smn-deficient cells (**Fig. 14 a**), we tested whether this defect can be rescued by hPLS3 overexpression. Indeed, when hPLS3 was overexpressed in motoneurons lacking Smn, 8-CPT-cAMP stimulation was efficiently triggering the recruitment of TrkB to the cell surface within axon terminals (**Fig. 26**). This further argues that Pls3 is required for the proper translocation of transmembrane receptors from the intracellular store to the cell surface.
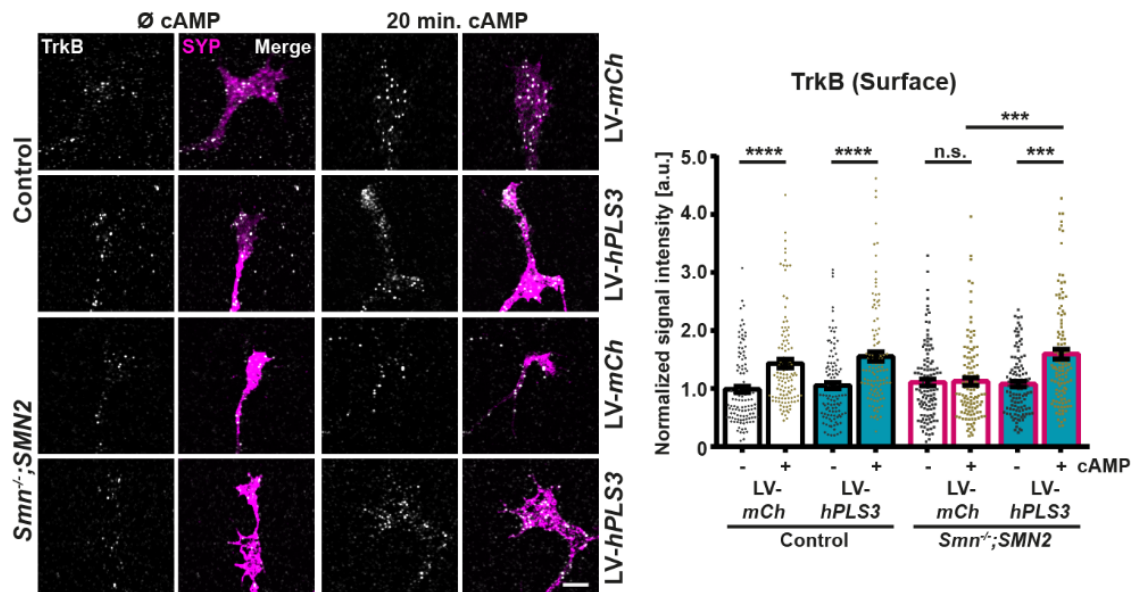
Fig. 26: Overexpression of hPLS3 rescues deficient cAMP-induced cell surface translocation of TrkB in SMA axon terminals. *LV-mCh and LV-hPLS3 transduced control and Smn$^{-/-}$;SMN2 growth cones unstimulated and 20 min. 8-CPT-cAMP stimulated stained against surface TrkB (gray) and Synaptophysin-1 (SYP, magenta). Normalized mean gray values of surface TrkB (n=4, N=115; ANOVA Kruskal-Wallis test, *** p ≤ 0.001; **** p ≤ 0.0001; n.s. not significant). Data are presented as scatter dot plot with bar. Bar represent the mean ± SEM. Scale bar: 5 μm.*

As a subsequent step, we focused on the activation of the receptor. BDNF stimulation failed to induce a transient increase in p-TrkB immunoreactivity in Smn-deficient axon terminals; however, lentivirus-mediated hPLS3 overexpression was able to rescue this defect. After 15 min. BDNF exposure, hPLS3-overexpressing *Smn$^{-/-}$;SMN2* showed a marked raise in p-TrkB levels within their growth cones (**Fig. 27 a**). To test if the activation of TrkB is indeed functional, we assessed the activation of downstream signaling cascades. Therefore, motoneurons were again stimulated with BDNF and the activation of the downstream PI3K – Akt pathway downstream was examined using a p-Akt antibody. Although a slight increase in p-Akt immunosignal was also observed in Smn-deficient cells transduced with LV-*mCh*, this elevation was markedly enhanced upon hPLS3 overexpression (**Fig. 27 b**). In conclusion, increasing Pls3 levels and thereby beneficially modulating the actin cytoskeleton in Smn-deficient motoneurons rescues motoneuron axon elongation and differentiation and restores cAMP-mediated TrkB membrane translation and its BDNF-induced activation.
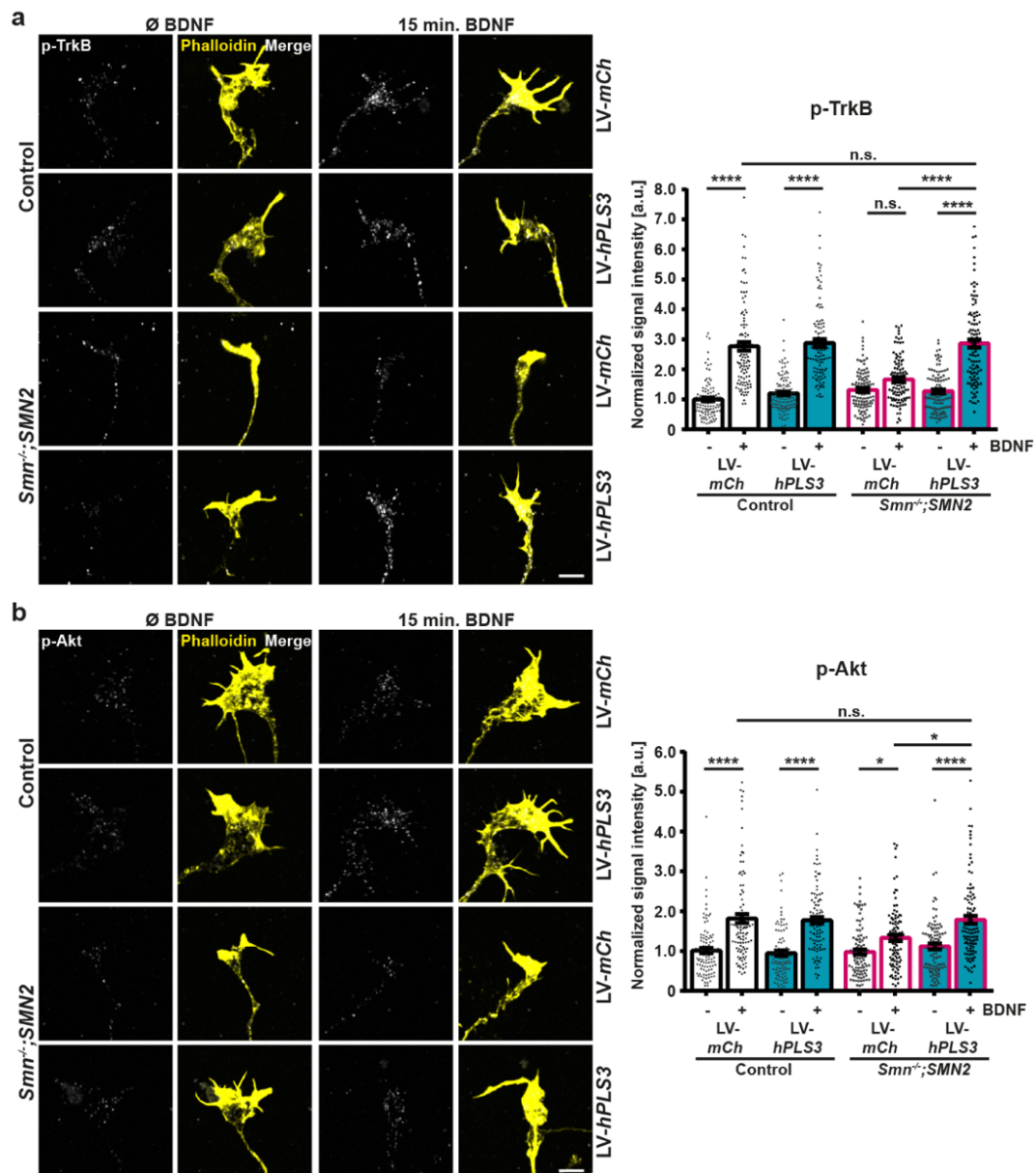
Fig. 27: Overexpression of hPLS3 restores BDNF-induced TrkB activation and downstream Akt phosphorylation in SMA axon terminals. a) – b) *Unstimulated or 15 min. BDNF stimulated growth cones from control and Smn$^{-/-}$;SMN2 motoneurons transduced with LV-mCh and LV-hPLS3 stained against **a)** p-TrkB (gray) or **b)** p-Akt and F-actin (Phalloidin, yellow), scale bars: 5 µm. **a)** Normalized mean gray values of p-TrkB in LV-mCh or LV-hPLS3 transduced control and Smn$^{-/-}$;SMN2 terminals (n=4, N=105; ANOVA Kruskal-Wallis test, **** p ≤ 0.0001; n.s. not significant). **b)** Normalized mean gray values of p-Akt in LV-mCh or LV-hPLS3 transduced control and Smn$^{-/-}$;SMN2 terminals (n=4, N=98; ANOVA Kruskal-Wallis test, * p ≤ 0.05; **** p ≤ 0.0001; n.s. not significant). Data are presented as scatter dot plot with bar. Bar represent the mean ± SEM.*

3.4.3. hPLS3 overexpression improves Ca$_v$2.2. localization, accumulation and spontaneous Ca^{2+} influx in axon terminals

In order to investigate whether Pls3 beneficially affects further transmembrane proteins, we checked the impact of its overexpression on VGCCs, which were previously shown to be affected in SMA (Jablonka et al., 2007). In a further subset of experiments performed with the support of my colleague Eduardo Palominos-Garcia, the localization of Ca$_v$2.2 and spontaneous Ca^{2+} influx were examined upon hPLS3 overexpression in *Smn$^{-/-}$;SMN2* motoneurons.

Immunocytchemical analysis revealed that the signal intensities of $Ca_v2.2$ was markedly reduced in SMA motoneurons transduced with LV-*mCh*, but hPLS3 overexpression significantly improved the VGCC signal in Smn-deficient growth cones when hPLS3 is overexpressed (**Fig. 28 a**). In addition, high resolution SIM images revealed that the accumulation of $Ca_v2.2$ in cluster-like structures seemed to be impaired in Smn-deficient axon terminals as previously described by (Jablonka et al., 2007), which is strongly improved in Smn-deficient cells overexpressing hPLS3 (**Fig. 28 b**). Moreover, the frequency of spontaneous spike-like Ca^{2+} transients in axon terminals was markedly increased in these cells when compared to SMA motoneurons (**Fig. 28 c**).

Hence, this data implicates that the reconstitution of Pls3 levels and its supportive function on the actin cytoskeleton is in general required for the proper alignment of transmembrane proteins.
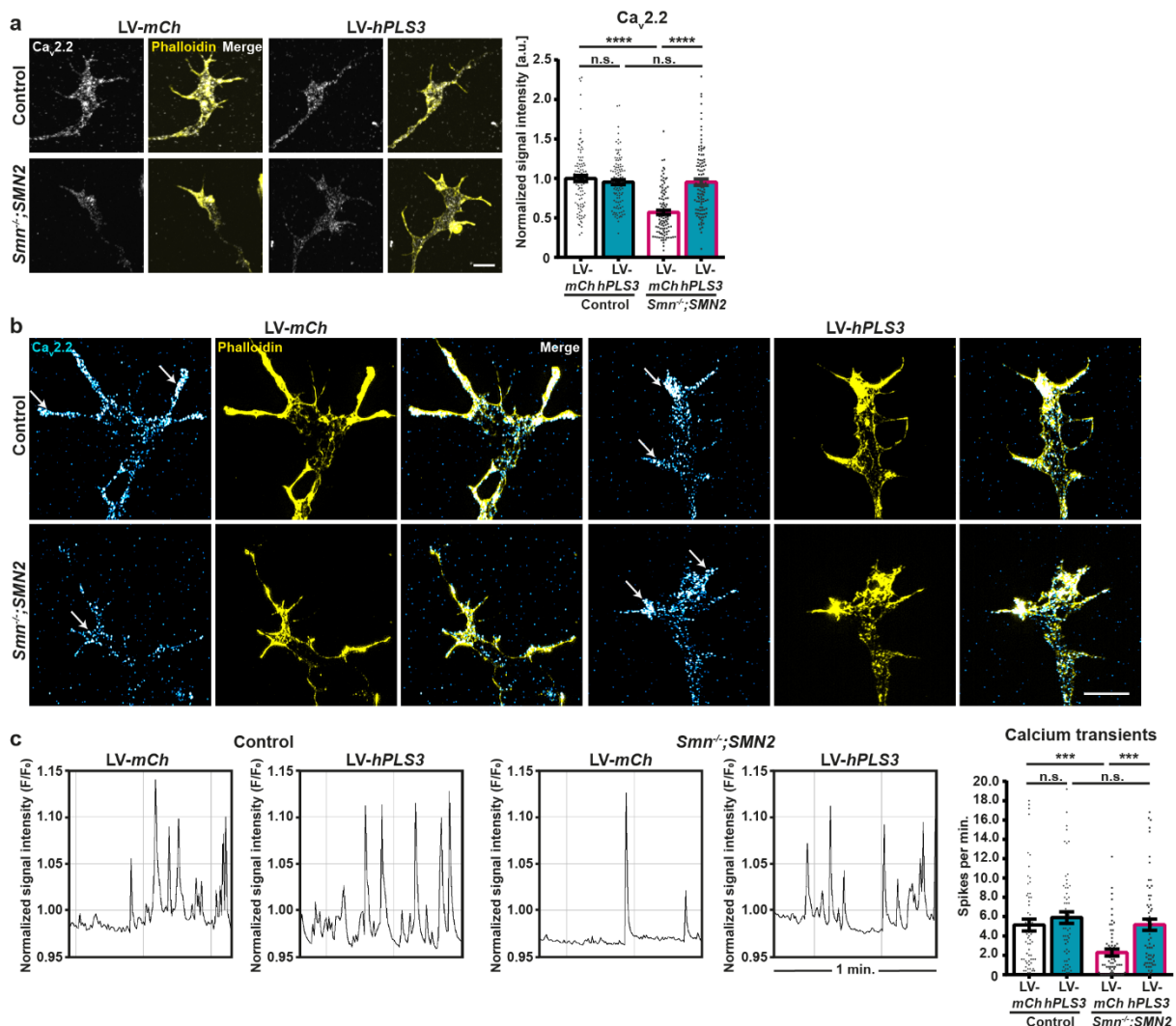
Fig. 28: Overexpression of hPLS3 restores $Ca_v2.2$ localization, cluster-like formation and function. a) *Growth cones from control and Smn⁻/⁻;SMN2 motoneurons transduced with LV-mCh and LV-hPLS3 stained against $Ca_v2.2$ (gray) and F-actin (Phalloidin, yellow) Normalized mean gray values of $Ca_v2.2$ in LV-mCh or LV-hPLS3 transduced control and Smn⁻/⁻;SMN2 terminals (n=5, N=105; ANOVA Kruskal-Wallis test, **** p ≤ 0.0001; n.s. not significant).* ***b)*** *Maximum intensity projections of SIM images of control and Smn⁻/⁻;SMN2 growth cones transduced with LV-mCh and LV-hPLS3 stained against $Ca_v2.2$ (cyan) and F-actin (Phalloidin, yellow). Arrows indicate high-density cluster-like formations of $Ca_v2.2$.* ***c)*** *Representative plots of Oregon Green™ 488 BAPTA-1 fluorescent changes over min. indicating spontaneous Ca^{2+} spikes of control and Smn⁻/⁻ ;SMN2 motoneurons transduced with LV-mCh and LV-hPLS3. Quantification of spontaneous Ca^{2+} spikes per min. (n=4; N=60; ANOVA Kruskal-Wallis, *** p ≤ 0.001). Data are presented as scatter dot plot with bar. Bar represent the mean ± SEM. Scale bars: 5 µm.*

3.5. The reconstitution of TrkB surface levels after BDNF stimulation is disturbed in SMA motoneurons

3.5.1. The actin-dependent process of TrkB surface level recovery after BDNF stimulation is disturbed in upon Smn deficiency

As apparent from the data generated so far, baseline TrkB levels on the cell surface and its BDNF-induced internalization are not affected in Smn-deficient motoneurons. Therefore, it is not clear why TrkB phosphorylation after BDNF stimulation is greatly diminished in the axon terminals of these neurons compared to controls. A possible mechanistic scenario that could explain the failure in TrkB activation in SMA motoneurons is based on the described self-amplifying actions of BDNF (Cheng et al., 2011) together with the observation that the activity-dependent TrkB membrane translocation is disturbed upon Smn deficiency. Cheng and colleagues reported that BDNF acts in an autocrine manner, by which cAMP levels are elevated following TrkB activation that in turn promotes further membrane translocation and local availability of TrkB resulting in a signal amplification (Cheng et al., 2011). Furthermore, the fact that the marked increase in p-TrkB immunoreactivity after BDNF exposure is abolished by pre-treatment with CytoD in control motoneurons, and the actin-dependency of TrkB translocation, implicate that the disturbed actin cytoskeleton in SMA plays a key role in this scenario.
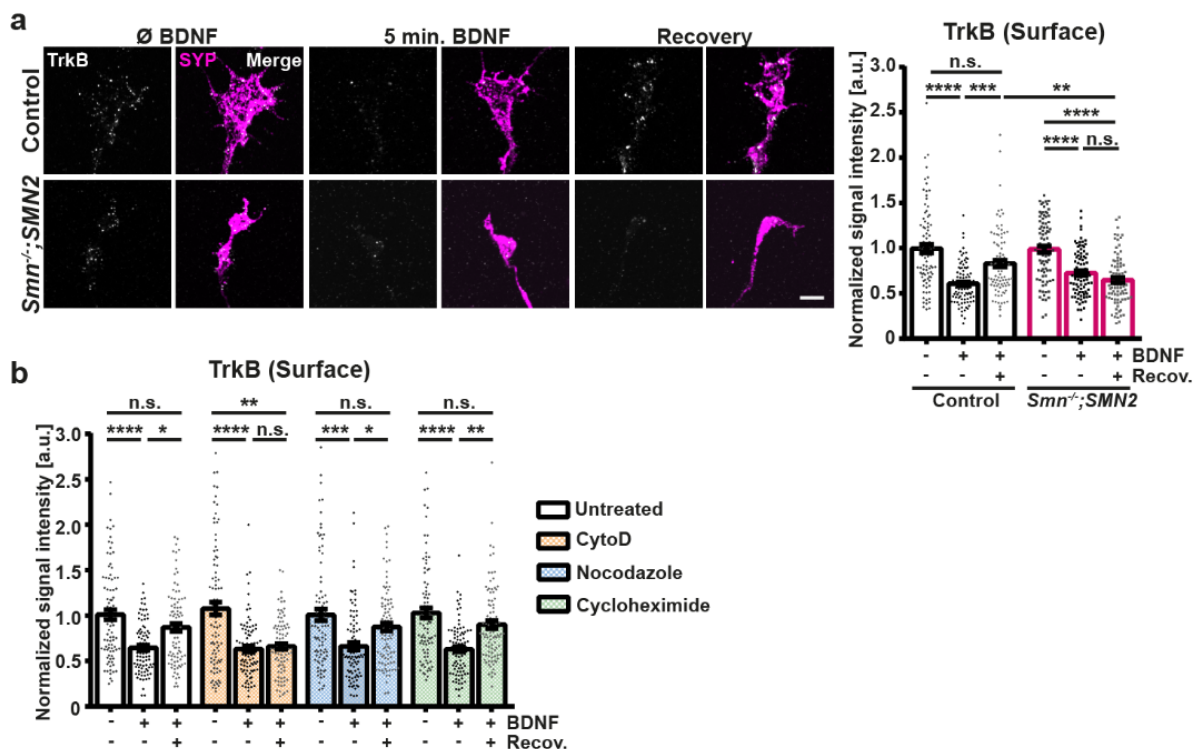

Fig. 29: Retranslocation of surface TrkB surface upon BDNF stimulation is dysfunctional in SMA axon terminals. a) *Control and Smn⁻/⁻;SMN2 growth cones unstimulated and stimulated for 5 min. BDNF followed by a 10 min. recovery phase (recovery assay) stained against surface TrkB (gray) and Synaptophysin-1 (SYP, magenta), scale bar: 5 µm. Normalized mean gray values of surface TrkB (n=3, N=90; ANOVA Kruskal-Wallis test, ** p ≤ 0.01; *** p ≤ 0.001; **** p ≤ 0.0001; n.s. not significant).* ***b)*** *Normalized mean gray values of surface TrkB in axon terminals of control motoneurons that were treated with 0,5 µM CytoD, 10 µM Nocodazole and 20 µM Cycloheximide prior to the recovery assay (n=4, N=90; ANOVA Kruskal-Wallis test, * p ≤ 0.05; ** p ≤ 0.01; *** p ≤ 0.001; **** p ≤ 0.0001; n.s. not significant). Data are presented as scatter dot plot with bar. Bar represent the mean ± SEM.*

To test this hypothesis, we used our live-cell staining assay to examine the reconstitution of TrkB cell surface levels after exposure to its ligand. Prior to the surface TrkB staining, motoneurons were stimulated with BDNF for 5 min. before the BDNF-containing medium was washed out and they were allowed to recover for 10 min. Similar to our previous results (**Fig. 13 a**), BDNF stimulation alone promoted the internalization of TrkB leading to a decrease in cell surface TrkB levels (**Fig. 29 a**). However, during the recovery time of 10 min. after BDNF stimulation the quantity of receptors at the plasma membrane of growth cones started to reconstitute in control motoneurons (**Fig. 29 a**). In contrast to control neurons, in axon terminals of Smn-deficient motoneurons no increase in surface TrkB levels could be detected after the recovery period (**Fig. 29 a**). Hence, these observations demonstrate that TrkB is re-located to the plasma membrane after it has been endocytosed in response to BDNF stimulation and that this process is impaired in SMA motoneurons. To confirm that the TrkB recovery is mediated via the actin cytoskeleton, the experiment was performed on control motoneurons that were pre-treated with CytoD, and in addition Nocodazole that blocks microtubule polymerization or CHX to interfere with protein synthesis. Similar to our previous observation that cAMP-induced TrkB recruitment is abolished when the actin cytoskeleton was disrupted, CytoD treatment prior to the recovery assay prevented to reconstitution of surface TrkB after BDNF stimulation in growth cones of motoneurons (**Fig. 29 b**). In contrast to that, blockage of microtubule polymerization by incubation with Nocodazole had no effect on TrkB recovery in axon terminals (**Fig. 29 b**). Moreover, the fact that inhibition of protein translational elongation by CHX does not prevent the re-location of TrkB to the cell surface (**Fig. 29 b**) provides evidence that TrkB is recruited from an already available intracellular pool instead of being dependent on newly synthesized proteins.

3.5.2. Pls3 is involved in the recovery of cell surface TrkB after BDNF stimulation

Focusing on the actin cytoskeleton as key player in TrkB translocation, we wanted to test whether a lack of Pls3 is interfering with the dynamic surface presentation of TrkB after BDNF stimulation. Therefore, the recovery assay was performed on motoneurons transduced with the sh*Pls3*-containing lentivirus. Similar to the failure in cAMP-mediated TrkB recruitment, no increase in TrkB re-location to the cell surface was detected after recovery in growth cones of Pls3 knockdown motoneurons (**Fig. 30 a**). On the other hand, overexpression of hPLS3 in *Smn⁻ᐟ⁻;SMN2* motoneurons beneficially modified the actin cytoskeleton resulting in a significant improvement of TrkB recruitment during the recovery phase following BDNF stimulation compared to LV-*mCh* transduced *Smn⁻ᐟ⁻;SMN2* motoneurons (**Fig. 30 b**).
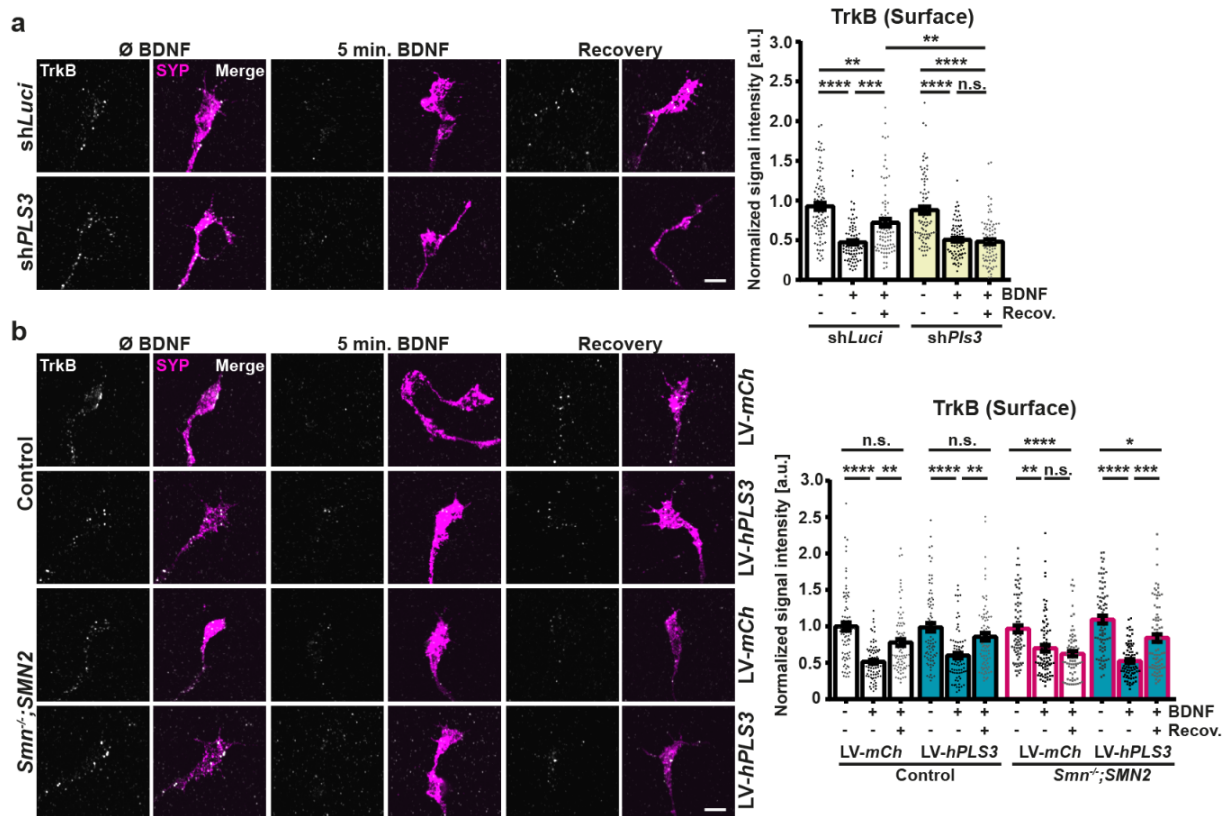
Fig. 30: Pls3 functionally participates in the TrkB surface recovery after BDNF stimulation in motoneuron axon terminals. *a) shLuci and shPls3 growth cones subjected to the recovery assay and stained against surface TrkB (gray) and Synaptophysin-1 (SYP, magenta). Normalized mean gray values of surface TrkB (n=3, N=85; ANOVA Kruskal-Wallis test, ** p ≤ 0.01; *** p ≤ 0.001; **** p ≤ 0.0001; n.s. not significant). b) LV-mCh and LV-hPLS3 transduced control and Smn⁻/⁻;SMN2 growth cones were subjected to the recovery assay and stained against surface TrkB (gray) and SYP (magenta). Normalized mean gray values of surface TrkB (n=3, N=80; ANOVA Kruskal-Wallis test, * p ≤ 0.05; ** p ≤ 0.01; *** p ≤ 0.001; **** p ≤ 0.0001; n.s. not significant). Data are presented as scatter dot plot with bar. Bar represent the mean ± SEM. Scale bars: 5 µm.*

As a next step, we wanted to investigate the origin of the rapidly recovered TrkB in more detail to answer the question whether they are recycled receptors that had been on the cell surface before or whether they are recruited from intracellular stores. In order to follow the track of the receptors, we established a TrkB recycling assay on living motoneurons. Therefore, living motoneurons were incubated with the anti-TrkB antibody and secondary antibody prior to the BNDF stimulation to visualize receptors present on the cell surface under basal conditions. After BDNF stimulation and recovery phase, a second round of cell surface TrkB staining with a different secondary antibody was performed to label the recovered receptors. Thus, recovered TrkB that display both fluorescent tags are the recycled receptors that were present at the surface before (**Fig. 31 a**). In control motoneurons, the baseline TrkB quantities are reconstituted to ~67 % during the recovery phase. Interestingly, approximately half of the receptors (57.7 %) are labeled with both fluorescent tags showing that they are recycled receptors (**Fig. 31 b**). In terminals of *Smn⁻/⁻;SMN2* motoneurons only ~40 % of the basal TrkB surface level are detectable upon recovery, confirming that the re-location of TrkB initiated after BDNF exposure is impaired in these neurons.

However, the rate of recycled receptor is similar in Smn-deficient (55.8 %) and control motoneurons. To improve the actin dynamics in SMA motoneurons, we overexpressed hPLS3 in these neurons and performed the TrkB recycling assay. Increasing the levels of hPLS3 resulted in a restoration of the baseline TrkB numbers to ~72 % following recovery after BDNF stimulation (**Fig. 31 b – c**). Thus, this set of experiments revealed that the impaired reconstitution of surface TrkB levels that is initiated after BDNF stimulation seen in SMA motoneurons is resulting from an actin-dependent translocation defect of intracellular available TrkB, which can be rescued by overexpression of hPLS3. The mechanism of rapid recycling of cell surface receptors doesn't seem to be disturbed upon Smn deficiency, since the rate of recycled receptors is similar in control (57.7 %) and Smn-deficient axon terminals (55.8 %) and is not altered upon hPLS3 overexpression (56.7 %) (**Fig. 31 b – c**).
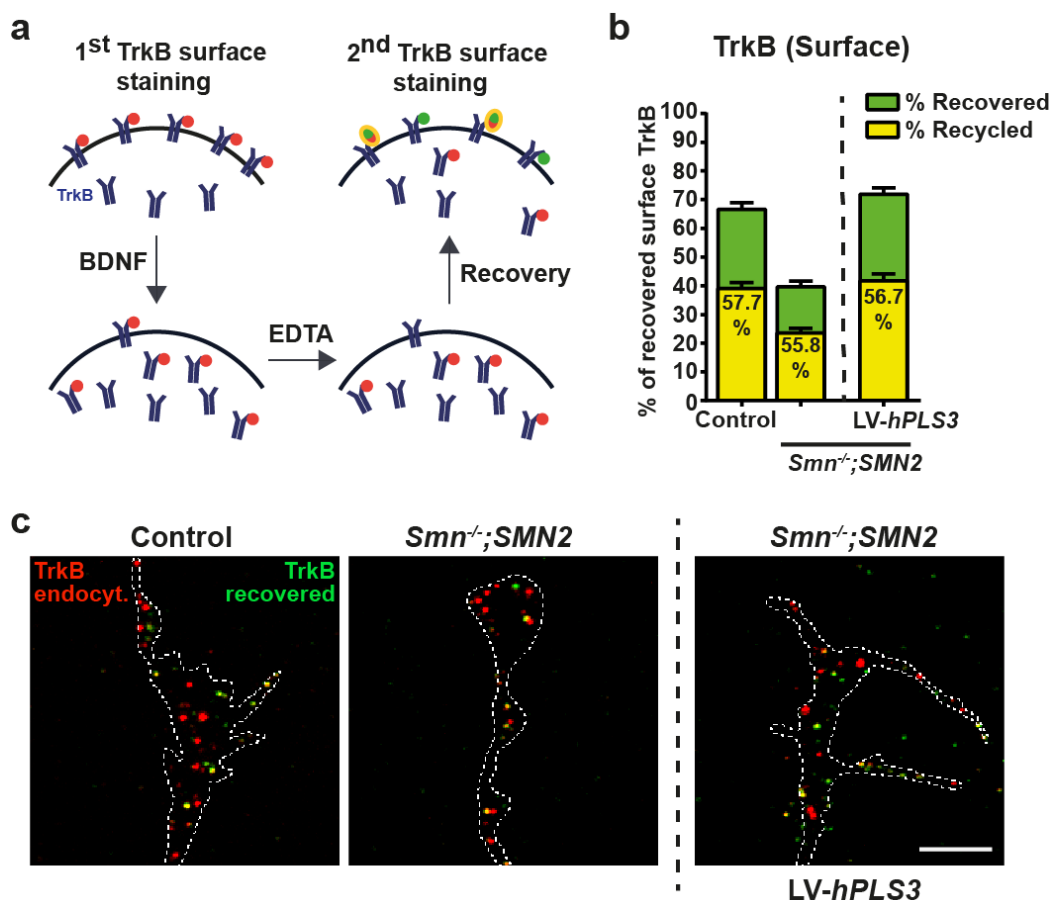

Fig. 31: TrkB recycling assay confirmes defective TrkB cell surface translocation after BDNF stimulation, while TrkB recycling is unaffected in SMA axon terminals. *a) Schematic illustration of the TrkB recycling assay (for details see Methods). b) – c) Growth cones of control, Smn⁻ᐟ⁻;SMN2 and LV-hPLS3-transduced Smn⁻ᐟ⁻;SMN2 motoneurons double stained against surface TrkB (red= receptors that have been on the cell surface prior to BDNF stimulation, green= receptors located at the cell surface after recovery, yellow= co-localizing). Quantification (n=3, N=98) of (**green**), the number of recovered receptors (percentage of total TrkB) and (**yellow**) the number of recycled receptors (percentage of recovered TrkB). Data are presented as bar. Bar represent the mean ± SEM. Scale bar: 5 µm.*

3.6. The interplay between Pls3 and Arp2/3 is required for proper surface translocation of TrkB

Our results so far revealed that Pls3 is functionally participating in the dynamic actin-dependent cell surface translocation of TrkB from the intracellular pool in response to stimulation. In order to gain further knowledge about the role of Pls3 in this scenario, we wanted to know whether additional actin-modulators play a role and whether there is an interaction with Pls3. One candidate that attracted our interest is the Arp2/3 complex due to two reasons. First, two subunits of the actin nucleator complex, Arpc4 and Arpc1b were identified as downregulated transcripts upon Smn knockdown in the axonal compartment of motoneurons **(Fig. 15 e)**. Second, the Arp2/3 complex was recently found to be diminished in the leading edge of human endothelial cells upon knockdown of PLS3 (Garbett et al., 2020). Arp2/3 is known as actin nucleator that is responsible for the generation of branched actin filaments (Suraneni et al., 2012; Welch et al., 1997; Wu et al., 2012b). Furthermore, it has been shown that Pls3 preferably localizes to Arp2/3-branched actin filaments (Skau et al., 2011). Initially, we checked the levels and distribution of Arp2/3 in Smn-deficient axon terminals using an antibody direct against Arp3 that was also used in the study by Garbett et al., 2020. Intriguingly, in growth cones of Smn-deficient motoneurons we found significantly reduced levels of Arp3 (**Fig. 32 a**). For a better resolution we used SIM to examine the spatial relation of the Arp2/3 complex and Pls3. As already observed with confocal microscopy, in control motoneurons Pls3 is distributed in all places within a growth cone but shows higher abundance in F-actin rich protrusions, while Arp3 is predominantly located in the center of the growth cone (**Fig. 32 b**). Furthermore, SIM confirmed the previous findings showing reduced levels of both proteins in Smn-deficient axon terminals (**Fig. 32 b**).
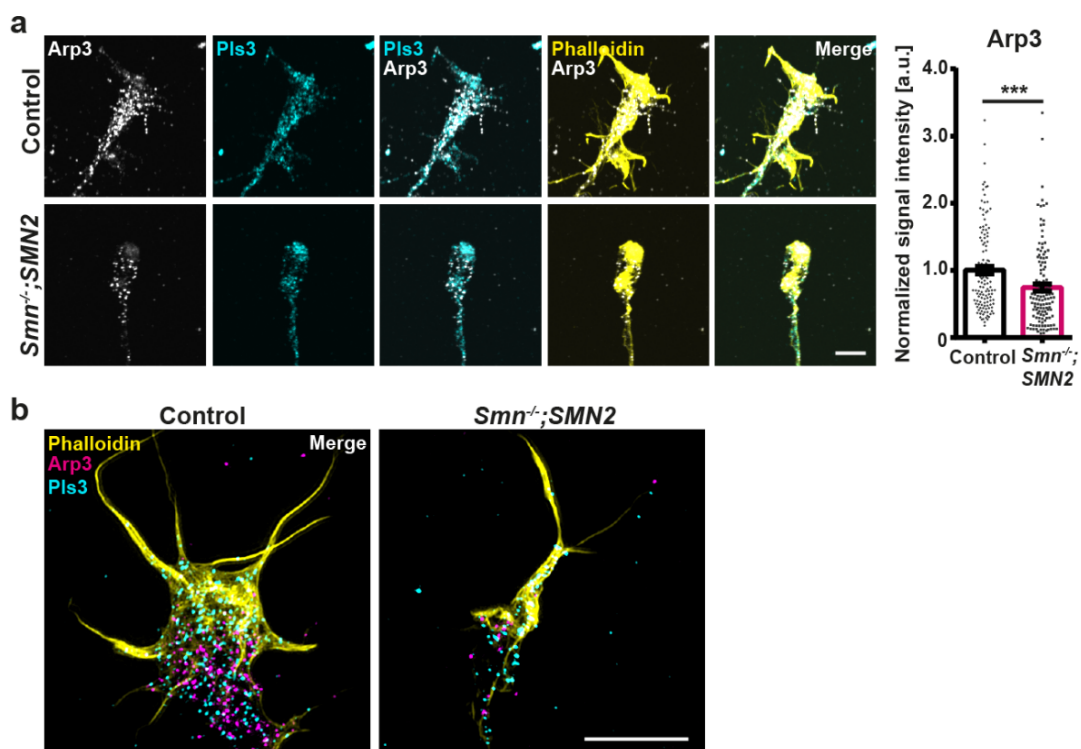

Fig. 32: SMA axon terminals display reduced levels of Arp3. a) *Control and Smn$^{-/-}$;SMN2 growth cones stained against Arp3 (gray), Pls3 (cyan) and F-actin (Phalloidin, yellow). Normalized mean gray values of Arp3 (n=4, N=130; Mann-Whitney test, *** p ≤ 0.001). Data are presented as scatter dot plot with bar. Bar represent the mean ± SEM.* ***b)*** *Maximum intensity projections of SIM images of control and Smn$^{-/-}$;SMN2 growth cones stained against Arp3 (magenta), Pls3 (cyan) and F-actin (Phalloidin, yellow). Scale bars: 5 µm.*

Next, we examined whether absence of Pls3 in motoneurons would diminish the Arp3 levels within axon terminals, similarly to the previous reports in endothelial cells (Garbett et al., 2020). Indeed, control motoneurons transduced with the sh*Pls3*-harboring lentivirus display markedly reduced Arp3 levels in comparison to sh*Luci* control axon terminals (**Fig. 33 a**).

Hence, we hypothesized that overexpression of hPLS3 in Smn-deficient terminals would rescue the altered Arp3 expression. Quantification of the Arp3 signal intensity revealed that expression of hPLS3 in Smn-deficient motoneurons beneficially influenced the presence of Arp3 in their axon terminals leading to increased Arp3 levels in comparison to LV-*mCh* transduced SMA motoneurons (**Fig. 33 b**).
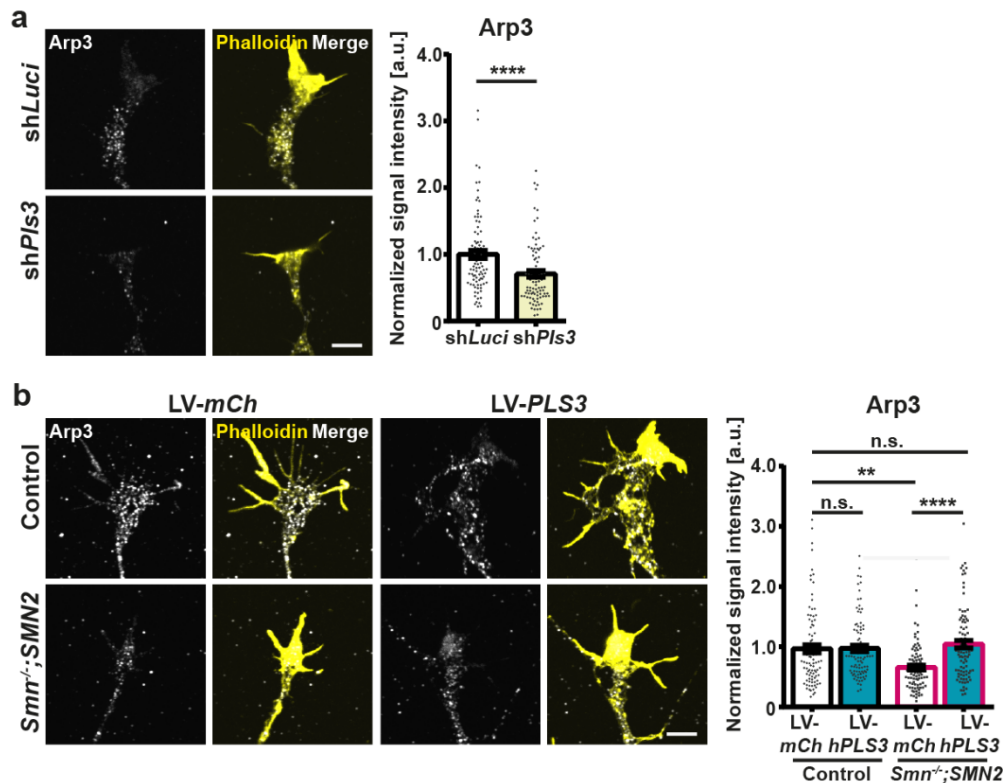

Fig. 33: Pls3 levels and Arp3 levels correlate in motoneuron axon terminals. a) *shLuci and shPls3 growth cones stained against Arp3 (gray) and F-actin (Phalloidin, yellow). Normalized mean gray values of Arp3 (n=3, N=90; Mann-Whitney test, p **** ≤ 0.0001).* **b)** *Growth cones from control and Smn⁻/⁻;SMN2 motoneurons transduced with LV-mCh and LV-hPLS3 stained against Arp3 (gray) and F-actin (Phalloidin, yellow). Normalized mean gray values of Arp3 (n=3, N=90; ANOVA Kruskal-Wallis test, p ** ≤ 0.01; p **** ≤ 0.0001; n.s. not significant). Data are presented as scatter dot plot with bar. Bar represent the mean ± SEM. Scale bars: 5 µm.*

To investigate whether both processes, actin branching by Arp2/3 and actin-bundling by Pls3, are required for proper TrkB membrane recruitment in response to BDNF stimulation, we blocked Arp2/3 activation by the inhibitor CK-666 and performed the TrkB cell surface staining on living motoneurons. Motoneurons were pre-treated with CK-666 for 30 min. prior to the experiments and the following BDNF stimulation and recovery were also performed in presence of CK-666 in the respective media. Quantification of the surface TrkB immunosignal of control motoneurons revealed that similar to Smn deficiency (**Fig. 29 a**), inhibition of actin polymerization by CytoD (**Fig. 29 b**) or Pls3 knockdown (**Fig. 30 a**), the inhibition of Arp2/3 by CK-666 prevents the TrkB cell surface re-location after BDNF stimulation during the recovery phase (**Fig. 34 a**). In contrast to that, no further effect was observed when Smn-deficient motoneurons were treated with the Arp2/3 inhibitor (**Fig. 34 a**).

To see whether the rescuing effect of hPLS3 overexpression on plasma membrane re-location of TrkB is inhibited by blockage of Arp2/3 activation, we performed the same experimental setup on Smn-deficient cells transduced with LV-*hPLS3* and quantified the surface level of TrkB normalized to LV-*mCh* transduced control motoneurons. Indeed, CK-666 treatment counteracted the improved TrkB cell surface recruitment after BDNF stimulation and no shift in TrkB to the cell surface could be detected (**Fig. 34 b**). Thus, inhibition of Arp2/3 reversed the beneficial effects of hPLS3 overexpression in SMA motoneurons arguing for the importance of both actin modulatory proteins for proper alignment of transmembrane proteins such as TrkB. In conclusion, our data indicates that the interplay between the Arp2/3 complex and Pls3 is important for the proper formation of the actin cytoskeleton in mediating TrkB cell surface recruitment in response to BDNF exposure.
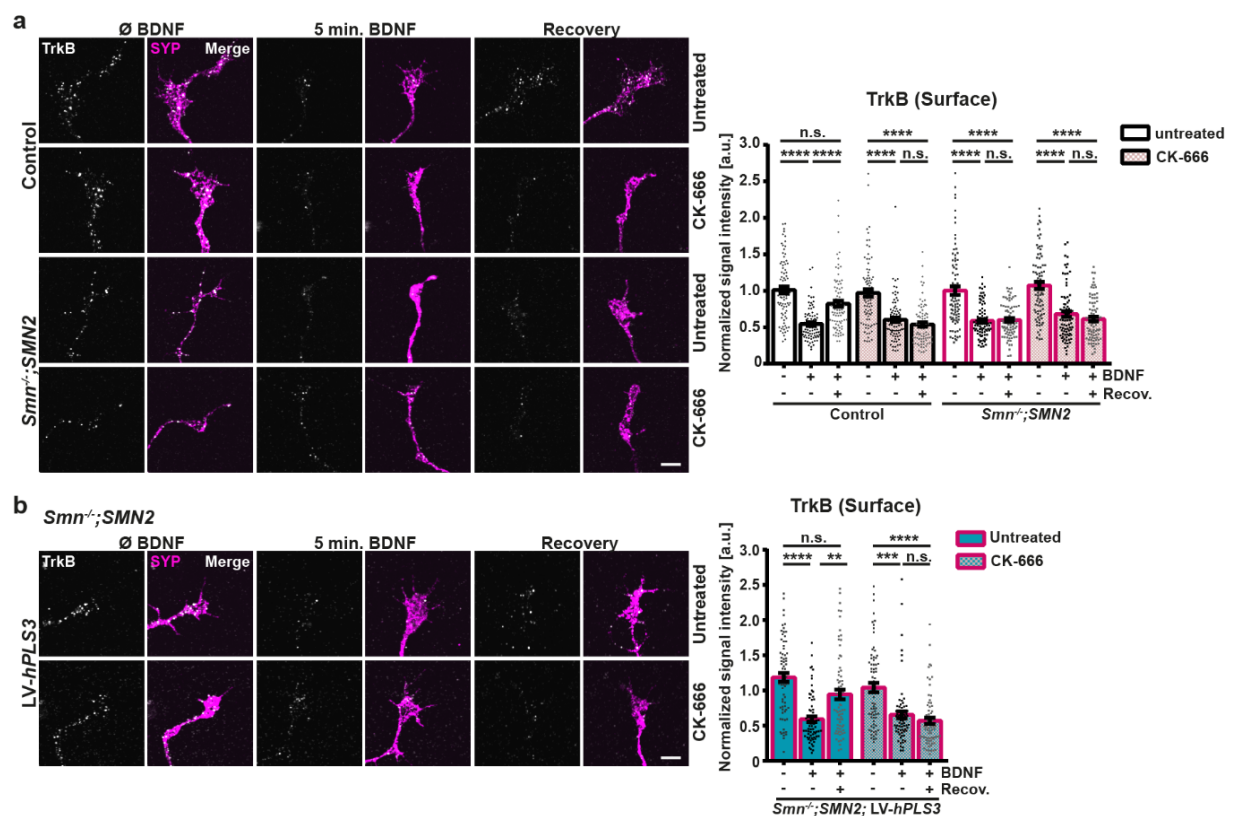

Fig. 34: The Arp2/3 complex and Pls3 are required for proper TrkB cell surface translocation after BDNF stinmulation in motoneuron axon terminals. a) *Growth cones from control and Smn$^{-/-}$;SMN2 motoneurons that were pre-treated with 50 µM CK-666 prior to the recovery assay and stained against surface TrkB (gray) and Synaptophysin-1 (SYP, magenta). Normalized mean gray values of surface TrkB (n=4, N=83; ANOVA Kruskal-Wallis test, **** p ≤ 0.0001; n.s. not significant).* **b)** *Growth cones from Smn$^{-/-}$;SMN2 motoneurons transduced with LV-hPLS3 that were pre-treated with CK-666 prior to the recovery assay and stained against surface TrkB (gray) and SYP (magenta). Normalized mean gray values of surface TrkB (LV-mCh data not shown) (n=3, N=72; ANOVA Kruskal-Wallis test, ** p ≤ 0.01; *** p ≤ 0.001; **** p ≤ 0.0001; n.s. not significant). Data are presented as scatter dot plot with bar. Bar represent the mean ± SEM. Scale bars: 5 µm.*

3.7. Overexpression of Pls3 beneficially regulates profilin levels and its activation via BDNF

In addition to subunits of the Arp2/3 complex, the transcript encoding profilin I (*Pfn1*) appeared to be downregulated in the axonal compartment of Smn knockdown motoneurons **(Fig. 15 e)**. As stated before, profilins are important regulators of actin dynamics (Hensel and Claus, 2018) and imbalances in the protein homeostasis were shown to be possibly involved in the pathomechanism of SMA. Interestingly, it has been shown that depletion of profilin II in Smn-deficient PC12 cells, that show enhanced levels of this specific protein isoform, results in an upregulation of Pls3 in a Smn-dependent manner (Bowerman et al., 2009). Hence, we wanted to examine whether inversely, Pls3 can regulate profilin. First, we used a pan-profilin antibody and checked the expression of both profilin isoforms in motoneuron axon terminals. In SMA motoneurons transduced with LV-*mCh*, significantly less quantities of profilin were detected when compared to control motoneurons **(Fig. 35 a)**, confirming the RNA sequencing results. Indeed, when hPLS3 was overexpressed in Smn-deficient motoneurons, markedly increased profilin levels could be detected **(Fig. 35 a)**.
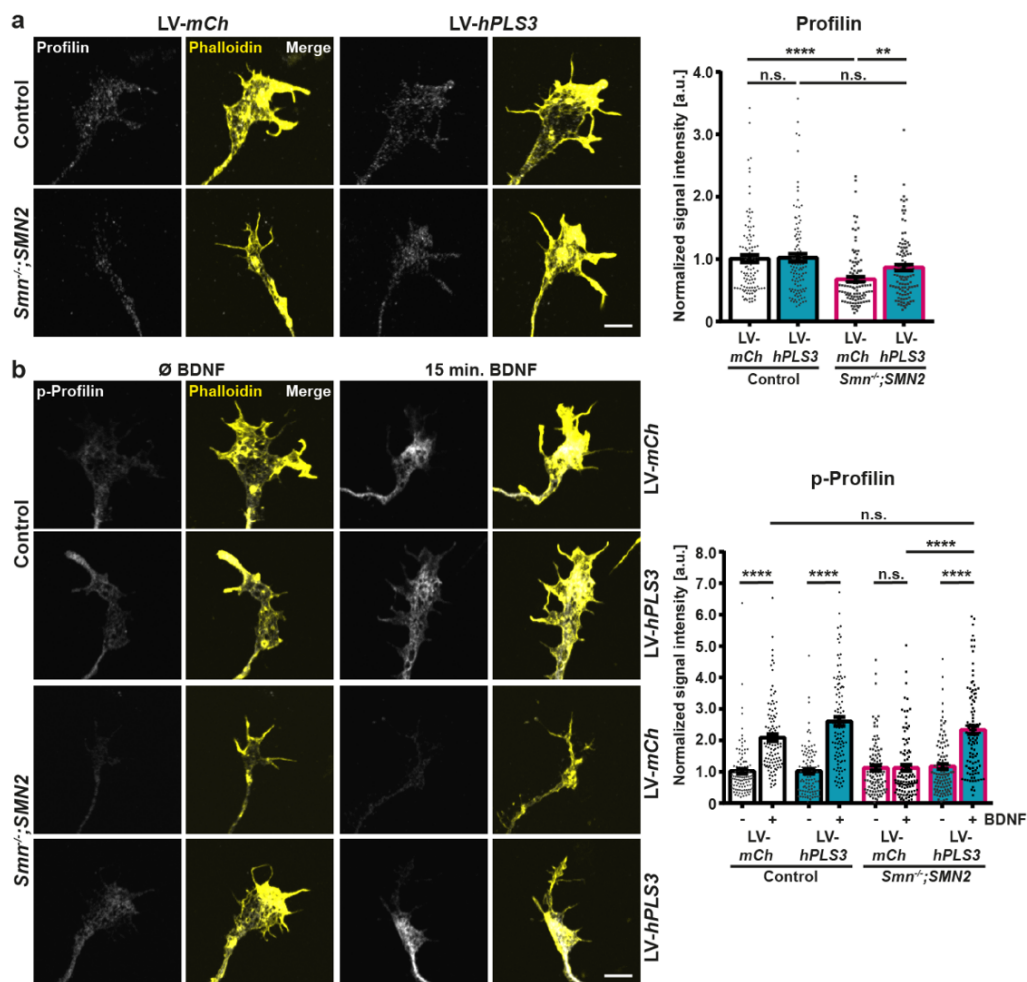

Fig. 35: Overexpression of hPLS3 restores localization and BDNF-induced activation of profilin in SMA axon terminals. a) *Growth cones from control and Smn⁻/⁻;SMN2 motoneurons transduced with LV-mCh and LV-hPLS3 stained against Profilin (gray) and F-actin (Phalloidin, yellow). Normalized mean gray values of Profilin in LV-mCh or LV-hPLS3 transduced control and Smn⁻/⁻;SMN2 terminals (n=3, N=110; ANOVA Kruskal-Wallis test, **** p ≤ 0.01; **** p ≤ 0.0001; n.s. not significant).* **b)** *Unstimulated or 15 min. BDNF stimulated growth cones from control and Smn⁻/⁻;SMN2 motoneurons transduced with LV-mCh and LV-hPLS3 stained against p-Profilin (gray) and F-actin (Phalloidin, yellow). Normalized mean gray values of p-Profilin in LV-mCh or LV-hPLS3 transduced control and Smn⁻/⁻;SMN2 terminals (n=3, N=105; ANOVA Kruskal-Wallis test, **** p ≤ 0.0001; n.s. not significant). Data are presented as scatter dot plot with bar. Bar represent the mean ± SEM. Scale bars: 5 µm.*

As the activity of profilins is modulated by phosphorylation and BDNF was demonstrated to induce robust elevation of p-profilin in motoneurons leading to increased F-actin levels (Dombert et al., 2017), we further investigated the activation of profilin after BDNF stimulation using a p-profilin antibody recognizing the tyrosine 129 phosphorylation site. Indeed, a 15 min. BDNF stimulation could evoke a marked increase in p-profilin in control motoneurons independent from virus transduction (**Fig. 35 b**). However, *Smn*$^{-/-}$*;SMN2* motoneurons transduced with LV-*mCh* showed no raise in p-profilin after BDNF stimulation (**Fig. 35 b**). In turn, upon upregulation of hPLS3 BDNF stimulation could significantly evoke a phosphorylation of profilin in SMA motoneurons comparable to control motoneurons (**Fig. 35 b**).

Thus, this data further confirms that Pls3 seems to act as an general modifier of SMA pathology beneficially modulating the actin cytoskeleton and further actin-regulatory proteins such as the Arp2/3 complex and profilins.

3.8. Overexpression of hPLS3 *in vivo* rescues BDNF-induced TrkB activation and ameliorates the neuromuscular phenotype and in SMNΔ7 mice

The function of Pls3 as protective SMA modifier was further strengthened by our data revealing its key role in the dynamic cell surface presentation of TrkB and the fact that overexpression of hPLS3 in Smn-deficient motoneurons beneficially interferes with the BDNF/TrkB defects observed in SMA motoneurons. To figure out whether the neuromucular phenotype of severly-affected *SMNΔ7* mice is improved when hPLS3 is overexpressed, we used an adeno-associated virus (AAV) mediated approach. Virus injection, tissue preparation and spinal cord immunohistochemistry were performed by our collaborators Dr. Christian Simon and Florian Gerstner at the Carl-Ludwig-Institute for Physiology, Leipzig University. AAV9-*hPLS3* or AAV9-*EGFP* as control were delivered via *cisterna magna* injection in mice at P1/P2. Examination of the *TVA* NMJs was performed at the later symptomatic stage at P10-11. To confirm virus expression within motoneurons, transverse sections of the spinal cord obtained from control mice injected with either AAV9-*hPLS3* or AAV9-*EGFP* were stained against the HA-tag of hPLS3 and EGFP. Quantification of the GFP- or HA- expressing motoneurons revealed that ~68 % or respectively ~49 % of the L1 spinal motoneurons showed robust virus expression, respectively (**Fig. 36 a**). To investigate the NMJs in detail, first the ratio of the pre- and postsynaptic area was determined. As demonstrated before (**Fig. 10 a**), *SMNΔ7* mice injected with the control virus displayed reduced NMJ size and degenerating presynapse, as reflected by a significant reduction in the area ratio (**Fig. 36 b**). However, AAV9-mediated hPLS3 overexpression slightly improved the area ratio showing a stabilizing effect of hPLS3 on neuromuscular endplates (**Fig. 36 b**).
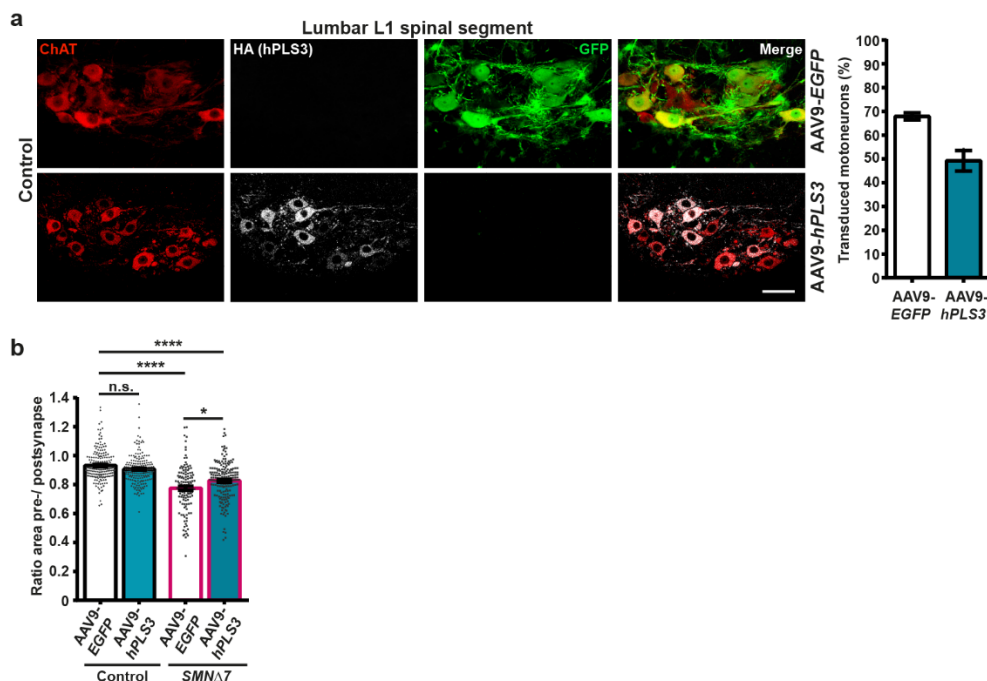

Fig. 36: Verification of virus expression in motoneurons of the L1 spinal segement and influence of hPLS3 overexpression in SMA neuromuscular endplates. a) *Motoneuron soma within the L1 lumbar spinal segment of P10 control animals injected with AAV9-EGFP or AAV9-hPLS3, stained against choline acetyltransferase (ChAT, red), HA (gray) and GFP (green), scale bar: 50 µm. Quantification of the percentage of GFP (AAV9-EGFP) or HA (AAV9-hPLS3)-expressing motoneurons (n=3/4). Data are presented as mean ± SD.* **b)** *Ratio of the area of the presynapse (SYP) vs. postsynapse (BTX) in NMJs from TVA of control and SMNΔ7 P10 animals that were injected with AAV9-EGFP and AAV9-hPLS3 (n=10/10/5/7, N=185/185/130/185; ANOVA Kruskal-Wallis test, * p ≤ 0.05; **** p ≤ 0.0001; n.s. not significant). Data are presented as scatter dot plot with bar. Bar represent the mean ± SEM.*

To further explore the effects of hPLS3 overexpression on the structure and functionality of NMJs in Smn-deficient mice, TrkB localization and its BDNF-induced phosphorylation were quantified in NMJs of the *TVA*. Analysis of the TrkB immunosignal revealed a small but significant increase in TrkB expression within the presynaptic compartment (**Fig. 37 a**). To test whether the activation of TrkB is improved by hPLS3 expression as well, muscle explants were stimulated with BDNF and the p-TrkB immunosignal was analyzed. Comparison of the p-TrkB levels in control and SMA pubs injected with AAV9-*EGFP* confirmed our previous results showing no increase in TrkB activation following BDNF stimulation in *SMNΔ7* mice (**Fig. 11 c**). Strikingly, when hPLS3 was overexpressed in *SMNΔ7* mice the activation of TrkB in response to BDNF stimulation was rescued showing a marked p-TrkB elevation upon BDNF stimulation within axonal terminals (**Fig. 37 b**). Thus, hPLS3 overexpression markedly ameliorated the TrkB activation defect in later symptomatic *SMNΔ7* mice, while only minor improvements were observed in TrkB expression and structure of Smn-deficient NMJs.
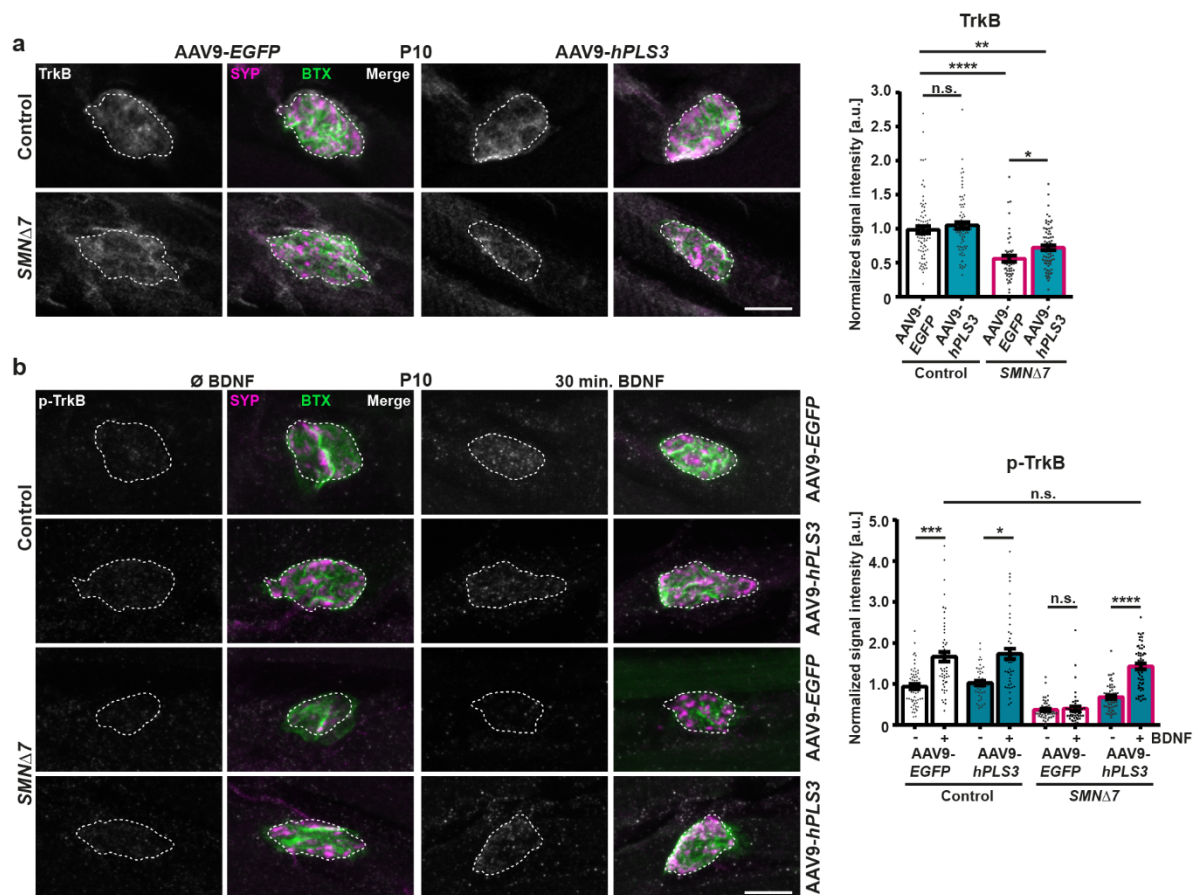

Fig. 37: In vivo hPLS3 overexpression rescues defective BDNF-induced TrkB activation and ameliorates TrkB localiztaion in SMA neuromuscular endplates. a) *NMJs in the TVA muscle of control and SMNΔ7 P10 animals that were injected with AAV9-EGFP or AAV9-hPLS3 stained against TrkB (gray), SYP (magenta) and BTX (green). Normalized mean gray values of TrkB (n=5/5/3/4, N=78/78/52/75; ANOVA Kruskal-Wallis test, * p ≤ 0.05; ** p ≤ 0.01; **** p ≤ 0.0001; n.s. not significant).* ***b)*** *Unstimulated and 30 min. BDNF stimulated NMJs in TVA muscle of control and SMNΔ7 P10 animals that were injected with AAV9-EGFP and AAV9-hPLS3 and stained against p-TrkB (gray), Synaptophysin-1 (SYP, magenta) and postsynaptic ACh receptors (BTX, green). Normalized mean gray values of p-TrkB (n=6/4/3/3, N=54/46/46/54; ANOVA Kruskal-Wallis test, * p ≤ 0.05; *** p ≤ 0.001 **** p ≤ 0.0001; n.s. not significant). Dotted line depicts outline of the presynapse (SYP). Data are presented as scatter dot plot with bar. Bar represent the mean ± SEM. Scale bars: 10 µm.*

To gain further insights into the organization of the neuromuscular endplates when hPLS3 is overexpressed we performed Ca$_v$2.1 immunostainings to investigate the localization and cluster-like formation of VGCCs in *SMNΔ7* mice. As shown in **Fig. 38**, Ca$_v$2.1 accumulation was significantly impaired in SMA mice injected with AAV-*EGFP* which is in accordance with previous reports (Tejero et al., 2020). In contrast, increased Ca$_v$2.1 signal intensity could be detected in endplates obtained from AAV9-*hPLS3*-injected SMA mice (**Fig. 38**). Hence, hPLS3 overexpression in *SMNΔ7* mice rescues the impaired TrkB activation and partially ameliorates the progressive NMJ deterioration as reflected by improved TrkB and Ca$_v$2.1 localization. In conclusion, our *in vivo* data provides further evidence for the beneficial effects of hPLS3 overexpression in a severe SMA mouse model.
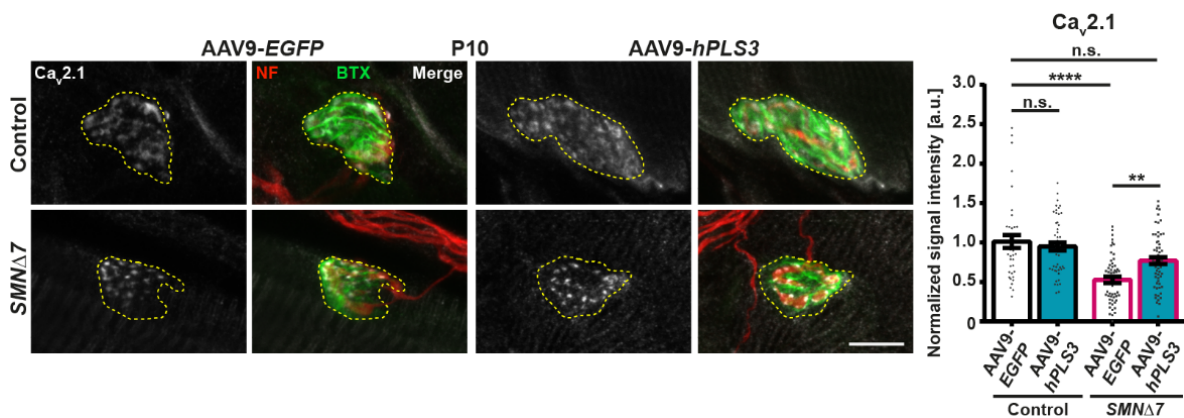

***Fig. 38: In vivo hPLS3 overexpression improves disturbed VGCC cluster-like formation in SMA neuromuscular endplates**. NMJs in the TVA muscle of control and SMNΔ7 P10 animals that were injected with AAV9-EGFP or AAV9-hPLS3 stained against Ca$_v$2.1 (gray), neurofilament (NF, red) and postsynaptic ACh receptors (BTX, green), scale bar: 10 μm. Dotted yellow line depicts outline of the postsynapse (BTX). Normalized mean gray values of Ca$_v$2.1 (n=3/4/3/4, N=40/50/54/62; ANOVA Kruskal-Wallis test, ** p ≤ 0.01; **** p ≤ 0.0001; n.s. not significant). Data are presented as scatter dot plot with bar. Bar represent the mean ± SEM.*

4. Discussion

Since SMA is a fetal progressive neuromuscular disease and one of the leading genetic causes of mortality in infants (Kingsmore et al., 2020), the primary mission during the last decades was to understand the cellular mechanisms underlying SMN deficiency and motoneuron degeneration in order to develop suitable therapies for the affected children. The impressive milestones that have been made in generating therapeutics by increasing the level of functional SMN protein via ASOs or viral vectors, are simultaneously dampened by the limitations of these approaches (Jablonka et al., 2022; Wirth et al., 2020) . Therefore, considering pathways that mediate SMA pathogenesis downstream of SMN or even in an SMN-independent manner broadens the possibilities for additional therapeutic strategies. Given the fact that morphological and functional abnormalities of SMA motoneurons are comparable with defects in motoneurons affected by TrkB deficiency (Dombert et al., 2017), examination of the BDNF/TrkB signaling cascade in SMA motoneurons would deliver insights into affected signaling pathways that could be targeted in an SMN-independent way. Moreover, recent findings indicate disease modifier genes beyond *SMN2* that bear a high potential to modulate the SMA phenotype. One of these modifiers shown to protect from SMA is the actin-bundling protein PLS3, however the underlying mechanism of how PLS3 beneficially interferes with SMN deficiency is not well understood. Hence, identification of PLS3's role in F-actin mediated processes will facilitate the understanding of disease-modifying genes and may provide the basis for the development of combinatorial therapeutic approaches.

Therefore, we used various imaging techniques and molecular biology methods to investigate the localization and activation of TrkB in SMA motoneuron growth cones in relation to the affected actin cytoskeleton and its modulators such as PLS3 and Arp2/3. The results of this thesis expand the current knowledge of SMA pathology by revealing impaired BDNF/TrkB signaling and describes a novel role for Pls3 in mediating correct F-actin assembly for proper cell surface recruitment of transmembrane proteins such as TrkB. More precisely, the key findings described in this study are listed below, which are discussed separately in the following chapters:

1) Smn-deficient axon terminals display impaired TrkB translocation and ligand-induced TrkB activation that corresponds to the disturbed actin cytoskeleton

2) TrkB surface level recovery after BDNF stimulation is disturbed in SMA axon terminals

3) Pls3 deficiency mimics SMA phenotype in cultured motoneurons

4) Overexpression of hPLS3 rescues the SMA phenotype in cultured motoneurons

5) Overexpression of hPLS3 in vivo rescues BDNF-induced TrkB activation and ameliorates the neuromuscular phenotype and in SMNΔ7 mice

6) Pls3 and Arp2/3 cooperate for proper surface translocation of TrkB

7) Overexpression of hPLS3 regulates profilin localization and phosphorylation

4.1. Smn-deficient axon terminals display impaired TrkB translocation and ligand-induced TrkB activation that corresponds to the disturbed actin cytoskeleton

Considering a proper functioning actin cytoskeleton as prerequisite for processes like axonal outgrowth and arrangement of the presynaptic compartment in neurons, disturbed F-actin assembly might play a fundamental role in the SMA disease scenario leading to alterations in motoneuron differentiation, diminished neurotransmission and muscle atrophy (Jablonka et al., 2007; Ruiz et al., 2010; Tejero et al., 2020; Tejero et al., 2016). Proof for an affected actin cytoskeleton was provided early by Rossoll and colleagues showing impaired *β-actin* mRNA translocation to distal axons (Rossoll et al., 2003). Subsequently, findings of local translation defects (Rathod et al., 2012) and a dysfunctional network of regulatory proteins (Ackermann et al., 2013; Alrafiah et al., 2018; Bowerman et al., 2009; Bowerman et al., 2007; Oprea et al., 2008; Riessland et al., 2017) further added evidence for the defective microfilament organization under Smn deficiency, that might be responsible for the observed motoneuron defects. This is from major importance especially with regard to the axonal terminals, since formation and maintenance of functional NMJs requires a proper presynaptic orchestration. Indeed, perturbed cluster formation of VGCCs was detected in Smn-deficient growth cones that correlates with reduced cellular excitability (Jablonka et al., 2007). Therefore, it might be possible that further transmembrane proteins are affected under Smn-deficient conditions that could contribute to the pathological mechanisms leading to motoneuron degeneration.

One candidate that aroused our interest is the BDNF receptor TrkB, since cellular differentiation defects of TrkB-deficient motoneurons resemble those observed in SMA motoneurons (Dombert et al., 2017). Moreover, mice that express TrkB with mutated kinase domain (*trkBTK^-/-*) (Klein et al., 1993) or full TrkB-KO mice (*Ntrk2^-/-*) (Rohrer et al., 1999) die during early postnatal development with severe motor defects such as righting difficulties (Klein et al., 1993; Rohrer et al., 1999), which reminded of the phenotypic SMA manifestations observed in *SMNΔ7* animals. The initial results obtained from immunostainings of primary cultured embryonic motoneurons isolated from *Smn^-/-;SMN2* embryos revealed only minor alterations in TrkB localization within the somatodendritic compartment and the axonal compartment, although overall no great reduction could be detected in western blots or RNA extracts of whole-cell lysates (**Fig. 5**). Similarly, activation of TrkB by its ligand BDNF was working properly in the somatodendritic compartment of Smn-deficient motoneurons. However, looking at the axon terminals of these motoneurons we observed that BDNF stimulation was not able to induce a robust elevation of p-TrkB in SMA motoneurons, in contrast to control neurons (**Fig. 7**). Hence, the localization of TrkB is only slightly affected in SMA motoneurons, but its activation is defective locally at the growth cones. Investigations of the neuromuscular endplates of severely affected muscles obtained from *SMNΔ7* mice revealed similar results. Although TrkB levels were significantly reduced already at the early disease stage at P5, BDNF could still evoke a marked phosphorylation of TrkB, even if the signal intensities were reduced when compared to control NMJs (**Fig. 10**). At P10, when the disease progressed and the mice start to show a more pronounced phenotype, BDNF stimulation failed to induce TrkB phosphorylation in Smn-deficient NMJs (**Fig. 11**).

Therefore, the question arises whether SMN deficiency and loss of BDNF/TrkB signaling within growth cones and presynaptic terminals are directly interlinked or whether a more indirect link could be possible. Since the *in vitro* data did not reveal marked differences in total TrkB levels upon Smn deficiency, we

hypothesized that the affected actin cytoskeleton could play a role in this scenario. Indeed, when actin polymerization was inhibited, control motoneurons showed the same TrkB activation defect within their axon terminals upon ligand stimulation as Smn-deficient motoneurons (**Fig. 8**).

Since responsiveness to BDNF is highly regulated by surface expression of the receptor, which on the one hand is modulated by neuronal activity and on the other hand requires an intact cytoskeleton (Andreska et al., 2020), we tested whether changes in the plasma membrane presentation of the receptor would explain the observed activation defects. Using live-cell stainings, we found out that the baseline cell surface TrkB expression is unaltered upon Smn deficiency. After ligand binding and activation, TrkB is rapidly endocytosed into the cell to form signaling endosomes (Barford et al., 2017; Cosker and Segal, 2014). Hence, access to BDNF would cause internalization of TrkB and thus reduction of TrkB cell surface levels as shown in **Fig. 13**. This endocytosis is either realized in a clathrin-dependent way or via Pincher-mediated micropinocytosis (Barford et al., 2017; Cosker and Segal, 2014). The mechanism of TrkB endocytosis appeared to be unaffected by the disturbed actin cytoskeleton in SMA motoneurons, since similar to control cells, BDNF stimulation induced a internalization of TrkB in *Smn*$^{-/-}$*;SMN2* growth cones (**Fig. 13**). Moreover, the levels of myosin VI, which was shown to be responsible for the retrograde transport of BDNF/TrkB signaling endosomes (Yano et al., 2006), were unaltered in SMA motoneurons further arguing for a functional BDNF/TrkB complex endocytosis and signaling.

Hence, neither the baseline TrkB cell surface presentation nor the mechanism of ligand-induced internalization were shown to be defective in SMA axon terminals and therefore could not explain the defective TrkB phosphorylation seen upon BDNF stimulation. However, what these live-cell stainings further demonstrated was that the amount of TrkB presented at the cell surface only corresponds to a small portion of total TrkB and most of them are located intracellularly. These results confirmed early observations on retinal ganglion cells and spinal motoneurons made in the laboratory of Ben Barres (Meyer-Franke et al., 1998). Unlike neurons in the PNS, these CNS neurons were shown to express only low levels of TrkB on the cell membrane under basal conditions, but depolarization or elevation of cAMP rapidly triggered a shift of these intracellular located receptors to the cell surface (Meyer-Franke et al., 1998). Thus, to test this activity-induced TrkB translocation mechanism in Smn-deficient axon terminals, motoneurons were stimulated with 8-CPT-cAMP prior to the cell surface staining of TrkB. In growth cones of control motoneurons, a marked increase of receptors at the membrane was observed after the exposure to cAMP, while no changes at all could be detected in SMA axon terminals (**Fig. 14**). Hence, *Smn*$^{-/-}$*;*SMN2 motoneurons display a defective translocation of TrkB to the cell surface in response to cellular activity. These findings, together with the fact that TrkB translocation in response to cAMP could be blocked by disruption of actin polymerization provided the first evidence that an actin-dependent translocation defect could be causative for the disturbed BDNF-induced TrkB activation seen in SMA axon terminals.

4.2. TrkB surface level recovery after BDNF stimulation is disturbed in SMA axon terminals

As described before, Smn-deficient motoneurons show only minor reductions in total TrkB levels and normal presentation of TrkB at the cell surface within axon terminals. Therefore, it remains elusive why the amount of phosphorylated TrkB after BDNF stimulation is much lower in SMA axon terminals when

compared to controls growth cones, which display similar baseline cell surface TrkB levels. On the basis of our previous observations that cAMP-induced TrkB membrane translocation is defective in Smn-deficient growth cones, we hypothesized that the self-amplifying actions of BDNF postulated by Cheng et al. in 2011 are impaired upon Smn deficiency. This autocrine mechanism of BDNF is based on the finding that BDNF/TrkB signaling itself can induce elevation of intracellular cAMP levels leading to elevated BDNF secretion on the one hand and recruitment of TrkB and its insertion into the plasma membrane on the other hand (Cheng et al., 2011). In turn, it might be possible that BDNF stimulation not only leads to activation and endocytosis of TrkB, but also triggers further recruitment of TrkB to the cell surface in a positive feedback loop, resulting in a marked signal amplification. Similar to the cAMP-mediated TrkB translocation, this autocrine mechanism of BDNF by locally enhancing available receptors at the membrane is dependent on a well-functioning actin cytoskeleton, which could provide an explanation for the impaired TrkB phosphorylation in SMA.

The results from our live-cell recovery experiments revealed that indeed during a recovery period after BDNF-induced TrkB internalization, the quantities of the receptors presented at the cell surface started to reconstitute (**Fig. 29**). Blockade experiments using inhibitors of either actin polymerization, microtubule polymerization or protein biosynthesis further confirmed the requirement of an intact actin cytoskeleton as prerequisite for this TrkB re-translocation (**Fig. 29**). Furthermore, the recruitment of TrkB is realized from a pool of already existing receptors, since CHX treatment did not inhibit the recovery after BDNF stimulation in control motoneurons. Based on the experimental setup, we were not able to distinguish whether the recovered receptors were directly recycled TrkBs, that have been at the cell surface prior to BDNF stimulation, or whether they originate from the intracellular storage. This question was answered using two rounds of cell surface TrkB stainings in our TrkB recycling assay. Again, the previous results were confirmed showing a reconstitution of about ~70 % of the baseline TrkB levels in control growth cones during this short recovery period. Surprisingly, this experiment additionally revealed that approximately half of the recovered surface receptors after BDNF stimulation are recycled receptors that already have been at the plasma membrane, while the other half is translocated from the intracellular pool (**Fig. 31**). In contrast, the amount of recovered TrkB after BDNF stimulation in Smn-deficient axon terminals is only about ~40 %. But again, half of the recovered receptors are directly recycled TrkBs from the cell surface (**Fig. 31**). Thus, the defect in TrkB reconstitution at the plasma membrane after BDNF stimulation in SMA motoneuron terminals is based on an actin-dependent translocation defect and not caused by a TrkB recycling defect *per se*. In conclusion, we postulate a mechanism for control motoneurons in which BDNF stimulation triggers a highly dynamic recruitment and membrane insertion of additional receptors in axon terminals leading to a signal amplification resembled by a great amount of phosphorylated TrkB upon BDNF stimulation. In contrast to that, in SMA growth cones activation of available TrkB at the plasma membrane and endocytosis is not altered, however the BNDF-induced TrkB translocation and membrane inclusion is absent due to the affected actin cytoskeleton resulting in impaired signal amplification.

Bearing in mind that BDNF/TrkB signaling is one of the key regulators of neuronal survival, regeneration as well as growth and differentiation and therefore takes places in various cellular processes, it is not surprising that disequilibrium of BDNF and its signaling cascade are prominent features in disease conditions with particular attention on neurodegenerative diseases (Colucci-D'Amato et al., 2020).

Although neuroprotective functions of BDNF are widely recognized making it a potential target for protective intervention of motoneuron survival, most attempts of BDNF upregulation either via direct delivery or upregulation of its expression did not deliver successful outcomes in patients as shown for PD (Palasz et al., 2020). Moreover, it is well documented that elevated amounts of BDNF were also associated with detrimental cellular ramifications such as increased excitability contributing to neuronal damage in the context of ALS or epilepsy (Iughetti et al., 2018; Pradhan et al., 2019). Therefore, key challenge is to unravel the underlying mechanisms in order to understand the particular role of BDNF/TrkB signaling in the corresponding disease context, in order to find tools to specifically modulate its signaling in distinct cell types or even subcellular localizations.

With regard to SMA, we were able to demonstrate that the stimulus-induced translocation of the BDNF receptor TrkB is altered locally in axon terminals, leading to impaired signal amplification upon BDNF stimulation. Since pathological features of TrkB- and SMN-deficient motoneurons are quite similar, our data implicates that, at least in part, some of the observed dysregulations in SMA are likely to be results of disturbed BDNF/TrkB signaling.

4.3. Pls3 deficiency mimics SMA phenotype in cultured motoneurons

So far, we provide evidence that the affected actin cytoskeleton functionally participates in the observed TrkB translocation and activation defects; however, the underlying mechanism remains fragmented. To further investigate this in detail, a transcriptome analysis was performed in the interest of modulatory proteins associated with the defective cytoskeleton. RNA-sequencing of Smn knockdown motoneurons grown in compartmentalized microfluidic chambers revealed a multitude of genes showing altered expression in the somatodendritic compartment as well as in the axonal compartment **(Fig. 15)**. Intriguingly, gene ontology term analysis of the affected genes showed that especially in the axonal compartment of Smn-deficient motoneurons, transcripts that encode proteins with functions associated to the actin cytoskeleton were downregulated. With strong emphasis on these transcripts, we found that the gene encoding the actin-bundling protein Pls3 appeared to be downregulated upon Smn deficiency **(Fig. 16)**. Interestingly, in control motoneurons Pls3 transcripts showed a higher abundance in the axonal compartment compared to the somatodendritic compartment, however in both compartments lower levels of *Pls3* could be detected in Smn knockdown motoneurons.

PLS3 gained special attention as protective SMA modifier, since it was shown to be upregulated in asymptomatic female SMA type I patients harbouring deletions of *SMN1* (Oprea et al., 2008). Since then, extensive research focussing on its role in SMA pathophysiology was carried out, demonstrating the ability of Pls3 overexpression to counteract typical SMA hallmarks across species in various SMA animal models such as mice, zebrafish, flies or worms (Ackermann et al., 2013; Alrafiah et al., 2018; Dimitriadi et al., 2010; Hao le et al., 2012; Hosseinibarkooie et al., 2016; Oprea et al., 2008). According to the very first descriptions, Pls3, a 68 kDa protein that initially was termed fimbrin, was found to be associated with microfilaments in microvilli and membrane ruffles chicken fibroblast cells (Bretscher and Weber, 1980). Later on, its capability of actin-binding and cross-linking was reported, demonstrating its important function in cytoskeletal organization and re-organization (Arpin et al., 1994; Delanote et al., 2005; Giganti et al., 2005; Karpova et al., 1995; Shinomiya, 2012). Therefore, it acts as a powerful

modulator of actin-related processes such as cell motility and migration (Brun et al., 2014; Garbett et al., 2020; Serio et al., 2010; Xue et al., 2010), and endocytosis (Hagiwara et al., 2011; Jorde et al., 2011; Kubler and Riezman, 1993). Dysregulations of Pls3, on the one hand lack of the protein but also increased levels of Pls3, can influence actin-dependent cellular processes that are related various pathological conditions. For instance, reduced PLS3 levels were shown to interfere with bone remodelling cells that is causative for osteoporosis, while enhanced levels are associated with osteoarthritis or cancer (Wolff et al., 2021). In neurodegenerative diseases such as SMA or ALS, where motoneurons suffer from reduced F-actin levels, an upregulation of PLS3 has beneficial effects (Wolff et al., 2021).

In the context of SMA, numerous studies have addressed its protective characteristics: PLS3 overexpression on a severe SMA background restores motoneuron soma size, improves neuronal connectivity and rescues the NMJ defects including the endplate size, increases the amount of F-actin within the presynapse, improves organization of the active zones and synaptic vesicles leading to improved neurotransmission (Ackermann et al., 2013; Alrafiah et al., 2018; Oprea et al., 2008). Furthermore, endocytotic processes and synaptic vesicle recycling are significantly improved by increased PLS3 levels in SMA mice (Hosseinibarkooie et al., 2016). In contrast, depletion of Pls3 interferes with axon outgrowth and growth cone morphology (Oprea et al., 2008).

Since our immunohistochemical investigations of $Smn^{-/-};SMN2$ motoneurons confirmed the lack of Pls3 in axon terminals of SMA motoneurons revealed by RNA sequencing, we aimed to find out whether Pls3 could be involved in the previously observed actin-dependent TrkB translocation and activation defects. Therefore, a shRNA-containing knockdown construct was designed targeting endogenous $Pls3$. Interestingly, lentivirus-mediated $Pls3$ knockdown in cultured control motoneurons phenocopied SMA motoneurons. Not only morphological abnormalities including reduced growth cone size, impaired axon elongation of functional disturbances in actin dynamics were observed **(Fig. 17)**, but also decreased TrkB levels and defective BDNF-induced TrkB phosphorylation could be detected (**Fig. 18**). Moreover, the cAMP-mediated TrkB surface translocation was absent in growth cones of Pls3 knockdown motoneurons, while similar to SMA axon terminals, the BDNF-induced TrkB endocytosis was working **(Fig.19)**. Therefore, we concluded that Pls3 functionally participates in the translocation and plasma membrane presentation of TrkB as well as its ligand-induced activation. In addition to that, proper Pls3-bundled actin filaments seems to be important for the alignment of further transmembrane proteins such as VGCCs. Similar to SMA motoneuron axon terminals (Jablonka et al., 2007), $Ca_v2.2$ localization, cluster-like accumulation and functionality were shown to be disturbed upon Pls3 knockdown in motoneurons **(Fig. 20)**. However, to exclude to possibility of unspecific off-target effects that could be possibly induced by virus transduction, we cloned a shRNA-resistant $hPLS3$ cDNA tagged with HA into the $shPls3$-containing pSIH vector. Since analysis of HA-expressing motoneurons, which harbor the tagged version of hPLS3 to compensate for the shRNA-mediated knockdown of endogenous Pls3, did not reveal any morphological or functional abnormalities (**Fig. 21**), we assume that the lack of Pls3 was specifically responsible for the observed defects in these knockdown motoneurons. Our results upon Pls3 depletion are in line with previous observations in cultured PC12 cells (Oprea et al., 2008), demonstrating the high potential of Pls3 to modulate actin-dependent processes such as growth cone morphology or translocation of transmembrane proteins.

4.4. Overexpression of hPLS3 rescues the SMA phenotype in cultured motoneurons

Based on the initial results and the fact that lack of Pls3 phenocopies SMA motoneurons, we hypothesized that enhancing the Pls3 levels in Smn-deficient motoneurons would improve the observed defects of the BDNF/TrkB signaling cascade due to its direct impact on the cytoskeleton. Indeed, upon overexpression of hPLS3 in Smn-deficient motoneurons, morphological and functional improvements could be observed. Axon length as well as growth cone size and morphology of hPLS3-expressing SMA motoneurons were normalized to wild type levels. Furthermore, on the functional level increased actin dynamics could be detected arguing for the beneficial effects of enhanced hPLS3 levels on the cytoskeleton (**Figs. 22 - 23**). Therefore, we hypothesized that the actin-dependent processes like TrkB membrane translocation upon stimulation or its BDNF-induced activation are rescued upon hPLS3 overexpression.

Indeed, improved TrkB localization, rescued cAMP-induced TrkB surface translocation and normal TrkB phosphorylation could be detected in *Smn^{-/-};SMN2* motoneurons overexpressing hPLS3 (**Figs. 24 - 27**). Since the BDNF/TrkB signaling cascade leads to the induction of further signaling pathways including the activation of Akt, we also checked this downstream signaling target in SMA motoneurons. As expected, Smn-deficient motoneurons display significantly reduced, albeit not absent, Akt phosphorylation after BDNF stimulation when compared to control motoneurons. However, when hPLS3 was overexpressed, the observed activation defects and its downstream signaling cascade of TrkB were abolished (**Fig. 27**). Thus, restoring the Pls3 levels in SMA motoneurons beneficially interferes with the TrkB translocation and activation defects. Moreover, the TrkB recovery and recycling assays confirmed our hypothesis that the actin-dependent translocation defects in SMA motoneurons is responsible for the disturbed signal amplification after BDNF stimulation resulting in decreased levels of phosphorylated TrkB. Overexpression of hPLS3 resulted in a marked rescue of the TrkB re-location to the cell membrane after BDNF stimulation (**Fig. 30**), which is not attributable to a disturbed recycling of cell surface receptors but rather to an actin-dependent TrkB translocation defect that is removed by overexpression of hPLS3 (**Fig. 31**). Hence, we conclude that the expression of hPLS3 stabilizes the actin cytoskeleton in Smn-deficient motoneurons resulting in a marked recovery from the observed TrkB translocation and activation impairments.

Early investigations using yeast mutants lacking the Pls3/fimbrin homologue Sac6 already addressed the stabilizing effect of Pls3 on the actin cytoskeleton. Using different strategies it has been demonstrated that Sac6 yeast mutants display reduced levels of F-actin and increased levels of G-actin, while the overall amount of actin remained unchanged (Karpova et al., 1995). Thus, depletion of Sac6 resulted in a yeast phenotype that lacks actin cables and shows depolarized actin patches (Belmont and Drubin, 1998). This is in agreement with the observation that lymphoblastoid cell lines derived from unaffected *SMN1*-deleted children with increased PLS3 expression displayed higher levels of F-actin (Oprea et al., 2008). Additionally, similar results were obtained from overexpression studies in HEK293 cells (Oprea et al., 2008). Hence, altogether these findings argue that besides actin-bundling, Pls3 inheres crucial roles for actin stabilization by inhibiting actin depolymerization on the one hand and directing the orientation of actin filaments on the other hand. This could explain the beneficial effects of increased Pls3 levels on actin-dependent processes like axogenesis, growth cone formation and

composition of the presynaptic compartment in SMA motoneurons as described by us and others (Ackermann et al., 2013; Hosseinibarkooie et al., 2016; Oprea et al., 2008).

To examine whether hPLS3 overexpression also advantageously impacts further transmembrane proteins, we investigated the localization and accumulation of cluster-like formations of VGCCs that previously have been shown to be disturbed in SMA (Jablonka et al., 2007). Intriguingly, hPLS3-overexpressing SMA motoneurons display increased amount of $Ca_v2.2$ in their axon terminals that corresponds to increased frequencies of spontaneous Ca^{2+} transients (**Fig. 28**). Similar observations were made using the small molecule R-Roscovitine. R-Roscovitine extends the open-stated of VGCCs and thereby modulates Ca^{2+} influx leading to increased spontaneous Ca^{2+} transients. Thus, application of this drug *in vivo* results in increased survival of severely affected SMA mice and improved NMJ phenotype and rescues the SMA motoneuron phenotype *in vitro* (Tejero et al., 2020).

In conclusion, Pls3 is an important regulator of actin-bundling as well as actin-stabilization and filament direction and therefore modulates a vast number of cellular processes including translocation of transmembrane proteins. Depletion of this protein results in a SMA-like motoneurons phenotype, while overexpression generously rescues the SMA motoneuron phenotype *in vitro* that is likely due to its stabilizing effect on the actin cytoskeleton.

4.5. Overexpression of hPLS3 *in vivo* rescues BDNF-induced TrkB activation and ameliorates the neuromuscular phenotype and in *SMNΔ7* mice

Since hPLS3 effectively rescued the TrkB translocation and activation defects *in vitro* we hypothesized similar beneficial effects *in vivo*. Therefore, neonatal *SMNΔ7* mice were injected into the right lateral ventricle with an AAV9 harboring the cDNA for hPLS3 and the neuromuscular endplates were investigated at the later disease stage at P10-11. Impressively, BDNF stimulation experiments revealed that the activation of TrkB is almost normalized to wild type level in NMJs of SMA mice with increased hPLS3 levels (**Fig. 37**). However, the effects on TrkB localization and overall NMJs size as reflected by the area of the pre- vs. postsynapse was only mildly improved upon AAV9-mediated hPLS3 delivery (**Figs. 36 and 37**). In contrast to that, the influence of hPLS3 on clustering of $Ca_v2.1$ was conspicuous in the NMJs of *SMNΔ7* mice (**Fig. 38**). Hence, improving actin dynamics by elevating Pls3 levels *in vivo* ameliorates the NMJ phenotype and rescues the defective ligand-induced TrkB activation in a severely affected SMA mouse model.

However, in our experiments no increase in body weight or improvement of motoric functions as indicated by the righting reflex could be detected (*data not shown*). With regard to the survival rate of hPLS3-overexpressing SMA mice, previous studies showed contradictory findings. While rescuing effects could previously only be detected on a milder SMA background or upon simultaneously administration of ASOs to insufficiently increase the Smn levels (Ackermann et al., 2013; Kaifer et al., 2017), more recent investigations revealed a significant rescuing effect on mean survival rate and body weight of AAV9-PLS3 administration alone (Alrafiah et al., 2018). But noteworthy, the observed improvements on the body weight were first obvious when the disease had progressed starting from P10 and survival elongation is confined to about three days (Alrafiah et al., 2018). This discrepancy could be based on several factors. One is rooted back to the fact that a highly dynamic and well-

functioning actin cytoskeleton is already required during early embryonic development, especially when motoneurons grow out to their target muscles to build functional nerve-muscle connections. Thus, the relatively late postnatal delivery of hPLS3 could have exceeded the relevant window for therapeutic intervention leading to mitigation of the positive impact. This idea is further supported by the fact, that R-Roscovitine, when applied only postnatally had less pro-survival effects on *SMNΔ7* mice compared to a prenatal application starting from E11.5 in these mice (Tejero et al., 2020). Furthermore, as demonstrated in motoneuron soma of the L1 spinal segment, transduction rate of AAV9-*hPLS3* is only about 50 % (**Fig. 36**). It might be that hPLS3-mediated rescuing effects would be stronger if higher transduction rates could be achieved. Secondly, *SMNΔ7* mice account for a severely affected SMA mouse model and motoneurons are not the only cell type suffering from Smn depletion. For instance, various studies using animal models and SMA patients have demonstrated how loss of Smn affects sensory neurons (Jablonka et al., 2006; Ling et al., 2010; Mentis et al., 2011; Rudnik-Schoneborn et al., 2003), sympathetic neurons (Heier et al., 2010) or even bone mineral density (Khatri et al., 2008). Hence, stabilizing motoneurons and maintenance of the presynaptic compartment and neuromuscular endplates may not be able to counteract the overall detrimental effects in an advanced state of the disease. In addition, PLS3 is supposed to act as a gender-specific modifier in female SMA patients, while in highly *PLS3*-expressing male SMA patients the disease phenotype only correlated with the copy number of SMN2 and was not improved by PLS3 (Oprea et al., 2008). Therefore, it might be possible that varying results can be obtained according to the gender of *SMNΔ7* mice. Moreover, all asymptomatic female SMN1-depleted SMA patients examined in the original publication from Oprea et al., in 2008 harbored at least three or even four SMN2 copies that mitigate the SMA disease type by increasing levels of full-length SMN protein (Oprea et al., 2008).

Thus, it seems that a certain amount of Smn is required for Pls3 to develop its full therapeutic potential, which might explain the low beneficial impact of postnatal hPLS3 overexpression on the overall phenotype of *SMNΔ7* mice.

4.6. Pls3 and Arp2/3 cooperate for proper surface translocation of TrkB

Up to now, our data provide evidence that Pls3 is functionally participating in the organization of the actin cytoskeleton responsible for proper membrane recruitment of TrkB in response to external stimuli from the intracellular available pool. Based on our findings and previous observations we assume that besides actin-bundling, Pls3 also inheres an actin-stabilizing function probably by preventing actin depolymerization. Moreover, it has been shown that Pls3 is involved in directing the orientation of bundled F-actin filaments (Belmont and Drubin, 1998). This is in accordance with the recent observations that selectively PLS3 has a crucial role in promoting membrane protrusions in human endothelial cells enabling them to bridge gaps in the extracellular matrix (Garbett et al., 2020). In addition to that, the authors of this publication show that PLS3 is especially responsible for strengthening the protrusive actin network that is generated by the actin nucleator complex Arp2/3, and depletion of PLS3 results in reduced Arp2/3 levels (Garbett et al., 2020). The Arp2/3 protein complex of humans consist of seven subunits with the ability to induce actin polymerization and more specifically actin branching (Rouiller et al., 2008; Welch et al., 1997). In fission yeast, the related function of the proteins was previously reported. Pls3 primarily localizes and bundles actin filaments, which are branched by Arp2/3

(Skau et al., 2011). However, the Arp2/3 protein complex is rather responsible for generating dynamic leading edges for establishing filopodia-like protrusions but is not necessary for elongation of these filaments (Lee et al., 2010; Suraneni et al., 2012). Especially in terms of growth cones the importance of these two actin modulators become obvious, since both are required for the formation of the prominent finger-like filopodia (Lee et al., 2010; Xue et al., 2010).

Given the interrelated functions of PLS3 and the Arp2/3 complex for filopodia formation and direction, we asked whether the latter one is also required for proper cell surface translocation of TrkB. Therefore, we examined the expression and localization of the Arp3 subunit in SMA axon terminals and found out that Arp3 is significantly reduced in SMA growth cones. Furthermore, SIM imaging confirmed the differential localization of the two proteins. While Pls3 is distributed anywhere in the growth cones but is abundantly located in F-actin-rich protrusions, Arp3 is preferably found in the center of the growth cones (**Fig. 32**). This in in line with previous observations reporting the absence of Arp2/3 in cellular actin filament bundles (Welch et al., 1997) and in accordance with its function in induction of filopodia, but not their elongation (Lee et al., 2010; Suraneni et al., 2012). Similar to the findings of (Garbett et al., 2020), a knockdown of Pls3 in control motoneurons caused a decline in Arp3 localization within growth cones of control motoneurons. The other way around, overexpression of hPLS3 restored the Arp3 levels in Smn-deficient axon terminals (**Fig. 33**). Garbett and colleagues further showed, that localization of PLS3 in the front of filopodia requires stabilized actin filaments, while inhibition of Arp2/3-induced actin branching by the selective inhibitor CK-666 leads to a reduction of PLS3 in the front (Garbett et al., 2020). Thus, to investigate the role of Arp2/3 in TrkB cell surface recruitment after BDNF stimulation motoneurons were treated with the Arp2/3 inhibitor and subjected to our live-cell recovery assay. Indeed, inhibition of Arp2/3 complex activity by CK-666 prevented the recovery of cell surface TrkB levels induced by BDNF stimulation in control cells, to a similar extend as seen in SMA axon terminals (**Fig. 34**). Moreover, CK-666 pretreatment abolished the beneficial effects of hPLS3 overexpression on TrkB membrane recruitment in SMA motoneurons (**Fig. 34**).

Hence, these experiments reveal that a branched actin network by Arp2/3 is a prerequisite for proper formation of filopodia that can be bundled and stabilized by Pls3. Importantly, the cooperation of both proteins is important for proper cell surface recruitment of transmembrane proteins such as TrkB. It seems that the interrelation of these two actin modulators is from major importance and their relation is based on mutual presence, since both ablation of Pls3 results in decreased Arp3 levels, but also inhibition of Arp2/3 results in reduction of Pls3 levels in the front.

4.7. Overexpression of hPLS3 regulates profilin localization and activation

In addition to the cooperation of Pls3 and Arp2/3 for proper actin cytoskeleton function, further actin-regulatory proteins are required. Profilins act primarily as modulatory proteins regulating the addition of G-actin to the barbed end of the actin filament thereby generating a directed force to functionally participate in a wide range of cellular processes including motility or transport of cargos (Hensel and Claus, 2018). The different isoforms of the protein showing distinct expression profiles; while profilin I is ubiquitously expressed, profilin II is mainly found in the CNS and the isoform III and IV are only expressed in testis and sperm (Hensel and Claus, 2018). Moreover, the two isoforms I and II were

shown to inherit distinct expression patterns during development with different functions in the brain (Michaelsen-Preusse et al., 2016). For instance, profilin I was observed to play a major role during the formation of spines in the hippocampus during early development, while later-one mainly profilin IIa was required for spine stabilization and plasticity (Michaelsen-Preusse et al., 2016). Due to their structure, profilins can bind to poly-L-proline-containing proteins, such as SMN or formins, the latter one which are responsible for the catalyzation of profilin-actin assembly at the bared F-actin end (Hensel and Claus, 2018; Romero et al., 2004).

The importance of a regulated profilin homeostasis for a controlled F-actin formation is demonstrated by recent findings that link profilins to multiple diseases such as cancer, ALS, Huntington's Disease or SMA (Murk et al., 2021). For familial ALS is has been shown that toxic gain-of-function mutations in the *PFN1* gene are associated with conformational change of TDP-43 contributing to ALS pathomechanism (Smith et al., 2015; Tanaka et al., 2016; Wu et al., 2012a). Interestingly, ALS-linked mutant *PFN1* expression in primary murine motoneurons resulted in impaired axon outgrowth, smaller growth cones that lack filopodia accompanied by a lower F/G-actin ratio (Wu et al., 2012a), a phenotype which strongly reminds of SMA motoneurons. With regard to the latter one, it has been demonstrated that loss of Smn is linked to higher levels of the profilin IIa isoform in PC12 cells, leading its hyperphosphorylation and inactivation eventually resulting in an affected cytoskeleton (Bowerman et al., 2009; Bowerman et al., 2007; Nolle et al., 2011). On the other hand, SMA fission yeast mutants were shown to exhibit splicing defects in the profilin gene leading to a decline in profilin levels. This in turn was associated with perturbed actin turnover and a more accessible barbed end of F-actin which led to enhanced occupation by capping proteins (Antoine et al., 2020). The findings of the Antoine and colleagues are in line with the RNA sequencing data that revealed reduced *Pfn1* transcripts in the axonal compartment of Smn knockdown motoneurons (**Fig. 15**). Immunocytochemical analysis of our SMA motoneurons using a pan-profilin antibody confirmed the lack of profilin within growth cones (**Fig. 35**). Since an association of profilin and Pls3 was already observed in Smn-deficient PC12 cells (Bowerman et al., 2009), we wanted to see whether the beneficial impact of hPLS3 overexpression on SMA motoneurons also affects profilin. Indeed, $Smn^{-/-};SMN2$ motoneurons transduced with LV-*hPLS3* showed significantly higher abundance of profilin compared to the LV-*mCh* transduced motoneurons **(Fig. 35)**. The activation of profilins is tightly regulated and was shown to be modulated by stimulation with vascular endothelial growth factor (Fan et al., 2012) or BDNF (Dombert et al., 2017). Since BDNF/TrkB signaling is defective in SMA, we hypothesized that BDNF-induced profilin phosphorylation is disturbed in Smn-deficient motor axon terminals. Indeed, a transient BDNF stimulation was not able to evoke an increase in p-profilin levels in LV-*mCh* transduced $Smn^{-/-};SMN2$ motoneurons, while control motoneurons showed a significant upregulation in p-profilin levels **(Fig. 35)**. Again, the overexpression of hPLS3 had a positive effect on profilin activation showing a marked raise in profilin phosphorylation upon BDNF stimulation **(Fig. 35)**.

In addition to our pervious results that revealed and important interplay between Pls3 and the Arp2/3 complex for proper actin cytoskeleton function responsible for translocation and assembly of transmembrane proteins, we provide evidence that Pls3 is also linked to further actin-regulatory proteins such as profilin. However, in the future more investigation in the connection between Pls3 and profilin is required to decipher their complex interaction and the resulting implications on the regulation of the actin cytoskeleton.

4.8. Conclusions

Altogether, our comprehensive study revealed that SMA pathogenesis is tightly associated with the defective activity-induced translocation of TrkB from an intracellular available pool along bundled actin filaments to the plasma membrane in growth cones of motoneurons. Consequently, exposure to BDNF can induce activation of TrkB located at the cell surface, but the recruitment of further receptors which are required for signal amplification is disturbed. Moreover, we identified the SMA modifier PLS3 as important regulator of actin cytoskeleton dynamics and function and showed that lack of this protein is associated with the defective BDNF/TrkB signaling. In turn, increasing the levels of PLS3 in SMA motoneurons could effectively rescue their phenotype leading to an improved dynamic and functional actin cytoskeleton required for proper TrkB cell surface recruitment and ligand-induced activation. Moreover, accumulation of Ca$_v$2.2 was normalized to wild type level upon overexpression of PLS3 resulting in enhanced frequency of spontaneous Ca^{2+} transients, which together with BDNF/TrkB signaling are prerequisite for proper motoneurons maturation and function. Lastly, our experiments showed that PLS3 cooperates with a variety of other actin-regulatory proteins.

In conclusion, we provide a novel role for PLS3 in mediating accurate translocation and alignment of transmembrane proteins via the actin cytoskeleton in motor axon terminals. Thus, PLS3 is from major importance for key mechanisms required for normal motoneuron differentiation and regular function beyond the scope of SMA.
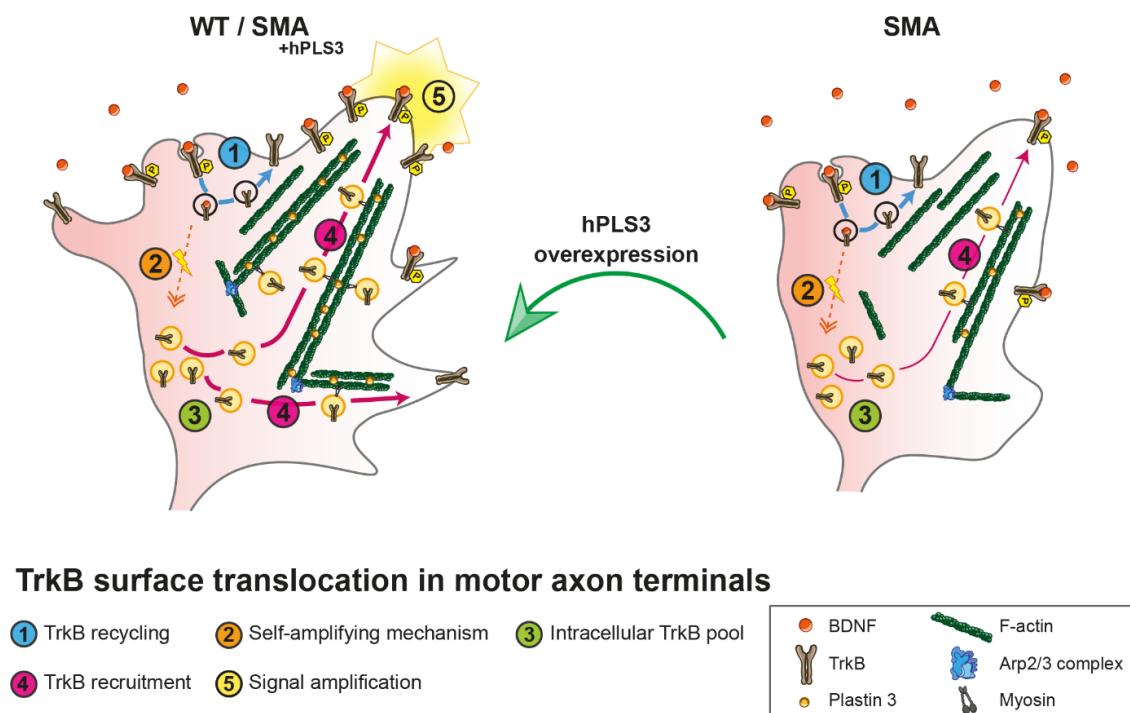
***Fig. 39: Defective TrkB translocation in SMA leading to decreased BDNF-induced signal amplification that can be rescued by overexpression of hPLS3**. In wild type motoneuron axon terminals, a small portion of TrkB is located at the cell surface that can be activated by BDNF stimulation. Internalized BDNF/TrkB receptor ligand complexes can be **(1)** directly recycled and transferred back to the cell membrane. **(2)** Furthermore, BDNF/TrkB signaling acts in an autocrine self-amplifying mechanism to promote further TrkB recruitment from the **(3)** available intracellular pool to **(4)** the plasma membrane via Arp2/3-branched and Pls3-bundeled actin filaments, which in turn can get activated by BDNF leading to a **(5)** signal amplification reflected by a marked raise in phosphorylated TrkB. In SMA motoneuron axon terminals, TrkB translocation in response to external stimuli that is realized via actin filaments is disturbed due to a lack of Pls3. Consequently, available TrkB at the membrane get activated, but translocation of further receptors to the cell surface after BDNF stimulation is dysfunctional, leading to markedly low p-TrkB levels when compared to wild type neurons. In contrast, overexpression of hPLS3 in SMA motoneurons stabilizes actin filaments resulting in a rescue of the observed TrkB translocation and activation defects.*

5. References

Ackermann, B., S. Krober, L. Torres-Benito, A. Borgmann, M. Peters, S.M. Hosseini Barkooie, R. Tejero, M. Jakubik, J. Schreml, J. Milbradt, T.F. Wunderlich, M. Riessland, L. Tabares, and B. Wirth. 2013. Plastin 3 ameliorates spinal muscular atrophy via delayed axon pruning and improves neuromuscular junction functionality. *Human molecular genetics*. 22:1328-1347.

Adachi, N., K. Kohara, and T. Tsumoto. 2005. Difference in trafficking of brain-derived neurotrophic factor between axons and dendrites of cortical neurons, revealed by live-cell imaging. *BMC neuroscience*. 6:42.

Aid, T., A. Kazantseva, M. Piirsoo, K. Palm, and T. Timmusk. 2007. Mouse and rat BDNF gene structure and expression revisited. *Journal of neuroscience research*. 85:525-535.

Akten, B., M.J. Kye, T. Hao le, M.H. Wertz, S. Singh, D. Nie, J. Huang, T.T. Merianda, J.L. Twiss, C.E. Beattie, J.A. Steen, and M. Sahin. 2011. Interaction of survival of motor neuron (SMN) and HuD proteins with mRNA cpg15 rescues motor neuron axonal deficits. *Proceedings of the National Academy of Sciences of the United States of America*. 108:10337-10342.

Alrafiah, A., E. Karyka, I. Coldicott, K. Iremonger, K.E. Lewis, K. Ning, and M. Azzouz. 2018. Plastin 3 Promotes Motor Neuron Axonal Growth and Extends Survival in a Mouse Model of Spinal Muscular Atrophy. *Molecular therapy. Methods & clinical development*. 9:81-89.

Andreska, T., S. Aufmkolk, M. Sauer, and R. Blum. 2014. High abundance of BDNF within glutamatergic presynapses of cultured hippocampal neurons. *Frontiers in cellular neuroscience*. 8:107.

Andreska, T., P. Luningschror, and M. Sendtner. 2020. Regulation of TrkB cell surface expression-a mechanism for modulation of neuronal responsiveness to brain-derived neurotrophic factor. *Cell and tissue research*. 382:5-14.

Antoine, M., K.L. Patrick, J. Soret, P. Duc, F. Rage, R. Cacciottolo, K.E. Nissen, R.J. Cauchi, N.J. Krogan, C. Guthrie, Y. Gachet, and R. Bordonne. 2020. Splicing Defects of the Profilin Gene Alter Actin Dynamics in an S. pombe SMN Mutant. *iScience*. 23:100809.

Aoki, C., K. Wu, A. Elste, G. Len, S. Lin, G. McAuliffe, and I.B. Black. 2000. Localization of brain-derived neurotrophic factor and TrkB receptors to postsynaptic densities of adult rat cerebral cortex. *Journal of neuroscience research*. 59:454-463.

Arpin, M., E. Friederich, M. Algrain, F. Vernel, and D. Louvard. 1994. Functional differences between L- and T-plastin isoforms. *The Journal of cell biology*. 127:1995-2008.

Atwal, J.K., B. Massie, F.D. Miller, and D.R. Kaplan. 2000. The TrkB-Shc site signals neuronal survival and local axon growth via MEK and P13-kinase. *Neuron*. 27:265-277.

Ayloo, S., P. Guedes-Dias, A.E. Ghiretti, and E.L.F. Holzbaur. 2017. Dynein efficiently navigates the dendritic cytoskeleton to drive the retrograde trafficking of BDNF/TrkB signaling endosomes. *Molecular biology of the cell*. 28:2543-2554.

Baj, G., E. Leone, M.V. Chao, and E. Tongiorgi. 2011. Spatial segregation of BDNF transcripts enables BDNF to differentially shape distinct dendritic compartments. *Proceedings of the National Academy of Sciences of the United States of America*. 108:16813-16818.

Balkowiec, A., and D.M. Katz. 2000. Activity-dependent release of endogenous brain-derived neurotrophic factor from primary sensory neurons detected by ELISA in situ. *The Journal of neuroscience : the official journal of the Society for Neuroscience*. 20:7417-7423.

Balkowiec, A., and D.M. Katz. 2002. Cellular mechanisms regulating activity-dependent release of native brain-derived neurotrophic factor from hippocampal neurons. *The Journal of neuroscience : the official journal of the Society for Neuroscience*. 22:10399-10407.

Bamji, S.X., M. Majdan, C.D. Pozniak, D.J. Belliveau, R. Aloyz, J. Kohn, C.G. Causing, and F.D. Miller. 1998. The p75 neurotrophin receptor mediates neuronal apoptosis and is essential for naturally occurring sympathetic neuron death. *The Journal of cell biology*. 140:911-923.

Banuelos, S., M. Saraste, and K. Djinovic Carugo. 1998. Structural comparisons of calponin homology domains: implications for actin binding. *Structure*. 6:1419-1431.

Barbacid, M. 1994. The Trk family of neurotrophin receptors. *Journal of neurobiology*. 25:1386-1403.

Barde, Y.A. 1990. The nerve growth factor family. *Progress in growth factor research*. 2:237-248.

Barde, Y.A., D. Edgar, and H. Thoenen. 1982. Purification of a new neurotrophic factor from mammalian brain. *The EMBO journal*. 1:549-553.

Barford, K., C. Deppmann, and B. Winckler. 2017. The neurotrophin receptor signaling endosome: Where trafficking meets signaling. *Developmental neurobiology*. 77:405-418.

Bartkowska, K., A. Paquin, A.S. Gauthier, D.R. Kaplan, and F.D. Miller. 2007. Trk signaling regulates neural precursor cell proliferation and differentiation during cortical development. *Development*. 134:4369-4380.

Battaglia, G., A. Princivalle, F. Forti, C. Lizier, and M. Zeviani. 1997. Expression of the SMN gene, the spinal muscular atrophy determining gene, in the mammalian central nervous system. *Human molecular genetics*. 6:1961-1971.

Baumer, D., S. Lee, G. Nicholson, J.L. Davies, N.J. Parkinson, L.M. Murray, T.H. Gillingwater, O. Ansorge, K.E. Davies, and K. Talbot. 2009. Alternative splicing events are a late feature of pathology in a mouse model of spinal muscular atrophy. *PLoS genetics*. 5:e1000773.

Baxter, G.T., M.J. Radeke, R.C. Kuo, V. Makrides, B. Hinkle, R. Hoang, A. Medina-Selby, D. Coit, P. Valenzuela, and S.C. Feinstein. 1997. Signal transduction mediated by the truncated trkB receptor isoforms, trkB.T1 and trkB.T2. *The Journal of neuroscience : the official journal of the Society for Neuroscience*. 17:2683-2690.

Beattie, E.C., C.L. Howe, A. Wilde, F.M. Brodsky, and W.C. Mobley. 2000. NGF signals through TrkA to increase clathrin at the plasma membrane and enhance clathrin-mediated membrane trafficking. *The Journal of neuroscience : the official journal of the Society for Neuroscience*. 20:7325-7333.

Belmont, L.D., and D.G. Drubin. 1998. The yeast V159N actin mutant reveals roles for actin dynamics in vivo. *The Journal of cell biology*. 142:1289-1299.

Birbach, A. 2008. Profilin, a multi-modal regulator of neuronal plasticity. *BioEssays : news and reviews in molecular, cellular and developmental biology*. 30:994-1002.

Blum, R., and A. Konnerth. 2005. Neurotrophin-mediated rapid signaling in the central nervous system: mechanisms and functions. *Physiology (Bethesda)*. 20:70-78.

Bolte, S., and F.P. Cordelieres. 2006. A guided tour into subcellular colocalization analysis in light microscopy. *J Microsc*. 224:213-232.

Borg, R.M., B. Fenech Salerno, N. Vassallo, R. Bordonne, and R.J. Cauchi. 2016. Disruption of snRNP biogenesis factors Tgs1 and pICln induces phenotypes that mirror aspects of SMN-Gemins complex perturbation in Drosophila, providing new insights into spinal muscular atrophy. *Neurobiology of disease*. 94:245-258.

Bowerman, M., C.L. Anderson, A. Beauvais, P.P. Boyl, W. Witke, and R. Kothary. 2009. SMN, profilin IIa and plastin 3: a link between the deregulation of actin dynamics and SMA pathogenesis. *Molecular and cellular neurosciences*. 42:66-74.

Bowerman, M., D. Shafey, and R. Kothary. 2007. Smn depletion alters profilin II expression and leads to upregulation of the RhoA/ROCK pathway and defects in neuronal integrity. *Journal of molecular neuroscience : MN*. 32:120-131.

Boyd, J.G., and T. Gordon. 2003. Glial cell line-derived neurotrophic factor and brain-derived neurotrophic factor sustain the axonal regeneration of chronically axotomized motoneurons in vivo. *Experimental neurology*. 183:610-619.

Boza-Moran, M.G., R. Martinez-Hernandez, S. Bernal, K. Wanisch, E. Also-Rallo, A. Le Heron, L. Alias, C. Denis, M. Girard, J.K. Yee, E.F. Tizzano, and R.J. Yanez-Munoz. 2015. Decay in survival motor neuron and plastin 3 levels during differentiation of iPSC-derived human motor neurons. *Scientific reports*. 5:11696.

Bretscher, A., and K. Weber. 1980. Fimbrin, a new microfilament-associated protein present in microvilli and other cell surface structures. *The Journal of cell biology*. 86:335-340.

Briese, M., D.U. Richter, D.B. Sattelle, and N. Ulfig. 2006. SMN, the product of the spinal muscular atrophy-determining gene, is expressed widely but selectively in the developing human forebrain. *The Journal of comparative neurology*. 497:808-816.

Briese, M., L. Saal-Bauernschubert, C. Ji, M. Moradi, H. Ghanawi, M. Uhl, S. Appenzeller, R. Backofen, and M. Sendtner. 2018. hnRNP R and its main interactor, the noncoding RNA 7SK, coregulate the axonal transcriptome of motoneurons. *Proceedings of the National Academy of Sciences of the United States of America*. 115:E2859-E2868.

Briese, M., L. Saal, S. Appenzeller, M. Moradi, A. Baluapuri, and M. Sendtner. 2016. Whole transcriptome profiling reveals the RNA content of motor axons. *Nucleic acids research*. 44:e33.

Brigadski, T., and V. Lessmann. 2020. The physiology of regulated BDNF release. *Cell and tissue research*. 382:15-45.

Brun, C., A. Demeaux, F. Guaddachi, F. Jean-Louis, T. Oddos, M. Bagot, A. Bensussan, S. Jauliac, and L. Michel. 2014. T-plastin expression downstream to the calcineurin/NFAT pathway is involved in keratinocyte migration. *PloS one*. 9:e104700.

Brunet, A., S.R. Datta, and M.E. Greenberg. 2001. Transcription-dependent and -independent control of neuronal survival by the PI3K-Akt signaling pathway. *Current opinion in neurobiology*. 11:297-305.

Brzustowicz, L.M., T. Lehner, L.H. Castilla, G.K. Penchaszadeh, K.C. Wilhelmsen, R. Daniels, K.E. Davies, M. Leppert, F. Ziter, D. Wood, and et al. 1990. Genetic mapping of chronic childhood-onset spinal muscular atrophy to chromosome 5q11.2-13.3. *Nature*. 344:540-541.

Buchman, A.S., L. Yu, P.A. Boyle, J.A. Schneider, P.L. De Jager, and D.A. Bennett. 2016. Higher brain BDNF gene expression is associated with slower cognitive decline in older adults. *Neurology*. 86:735-741.

Buettner, J.M., J.K. Sime Longang, F. Gerstner, K.S. Apel, B. Blanco-Redondo, L. Sowoidnich, E. Janzen, T. Langenhan, B. Wirth, and C.M. Simon. 2021. Central synaptopathy is the most conserved feature of motor circuit pathology across spinal muscular atrophy mouse models. *iScience*. 24:103376.

Buhler, D., V. Raker, R. Luhrmann, and U. Fischer. 1999. Essential role for the tudor domain of SMN in spliceosomal U snRNP assembly: implications for spinal muscular atrophy. *Human molecular genetics*. 8:2351-2357.

Burglen, L., S. Lefebvre, O. Clermont, P. Burlet, L. Viollet, C. Cruaud, A. Munnich, and J. Melki. 1996. Structure and organization of the human survival motor neurone (SMN) gene. *Genomics*. 32:479-482.

Burk, K., J.D. Murdoch, S. Freytag, M. Koenig, V. Bharat, R. Markworth, S. Burkhardt, A. Fischer, and C. Dean. 2017. EndophilinAs regulate endosomal sorting of BDNF-TrkB to mediate survival signaling in hippocampal neurons. *Scientific reports*. 7:2149.

Burlet, P., C. Huber, S. Bertrandy, M.A. Ludosky, I. Zwaenepoel, O. Clermont, J. Roume, A.L. Delezoide, J. Cartaud, A. Munnich, and S. Lefebvre. 1998. The distribution of SMN protein complex in human fetal tissues and its alteration in spinal muscular atrophy. *Human molecular genetics*. 7:1927-1933.

Bussaglia, E., O. Clermont, E. Tizzano, S. Lefebvre, L. Burglen, C. Cruaud, J.A. Urtizberea, J. Colomer, A. Munnich, M. Baiget, and et al. 1995. A frame-shift deletion in the survival motor neuron gene in Spanish spinal muscular atrophy patients. *Nature genetics*. 11:335-337.

Campbell, L., A. Potter, J. Ignatius, V. Dubowitz, and K. Davies. 1997. Genomic variation and gene conversion in spinal muscular atrophy: implications for disease process and clinical phenotype. *American journal of human genetics*. 61:40-50.

Canossa, M., A. Gartner, G. Campana, N. Inagaki, and H. Thoenen. 2001. Regulated secretion of neurotrophins by metabotropic glutamate group I (mGluRI) and Trk receptor activation is mediated via phospholipase C signalling pathways. *The EMBO journal*. 20:1640-1650.

Carrel, T.L., M.L. McWhorter, E. Workman, H. Zhang, E.C. Wolstencroft, C. Lorson, G.J. Bassell, A.H. Burghes, and C.E. Beattie. 2006. Survival motor neuron function in motor axons is independent of functions required for small nuclear ribonucleoprotein biogenesis. *The Journal of neuroscience : the official journal of the Society for Neuroscience*. 26:11014-11022.

Carroll, P., G.R. Lewin, M. Koltzenburg, K.V. Toyka, and H. Thoenen. 1998. A role for BDNF in mechanosensation. *Nature neuroscience*. 1:42-46.

Cartegni, L., and A.R. Krainer. 2002. Disruption of an SF2/ASF-dependent exonic splicing enhancer in SMN2 causes spinal muscular atrophy in the absence of SMN1. *Nature genetics*. 30:377-384.

Chan, Y.B., I. Miguel-Aliaga, C. Franks, N. Thomas, B. Trulzsch, D.B. Sattelle, K.E. Davies, and M. van den Heuvel. 2003. Neuromuscular defects in a Drosophila survival motor neuron gene mutant. *Human molecular genetics*. 12:1367-1376.

Chao, M.V. 2003. Neurotrophins and their receptors: a convergence point for many signalling pathways. *Nature reviews. Neuroscience*. 4:299-309.

Chen, Z.Y., A. Ieraci, H. Teng, H. Dall, C.X. Meng, D.G. Herrera, A. Nykjaer, B.L. Hempstead, and F.S. Lee. 2005. Sortilin controls intracellular sorting of brain-derived neurotrophic factor to the regulated secretory pathway. *The Journal of neuroscience : the official journal of the Society for Neuroscience*. 25:6156-6166.

Cheng, P.L., A.H. Song, Y.H. Wong, S. Wang, X. Zhang, and M.M. Poo. 2011. Self-amplifying autocrine actions of BDNF in axon development. *Proceedings of the National Academy of Sciences of the United States of America*. 108:18430-18435.

Cheung, Z.H., W.H. Chin, Y. Chen, Y.P. Ng, and N.Y. Ip. 2007. Cdk5 is involved in BDNF-stimulated dendritic growth in hippocampal neurons. *PLoS biology*. 5:e63.

Chevrel, G., R. Hohlfeld, and M. Sendtner. 2006. The role of neurotrophins in muscle under physiological and pathological conditions. *Muscle & nerve*. 33:462-476.

Chiaruttini, C., A. Vicario, Z. Li, G. Baj, P. Braiuca, Y. Wu, F.S. Lee, L. Gardossi, J.M. Baraban, and E. Tongiorgi. 2009. Dendritic trafficking of BDNF mRNA is mediated by translin and blocked by the G196A (Val66Met) mutation. *Proceedings of the National Academy of Sciences of the United States of America*. 106:16481-16486.

Cho, S., and G. Dreyfuss. 2010. A degron created by SMN2 exon 7 skipping is a principal contributor to spinal muscular atrophy severity. *Genes & development*. 24:438-442.

Cifuentes-Diaz, C., S. Nicole, M.E. Velasco, C. Borra-Cebrian, C. Panozzo, T. Frugier, G. Millet, N. Roblot, V. Joshi, and J. Melki. 2002. Neurofilament accumulation at the motor endplate and lack of axonal sprouting in a spinal muscular atrophy mouse model. *Human molecular genetics*. 11:1439-1447.

Clatterbuck, R.E., D.L. Price, and V.E. Koliatsos. 1994. Further characterization of the effects of brain-derived neurotrophic factor and ciliary neurotrophic factor on axotomized neonatal and adult mammalian motor neurons. *The Journal of comparative neurology*. 342:45-56.

Cobben, J.M., G. van der Steege, P. Grootscholten, M. de Visser, H. Scheffer, and C.H. Buys. 1995. Deletions of the survival motor neuron gene in unaffected siblings of patients with spinal muscular atrophy. *American journal of human genetics*. 57:805-808.

Colucci-D'Amato, L., L. Speranza, and F. Volpicelli. 2020. Neurotrophic Factor BDNF, Physiological Functions and Therapeutic Potential in Depression, Neurodegeneration and Brain Cancer. *International journal of molecular sciences*. 21.

Conner, J.M., J.C. Lauterborn, Q. Yan, C.M. Gall, and S. Varon. 1997. Distribution of brain-derived neurotrophic factor (BDNF) protein and mRNA in the normal adult rat CNS: evidence for anterograde axonal transport. *The Journal of neuroscience : the official journal of the Society for Neuroscience*. 17:2295-2313.

Connor, B., D. Young, Q. Yan, R.L. Faull, B. Synek, and M. Dragunow. 1997. Brain-derived neurotrophic factor is reduced in Alzheimer's disease. *Brain research. Molecular brain research*. 49:71-81.

Coovert, D.D., T.T. Le, P.E. McAndrew, J. Strasswimmer, T.O. Crawford, J.R. Mendell, S.E. Coulson, E.J. Androphy, T.W. Prior, and A.H. Burghes. 1997. The survival motor neuron protein in spinal muscular atrophy. *Human molecular genetics*. 6:1205-1214.

Corbit, K.C., D.A. Foster, and M.R. Rosner. 1999. Protein kinase Cdelta mediates neurogenic but not mitogenic activation of mitogen-activated protein kinase in neuronal cells. *Molecular and cellular biology*. 19:4209-4218.

Cosker, K.E., and R.A. Segal. 2014. Neuronal signaling through endocytosis. *Cold Spring Harbor perspectives in biology*. 6.

Crawford, T.O., and C.A. Pardo. 1996. The neurobiology of childhood spinal muscular atrophy. *Neurobiology of disease*. 3:97-110.

Crowder, R.J., and R.S. Freeman. 1998. Phosphatidylinositol 3-kinase and Akt protein kinase are necessary and sufficient for the survival of nerve growth factor-dependent sympathetic neurons. *The Journal of neuroscience : the official journal of the Society for Neuroscience*. 18:2933-2943.

Cunningham, M.E., and L.A. Greene. 1998. A function-structure model for NGF-activated TRK. *The EMBO journal*. 17:7282-7293.

Cusco, I., M.J. Barcelo, E. del Rio, M. Baiget, and E.F. Tizzano. 2004. Detection of novel mutations in the SMN Tudor domain in type I SMA patients. *Neurology*. 63:146-149.

Darras, B.T. 2011. Non-5q spinal muscular atrophies: the alphanumeric soup thickens. *Neurology*. 77:312-314.

Davey, R.J., and P.D. Moens. 2020. Profilin: many facets of a small protein. *Biophys Rev*. 12:827-849.

de Arruda, M.V., S. Watson, C.S. Lin, J. Leavitt, and P. Matsudaira. 1990. Fimbrin is a homologue of the cytoplasmic phosphoprotein plastin and has domains homologous with calmodulin and actin gelation proteins. *The Journal of cell biology*. 111:1069-1079.

Dechant, G., and Y.A. Barde. 2002. The neurotrophin receptor p75(NTR): novel functions and implications for diseases of the nervous system. *Nature neuroscience*. 5:1131-1136.

Delanote, V., K. Van Impe, V. De Corte, E. Bruyneel, G. Vetter, C. Boucherie, M. Mareel, J. Vandekerckhove, E. Friederich, and J. Gettemans. 2005. Molecular basis for dissimilar nuclear trafficking of the actin-bundling protein isoforms T- and L-plastin. *Traffic*. 6:335-345.

Dhillon, S. 2020. Risdiplam: First Approval. *Drugs*. 80:1853-1858.

DiDonato, C.J., X.N. Chen, D. Noya, J.R. Korenberg, J.H. Nadeau, and L.R. Simard. 1997. Cloning, characterization, and copy number of the murine survival motor neuron gene: homolog of the spinal muscular atrophy-determining gene. *Genome research*. 7:339-352.

Dieni, S., T. Matsumoto, M. Dekkers, S. Rauskolb, M.S. Ionescu, R. Deogracias, E.D. Gundelfinger, M. Kojima, S. Nestel, M. Frotscher, and Y.A. Barde. 2012. BDNF and its pro-peptide are stored in presynaptic dense core vesicles in brain neurons. *The Journal of cell biology*. 196:775-788.

Dijkhuizen, P.A., and A. Ghosh. 2005. BDNF regulates primary dendrite formation in cortical neurons via the PI3-kinase and MAP kinase signaling pathways. *Journal of neurobiology*. 62:278-288.

Dimitriadi, M., J.N. Sleigh, A. Walker, H.C. Chang, A. Sen, G. Kalloo, J. Harris, T. Barsby, M.B. Walsh, J.S. Satterlee, C. Li, D. Van Vactor, S. Artavanis-Tsakonas, and A.C. Hart. 2010. Conserved genes act as modifiers of invertebrate SMN loss of function defects. *PLoS genetics*. 6:e1001172.

DiStefano, P.S., B. Friedman, C. Radziejewski, C. Alexander, P. Boland, C.M. Schick, R.M. Lindsay, and S.J. Wiegand. 1992. The neurotrophins BDNF, NT-3, and NGF display distinct patterns of retrograde axonal transport in peripheral and central neurons. *Neuron*. 8:983-993.

Doktor, T.K., Y. Hua, H.S. Andersen, S. Broner, Y.H. Liu, A. Wieckowska, M. Dembic, G.H. Bruun, A.R. Krainer, and B.S. Andresen. 2017. RNA-sequencing of a mouse-model of spinal muscular atrophy reveals tissue-wide changes in splicing of U12-dependent introns. *Nucleic acids research*. 45:395-416.

Dolcet, X., J. Egea, R.M. Soler, D. Martin-Zanca, and J.X. Comella. 1999. Activation of phosphatidylinositol 3-kinase, but not extracellular-regulated kinases, is necessary to mediate brain-derived neurotrophic factor-induced motoneuron survival. *Journal of neurochemistry*. 73:521-531.

Dombert, B., S. Balk, P. Luningschror, M. Moradi, R. Sivadasan, L. Saal-Bauernschubert, and S. Jablonka. 2017. BDNF/trkB Induction of Calcium Transients through Cav2.2 Calcium Channels in Motoneurons Corresponds to F-actin Assembly and Growth Cone Formation on beta2-Chain Laminin (221). *Frontiers in molecular neuroscience*. 10:346.

Dombert, B., R. Sivadasan, C.M. Simon, S. Jablonka, and M. Sendtner. 2014. Presynaptic localization of Smn and hnRNP R in axon terminals of embryonic and postnatal mouse motoneurons. *PLoS one*. 9:e110846.

Dong, Q., Y.S. Ji, C. Cai, and Z.Y. Chen. 2012. LIM kinase 1 (LIMK1) interacts with tropomyosin-related kinase B (TrkB) and Mediates brain-derived neurotrophic factor (BDNF)-induced axonal elongation. *The Journal of biological chemistry*. 287:41720-41731.

Donlin-Asp, P.G., C. Fallini, J. Campos, C.C. Chou, M.E. Merritt, H.C. Phan, G.J. Bassell, and W. Rossoll. 2017. The Survival of Motor Neuron Protein Acts as a Molecular Chaperone for mRNP Assembly. *Cell reports*. 18:1660-1673.

Dor-On, E., S. Raviv, Y. Cohen, O. Adir, K. Padmanabhan, and C. Luxenburg. 2017. T-plastin is essential for basement membrane assembly and epidermal morphogenesis. *Science signaling*. 10.

Drake, C.T., T.A. Milner, and S.L. Patterson. 1999. Ultrastructural localization of full-length trkB immunoreactivity in rat hippocampus suggests multiple roles in modulating activity-dependent synaptic plasticity. *The Journal of neuroscience : the official journal of the Society for Neuroscience*. 19:8009-8026.

Du, J., L. Feng, F. Yang, and B. Lu. 2000. Activity- and Ca(2+)-dependent modulation of surface expression of brain-derived neurotrophic factor receptors in hippocampal neurons. *The Journal of cell biology*. 150:1423-1434.

Du, J., L. Feng, E. Zaitsev, H.S. Je, X.W. Liu, and B. Lu. 2003. Regulation of TrkB receptor tyrosine kinase and its internalization by neuronal activity and Ca2+ influx. *The Journal of cell biology*. 163:385-395.

Dubowitz, V. 1964. Infantile Muscular Atrophy. A Prospective Study with Particular Reference to a Slowly Progressive Variety. *Brain : a journal of neurology*. 87:707-718.

Dubowitz, V. 1999. Very severe spinal muscular atrophy (SMA type 0): an expanding clinical phenotype. *European journal of paediatric neurology : EJPN : official journal of the European Paediatric Neurology Society*. 3:49-51.

Edens, B.M., S. Ajroud-Driss, L. Ma, and Y.C. Ma. 2015. Molecular mechanisms and animal models of spinal muscular atrophy. *Biochimica et biophysica acta*. 1852:685-692.

Eggermann, K., D. Gläser, A. Abicht, and B. Wirth. 2020. Spinal muscular atrophy (5qSMA): best practice of diagnostics, newborn screening and therapy. *Medizinische Genetik*. 32:263-272.

Erickson, J.T., J.C. Conover, V. Borday, J. Champagnat, M. Barbacid, G. Yancopoulos, and D.M. Katz. 1996. Mice lacking brain-derived neurotrophic factor exhibit visceral sensory neuron losses distinct from mice

lacking NT4 and display a severe developmental deficit in control of breathing. *The Journal of neuroscience : the official journal of the Society for Neuroscience*. 16:5361-5371.

Ernfors, P., K.F. Lee, and R. Jaenisch. 1994. Mice lacking brain-derived neurotrophic factor develop with sensory deficits. *Nature*. 368:147-150.

Ernfors, P., C. Wetmore, L. Olson, and H. Persson. 1990. Identification of cells in rat brain and peripheral tissues expressing mRNA for members of the nerve growth factor family. *Neuron*. 5:511-526.

Fallini, C., J.P. Rouanet, P.G. Donlin-Asp, P. Guo, H. Zhang, R.H. Singer, W. Rossoll, and G.J. Bassell. 2014. Dynamics of survival of motor neuron (SMN) protein interaction with the mRNA-binding protein IMP1 facilitates its trafficking into motor neuron axons. *Developmental neurobiology*. 74:319-332.

Fallini, C., H. Zhang, Y. Su, V. Silani, R.H. Singer, W. Rossoll, and G.J. Bassell. 2011. The survival of motor neuron (SMN) protein interacts with the mRNA-binding protein HuD and regulates localization of poly(A) mRNA in primary motor neuron axons. *The Journal of neuroscience : the official journal of the Society for Neuroscience*. 31:3914-3925.

Fan, L., and L.R. Simard. 2002. Survival motor neuron (SMN) protein: role in neurite outgrowth and neuromuscular maturation during neuronal differentiation and development. *Human molecular genetics*. 11:1605-1614.

Fan, Y., A. Arif, Y. Gong, J. Jia, S.M. Eswarappa, B. Willard, A. Horowitz, L.M. Graham, M.S. Penn, and P.L. Fox. 2012. Stimulus-dependent phosphorylation of profilin-1 in angiogenesis. *Nature cell biology*. 14:1046-1056.

Fawcett, J.P., M.A. Alonso-Vanegas, S.J. Morris, F.D. Miller, A.F. Sadikot, and R.A. Murphy. 2000. Evidence that brain-derived neurotrophic factor from presynaptic nerve terminals regulates the phenotype of calbindin-containing neurons in the lateral septum. *The Journal of neuroscience : the official journal of the Society for Neuroscience*. 20:274-282.

Feldkotter, M., V. Schwarzer, R. Wirth, T.F. Wienker, and B. Wirth. 2002. Quantitative analyses of SMN1 and SMN2 based on real-time lightCycler PCR: fast and highly reliable carrier testing and prediction of severity of spinal muscular atrophy. *American journal of human genetics*. 70:358-368.

Feng, W., A.K. Gubitz, L. Wan, D.J. Battle, J. Dostie, T.J. Golembe, and G. Dreyfuss. 2005. Gemins modulate the expression and activity of the SMN complex. *Human molecular genetics*. 14:1605-1611.

Finkbeiner, S., S.F. Tavazoie, A. Maloratsky, K.M. Jacobs, K.M. Harris, and M.E. Greenberg. 1997. CREB: a major mediator of neuronal neurotrophin responses. *Neuron*. 19:1031-1047.

Finsterwald, C., H. Fiumelli, J.R. Cardinaux, and J.L. Martin. 2010. Regulation of dendritic development by BDNF requires activation of CRTC1 by glutamate. *The Journal of biological chemistry*. 285:28587-28595.

Fischer, U., Q. Liu, and G. Dreyfuss. 1997. The SMN-SIP1 complex has an essential role in spliceosomal snRNP biogenesis. *Cell*. 90:1023-1029.

Foltran, R.B., and S.L. Diaz. 2016. BDNF isoforms: a round trip ticket between neurogenesis and serotonin? *Journal of neurochemistry*. 138:204-221.

Foust, K.D., X. Wang, V.L. McGovern, L. Braun, A.K. Bevan, A.M. Haidet, T.T. Le, P.R. Morales, M.M. Rich, A.H. Burghes, and B.K. Kaspar. 2010. Rescue of the spinal muscular atrophy phenotype in a mouse model by early postnatal delivery of SMN. *Nature biotechnology*. 28:271-274.

Friedman, B., D. Kleinfeld, N.Y. Ip, V.M. Verge, R. Moulton, P. Boland, E. Zlotchenko, R.M. Lindsay, and L. Liu. 1995. BDNF and NT-4/5 exert neurotrophic influences on injured adult spinal motor neurons. *The Journal of neuroscience : the official journal of the Society for Neuroscience*. 15:1044-1056.

Fu, X., Y. Yang, C. Xu, Y. Niu, T. Chen, Q. Zhou, and J.J. Liu. 2011. Retrolinkin cooperates with endophilin A1 to mediate BDNF-TrkB early endocytic trafficking and signaling from early endosomes. *Molecular biology of the cell*. 22:3684-3698.

Gabanella, F., M.E. Butchbach, L. Saieva, C. Carissimi, A.H. Burghes, and L. Pellizzoni. 2007. Ribonucleoprotein assembly defects correlate with spinal muscular atrophy severity and preferentially affect a subset of spliceosomal snRNPs. *PloS one*. 2:e921.

Gabanella, F., C. Pisani, A. Borreca, S. Farioli-Vecchioli, M.T. Ciotti, T. Ingegnere, A. Onori, M. Ammassari-Teule, N. Corbi, N. Canu, L. Monaco, C. Passananti, and M.G. Di Certo. 2016. SMN affects membrane remodelling and anchoring of the protein synthesis machinery. *Journal of cell science*. 129:804-816.

Galkin, V.E., A. Orlova, O. Cherepanova, M.C. Lebart, and E.H. Egelman. 2008. High-resolution cryo-EM structure of the F-actin-fimbrin/plastin ABD2 complex. *Proceedings of the National Academy of Sciences of the United States of America*. 105:1494-1498.

Gan, K.J., and M.A. Silverman. 2015. Dendritic and axonal mechanisms of Ca2+ elevation impair BDNF transport in Abeta oligomer-treated hippocampal neurons. *Molecular biology of the cell*. 26:1058-1071.

Garbett, D., A. Bisaria, C. Yang, D.G. McCarthy, A. Hayer, W.E. Moerner, T.M. Svitkina, and T. Meyer. 2020. T-Plastin reinforces membrane protrusions to bridge matrix gaps during cell migration. *Nature communications*. 11:4818.

Garcia, E.L., Z. Lu, M.P. Meers, K. Praveen, and A.G. Matera. 2013. Developmental arrest of Drosophila survival motor neuron (Smn) mutants accounts for differences in expression of minor intron-containing genes. *RNA*. 19:1510-1516.

Gartner, A., and V. Staiger. 2002. Neurotrophin secretion from hippocampal neurons evoked by long-term-potentiation-inducing electrical stimulation patterns. *Proceedings of the National Academy of Sciences of the United States of America*. 99:6386-6391.

Gennarelli, M., M. Lucarelli, F. Capon, A. Pizzuti, L. Merlini, C. Angelini, G. Novelli, and B. Dallapiccola. 1995. Survival motor neuron gene transcript analysis in muscles from spinal muscular atrophy patients. *Biochemical and biophysical research communications*. 213:342-348.

Gezen-Ak, D., E. Dursun, H. Hanagasi, B. Bilgic, E. Lohman, O.S. Araz, I.L. Atasoy, M. Alaylioglu, B. Onal, H. Gurvit, and S. Yilmazer. 2013. BDNF, TNFalpha, HSP90, CFH, and IL-10 serum levels in patients with early or late onset Alzheimer's disease or mild cognitive impairment. *Journal of Alzheimer's disease : JAD*. 37:185-195.

Giavazzi, A., V. Setola, A. Simonati, and G. Battaglia. 2006. Neuronal-specific roles of the survival motor neuron protein: evidence from survival motor neuron expression patterns in the developing human central nervous system. *Journal of neuropathology and experimental neurology*. 65:267-277.

Gibon, J., S.M. Buckley, N. Unsain, V. Kaartinen, P. Seguela, and P.A. Barker. 2015. proBDNF and p75NTR Control Excitability and Persistent Firing of Cortical Pyramidal Neurons. *The Journal of neuroscience : the official journal of the Society for Neuroscience*. 35:9741-9753.

Gidaro, T., and L. Servais. 2019. Nusinersen treatment of spinal muscular atrophy: current knowledge and existing gaps. *Developmental medicine and child neurology*. 61:19-24.

Giesemann, T., S. Rathke-Hartlieb, M. Rothkegel, J.W. Bartsch, S. Buchmeier, B.M. Jockusch, and H. Jockusch. 1999. A role for polyproline motifs in the spinal muscular atrophy protein SMN. Profilins bind to and colocalize with smn in nuclear gems. *The Journal of biological chemistry*. 274:37908-37914.

Giesemann, T., G. Schwarz, R. Nawrotzki, K. Berhorster, M. Rothkegel, K. Schluter, N. Schrader, H. Schindelin, R.R. Mendel, J. Kirsch, and B.M. Jockusch. 2003. Complex formation between the postsynaptic scaffolding protein gephyrin, profilin, and mena: A possible link of the microfilament system. *Journal of Neuroscience*. 23:8330-8339.

Giganti, A., J. Plastino, B. Janji, M. Van Troys, D. Lentz, C. Ampe, C. Sykes, and E. Friederich. 2005. Actin-filament cross-linking protein T-plastin increases Arp2/3-mediated actin-based movement. *Journal of cell science*. 118:1255-1265.

Glass, D.J., S.H. Nye, P. Hantzopoulos, M.J. Macchi, S.P. Squinto, M. Goldfarb, and G.D. Yancopoulos. 1991. TrkB mediates BDNF/NT-3-dependent survival and proliferation in fibroblasts lacking the low affinity NGF receptor. *Cell*. 66:405-413.

Glinka, M., T. Herrmann, N. Funk, S. Havlicek, W. Rossoll, C. Winkler, and M. Sendtner. 2010. The heterogeneous nuclear ribonucleoprotein-R is necessary for axonal beta-actin mRNA translocation in spinal motor neurons. *Human molecular genetics*. 19:1951-1966.

Goldsmith, S.C., N. Pokala, W. Shen, A.A. Fedorov, P. Matsudaira, and S.C. Almo. 1997. The structure of an actin-crosslinking domain from human fimbrin. *Nature structural biology*. 4:708-712.

Gomes, R.A., C. Hampton, F. El-Sabeawy, S.L. Sabo, and A.K. McAllister. 2006. The dynamic distribution of TrkB receptors before, during, and after synapse formation between cortical neurons. *The Journal of neuroscience : the official journal of the Society for Neuroscience*. 26:11487-11500.

Gonzalez-Gutierrez, A., O.M. Lazo, and F.C. Bronfman. 2020. The Rab5-Rab11 Endosomal Pathway is Required for BDNF-Induced CREB Transcriptional Regulation in Hippocampal Neurons. *The Journal of neuroscience : the official journal of the Society for Neuroscience*. 40:8042-8054.

Gonzalez, A., G. Moya-Alvarado, C. Gonzalez-Billault, and F.C. Bronfman. 2016. Cellular and molecular mechanisms regulating neuronal growth by brain-derived neurotrophic factor. *Cytoskeleton (Hoboken)*. 73:612-628.

Griesbeck, O., A.S. Parsadanian, M. Sendtner, and H. Thoenen. 1995. Expression of neurotrophins in skeletal muscle: quantitative comparison and significance for motoneuron survival and maintenance of function. *Journal of neuroscience research*. 42:21-33.

Grimes, M.L., E. Beattie, and W.C. Mobley. 1997. A signaling organelle containing the nerve growth factor-activated receptor tyrosine kinase, TrkA. *Proceedings of the National Academy of Sciences of the United States of America*. 94:9909-9914.

Grimes, M.L., J. Zhou, E.C. Beattie, E.C. Yuen, D.E. Hall, J.S. Valletta, K.S. Topp, J.H. LaVail, N.W. Bunnett, and W.C. Mobley. 1996. Endocytosis of activated TrkA: evidence that nerve growth factor induces formation of signaling endosomes. *The Journal of neuroscience : the official journal of the Society for Neuroscience*. 16:7950-7964.

Guo, S.L., G.H. Tan, S. Li, X.W. Cheng, Y. Zhou, Y.F. Jia, H. Xiong, J. Tao, and Z.Q. Xiong. 2012. Serum inducible kinase is a positive regulator of cortical dendrite development and is required for BDNF-promoted dendritic arborization. *Cell research*. 22:387-398.

Ha, J., K.W. Lo, K.R. Myers, T.M. Carr, M.K. Humsi, B.A. Rasoul, R.A. Segal, and K.K. Pfister. 2008. A neuron-specific cytoplasmic dynein isoform preferentially transports TrkB signaling endosomes. *The Journal of cell biology*. 181:1027-1039.

Haapasalo, A., I. Sipola, K. Larsson, K.E. Akerman, P. Stoilov, S. Stamm, G. Wong, and E. Castren. 2002. Regulation of TRKB surface expression by brain-derived neurotrophic factor and truncated TRKB isoforms. *The Journal of biological chemistry*. 277:43160-43167.

Hagiwara, M., H. Shinomiya, M. Kashihara, K. Kobayashi, T. Tadokoro, and Y. Yamamoto. 2011. Interaction of activated Rab5 with actin-bundling proteins, L- and T-plastin and its relevance to endocytic functions in mammalian cells. *Biochemical and biophysical research communications*. 407:615-619.

Hahnen, E., J. Schonling, S. Rudnik-Schoneborn, H. Raschke, K. Zerres, and B. Wirth. 1997. Missense mutations in exon 6 of the survival motor neuron gene in patients with spinal muscular atrophy (SMA). *Human molecular genetics*. 6:821-825.

Hanein, D., N. Volkmann, S. Goldsmith, A.M. Michon, W. Lehman, R. Craig, D. DeRosier, S. Almo, and P. Matsudaira. 1998. An atomic model of fimbrin binding to F-actin and its implications for filament crosslinking and regulation. *Nature structural biology*. 5:787-792.

Hannus, S., D. Buhler, M. Romano, B. Seraphin, and U. Fischer. 2000. The Schizosaccharomyces pombe protein Yab8p and a novel factor, Yip1p, share structural and functional similarity with the spinal muscular atrophy-associated proteins SMN and SIP1. *Human molecular genetics*. 9:663-674.

Hanson, I.M., A. Seawright, and V. van Heyningen. 1992. The human BDNF gene maps between FSHB and HVBS1 at the boundary of 11p13-p14. *Genomics*. 13:1331-1333.

Hao le, T., M. Wolman, M. Granato, and C.E. Beattie. 2012. Survival motor neuron affects plastin 3 protein levels leading to motor defects. *J Neurosci*. 32:5074-5084.

Harding, B.N., S. Kariya, U.R. Monani, W.K. Chung, M. Benton, S.W. Yum, G. Tennekoon, and R.S. Finkel. 2015. Spectrum of neuropathophysiology in spinal muscular atrophy type I. *Journal of neuropathology and experimental neurology*. 74:15-24.

Harrington, A.W., and D.D. Ginty. 2013. Long-distance retrograde neurotrophic factor signalling in neurons. *Nature reviews. Neuroscience*. 14:177-187.

Hartmann, M., R. Heumann, and V. Lessmann. 2001. Synaptic secretion of BDNF after high-frequency stimulation of glutamatergic synapses. *The EMBO journal*. 20:5887-5897.

Harward, S.C., N.G. Hedrick, C.E. Hall, P. Parra-Bueno, T.A. Milner, E. Pan, T. Laviv, B.L. Hempstead, R. Yasuda, and J.O. McNamara. 2016. Autocrine BDNF-TrkB signalling within a single dendritic spine. *Nature*. 538:99-103.

Heerssen, H.M., M.F. Pazyra, and R.A. Segal. 2004. Dynein motors transport activated Trks to promote survival of target-dependent neurons. *Nature neuroscience*. 7:596-604.

Heesen, L., M. Peitz, L. Torres-Benito, I. Holker, K. Hupperich, K. Dobrindt, J. Jungverdorben, S. Ritzenhofen, B. Weykopf, D. Eckert, S.M. Hosseini-Barkooie, M. Storbeck, N. Fusaki, R. Lonigro, R. Heller, M.J. Kye, O. Brustle, and B. Wirth. 2016. Plastin 3 is upregulated in iPSC-derived motoneurons from asymptomatic SMN1-deleted individuals. *Cellular and molecular life sciences : CMLS*. 73:2089-2104.

Heier, C.R., R. Satta, C. Lutz, and C.J. DiDonato. 2010. Arrhythmia and cardiac defects are a feature of spinal muscular atrophy model mice. *Human molecular genetics*. 19:3906-3918.

Helgager, J., Y.Z. Huang, and J.O. McNamara. 2014. Brain-derived neurotrophic factor but not vesicular zinc promotes TrkB activation within mossy fibers of mouse hippocampus in vivo. *The Journal of comparative neurology*. 522:3885-3899.

Henderson, C.E., W. Camu, C. Mettling, A. Gouin, K. Poulsen, M. Karihaloo, J. Rullamas, T. Evans, S.B. McMahon, M.P. Armanini, and et al. 1993. Neurotrophins promote motor neuron survival and are present in embryonic limb bud. *Nature*. 363:266-270.

Hensel, N., and P. Claus. 2018. The Actin Cytoskeleton in SMA and ALS: How Does It Contribute to Motoneuron Degeneration? *The Neuroscientist : a review journal bringing neurobiology, neurology and psychiatry*. 24:54-72.

Hetman, M., K. Kanning, J.E. Cavanaugh, and Z. Xia. 1999. Neuroprotection by brain-derived neurotrophic factor is mediated by extracellular signal-regulated kinase and phosphatidylinositol 3-kinase. *The Journal of biological chemistry*. 274:22569-22580.

Hirokawa, N., S. Niwa, and Y. Tanaka. 2010. Molecular motors in neurons: transport mechanisms and roles in brain function, development, and disease. *Neuron*. 68:610-638.

Hock, C., K. Heese, C. Hulette, C. Rosenberg, and U. Otten. 2000. Region-specific neurotrophin imbalances in Alzheimer disease: decreased levels of brain-derived neurotrophic factor and increased levels of nerve growth factor in hippocampus and cortical areas. *Archives of neurology*. 57:846-851.

Hoehner, J.C., T. Wester, S. Pahlman, and L. Olsen. 1996. Localization of neurotrophins and their high-affinity receptors during human enteric nervous system development. *Gastroenterology*. 110:756-767.

Hofer, M., S.R. Pagliusi, A. Hohn, J. Leibrock, and Y.A. Barde. 1990. Regional distribution of brain-derived neurotrophic factor mRNA in the adult mouse brain. *The EMBO journal*. 9:2459-2464.

Hoffmann, J. 1893. Ueber chronische spinal Muskelatrophie im Kindesalter, auf familiärer Basis. 1893. *Deutsche Zeitschrift fur Nervenheilkunde*. 3:427.

Hofmann, Y., and B. Wirth. 2002. hnRNP-G promotes exon 7 inclusion of survival motor neuron (SMN) via direct interaction with Htra2-beta1. *Human molecular genetics*. 11:2037-2049.

Hong, E.J., A.E. McCord, and M.E. Greenberg. 2008. A biological function for the neuronal activity-dependent component of Bdnf transcription in the development of cortical inhibition. *Neuron*. 60:610-624.

Hosseinibarkooie, S., M. Peters, L. Torres-Benito, R.H. Rastetter, K. Hupperich, A. Hoffmann, N. Mendoza-Ferreira, A. Kaczmarek, E. Janzen, J. Milbradt, T. Lamkemeyer, F. Rigo, C.F. Bennett, C. Guschlbauer, A. Buschges, M. Hammerschmidt, M. Riessland, M.J. Kye, C.S. Clemen, and B. Wirth. 2016. The Power of Human Protective Modifiers: PLS3 and CORO1C Unravel Impaired Endocytosis in Spinal Muscular Atrophy and Rescue SMA Phenotype. *American journal of human genetics*. 99:647-665.

Howe, C.L., J.S. Valletta, A.S. Rusnak, and W.C. Mobley. 2001. NGF signaling from clathrin-coated vesicles: evidence that signaling endosomes serve as a platform for the Ras-MAPK pathway. *Neuron*. 32:801-814.

Howells, D.W., M.J. Porritt, J.Y. Wong, P.E. Batchelor, R. Kalnins, A.J. Hughes, and G.A. Donnan. 2000. Reduced BDNF mRNA expression in the Parkinson's disease substantia nigra. *Experimental neurology*. 166:127-135.

Hoy, S.M. 2019. Onasemnogene Abeparvovec: First Global Approval. *Drugs*. 79:1255-1262.

Hsieh-Li, H.M., J.G. Chang, Y.J. Jong, M.H. Wu, N.M. Wang, C.H. Tsai, and H. Li. 2000. A mouse model for spinal muscular atrophy. *Nature genetics*. 24:66-70.

Hua, Y., T.A. Vickers, H.L. Okunola, C.F. Bennett, and A.R. Krainer. 2008. Antisense masking of an hnRNP A1/A2 intronic splicing silencer corrects SMN2 splicing in transgenic mice. *American journal of human genetics*. 82:834-848.

Huang da, W., B.T. Sherman, and R.A. Lempicki. 2009. Systematic and integrative analysis of large gene lists using DAVID bioinformatics resources. *Nature protocols*. 4:44-57.

Huang, E.J., and L.F. Reichardt. 2001. Neurotrophins: roles in neuronal development and function. *Annual review of neuroscience*. 24:677-736.

Huang, E.J., and L.F. Reichardt. 2003. Trk receptors: roles in neuronal signal transduction. *Annual review of biochemistry*. 72:609-642.

Huang, Y.Z., E. Pan, Z.Q. Xiong, and J.O. McNamara. 2008. Zinc-mediated transactivation of TrkB potentiates the hippocampal mossy fiber-CA3 pyramid synapse. *Neuron*. 57:546-558.

Hubers, L., H. Valderrama-Carvajal, J. Laframboise, J. Timbers, G. Sanchez, and J. Cote. 2011. HuD interacts with survival motor neuron protein and can rescue spinal muscular atrophy-like neuronal defects. *Human molecular genetics*. 20:553-579.

Iughetti, L., L. Lucaccioni, F. Fugetto, B. Predieri, A. Berardi, and F. Ferrari. 2018. Brain-derived neurotrophic factor and epilepsy: a systematic review. *Neuropeptides*. 72:23-29.

Iwakura, Y., H. Nawa, I. Sora, and M.V. Chao. 2008. Dopamine D1 receptor-induced signaling through TrkB receptors in striatal neurons. *The Journal of biological chemistry*. 283:15799-15806.

Jablonka, S., M. Bandilla, S. Wiese, D. Buhler, B. Wirth, M. Sendtner, and U. Fischer. 2001. Co-regulation of survival of motor neuron (SMN) protein and its interactor SIP1 during development and in spinal muscular atrophy. *Human molecular genetics*. 10:497-505.

Jablonka, S., M. Beck, B.D. Lechner, C. Mayer, and M. Sendtner. 2007. Defective Ca2+ channel clustering in axon terminals disturbs excitability in motoneurons in spinal muscular atrophy. *The Journal of cell biology*. 179:139-149.

Jablonka, S., L. Hennlein, and M. Sendtner. 2022. Therapy development for spinal muscular atrophy: perspectives for muscular dystrophies and neurodegenerative disorders. *Neurol Res Pract*. 4:2.

Jablonka, S., K. Karle, B. Sandner, C. Andreassi, K. von Au, and M. Sendtner. 2006. Distinct and overlapping alterations in motor and sensory neurons in a mouse model of spinal muscular atrophy. *Human molecular genetics*. 15:511-518.

Jablonka, S., B. Schrank, M. Kralewski, W. Rossoll, and M. Sendtner. 2000. Reduced survival motor neuron (Smn) gene dose in mice leads to motor neuron degeneration: an animal model for spinal muscular atrophy type III. *Human molecular genetics*. 9:341-346.

Jablonka, S., and M. Sendtner. 2017. Developmental regulation of SMN expression: pathophysiological implications and perspectives for therapy development in spinal muscular atrophy. *Gene therapy*. 24:506-513.

Jaworski, J., S. Spangler, D.P. Seeburg, C.C. Hoogenraad, and M. Sheng. 2005. Control of dendritic arborization by the phosphoinositide-3'-kinase-Akt-mammalian target of rapamycin pathway. *The Journal of neuroscience : the official journal of the Society for Neuroscience*. 25:11300-11312.

Je, H.S., F. Yang, Y. Ji, G. Nagappan, B.L. Hempstead, and B. Lu. 2012. Role of pro-brain-derived neurotrophic factor (proBDNF) to mature BDNF conversion in activity-dependent competition at developing neuromuscular synapses. *Proceedings of the National Academy of Sciences of the United States of America*. 109:15924-15929.

Jodelka, F.M., A.D. Ebert, D.M. Duelli, and M.L. Hastings. 2010. A feedback loop regulates splicing of the spinal muscular atrophy-modifying gene, SMN2. *Human molecular genetics*. 19:4906-4917.

Johnson, J.E., Y.A. Barde, M. Schwab, and H. Thoenen. 1986. Brain-derived neurotrophic factor supports the survival of cultured rat retinal ganglion cells. *The Journal of neuroscience : the official journal of the Society for Neuroscience*. 6:3031-3038.

Jones, K.R., I. Farinas, C. Backus, and L.F. Reichardt. 1994. Targeted disruption of the BDNF gene perturbs brain and sensory neuron development but not motor neuron development. *Cell*. 76:989-999.

Jorde, S., A. Walther, and J. Wendland. 2011. The Ashbya gossypii fimbrin SAC6 is required for fast polarized hyphal tip growth and endocytosis. *Microbiol Res*. 166:137-145.

Kaifer, K.A., E. Villalon, E.Y. Osman, J.J. Glascock, L.L. Arnold, D.D. Cornelison, and C.L. Lorson. 2017. Plastin-3 extends survival and reduces severity in mouse models of spinal muscular atrophy. *JCI insight*. 2:e89970.

Kalinowska-Lyszczarz, A., and J. Losy. 2012. The role of neurotrophins in multiple sclerosis-pathological and clinical implications. *International journal of molecular sciences*. 13:13713-13725.

Kaplan, D.R., and F.D. Miller. 2000. Neurotrophin signal transduction in the nervous system. *Current opinion in neurobiology*. 10:381-391.

Kariya, S., G.H. Park, Y. Maeno-Hikichi, O. Leykekhman, C. Lutz, M.S. Arkovitz, L.T. Landmesser, and U.R. Monani. 2008. Reduced SMN protein impairs maturation of the neuromuscular junctions in mouse models of spinal muscular atrophy. *Human molecular genetics*. 17:2552-2569.

Karpova, T.S., K. Tatchell, and J.A. Cooper. 1995. Actin filaments in yeast are unstable in the absence of capping protein or fimbrin. *The Journal of cell biology*. 131:1483-1493.

Kashima, T., and J.L. Manley. 2003. A negative element in SMN2 exon 7 inhibits splicing in spinal muscular atrophy. *Nature genetics*. 34:460-463.

Kashima, T., N. Rao, C.J. David, and J.L. Manley. 2007. hnRNP A1 functions with specificity in repression of SMN2 exon 7 splicing. *Human molecular genetics*. 16:3149-3159.

Katoh-Semba, R., I.K. Takeuchi, R. Semba, and K. Kato. 1997. Distribution of brain-derived neurotrophic factor in rats and its changes with development in the brain. *Journal of neurochemistry*. 69:34-42.

Kerschensteiner, M., E. Gallmeier, L. Behrens, V.V. Leal, T. Misgeld, W.E. Klinkert, R. Kolbeck, E. Hoppe, R.L. Oropeza-Wekerle, I. Bartke, C. Stadelmann, H. Lassmann, H. Wekerle, and R. Hohlfeld. 1999. Activated human T cells, B cells, and monocytes produce brain-derived neurotrophic factor in vitro and in inflammatory brain lesions: a neuroprotective role of inflammation? *The Journal of experimental medicine*. 189:865-870.

Khatri, I.A., U.S. Chaudhry, M.G. Seikaly, R.H. Browne, and S.T. Iannaccone. 2008. Low bone mineral density in spinal muscular atrophy. *Journal of clinical neuromuscular disease*. 10:11-17.

Kingsbury, T.J., P.D. Murray, L.L. Bambrick, and B.K. Krueger. 2003. Ca(2+)-dependent regulation of TrkB expression in neurons. *The Journal of biological chemistry*. 278:40744-40748.

Kingsmore, S.F., A. Henderson, M.J. Owen, M.M. Clark, C. Hansen, D. Dimmock, C.D. Chambers, L.L. Jeliffe-Pawlowski, and C. Hobbs. 2020. Measurement of genetic diseases as a cause of mortality in infants receiving whole genome sequencing. *Npj Genom Med*. 5.

Klein, M.G., W. Shi, U. Ramagopal, Y. Tseng, D. Wirtz, D.R. Kovar, C.J. Staiger, and S.C. Almo. 2004. Structure of the actin crosslinking core of fimbrin. *Structure*. 12:999-1013.

Klein, R., D. Conway, L.F. Parada, and M. Barbacid. 1990. The trkB tyrosine protein kinase gene codes for a second neurogenic receptor that lacks the catalytic kinase domain. *Cell*. 61:647-656.

Klein, R., V. Nanduri, S.A. Jing, F. Lamballe, P. Tapley, S. Bryant, C. Cordon-Cardo, K.R. Jones, L.F. Reichardt, and M. Barbacid. 1991. The trkB tyrosine protein kinase is a receptor for brain-derived neurotrophic factor and neurotrophin-3. *Cell*. 66:395-403.

Klein, R., L.F. Parada, F. Coulier, and M. Barbacid. 1989. trkB, a novel tyrosine protein kinase receptor expressed during mouse neural development. *The EMBO journal*. 8:3701-3709.

Klein, R., R.J. Smeyne, W. Wurst, L.K. Long, B.A. Auerbach, A.L. Joyner, and M. Barbacid. 1993. Targeted disruption of the trkB neurotrophin receptor gene results in nervous system lesions and neonatal death. *Cell*. 75:113-122.

Kohara, K., A. Kitamura, M. Morishima, and T. Tsumoto. 2001. Activity-dependent transfer of brain-derived neurotrophic factor to postsynaptic neurons. *Science*. 291:2419-2423.

Kolarow, R., T. Brigadski, and V. Lessmann. 2007. Postsynaptic secretion of BDNF and NT-3 from hippocampal neurons depends on calcium calmodulin kinase II signaling and proceeds via delayed fusion pore opening. *The Journal of neuroscience : the official journal of the Society for Neuroscience*. 27:10350-10364.

Koliatsos, V.E., R.E. Clatterbuck, J.W. Winslow, M.H. Cayouette, and D.L. Price. 1993. Evidence that brain-derived neurotrophic factor is a trophic factor for motor neurons in vivo. *Neuron*. 10:359-367.

Kong, L., X. Wang, D.W. Choe, M. Polley, B.G. Burnett, M. Bosch-Marce, J.W. Griffin, M.M. Rich, and C.J. Sumner. 2009. Impaired synaptic vesicle release and immaturity of neuromuscular junctions in spinal muscular atrophy mice. *The Journal of neuroscience : the official journal of the Society for Neuroscience*. 29:842-851.

Korte, M., P. Carroll, E. Wolf, G. Brem, H. Thoenen, and T. Bonhoeffer. 1995. Hippocampal long-term potentiation is impaired in mice lacking brain-derived neurotrophic factor. *Proceedings of the National Academy of Sciences of the United States of America*. 92:8856-8860.

Korte, M., V. Staiger, O. Griesbeck, H. Thoenen, and T. Bonhoeffer. 1996. The involvement of brain-derived neurotrophic factor in hippocampal long-term potentiation revealed by gene targeting experiments. *Journal of physiology, Paris*. 90:157-164.

Kowianski, P., G. Lietzau, E. Czuba, M. Waskow, A. Steliga, and J. Morys. 2018. BDNF: A Key Factor with Multipotent Impact on Brain Signaling and Synaptic Plasticity. *Cellular and molecular neurobiology*. 38:579-593.

Kroiss, M., J. Schultz, J. Wiesner, A. Chari, A. Sickmann, and U. Fischer. 2008. Evolution of an RNP assembly system: a minimal SMN complex facilitates formation of UsnRNPs in Drosophila melanogaster. *Proceedings of the National Academy of Sciences of the United States of America*. 105:10045-10050.

Kryl, D., T. Yacoubian, A. Haapasalo, E. Castren, D. Lo, and P.A. Barker. 1999. Subcellular localization of full-length and truncated Trk receptor isoforms in polarized neurons and epithelial cells. *The Journal of neuroscience : the official journal of the Society for Neuroscience*. 19:5823-5833.

Kubler, E., and H. Riezman. 1993. Actin and fimbrin are required for the internalization step of endocytosis in yeast. *The EMBO journal*. 12:2855-2862.

Kugelberg, E., and L. Welander. 1956. Heredofamilial juvenile muscular atrophy simulating muscular dystrophy. *A.M.A. archives of neurology and psychiatry*. 75:500-509.

Kulakowski, S.A., S.D. Parker, and K.E. Personius. 2011. Reduced TrkB expression results in precocious age-like changes in neuromuscular structure, neurotransmission, and muscle function. *J Appl Physiol (1985)*. 111:844-852.

Kumar, V., M.X. Zhang, M.W. Swank, J. Kunz, and G.Y. Wu. 2005. Regulation of dendritic morphogenesis by Ras-PI3K-Akt-mTOR and Ras-MAPK signaling pathways. *The Journal of neuroscience : the official journal of the Society for Neuroscience*. 25:11288-11299.

Kwon, M., J.R. Fernandez, G.F. Zegarek, S.B. Lo, and B.L. Firestein. 2011. BDNF-promoted increases in proximal dendrites occur via CREB-dependent transcriptional regulation of cypin. *The Journal of neuroscience : the official journal of the Society for Neuroscience*. 31:9735-9745.

Kwon, Y.W., and M.E. Gurney. 1996. Brain-derived neurotrophic factor transiently stabilizes silent synapses on developing neuromuscular junctions. *Journal of neurobiology*. 29:503-516.

La Bella, V., C. Cisterni, D. Salaun, and B. Pettmann. 1998. Survival motor neuron (SMN) protein in rat is expressed as different molecular forms and is developmentally regulated. *The European journal of neuroscience*. 10:2913-2923.

Lai, K.O., A.S. Wong, M.C. Cheung, P. Xu, Z. Liang, K.C. Lok, H. Xie, M.E. Palko, W.H. Yung, L. Tessarollo, Z.H. Cheung, and N.Y. Ip. 2012. TrkB phosphorylation by Cdk5 is required for activity-dependent structural plasticity and spatial memory. *Nature neuroscience*. 15:1506-1515.

Laske, C., K. Stellos, N. Hoffmann, E. Stransky, G. Straten, G.W. Eschweiler, and T. Leyhe. 2011. Higher BDNF serum levels predict slower cognitive decline in Alzheimer's disease patients. *The international journal of neuropsychopharmacology*. 14:399-404.

Le, T.T., L.T. Pham, M.E. Butchbach, H.L. Zhang, U.R. Monani, D.D. Coovert, T.O. Gavrilina, L. Xing, G.J. Bassell, and A.H. Burghes. 2005. SMNDelta7, the major product of the centromeric survival motor neuron (SMN2) gene, extends survival in mice with spinal muscular atrophy and associates with full-length SMN. *Human molecular genetics*. 14:845-857.

Lee, C.W., E.A. Vitriol, S. Shim, A.L. Wise, R.P. Velayutham, and J.Q. Zheng. 2013. Dynamic localization of G-actin during membrane protrusion in neuronal motility. *Current biology : CB*. 23:1046-1056.

Lee, F.S., and M.V. Chao. 2001. Activation of Trk neurotrophin receptors in the absence of neurotrophins. *Proceedings of the National Academy of Sciences of the United States of America*. 98:3555-3560.

Lee, F.S., R. Rajagopal, and M.V. Chao. 2002a. Distinctive features of Trk neurotrophin receptor transactivation by G protein-coupled receptors. *Cytokine & growth factor reviews*. 13:11-17.

Lee, F.S., R. Rajagopal, A.H. Kim, P.C. Chang, and M.V. Chao. 2002b. Activation of Trk neurotrophin receptor signaling by pituitary adenylate cyclase-activating polypeptides. *The Journal of biological chemistry*. 277:9096-9102.

Lee, K., J.L. Gallop, K. Rambani, and M.W. Kirschner. 2010. Self-assembly of filopodia-like structures on supported lipid bilayers. *Science*. 329:1341-1345.

Lefebvre, S., L. Burglen, S. Reboullet, O. Clermont, P. Burlet, L. Viollet, B. Benichou, C. Cruaud, P. Millasseau, M. Zeviani, and et al. 1995. Identification and characterization of a spinal muscular atrophy-determining gene. *Cell*. 80:155-165.

Lefebvre, S., P. Burlet, Q. Liu, S. Bertrandy, O. Clermont, A. Munnich, G. Dreyfuss, and J. Melki. 1997. Correlation between severity and SMN protein level in spinal muscular atrophy. *Nature genetics*. 16:265-269.

Leibrock, J., F. Lottspeich, A. Hohn, M. Hofer, B. Hengerer, P. Masiakowski, H. Thoenen, and Y.A. Barde. 1989. Molecular cloning and expression of brain-derived neurotrophic factor. *Nature*. 341:149-152.

Li, D.K., S. Tisdale, F. Lotti, and L. Pellizzoni. 2014. SMN control of RNP assembly: from post-transcriptional gene regulation to motor neuron disease. *Seminars in cell & developmental biology*. 32:22-29.

Li, L., R.W. Oppenheim, M. Lei, and L.J. Houenou. 1994. Neurotrophic agents prevent motoneuron death following sciatic nerve section in the neonatal mouse. *Journal of neurobiology*. 25:759-766.

Li, Y., D. Yui, B.W. Luikart, R.M. McKay, J.L. Rubenstein, and L.F. Parada. 2012. Conditional ablation of brain-derived neurotrophic factor-TrkB signaling impairs striatal neuron development. *Proceedings of the National Academy of Sciences of the United States of America*. 109:15491-15496.

Lima Giacobbo, B., J. Doorduin, H.C. Klein, R. Dierckx, E. Bromberg, and E.F.J. de Vries. 2019. Brain-Derived Neurotrophic Factor in Brain Disorders: Focus on Neuroinflammation. *Molecular neurobiology*. 56:3295-3312.

Lin, C.S., R.H. Aebersold, S.B. Kent, M. Varma, and J. Leavitt. 1988. Molecular cloning and characterization of plastin, a human leukocyte protein expressed in transformed human fibroblasts. *Molecular and cellular biology*. 8:4659-4668.

Lin, C.S., T. Park, Z.P. Chen, and J. Leavitt. 1993. Human plastin genes. Comparative gene structure, chromosome location, and differential expression in normal and neoplastic cells. *The Journal of biological chemistry*. 268:2781-2792.

Lin, C.S., W. Shen, Z.P. Chen, Y.H. Tu, and P. Matsudaira. 1994. Identification of I-plastin, a human fimbrin isoform expressed in intestine and kidney. *Molecular and cellular biology*. 14:2457-2467.

Lin, P.Y., E.T. Kavalali, and L.M. Monteggia. 2018. Genetic Dissection of Presynaptic and Postsynaptic BDNF-TrkB Signaling in Synaptic Efficacy of CA3-CA1 Synapses. *Cell reports*. 24:1550-1561.

Lindholm, D., G. Dechant, C.P. Heisenberg, and H. Thoenen. 1993. Brain-derived neurotrophic factor is a survival factor for cultured rat cerebellar granule neurons and protects them against glutamate-induced neurotoxicity. *The European journal of neuroscience*. 5:1455-1464.

Ling, K.K., R.M. Gibbs, Z. Feng, and C.P. Ko. 2012. Severe neuromuscular denervation of clinically relevant muscles in a mouse model of spinal muscular atrophy. *Human molecular genetics*. 21:185-195.

Ling, K.K., M.Y. Lin, B. Zingg, Z. Feng, and C.P. Ko. 2010. Synaptic defects in the spinal and neuromuscular circuitry in a mouse model of spinal muscular atrophy. *PloS one*. 5:e15457.

Linnarsson, S., A. Bjorklund, and P. Ernfors. 1997. Learning deficit in BDNF mutant mice. *The European journal of neuroscience*. 9:2581-2587.

Linnarsson, S., C.A. Willson, and P. Ernfors. 2000. Cell death in regenerating populations of neurons in BDNF mutant mice. *Brain research. Molecular brain research*. 75:61-69.

Liou, J.C., R.S. Yang, and W.M. Fu. 1997. Regulation of quantal secretion by neurotrophic factors at developing motoneurons in Xenopus cell cultures. *The Journal of physiology*. 503 (Pt 1):129-139.

Liu, Q., and G. Dreyfuss. 1996. A novel nuclear structure containing the survival of motor neurons protein. *The EMBO journal*. 15:3555-3565.

Liu, Q., U. Fischer, F. Wang, and G. Dreyfuss. 1997. The spinal muscular atrophy disease gene product, SMN, and its associated protein SIP1 are in a complex with spliceosomal snRNP proteins. *Cell*. 90:1013-1021.

Liu, X., P. Ernfors, H. Wu, and R. Jaenisch. 1995. Sensory but not motor neuron deficits in mice lacking NT4 and BDNF. *Nature*. 375:238-241.

Liu, X.H., Z. Geng, J. Yan, T. Li, Q. Chen, Q.Y. Zhang, and Z.Y. Chen. 2015. Blocking GSK3beta-mediated dynamin1 phosphorylation enhances BDNF-dependent TrkB endocytosis and the protective effects of BDNF in neuronal and mouse models of Alzheimer's disease. *Neurobiology of disease*. 74:377-391.

Livak, K.J., and T.D. Schmittgen. 2001. Analysis of relative gene expression data using real-time quantitative PCR and the 2(-Delta Delta C(T)) Method. *Methods*. 25:402-408.

Lohof, A.M., N.Y. Ip, and M.M. Poo. 1993. Potentiation of developing neuromuscular synapses by the neurotrophins NT-3 and BDNF. *Nature*. 363:350-353.

Lorson, C.L., and E.J. Androphy. 1998. The domain encoded by exon 2 of the survival motor neuron protein mediates nucleic acid binding. *Human molecular genetics*. 7:1269-1275.

Lorson, C.L., and E.J. Androphy. 2000. An exonic enhancer is required for inclusion of an essential exon in the SMA-determining gene SMN. *Human molecular genetics*. 9:259-265.

Lorson, C.L., E. Hahnen, E.J. Androphy, and B. Wirth. 1999. A single nucleotide in the SMN gene regulates splicing and is responsible for spinal muscular atrophy. *Proceedings of the National Academy of Sciences of the United States of America*. 96:6307-6311.

Lorson, C.L., J. Strasswimmer, J.M. Yao, J.D. Baleja, E. Hahnen, B. Wirth, T. Le, A.H. Burghes, and E.J. Androphy. 1998. SMN oligomerization defect correlates with spinal muscular atrophy severity. *Nature genetics*. 19:63-66.

Lotti, F., W.L. Imlach, L. Saieva, E.S. Beck, T. Hao le, D.K. Li, W. Jiao, G.Z. Mentis, C.E. Beattie, B.D. McCabe, and L. Pellizzoni. 2012. An SMN-dependent U12 splicing event essential for motor circuit function. *Cell*. 151:440-454.

Lou, H., S.K. Kim, E. Zaitsev, C.R. Snell, B. Lu, and Y.P. Loh. 2005. Sorting and activity-dependent secretion of BDNF require interaction of a specific motif with the sorting receptor carboxypeptidase e. *Neuron*. 45:245-255.

Lu, B. 2003. BDNF and activity-dependent synaptic modulation. *Learn Mem*. 10:86-98.

Lu, B., P.T. Pang, and N.H. Woo. 2005. The yin and yang of neurotrophin action. *Nature reviews. Neuroscience*. 6:603-614.

Luberg, K., J. Wong, C.S. Weickert, and T. Timmusk. 2010. Human TrkB gene: novel alternative transcripts, protein isoforms and expression pattern in the prefrontal cerebral cortex during postnatal development. *Journal of neurochemistry*. 113:952-964.

Luikart, B.W., W. Zhang, G.A. Wayman, C.H. Kwon, G.L. Westbrook, and L.F. Parada. 2008. Neurotrophin-dependent dendritic filopodial motility: a convergence on PI3K signaling. *The Journal of neuroscience : the official journal of the Society for Neuroscience*. 28:7006-7012.

Lush, M.E., L. Ma, and L.F. Parada. 2005. TrkB signaling regulates the developmental maturation of the somatosensory cortex. *International journal of developmental neuroscience : the official journal of the International Society for Developmental Neuroscience*. 23:523-536.

Lyon, A.N., R.H. Pineda, T. Hao le, E. Kudryashova, D.S. Kudryashov, and C.E. Beattie. 2014. Calcium binding is essential for plastin 3 function in Smn-deficient motoneurons. *Human molecular genetics*. 23:1990-2004.

MacKenzie, A., N. Roy, A. Besner, G. Mettler, P. Jacob, R. Korneluk, and L. Surh. 1993. Genetic linkage analysis of Canadian spinal muscular atrophy kindreds using flanking microsatellite 5q13 polymorphisms. *Human genetics*. 90:501-504.

Maisonpierre, P.C., L. Belluscio, B. Friedman, R.F. Alderson, S.J. Wiegand, M.E. Furth, R.M. Lindsay, and G.D. Yancopoulos. 1990. NT-3, BDNF, and NGF in the developing rat nervous system: parallel as well as reciprocal patterns of expression. *Neuron*. 5:501-509.

Martin, R., K. Gupta, N.S. Ninan, K. Perry, and G.D. Van Duyne. 2012. The survival motor neuron protein forms soluble glycine zipper oligomers. *Structure*. 20:1929-1939.

Matsuda, N., H. Lu, Y. Fukata, J. Noritake, H. Gao, S. Mukherjee, T. Nemoto, M. Fukata, and M.M. Poo. 2009. Differential activity-dependent secretion of brain-derived neurotrophic factor from axon and dendrite. *The Journal of neuroscience : the official journal of the Society for Neuroscience*. 29:14185-14198.

Matthews, V.B., M.B. Astrom, M.H. Chan, C.R. Bruce, K.S. Krabbe, O. Prelovsek, T. Akerstrom, C. Yfanti, C. Broholm, O.H. Mortensen, M. Penkowa, P. Hojman, A. Zankari, M.J. Watt, H. Bruunsgaard, B.K. Pedersen, and M.A. Febbraio. 2009. Brain-derived neurotrophic factor is produced by skeletal muscle cells in response to contraction and enhances fat oxidation via activation of AMP-activated protein kinase. *Diabetologia*. 52:1409-1418.

McAndrew, P.E., D.W. Parsons, L.R. Simard, C. Rochette, P.N. Ray, J.R. Mendell, T.W. Prior, and A.H. Burghes. 1997. Identification of proximal spinal muscular atrophy carriers and patients by analysis of SMNT and SMNC gene copy number. *American journal of human genetics*. 60:1411-1422.

McGovern, V.L., T.O. Gavrilina, C.E. Beattie, and A.H. Burghes. 2008. Embryonic motor axon development in the severe SMA mouse. *Human molecular genetics*. 17:2900-2909.

McWhorter, M.L., U.R. Monani, A.H. Burghes, and C.E. Beattie. 2003. Knockdown of the survival motor neuron (Smn) protein in zebrafish causes defects in motor axon outgrowth and pathfinding. *The Journal of cell biology*. 162:919-931.

Meister, G., D. Buhler, B. Laggerbauer, M. Zobawa, F. Lottspeich, and U. Fischer. 2000. Characterization of a nuclear 20S complex containing the survival of motor neurons (SMN) protein and a specific subset of spliceosomal Sm proteins. *Human molecular genetics*. 9:1977-1986.

Mendell, J.R., S. Al-Zaidy, R. Shell, W.D. Arnold, L.R. Rodino-Klapac, T.W. Prior, L. Lowes, L. Alfano, K. Berry, K. Church, J.T. Kissel, S. Nagendran, J. L'Italien, D.M. Sproule, C. Wells, J.A. Cardenas, M.D. Heitzer, A. Kaspar, S. Corcoran, L. Braun, S. Likhite, C. Miranda, K. Meyer, K.D. Foust, A.H.M. Burghes, and B.K. Kaspar. 2017. Single-Dose Gene-Replacement Therapy for Spinal Muscular Atrophy. *The New England journal of medicine*. 377:1713-1722.

Mentis, G.Z., D. Blivis, W. Liu, E. Drobac, M.E. Crowder, L. Kong, F.J. Alvarez, C.J. Sumner, and M.J. O'Donovan. 2011. Early functional impairment of sensory-motor connectivity in a mouse model of spinal muscular atrophy. *Neuron*. 69:453-467.

Meyer-Franke, A., M.R. Kaplan, F.W. Pfrieger, and B.A. Barres. 1995. Characterization of the signaling interactions that promote the survival and growth of developing retinal ganglion cells in culture. *Neuron*. 15:805-819.

Meyer-Franke, A., G.A. Wilkinson, A. Kruttgen, M. Hu, E. Munro, M.G. Hanson, Jr., L.F. Reichardt, and B.A. Barres. 1998. Depolarization and cAMP elevation rapidly recruit TrkB to the plasma membrane of CNS neurons. *Neuron*. 21:681-693.

Michaelsen-Preusse, K., S. Zessin, G. Grigoryan, F. Scharkowski, J. Feuge, A. Remus, and M. Korte. 2016. Neuronal profilins in health and disease: Relevance for spine plasticity and Fragile X syndrome. *Proceedings of the National Academy of Sciences of the United States of America*. 113:3365-3370.

Middlemas, D.S., R.A. Lindberg, and T. Hunter. 1991. trkB, a neural receptor protein-tyrosine kinase: evidence for a full-length and two truncated receptors. *Molecular and cellular biology*. 11:143-153.

Miguel-Aliaga, I., Y.B. Chan, K.E. Davies, and M. van den Heuvel. 2000. Disruption of SMN function by ectopic expression of the human SMN gene in Drosophila. *FEBS letters*. 486:99-102.

Miguel-Aliaga, I., E. Culetto, D.S. Walker, H.A. Baylis, D.B. Sattelle, and K.E. Davies. 1999. The Caenorhabditis elegans orthologue of the human gene responsible for spinal muscular atrophy is a maternal product critical for germline maturation and embryonic viability. *Human molecular genetics*. 8:2133-2143.

Minichiello, L. 2009. TrkB signalling pathways in LTP and learning. *Nature reviews. Neuroscience*. 10:850-860.

Minichiello, L., A.M. Calella, D.L. Medina, T. Bonhoeffer, R. Klein, and M. Korte. 2002. Mechanism of TrkB-mediated hippocampal long-term potentiation. *Neuron*. 36:121-137.

Miyakawa, T., H. Shinomiya, F. Yumoto, Y. Miyauchi, H. Tanaka, T. Ojima, Y.S. Kato, and M. Tanokura. 2012. Different Ca(2)(+)-sensitivities between the EF-hands of T- and L-plastins. *Biochemical and biophysical research communications*. 429:137-141.

Monani, U.R., C.L. Lorson, D.W. Parsons, T.W. Prior, E.J. Androphy, A.H. Burghes, and J.D. McPherson. 1999. A single nucleotide difference that alters splicing patterns distinguishes the SMA gene SMN1 from the copy gene SMN2. *Human molecular genetics*. 8:1177-1183.

Monani, U.R., M. Sendtner, D.D. Coovert, D.W. Parsons, C. Andreassi, T.T. Le, S. Jablonka, B. Schrank, W. Rossoll, T.W. Prior, G.E. Morris, and A.H. Burghes. 2000. The human centromeric survival motor neuron gene (SMN2) rescues embryonic lethality in Smn(-/-) mice and results in a mouse with spinal muscular atrophy. *Human molecular genetics*. 9:333-339.

Moradi, M., R. Sivadasan, L. Saal, P. Luningschror, B. Dombert, R.J. Rathod, D.C. Dieterich, R. Blum, and M. Sendtner. 2017. Differential roles of alpha-, beta-, and gamma-actin in axon growth and collateral branch formation in motoneurons. *The Journal of cell biology*. 216:793-814.

Mowla, S.J., H.F. Farhadi, S. Pareek, J.K. Atwal, S.J. Morris, N.G. Seidah, and R.A. Murphy. 2001. Biosynthesis and post-translational processing of the precursor to brain-derived neurotrophic factor. *The Journal of biological chemistry*. 276:12660-12666.

Moya-Alvarado, G., A. Gonzalez, N. Stuardo, and F.C. Bronfman. 2018. Brain-Derived Neurotrophic Factor (BDNF) Regulates Rab5-Positive Early Endosomes in Hippocampal Neurons to Induce Dendritic Branching. *Frontiers in cellular neuroscience*. 12:493.

Mullins, R.D., J.F. Kelleher, J. Xu, and T.D. Pollard. 1998. Arp2/3 complex from Acanthamoeba binds profilin and cross-links actin filaments. *Molecular biology of the cell*. 9:841-852.

Munsat, T.L., and K.E. Davies. 1992. International SMA consortium meeting. (26-28 June 1992, Bonn, Germany). *Neuromuscular disorders : NMD*. 2:423-428.

Murk, K., M. Ornaghi, and J. Schiweck. 2021. Profilin Isoforms in Health and Disease - All the Same but Different. *Frontiers in cell and developmental biology*. 9.

Murray, L.M., L.H. Comley, D. Thomson, N. Parkinson, K. Talbot, and T.H. Gillingwater. 2008. Selective vulnerability of motor neurons and dissociation of pre- and post-synaptic pathology at the neuromuscular junction in mouse models of spinal muscular atrophy. *Human molecular genetics*. 17:949-962.

Murray, L.M., S. Lee, D. Baumer, S.H. Parson, K. Talbot, and T.H. Gillingwater. 2010. Pre-symptomatic development of lower motor neuron connectivity in a mouse model of severe spinal muscular atrophy. *Human molecular genetics*. 19:420-433.

Nakagawara, A., X.G. Liu, N. Ikegaki, P.S. White, D.J. Yamashiro, L.M. Nycum, J.A. Biegel, and G.M. Brodeur. 1995. Cloning and chromosomal localization of the human TRK-B tyrosine kinase receptor gene (NTRK2). *Genomics*. 25:538-546.

Namba, Y., M. Ito, Y. Zu, K. Shigesada, and K. Maruyama. 1992. Human T cell L-plastin bundles actin filaments in a calcium-dependent manner. *Journal of biochemistry*. 112:503-507.

Nash, L.A., J.K. Burns, J.W. Chardon, R. Kothary, and R.J. Parks. 2016. Spinal Muscular Atrophy: More than a Disease of Motor Neurons? *Current molecular medicine*. 16:779-792.

Neugebauer, J., J. Heilig, S. Hosseinibarkooie, B.C. Ross, N. Mendoza-Ferreira, F. Nolte, M. Peters, I. Holker, K. Hupperich, T. Tschanz, V. Grysko, F. Zaucke, A. Niehoff, and B. Wirth. 2018. Plastin 3 influences bone homeostasis through regulation of osteoclast activity. *Human molecular genetics*. 27:4249-4262.

Nicklin, P.L., D. Bayley, J. Giddings, S.J. Craig, L.L. Cummins, J.G. Hastewell, and J.A. Phillips. 1998. Pulmonary bioavailability of a phosphorothioate oligonucleotide (CGP 64128A): comparison with other delivery routes. *Pharmaceutical research*. 15:583-591.

Nolle, A., A. Zeug, J. van Bergeijk, L. Tonges, R. Gerhard, H. Brinkmann, S. Al Rayes, N. Hensel, Y. Schill, D. Apkhazava, S. Jablonka, J. O'Mer, R.K. Srivastav, A. Baasner, P. Lingor, B. Wirth, E. Ponimaskin, R. Niedenthal, C. Grothe, and P. Claus. 2011. The spinal muscular atrophy disease protein SMN is linked to the Rho-kinase pathway via profilin. *Human molecular genetics*. 20:4865-4878.

Notaras, M., and M. van den Buuse. 2019. Brain-Derived Neurotrophic Factor (BDNF): Novel Insights into Regulation and Genetic Variation. *The Neuroscientist : a review journal bringing neurobiology, neurology and psychiatry*. 25:434-454.

Novikov, L., L. Novikova, and J.O. Kellerth. 1997. Brain-derived neurotrophic factor promotes axonal regeneration and long-term survival of adult rat spinal motoneurons in vivo. *Neuroscience*. 79:765-774.

Numakawa, T., T. Matsumoto, N. Adachi, D. Yokomaku, M. Kojima, N. Takei, and H. Hatanaka. 2001. Brain-derived neurotrophic factor triggers a rapid glutamate release through increase of intracellular Ca(2+) and Na(+) in cultured cerebellar neurons. *Journal of neuroscience research*. 66:96-108.

Numakawa, T., S. Yamagishi, N. Adachi, T. Matsumoto, D. Yokomaku, M. Yamada, and H. Hatanaka. 2002. Brain-derived neurotrophic factor-induced potentiation of Ca(2+) oscillations in developing cortical neurons. *The Journal of biological chemistry*. 277:6520-6529.

Ogawa, C., K. Usui, M. Aoki, F. Ito, M. Itoh, C. Kai, M. Kanamori-Katayama, Y. Hayashizaki, and H. Suzuki. 2007. Gemin2 plays an important role in stabilizing the survival of motor neuron complex. *The Journal of biological chemistry*. 282:11122-11134.

Olenick, M.A., R. Dominguez, and E.L.F. Holzbaur. 2019. Dynein activator Hook1 is required for trafficking of BDNF-signaling endosomes in neurons. *The Journal of cell biology*. 218:220-233.

Oppenheim, R.W. 1991. Cell death during development of the nervous system. *Annual review of neuroscience*. 14:453-501.

Oppenheim, R.W., Q.W. Yin, D. Prevette, and Q. Yan. 1992. Brain-derived neurotrophic factor rescues developing avian motoneurons from cell death. *Nature*. 360:755-757.

Oprea, G.E., S. Krober, M.L. McWhorter, W. Rossoll, S. Muller, M. Krawczak, G.J. Bassell, C.E. Beattie, and B. Wirth. 2008. Plastin 3 is a protective modifier of autosomal recessive spinal muscular atrophy. *Science*. 320:524-527.

Owen, N., C.L. Doe, J. Mellor, and K.E. Davies. 2000. Characterization of the Schizosaccharomyces pombe orthologue of the human survival motor neuron (SMN) protein. *Human molecular genetics*. 9:675-684.

Pagliardini, S., A. Giavazzi, V. Setola, C. Lizier, M. Di Luca, S. DeBiasi, and G. Battaglia. 2000. Subcellular localization and axonal transport of the survival motor neuron (SMN) protein in the developing rat spinal cord. *Human molecular genetics*. 9:47-56.

Pagliarini, V., L. Pelosi, M.B. Bustamante, A. Nobili, M.G. Berardinelli, M. D'Amelio, A. Musaro, and C. Sette. 2015. SAM68 is a physiological regulator of SMN2 splicing in spinal muscular atrophy. *The Journal of cell biology*. 211:77-90.

Palasz, E., A. Wysocka, A. Gasiorowska, M. Chalimoniuk, W. Niewiadomski, and G. Niewiadomska. 2020. BDNF as a Promising Therapeutic Agent in Parkinson's Disease. *International journal of molecular sciences*. 21.

Pang, P.T., H.K. Teng, E. Zaitsev, N.T. Woo, K. Sakata, S. Zhen, K.K. Teng, W.H. Yung, B.L. Hempstead, and B. Lu. 2004. Cleavage of proBDNF by tPA/plasmin is essential for long-term hippocampal plasticity. *Science*. 306:487-491.

Park, H., and M.M. Poo. 2013. Neurotrophin regulation of neural circuit development and function. *Nature reviews. Neuroscience*. 14:7-23.

Parsons, D.W., P.E. McAndrew, P.S. Allinson, W.D. Parker, Jr., A.H. Burghes, and T.W. Prior. 1998a. Diagnosis of spinal muscular atrophy in an SMN non-deletion patient using a quantitative PCR screen and mutation analysis. *Journal of medical genetics*. 35:674-676.

Parsons, D.W., P.E. McAndrew, S.T. Iannaccone, J.R. Mendell, A.H. Burghes, and T.W. Prior. 1998b. Intragenic telSMN mutations: frequency, distribution, evidence of a founder effect, and modification of the spinal muscular atrophy phenotype by cenSMN copy number. *American journal of human genetics*. 63:1712-1723.

Parsons, D.W., P.E. McAndrew, U.R. Monani, J.R. Mendell, A.H. Burghes, and T.W. Prior. 1996. An 11 base pair duplication in exon 6 of the SMN gene produces a type I spinal muscular atrophy (SMA) phenotype: further evidence for SMN as the primary SMA-determining gene. *Human molecular genetics*. 5:1727-1732.

Patterson, S.L., T. Abel, T.A. Deuel, K.C. Martin, J.C. Rose, and E.R. Kandel. 1996. Recombinant BDNF rescues deficits in basal synaptic transmission and hippocampal LTP in BDNF knockout mice. *Neuron*. 16:1137-1145.

Paushkin, S., B. Charroux, L. Abel, R.A. Perkinson, L. Pellizzoni, and G. Dreyfuss. 2000. The survival motor neuron protein of Schizosacharomyces pombe. Conservation of survival motor neuron interaction domains in divergent organisms. *The Journal of biological chemistry*. 275:23841-23846.

Pedrotti, S., P. Bielli, M.P. Paronetto, F. Ciccosanti, G.M. Fimia, S. Stamm, J.L. Manley, and C. Sette. 2010. The splicing regulator Sam68 binds to a novel exonic splicing silencer and functions in SMN2 alternative splicing in spinal muscular atrophy. *The EMBO journal*. 29:1235-1247.

Pellizzoni, L. 2007. Chaperoning ribonucleoprotein biogenesis in health and disease. *EMBO reports*. 8:340-345.

Pellizzoni, L., N. Kataoka, B. Charroux, and G. Dreyfuss. 1998. A novel function for SMN, the spinal muscular atrophy disease gene product, in pre-mRNA splicing. *Cell*. 95:615-624.

Perez-Pinera, P., O. Garcia-Suarez, A. Germana, B. Diaz-Esnal, F. de Carlos, I. Silos-Santiago, M.E. del Valle, J. Cobo, and J.A. Vega. 2008. Characterization of sensory deficits in TrkB knockout mice. *Neuroscience letters*. 433:43-47.

Phillips, H.S., J.M. Hains, M. Armanini, G.R. Laramee, S.A. Johnson, and J.W. Winslow. 1991. BDNF mRNA is decreased in the hippocampus of individuals with Alzheimer's disease. *Neuron*. 7:695-702.

Poirier, A., M. Weetall, K. Heinig, F. Bucheli, K. Schoenlein, J. Alsenz, S. Bassett, M. Ullah, C. Senn, H. Ratni, N. Naryshkin, S. Paushkin, and L. Mueller. 2018. Risdiplam distributes and increases SMN protein in both the central nervous system and peripheral organs. *Pharmacology research & perspectives*. 6:e00447.

Pradhan, J., P.G. Noakes, and M.C. Bellingham. 2019. The Role of Altered BDNF/TrkB Signaling in Amyotrophic Lateral Sclerosis. *Frontiers in cellular neuroscience*. 13:368.

Praveen, K., Y. Wen, and A.G. Matera. 2012. A Drosophila model of spinal muscular atrophy uncouples snRNP biogenesis functions of survival motor neuron from locomotion and viability defects. *Cell reports*. 1:624-631.

Pruunsild, P., A. Kazantseva, T. Aid, K. Palm, and T. Timmusk. 2007. Dissecting the human BDNF locus: bidirectional transcription, complex splicing, and multiple promoters. *Genomics*. 90:397-406.

Puehringer, D., N. Orel, P. Luningschror, N. Subramanian, T. Herrmann, M.V. Chao, and M. Sendtner. 2013. EGF transactivation of Trk receptors regulates the migration of newborn cortical neurons. *Nature neuroscience*. 16:407-415.

Rajagopal, R., Z.Y. Chen, F.S. Lee, and M.V. Chao. 2004. Transactivation of Trk neurotrophin receptors by G-protein-coupled receptor ligands occurs on intracellular membranes. *The Journal of neuroscience : the official journal of the Society for Neuroscience*. 24:6650-6658.

Rajendra, T.K., G.B. Gonsalvez, M.P. Walker, K.B. Shpargel, H.K. Salz, and A.G. Matera. 2007. A Drosophila melanogaster model of spinal muscular atrophy reveals a function for SMN in striated muscle. *The Journal of cell biology*. 176:831-841.

Ramser, E.M., K.J. Gan, H. Decker, E.Y. Fan, M.M. Suzuki, S.T. Ferreira, and M.A. Silverman. 2013. Amyloid-beta oligomers induce tau-independent disruption of BDNF axonal transport via calcineurin activation in cultured hippocampal neurons. *Molecular biology of the cell*. 24:2494-2505.

Rathod, R., S. Havlicek, N. Frank, R. Blum, and M. Sendtner. 2012. Laminin induced local axonal translation of beta-actin mRNA is impaired in SMN-deficient motoneurons. *Histochemistry and cell biology*. 138:737-748.

Rauskolb, S., M. Zagrebelsky, A. Dreznjak, R. Deogracias, T. Matsumoto, S. Wiese, B. Erne, M. Sendtner, N. Schaeren-Wiemers, M. Korte, and Y.A. Barde. 2010. Global deprivation of brain-derived neurotrophic factor in the CNS reveals an area-specific requirement for dendritic growth. *The Journal of neuroscience : the official journal of the Society for Neuroscience*. 30:1739-1749.

Rehberg, M., A. Lepier, B. Solchenberger, P. Osten, and R. Blum. 2008. A new non-disruptive strategy to target calcium indicator dyes to the endoplasmic reticulum. *Cell calcium*. 44:386-399.

Reichardt, L.F. 2006. Neurotrophin-regulated signalling pathways. *Philosophical transactions of the Royal Society of London. Series B, Biological sciences*. 361:1545-1564.

Renvoise, B., K. Khoobarry, M.C. Gendron, C. Cibert, L. Viollet, and S. Lefebvre. 2006. Distinct domains of the spinal muscular atrophy protein SMN are required for targeting to Cajal bodies in mammalian cells. *Journal of cell science*. 119:680-692.

Riessland, M., A. Kaczmarek, S. Schneider, K.J. Swoboda, H. Lohr, C. Bradler, V. Grysko, M. Dimitriadi, S. Hosseinibarkooie, L. Torres-Benito, M. Peters, A. Upadhyay, N. Biglari, S. Krober, I. Holker, L. Garbes, C. Gilissen, A. Hoischen, G. Nurnberg, P. Nurnberg, M. Walter, F. Rigo, C.F. Bennett, M.J. Kye, A.C. Hart, M. Hammerschmidt, P. Kloppenburg, and B. Wirth. 2017. Neurocalcin Delta Suppression Protects against Spinal Muscular Atrophy in Humans and across Species by Restoring Impaired Endocytosis. *American journal of human genetics*. 100:297-315.

Righi, M., E. Tongiorgi, and A. Cattaneo. 2000. Brain-derived neurotrophic factor (BDNF) induces dendritic targeting of BDNF and tyrosine kinase B mRNAs in hippocampal neurons through a phosphatidylinositol-3 kinase-dependent pathway. *The Journal of neuroscience : the official journal of the Society for Neuroscience*. 20:3165-3174.

Rochette, C.F., N. Gilbert, and L.R. Simard. 2001. SMN gene duplication and the emergence of the SMN2 gene occurred in distinct hominids: SMN2 is unique to Homo sapiens. *Human genetics*. 108:255-266.

Rodriguez-Tebar, A., G. Dechant, and Y.A. Barde. 1990. Binding of brain-derived neurotrophic factor to the nerve growth factor receptor. *Neuron*. 4:487-492.

Rohrer, B., J.I. Korenbrot, M.M. LaVail, L.F. Reichardt, and B. Xu. 1999. Role of neurotrophin receptor TrkB in the maturation of rod photoreceptors and establishment of synaptic transmission to the inner retina. *The Journal of neuroscience : the official journal of the Society for Neuroscience*. 19:8919-8930.

Romero, S., C. Le Clainche, D. Didry, C. Egile, D. Pantaloni, and M.F. Carlier. 2004. Formin is a processive motor that requires profilin to accelerate actin assembly and associated ATP hydrolysis. *Cell*. 119:419-429.

Rosch, H., R. Schweigreiter, T. Bonhoeffer, Y.A. Barde, and M. Korte. 2005. The neurotrophin receptor p75NTR modulates long-term depression and regulates the expression of AMPA receptor subunits in the hippocampus. *Proceedings of the National Academy of Sciences of the United States of America*. 102:7362-7367.

Rosenthal, A., D.V. Goeddel, T. Nguyen, E. Martin, L.E. Burton, A. Shih, G.R. Laramee, F. Wurm, A. Mason, K. Nikolics, and et al. 1991. Primary structure and biological activity of human brain-derived neurotrophic factor. *Endocrinology*. 129:1289-1294.

Ross, A.F., Y. Oleynikov, E.H. Kislauskis, K.L. Taneja, and R.H. Singer. 1997. Characterization of a beta-actin mRNA zipcode-binding protein. *Molecular and cellular biology*. 17:2158-2165.

Rossoll, W., S. Jablonka, C. Andreassi, A.K. Kroning, K. Karle, U.R. Monani, and M. Sendtner. 2003. Smn, the spinal muscular atrophy-determining gene product, modulates axon growth and localization of beta-actin mRNA in growth cones of motoneurons. *The Journal of cell biology*. 163:801-812.

Rossoll, W., A.K. Kroning, U.M. Ohndorf, C. Steegborn, S. Jablonka, and M. Sendtner. 2002. Specific interaction of Smn, the spinal muscular atrophy determining gene product, with hnRNP-R and gry-rbp/hnRNP-Q: a role for Smn in RNA processing in motor axons? *Human molecular genetics*. 11:93-105.

Rouiller, I., X.P. Xu, K.J. Amann, C. Egile, S. Nickell, D. Nicastro, R. Li, T.D. Pollard, N. Volkmann, and D. Hanein. 2008. The structural basis of actin filament branching by the Arp2/3 complex. *The Journal of cell biology*. 180:887-895.

Rudnik-Schoneborn, S., H.H. Goebel, W. Schlote, S. Molaian, H. Omran, U. Ketelsen, R. Korinthenberg, D. Wenzel, H. Lauffer, M. Kreiss-Nachtsheim, B. Wirth, and K. Zerres. 2003. Classical infantile spinal muscular atrophy with SMN deficiency causes sensory neuronopathy. *Neurology*. 60:983-987.

Ruggiu, M., V.L. McGovern, F. Lotti, L. Saieva, D.K. Li, S. Kariya, U.R. Monani, A.H. Burghes, and L. Pellizzoni. 2012. A role for SMN exon 7 splicing in the selective vulnerability of motor neurons in spinal muscular atrophy. *Molecular and cellular biology*. 32:126-138.

Ruiz, R., J.J. Casanas, L. Torres-Benito, R. Cano, and L. Tabares. 2010. Altered intracellular Ca2+ homeostasis in nerve terminals of severe spinal muscular atrophy mice. *The Journal of neuroscience : the official journal of the Society for Neuroscience*. 30:849-857.

Russman, B.S. 2007. Spinal muscular atrophy: clinical classification and disease heterogeneity. *Journal of child neurology*. 22:946-951.

Saal, L., M. Briese, S. Kneitz, M. Glinka, and M. Sendtner. 2014. Subcellular transcriptome alterations in a cell culture model of spinal muscular atrophy point to widespread defects in axonal growth and presynaptic differentiation. *RNA*. 20:1789-1802.

Saito, A., K. Miyajima, J. Akatsuka, H. Kondo, T. Mashiko, T. Kiuchi, K. Ohashi, and K. Mizuno. 2013. CaMKIIbeta-mediated LIM-kinase activation plays a crucial role in BDNF-induced neuritogenesis. *Genes to cells : devoted to molecular & cellular mechanisms*. 18:533-543.

Sakata, K., N.H. Woo, K. Martinowich, J.S. Greene, R.J. Schloesser, L. Shen, and B. Lu. 2009. Critical role of promoter IV-driven BDNF transcription in GABAergic transmission and synaptic plasticity in the prefrontal cortex. *Proceedings of the National Academy of Sciences of the United States of America*. 106:5942-5947.

Sanchez, A.L., B.J. Matthews, M.M. Meynard, B. Hu, S. Javed, and S. Cohen Cory. 2006. BDNF increases synapse density in dendrites of developing tectal neurons in vivo. *Development*. 133:2477-2486.

Sanes, J.R., and J.W. Lichtman. 1999. Development of the vertebrate neuromuscular junction. *Annual review of neuroscience*. 22:389-442.

Sasaki, Y., K. Welshhans, Z. Wen, J. Yao, M. Xu, Y. Goshima, J.Q. Zheng, and G.J. Bassell. 2010. Phosphorylation of zipcode binding protein 1 is required for brain-derived neurotrophic factor signaling of local beta-actin synthesis and growth cone turning. *The Journal of neuroscience : the official journal of the Society for Neuroscience*. 30:9349-9358.

Sasi, M., B. Vignoli, M. Canossa, and R. Blum. 2017. Neurobiology of local and intercellular BDNF signaling. *Pflugers Archiv : European journal of physiology*. 469:593-610.

Schecterson, L.C., and M. Bothwell. 1992. Novel roles for neurotrophins are suggested by BDNF and NT-3 mRNA expression in developing neurons. *Neuron*. 9:449-463.

Schrank, B., R. Gotz, J.M. Gunnersen, J.M. Ure, K.V. Toyka, A.G. Smith, and M. Sendtner. 1997. Inactivation of the survival motor neuron gene, a candidate gene for human spinal muscular atrophy, leads to massive cell death in early mouse embryos. *Proceedings of the National Academy of Sciences of the United States of America*. 94:9920-9925.

Schratt, G.M., E.A. Nigh, W.G. Chen, L. Hu, and M.E. Greenberg. 2004. BDNF regulates the translation of a select group of mRNAs by a mammalian target of rapamycin-phosphatidylinositol 3-kinase-dependent pathway during neuronal development. *The Journal of neuroscience : the official journal of the Society for Neuroscience*. 24:7366-7377.

Schwebach, C.L., R. Agrawal, S. Lindert, E. Kudryashova, and D.S. Kudryashov. 2017. The Roles of Actin-Binding Domains 1 and 2 in the Calcium-Dependent Regulation of Actin Filament Bundling by Human Plastins. *Journal of molecular biology*. 429:2490-2508.

See, K., P. Yadav, M. Giegerich, P.S. Cheong, M. Graf, H. Vyas, S.G. Lee, S. Mathavan, U. Fischer, M. Sendtner, and C. Winkler. 2014. SMN deficiency alters Nrxn2 expression and splicing in zebrafish and mouse models of spinal muscular atrophy. *Human molecular genetics*. 23:1754-1770.

Selenko, P., R. Sprangers, G. Stier, D. Buhler, U. Fischer, and M. Sattler. 2001. SMN tudor domain structure and its interaction with the Sm proteins. *Nature structural biology*. 8:27-31.

Sendtner, M. 2014. Motoneuron disease. *Handbook of experimental pharmacology*. 220:411-441.

Sendtner, M., B. Holtmann, R. Kolbeck, H. Thoenen, and Y.A. Barde. 1992. Brain-derived neurotrophic factor prevents the death of motoneurons in newborn rats after nerve section. *Nature*. 360:757-759.

Sendtner, M., G. Pei, M. Beck, U. Schweizer, and S. Wiese. 2000. Developmental motoneuron cell death and neurotrophic factors. *Cell and tissue research*. 301:71-84.

Serio, A.W., R.L. Jeng, C.M. Haglund, S.C. Reed, and M.D. Welch. 2010. Defining a core set of actin cytoskeletal proteins critical for actin-based motility of Rickettsia. *Cell Host Microbe*. 7:388-398.

Shinomiya, H. 2012. Plastin family of actin-bundling proteins: its functions in leukocytes, neurons, intestines, and cancer. *Int J Cell Biol*. 2012:213492.

Simon, C.M., Y. Dai, M. Van Alstyne, C. Koutsioumpa, J.G. Pagiazitis, J.I. Chalif, X. Wang, J.E. Rabinowitz, C.E. Henderson, L. Pellizzoni, and G.Z. Mentis. 2017. Converging Mechanisms of p53 Activation Drive Motor Neuron Degeneration in Spinal Muscular Atrophy. *Cell reports*. 21:3767-3780.

Singh, N.K., N.N. Singh, E.J. Androphy, and R.N. Singh. 2006. Splicing of a critical exon of human Survival Motor Neuron is regulated by a unique silencer element located in the last intron. *Molecular and cellular biology*. 26:1333-1346.

Skau, C.T., D.S. Courson, A.J. Bestul, J.D. Winkelman, R.S. Rock, V. Sirotkin, and D.R. Kovar. 2011. Actin filament bundling by fimbrin is important for endocytosis, cytokinesis, and polarization in fission yeast. *The Journal of biological chemistry*. 286:26964-26977.

Skau, C.T., and D.R. Kovar. 2010. Fimbrin and tropomyosin competition regulates endocytosis and cytokinesis kinetics in fission yeast. *Current biology : CB*. 20:1415-1422.

Skordis, L.A., M.G. Dunckley, L. Burglen, L. Campbell, K. Talbot, S. Patel, J. Melki, K.E. Davies, V. Dubowitz, and F. Muntoni. 2001. Characterisation of novel point mutations in the survival motor neuron gene SMN, in three patients with SMA. *Human genetics*. 108:356-357.

Slaugenhaupt, S.A., A. Blumenfeld, C.B. Liebert, J. Mull, D.E. Lucente, M. Monahan, X.O. Breakefield, C. Maayan, L. Parada, F.B. Axelrod, and et al. 1995. The human gene for neurotrophic tyrosine kinase receptor type 2 (NTRK2) is located on chromosome 9 but is not the familial dysautonomia gene. *Genomics*. 25:730-732.

Smith, B.N., C. Vance, E.L. Scotter, C. Troakes, C.H. Wong, S. Topp, S. Maekawa, A. King, J.C. Mitchell, K. Lund, A. Al-Chalabi, N. Ticozzi, V. Silani, P. Sapp, R.H. Brown, Jr., J.E. Landers, S. Al-Sarraj, and C.E. Shaw. 2015. Novel mutations support a role for Profilin 1 in the pathogenesis of ALS. *Neurobiology of aging*. 36:1602 e1617-1627.

Smith, M., V. Calabro, B. Chong, N. Gardiner, S. Cowie, and D. du Sart. 2007. Population screening and cascade testing for carriers of SMA. *European journal of human genetics : EJHG*. 15:759-766.

Smith, M.A., L.X. Zhang, W.E. Lyons, and L.A. Mamounas. 1997. Anterograde transport of endogenous brain-derived neurotrophic factor in hippocampal mossy fibers. *Neuroreport*. 8:1829-1834.

Sobreviela, T., M. Pagcatipunan, J.S. Kroin, and E.J. Mufson. 1996. Retrograde transport of brain-derived neurotrophic factor (BDNF) following infusion in neo- and limbic cortex in rat: relationship to BDNF mRNA expressing neurons. *The Journal of comparative neurology*. 375:417-444.

Song, M., J. Giza, C.C. Proenca, D. Jing, M. Elliott, I. Dincheva, S.V. Shmelkov, J. Kim, R. Schreiner, S.H. Huang, E. Castren, R. Prekeris, B.L. Hempstead, M.V. Chao, J.B. Dictenberg, S. Rafii, Z.Y. Chen, E. Rodriguez-Boulan, and F.S. Lee. 2015. Slitrk5 Mediates BDNF-Dependent TrkB Receptor Trafficking and Signaling. *Developmental cell*. 33:690-702.

Squinto, S.P., T.N. Stitt, T.H. Aldrich, S. Davis, S.M. Bianco, C. Radziejewski, D.J. Glass, P. Masiakowski, M.E. Furth, D.M. Valenzuela, and et al. 1991. trkB encodes a functional receptor for brain-derived neurotrophic factor and neurotrophin-3 but not nerve growth factor. *Cell*. 65:885-893.

Stoilov, P., E. Castren, and S. Stamm. 2002. Analysis of the human TrkB gene genomic organization reveals novel TrkB isoforms, unusual gene length, and splicing mechanism. *Biochemical and biophysical research communications*. 290:1054-1065.

Stratigopoulos, G., P. Lanzano, L. Deng, J. Guo, P. Kaufmann, B. Darras, R. Finkel, R. Tawil, M.P. McDermott, W. Martens, D.C. Devivo, and W.K. Chung. 2010. Association of plastin 3 expression with disease severity in spinal muscular atrophy only in postpubertal females. *Archives of neurology*. 67:1252-1256.

Sugarman, E.A., N. Nagan, H. Zhu, V.R. Akmaev, Z. Zhou, E.M. Rohlfs, K. Flynn, B.C. Hendrickson, T. Scholl, D.A. Sirko-Osadsa, and B.A. Allitto. 2012. Pan-ethnic carrier screening and prenatal diagnosis for spinal muscular atrophy: clinical laboratory analysis of >72,400 specimens. *European journal of human genetics : EJHG*. 20:27-32.

Sugimachi, K., T. Yokobori, H. Iinuma, M. Ueda, H. Ueo, Y. Shinden, H. Eguchi, T. Sudo, A. Suzuki, Y. Maehara, M. Mori, and K. Mimori. 2014. Aberrant expression of plastin-3 via copy number gain induces the epithelial-mesenchymal transition in circulating colorectal cancer cells. *Ann Surg Oncol*. 21:3680-3690.

Sun, Y., M. Grimmler, V. Schwarzer, F. Schoenen, U. Fischer, and B. Wirth. 2005. Molecular and functional analysis of intragenic SMN1 mutations in patients with spinal muscular atrophy. *Human mutation*. 25:64-71.

Suraneni, P., B. Rubinstein, J.R. Unruh, M. Durnin, D. Hanein, and R. Li. 2012. The Arp2/3 complex is required for lamellipodia extension and directional fibroblast cell migration. *Journal of Cell Biology*. 197:239-251.

Tabuchi, A., R. Nakaoka, K. Amano, M. Yukimine, T. Andoh, Y. Kuraishi, and M. Tsuda. 2000. Differential activation of brain-derived neurotrophic factor gene promoters I and III by Ca2+ signals evoked via L-type voltage-dependent and N-methyl-D-aspartate receptor Ca2+ channels. *The Journal of biological chemistry*. 275:17269-17275.

Talbot, K., C.P. Ponting, A.M. Theodosiou, N.R. Rodrigues, R. Surtees, R. Mountford, and K.E. Davies. 1997. Missense mutation clustering in the survival motor neuron gene: a role for a conserved tyrosine and glycine rich region of the protein in RNA metabolism? *Human molecular genetics*. 6:497-500.

Tamura, S., A. Nagasawa, Y. Masuda, T. Tsunematsu, K. Hayasaka, K. Matsuno, C. Shimizu, Y. Ozaki, and T. Moriyama. 2012. BDNF, produced by a TPO-stimulated megakaryocytic cell line, regulates autocrine proliferation. *Biochemical and biophysical research communications*. 427:542-546.

Tanaka, Y., T. Nonaka, G. Suzuki, F. Kametani, and M. Hasegawa. 2016. Gain-of-function profilin 1 mutations linked to familial amyotrophic lateral sclerosis cause seed-dependent intracellular TDP-43 aggregation. *Human molecular genetics*. 25:1420-1433.

Tao, X., S. Finkbeiner, D.B. Arnold, A.J. Shaywitz, and M.E. Greenberg. 1998. Ca2+ influx regulates BDNF transcription by a CREB family transcription factor-dependent mechanism. *Neuron*. 20:709-726.

Tao, X., A.E. West, W.G. Chen, G. Corfas, and M.E. Greenberg. 2002. A calcium-responsive transcription factor, CaRF, that regulates neuronal activity-dependent expression of BDNF. *Neuron*. 33:383-395.

Tejero, R., S. Balk, J. Franco-Espin, J. Ojeda, L. Hennlein, H. Drexl, B. Dombert, J.D. Clausen, L. Torres-Benito, L. Saal-Bauernschubert, R. Blum, M. Briese, S. Appenzeller, L. Tabares, and S. Jablonka. 2020. R-Roscovitine Improves Motoneuron Function in Mouse Models for Spinal Muscular Atrophy. *iScience*. 23:100826.

Tejero, R., M. Lopez-Manzaneda, S. Arumugam, and L. Tabares. 2016. Synaptotagmin-2, and -1, linked to neurotransmission impairment and vulnerability in Spinal Muscular Atrophy. *Human molecular genetics*. 25:4703-4716.

Teng, H.K., K.K. Teng, R. Lee, S. Wright, S. Tevar, R.D. Almeida, P. Kermani, R. Torkin, Z.Y. Chen, F.S. Lee, R.T. Kraemer, A. Nykjaer, and B.L. Hempstead. 2005. ProBDNF induces neuronal apoptosis via activation of a receptor complex of p75NTR and sortilin. *The Journal of neuroscience : the official journal of the Society for Neuroscience*. 25:5455-5463.

Timmusk, T., K. Palm, M. Metsis, T. Reintam, V. Paalme, M. Saarma, and H. Persson. 1993. Multiple promoters direct tissue-specific expression of the rat BDNF gene. *Neuron*. 10:475-489.

Todd, A.G., R. Morse, D.J. Shaw, H. Stebbings, and P.J. Young. 2010a. Analysis of SMN-neurite granules: Core Cajal body components are absent from SMN-cytoplasmic complexes. *Biochemical and biophysical research communications*. 397:479-485.

Todd, A.G., D.J. Shaw, R. Morse, H. Stebbings, and P.J. Young. 2010b. SMN and the Gemin proteins form sub-complexes that localise to both stationary and dynamic neurite granules. *Biochemical and biophysical research communications*. 394:211-216.

Tolino, M., M. Kohrmann, and M.A. Kiebler. 2012. RNA-binding proteins involved in RNA localization and their implications in neuronal diseases. *The European journal of neuroscience*. 35:1818-1836.

Tongiorgi, E., M. Righi, and A. Cattaneo. 1997. Activity-dependent dendritic targeting of BDNF and TrkB mRNAs in hippocampal neurons. *The Journal of neuroscience : the official journal of the Society for Neuroscience*. 17:9492-9505.

Torres-Benito, L., M.F. Neher, R. Cano, R. Ruiz, and L. Tabares. 2011. SMN requirement for synaptic vesicle, active zone and microtubule postnatal organization in motor nerve terminals. *PloS one*. 6:e26164.

Torres-Benito, L., R. Ruiz, and L. Tabares. 2012. Synaptic defects in spinal muscular atrophy animal models. *Developmental neurobiology*. 72:126-133.

Turner, B.J., D. Baumer, N.J. Parkinson, J. Scaber, O. Ansorge, and K. Talbot. 2008. TDP-43 expression in mouse models of amyotrophic lateral sclerosis and spinal muscular atrophy. *BMC neuroscience*. 9:104.

Vaillant, A.R., I. Mazzoni, C. Tudan, M. Boudreau, D.R. Kaplan, and F.D. Miller. 1999. Depolarization and neurotrophins converge on the phosphatidylinositol 3-kinase-Akt pathway to synergistically regulate neuronal survival. *The Journal of cell biology*. 146:955-966.

Valdez, G., W. Akmentin, P. Philippidou, R. Kuruvilla, D.D. Ginty, and S. Halegoua. 2005. Pincher-mediated macroendocytosis underlies retrograde signaling by neurotrophin receptors. *The Journal of neuroscience : the official journal of the Society for Neuroscience*. 25:5236-5247.

Valent, A., G. Danglot, and A. Bernheim. 1997. Mapping of the tyrosine kinase receptors trkA (NTRK1), trkB (NTRK2) and trkC(NTRK3) to human chromosomes 1q22, 9q22 and 15q25 by fluorescence in situ hybridization. *European journal of human genetics : EJHG*. 5:102-104.

Van Alstyne, M., I. Tattoli, N. Delestree, Y. Recinos, E. Workman, L.S. Shihabuddin, C. Zhang, G.Z. Mentis, and L. Pellizzoni. 2021. Gain of toxic function by long-term AAV9-mediated SMN overexpression in the sensorimotor circuit. *Nature neuroscience*. 24:930-940.

van Dijk, F.S., M.C. Zillikens, D. Micha, M. Riessland, C.L. Marcelis, C.E. de Die-Smulders, J. Milbradt, A.A. Franken, A.J. Harsevoort, K.D. Lichtenbelt, H.E. Pruijs, M.E. Rubio-Gozalbo, R. Zwertbroek, Y. Moutaouakil, J. Egthuijsen, M. Hammerschmidt, R. Bijman, C.M. Semeins, A.D. Bakker, V. Everts, J. Klein-Nulend, N. Campos-Obando, A. Hofman, G.J. te Meerman, A.J. Verkerk, A.G. Uitterlinden, A. Maugeri, E.A. Sistermans, Q. Waisfisz, H. Meijers-Heijboer, B. Wirth, M.E. Simon, and G. Pals. 2013. PLS3 mutations in X-linked osteoporosis with fractures. *The New England journal of medicine*. 369:1529-1536.

Verhaart, I.E.C., A. Robertson, I.J. Wilson, A. Aartsma-Rus, S. Cameron, C.C. Jones, S.F. Cook, and H. Lochmuller. 2017. Prevalence, incidence and carrier frequency of 5q-linked spinal muscular atrophy - a literature review. *Orphanet journal of rare diseases*. 12:124.

Viollet, L., S. Bertrandy, A.L. Bueno Brunialti, S. Lefebvre, P. Burlet, O. Clermont, C. Cruaud, J.L. Guenet, A. Munnich, and J. Melki. 1997. cDNA isolation, expression, and chromosomal localization of the mouse survival motor neuron gene (Smn). *Genomics*. 40:185-188.

Vitali, T., V. Sossi, F. Tiziano, S. Zappata, A. Giuli, M. Paravatou-Petsotas, G. Neri, and C. Brahe. 1999. Detection of the survival motor neuron (SMN) genes by FISH: further evidence for a role for SMN2 in the modulation of disease severity in SMA patients. *Human molecular genetics*. 8:2525-2532.

Vohra, P.K., M.A. Thompson, V. Sathish, A. Kiel, C. Jerde, C.M. Pabelick, B.B. Singh, and Y.S. Prakash. 2013. TRPC3 regulates release of brain-derived neurotrophic factor from human airway smooth muscle. *Biochimica et biophysica acta*. 1833:2953-2960.

Walsh, M.B., E. Janzen, E. Wingrove, S. Hosseinibarkooie, N.R. Muela, L. Davidow, M. Dimitriadi, E.M. Norabuena, L.L. Rubin, B. Wirth, and A.C. Hart. 2020. Genetic modifiers ameliorate endocytic and neuromuscular defects in a model of spinal muscular atrophy. *BMC biology*. 18:127.

Wan, L., D.J. Battle, J. Yong, A.K. Gubitz, S.J. Kolb, J. Wang, and G. Dreyfuss. 2005. The survival of motor neurons protein determines the capacity for snRNP assembly: biochemical deficiency in spinal muscular atrophy. *Molecular and cellular biology*. 25:5543-5551.

Wang, J., and G. Dreyfuss. 2001. Characterization of functional domains of the SMN protein in vivo. *The Journal of biological chemistry*. 276:45387-45393.

Watson, F.L., H.M. Heerssen, D.B. Moheban, M.Z. Lin, C.M. Sauvageot, A. Bhattacharyya, S.L. Pomeroy, and R.A. Segal. 1999. Rapid nuclear responses to target-derived neurotrophins require retrograde transport of ligand-receptor complex. *The Journal of neuroscience : the official journal of the Society for Neuroscience*. 19:7889-7900.

Welch, M.D., A.H. DePace, S. Verma, A. Iwamatsu, and T.J. Mitchison. 1997. The human Arp2/3 complex is composed of evolutionarily conserved subunits and is localized to cellular regions of dynamic actin filament assembly. *Journal of Cell Biology*. 138:375-384.

Werdnig, G. 1891. Two early infantile hereditary cases of progressive muscular atrophy simulating dystrophy, but on a neural basis. 1891. *Archives of neurology*. 25:276-278.

Wiese, S., T. Herrmann, C. Drepper, S. Jablonka, N. Funk, A. Klausmeyer, M.L. Rogers, R. Rush, and M. Sendtner. 2010. Isolation and enrichment of embryonic mouse motoneurons from the lumbar spinal cord of individual mouse embryos. *Nature protocols*. 5:31-38.

Wiese, S., S. Jablonka, B. Holtmann, N. Orel, R. Rajagopal, M.V. Chao, and M. Sendtner. 2007. Adenosine receptor A2A-R contributes to motoneuron survival by transactivating the tyrosine kinase receptor TrkB. *Proceedings of the National Academy of Sciences of the United States of America*. 104:17210-17215.

Wiese, S., F. Metzger, B. Holtmann, and M. Sendtner. 1999. The role of p75NTR in modulating neurotrophin survival effects in developing motoneurons. *The European journal of neuroscience*. 11:1668-1676.

Windisch, J.M., R. Marksteiner, M.E. Lang, B. Auer, and R. Schneider. 1995. Brain-derived neurotrophic factor, neurotrophin-3, and neurotrophin-4 bind to a single leucine-rich motif of TrkB. *Biochemistry*. 34:11256-11263.

Winkler, C., C. Eggert, D. Gradl, G. Meister, M. Giegerich, D. Wedlich, B. Laggerbauer, and U. Fischer. 2005. Reduced U snRNP assembly causes motor axon degeneration in an animal model for spinal muscular atrophy. *Genes & development*. 19:2320-2330.

Wirth, B., M. Herz, A. Wetter, S. Moskau, E. Hahnen, S. Rudnik-Schoneborn, T. Wienker, and K. Zerres. 1999. Quantitative analysis of survival motor neuron copies: identification of subtle SMN1 mutations in patients with spinal muscular atrophy, genotype-phenotype correlation, and implications for genetic counseling. *American journal of human genetics*. 64:1340-1356.

Wirth, B., M. Karakaya, M.J. Kye, and N. Mendoza-Ferreira. 2020. Twenty-Five Years of Spinal Muscular Atrophy Research: From Phenotype to Genotype to Therapy, and What Comes Next. *Annual review of genomics and human genetics*. 21:231-261.

Wishart, T.M., C.A. Mutsaers, M. Riessland, M.M. Reimer, G. Hunter, M.L. Hannam, S.L. Eaton, H.R. Fuller, S.L. Roche, E. Somers, R. Morse, P.J. Young, D.J. Lamont, M. Hammerschmidt, A. Joshi, P. Hohenstein, G.E. Morris, S.H. Parson, P.A. Skehel, T. Becker, I.M. Robinson, C.G. Becker, B. Wirth, and T.H. Gillingwater. 2014. Dysregulation of ubiquitin homeostasis and beta-catenin signaling promote spinal muscular atrophy. *The Journal of clinical investigation*. 124:1821-1834.

Witke, W. 2004. The role of profilin complexes in cell motility and other cellular processes. *Trends in cell biology*. 14:461-469.

Wolff, L., E.A. Strathmann, I. Muller, D. Mahlich, C. Veltman, A. Niehoff, and B. Wirth. 2021. Plastin 3 in health and disease: a matter of balance. *Cellular and molecular life sciences : CMLS*. 78:5275-5301.

Woo, N.H., H.K. Teng, C.J. Siao, C. Chiaruttini, P.T. Pang, T.A. Milner, B.L. Hempstead, and B. Lu. 2005. Activation of p75NTR by proBDNF facilitates hippocampal long-term depression. *Nature neuroscience*. 8:1069-1077.

Wottawa, M., S. Naas, J. Bottger, G.J. van Belle, W. Mobius, N.H. Revelo, D. Heidenreich, M. von Ahlen, A. Zieseniss, K. Krohnert, S. Lutz, C. Lenz, H. Urlaub, S.O. Rizzoli, and D.M. Katschinski. 2017. Hypoxia-stimulated membrane trafficking requires T-plastin. *Acta Physiol (Oxf)*. 221:59-73.

Wu, C.H., C. Fallini, N. Ticozzi, P.J. Keagle, P.C. Sapp, K. Piotrowska, P. Lowe, M. Koppers, D. McKenna-Yasek, D.M. Baron, J.E. Kost, P. Gonzalez-Perez, A.D. Fox, J. Adams, F. Taroni, C. Tiloca, A.L. Leclerc, S.C. Chafe, D. Mangroo, M.J. Moore, J.A. Zitzewitz, Z.S. Xu, L.H. van den Berg, J.D. Glass, G. Siciliano, E.T. Cirulli, D.B. Goldstein, F. Salachas, V. Meininger, W. Rossoll, A. Ratti, C. Gellera, D.A. Bosco, G.J. Bassell, V. Silani, V.E. Drory, R.H. Brown, Jr., and J.E. Landers. 2012a. Mutations in the profilin 1 gene cause familial amyotrophic lateral sclerosis. *Nature*. 488:499-503.

Wu, C.Y., S.B. Asokan, M.E. Berginski, E.M. Haynes, N.E. Sharpless, J.D. Griffith, S.M. Gomez, and J.E. Bear. 2012b. Arp2/3 Is Critical for Lamellipodia and Response to Extracellular Matrix Cues but Is Dispensable for Chemotaxis. *Cell*. 148:973-987.

Xin, Z., D. Li, F. Mao, Y. Du, X. Wang, P. Xu, Z. Li, J. Qian, and J. Yao. 2020. PLS3 predicts poor prognosis in pancreatic cancer and promotes cancer cell proliferation via PI3K/AKT signaling. *Journal of cellular physiology*. 235:8416-8423.

Xue, F., D.M. Janzen, and D.A. Knecht. 2010. Contribution of Filopodia to Cell Migration: A Mechanical Link between Protrusion and Contraction. *Int J Cell Biol*. 2010:507821.

Yamada, K., M. Mizuno, and T. Nabeshima. 2002. Role for brain-derived neurotrophic factor in learning and memory. *Life sciences*. 70:735-744.

Yan, Q., J. Elliott, and W.D. Snider. 1992. Brain-derived neurotrophic factor rescues spinal motor neurons from axotomy-induced cell death. *Nature*. 360:753-755.

Yan, Q., M.J. Radeke, C.R. Matheson, J. Talvenheimo, A.A. Welcher, and S.C. Feinstein. 1997a. Immunocytochemical localization of TrkB in the central nervous system of the adult rat. *The Journal of comparative neurology*. 378:135-157.

Yan, Q., R.D. Rosenfeld, C.R. Matheson, N. Hawkins, O.T. Lopez, L. Bennett, and A.A. Welcher. 1997b. Expression of brain-derived neurotrophic factor protein in the adult rat central nervous system. *Neuroscience*. 78:431-448.

Yang, J., L.C. Harte-Hargrove, C.J. Siao, T. Marinic, R. Clarke, Q. Ma, D. Jing, J.J. Lafrancois, K.G. Bath, W. Mark, D. Ballon, F.S. Lee, H.E. Scharfman, and B.L. Hempstead. 2014. proBDNF negatively regulates neuronal remodeling, synaptic transmission, and synaptic plasticity in hippocampus. *Cell reports*. 7:796-806.

Yano, H., I. Ninan, H. Zhang, T.A. Milner, O. Arancio, and M.V. Chao. 2006. BDNF-mediated neurotransmission relies upon a myosin VI motor complex. *Nature neuroscience*. 9:1009-1018.

Yanyan, C., Q. Yujin, B. Jinli, J. Yuwei, W. Hong, and S. Fang. 2014. Correlation of PLS3 expression with disease severity in children with spinal muscular atrophy. *Journal of human genetics*. 59:24-27.

Young, P.J., N.T. Man, C.L. Lorson, T.T. Le, E.J. Androphy, A.H. Burghes, and G.E. Morris. 2000. The exon 2b region of the spinal muscular atrophy protein, SMN, is involved in self-association and SIP1 binding. *Human molecular genetics*. 9:2869-2877.

Zagrebelsky, M., A. Holz, G. Dechant, Y.A. Barde, T. Bonhoeffer, and M. Korte. 2005. The p75 neurotrophin receptor negatively modulates dendrite complexity and spine density in hippocampal neurons. *The Journal of neuroscience : the official journal of the Society for Neuroscience*. 25:9989-9999.

Zahavi, E.E., N. Steinberg, T. Altman, M. Chein, Y. Joshi, T. Gradus-Pery, and E. Perlson. 2018. The receptor tyrosine kinase TrkB signals without dimerization at the plasma membrane. *Science signaling*. 11.

Zerres, K., S. Rudnik-Schoneborn, R. Forkert, and B. Wirth. 1995. Genetic basis of adult-onset spinal muscular atrophy. *Lancet*. 346:1162.

Zhang, H., L. Xing, W. Rossoll, H. Wichterle, R.H. Singer, and G.J. Bassell. 2006. Multiprotein complexes of the survival of motor neuron protein SMN with Gemins traffic to neuronal processes and growth cones of motor neurons. *The Journal of neuroscience : the official journal of the Society for Neuroscience*. 26:8622-8632.

Zhang, H.L., F. Pan, D. Hong, S.M. Shenoy, R.H. Singer, and G.J. Bassell. 2003. Active transport of the survival motor neuron protein and the role of exon-7 in cytoplasmic localization. *The Journal of neuroscience : the official journal of the Society for Neuroscience*. 23:6627-6637.

Zhang, H.T., L.Y. Li, X.L. Zou, X.B. Song, Y.L. Hu, Z.T. Feng, and T.T. Wang. 2007. Immunohistochemical distribution of NGF, BDNF, NT-3, and NT-4 in adult rhesus monkey brains. *The journal of histochemistry and cytochemistry : official journal of the Histochemistry Society*. 55:1-19.

Zhang, R., B.R. So, P. Li, J. Yong, T. Glisovic, L. Wan, and G. Dreyfuss. 2011. Structure of a key intermediate of the SMN complex reveals Gemin2's crucial function in snRNP assembly. *Cell*. 146:384-395.

Zhang, Z., F. Lotti, K. Dittmar, I. Younis, L. Wan, M. Kasim, and G. Dreyfuss. 2008. SMN deficiency causes tissue-specific perturbations in the repertoire of snRNAs and widespread defects in splicing. *Cell*. 133:585-600.

Zhang, Z., A.M. Pinto, L. Wan, W. Wang, M.G. Berg, I. Oliva, L.N. Singh, C. Dengler, Z. Wei, and G. Dreyfuss. 2013. Dysregulation of synaptogenesis genes antecedes motor neuron pathology in spinal muscular atrophy. *Proceedings of the National Academy of Sciences of the United States of America*. 110:19348-19353.

Zhao, L., A.L. Sheng, S.H. Huang, Y.X. Yin, B. Chen, X.Z. Li, Y. Zhang, and Z.Y. Chen. 2009. Mechanism underlying activity-dependent insertion of TrkB into the neuronal surface. *Journal of cell science*. 122:3123-3136.

Zheng, J., W.H. Shen, T.J. Lu, Y. Zhou, Q. Chen, Z. Wang, T. Xiang, Y.C. Zhu, C. Zhang, S. Duan, and Z.Q. Xiong. 2008. Clathrin-dependent endocytosis is required for TrkB-dependent Akt-mediated neuronal protection and dendritic growth. *The Journal of biological chemistry*. 283:13280-13288.

Zhou, B., Q. Cai, Y. Xie, and Z.H. Sheng. 2012. Snapin recruits dynein to BDNF-TrkB signaling endosomes for retrograde axonal transport and is essential for dendrite growth of cortical neurons. *Cell reports*. 2:42-51.

Zhou, X.F., and R.A. Rush. 1996. Endogenous brain-derived neurotrophic factor is anterogradely transported in primary sensory neurons. *Neuroscience*. 74:945-953.

6. Attachment
6.1 List of Abbreviations

A	A_{2A}	Adenosine 2A
	AAV9	Adeno-associated virus 9
	ABD	Actin binding domains
	AC	Adenylate cyclase
	AChR	Acetylcholine receptor
	AD	Alzheimer´s disease
	ADP	Adenosine diphosphate
	Akt	Protein kinase B
	ALS	Amyotrophic lateral sclerosis
	AMPA	α-amino-3-hydroxy-5-methyl-4-isoxazolepropionic acid
	ANOVA	One-way analysis of variance
	APS	Ammonium Persulfate
	Arp2/3	Actin-related protein 2/3 complex
	Arpc1b	Actin-related protein 2/3 complex subunit 1B
	Arpc4	Actin-related protein 2/3 complex subunit 4
	ASO	Antisense oligonucleotides
	ATP	Adenosine triphosphate
B	BDNF	Brain-derived neurotrophic factor
	bp	base pairs
	BSA	Bovine serum albumin
	BTX	Botulinum toxin
C	C	Cytosine
	CamKII	Ca^{2+}/calmodulin-dependent protein kinase II
	cAMP	Cyclic adenosine monophosphate
	Ca_v	Voltage-gated calcium channel
	Cdk5	Cyclin-dependent kinase 5
	cDNA	Complementary DNA
	ChAT	Choline acetyltransferase
	CHX	Cycloheximide
	CMV	Cytomegalovirus
	CNS	Central nervous system
	CNTF	Ciliary neurotrophic factor
	CORO1C	Coronin 1C
	CPE	Carboxypeptidase E
	CREB	cAMP responsive element binding protein
	CytoD	Cytochalasin D
D	DAG	Diacyl glycerol
	DBP	Vitamin D-binding protein
	DIV	Days in vitro
	DMEM	Dulbecco´s Modified Eagle Medium
	DMSO	Dimethyl sulfoxide
	DNA	Deoxyribonucleic acid
	dNTPs	Deoxyribonucleotides
E	E	Embryonic day
	E.coli	Escherichia coli
	EDTA	Ethylenediaminetetraacetic acid
	EGF	Epidermal growth factor
	EGFP	Enhanced green fluorescent protein
	EGFR	Epidermal growth factor receptor
	EMA	European Medicines Agency
	ER	Endoplasmic reticulum
	ESE	Exonic splicing enhancer
F	F-actin	Filamentous actin
	FCS	Fetal Calf Serum
	FDA	Food and Drug Administration
G	g	Gram
	G-actin	Globular actin
	GAPDH	Glyceraldehyde-3-phosphate dehydrogenase
	GDNF	Glial cell–derived neurotrophic factor

	GFP	Green fluorescent protein
	GPCR	G protein-coupled receptors
	GRB2	Receptor-bound protein 2
H	HA	Human influenza hemagglutinin
	HBSS	Hank's Balanced Salt Solution
	HEK	Human embyonic kidney cell
	HEPES	4-(2-hydroxyethyl)-1-piperazineethanesulfonic acid
	hnRNPs	Heterogeneous nuclear ribonucleoproteins
	hPLS3	Human PLS3
	HRP	Horseradish peroxidase
I	IMP1	Insulin-like growth factor II -mRNA binding protein 1
	IP_3	Inositol 1,4,5-trisphosphate
	iPSC	induced pluripotent stem cell
K	K	Lysine
	Kb	Kilobase pairs
	kDa	Kilodalton
	kg	Kilogram
L	l	Liter
	LAL	Levator auris longus
	LB	Lymphoblastoid
	LB medium	Lysogeny Broth medium
	LIMK1	LIM kinase 1
	LTD	Long-term depression
	LTFU	Long-term follow-up
	LTP	Long-term potentiation
	Luci	Luciferase
	LV	Lentivirus
M	M	Molar
	MAPK	Ras- mitogen-activated protein kinase
	mCh	mCherry
	min.	Minutes
	mg	Milligram
	ml	Milliliter
	mM	Millimolar
	mPLS3	Murine Pls3
	mRNA	Messenger RNA
N	NAIP	Neuronal apoptosis inhibitory protein
	NB	Neurobasal
	NCALD	Neurocalcin delta
	NF	Neurofilament
	NGF	Nerve growth factor
	NKRF	NFκB repressing factor
	NMDA	N-methyl-d-aspartate
	NMJs	Neuromuscular junctions
	NT	Neurotrophin
O	OIA	Obliquus internus abdominis
	ORF	Open reading frame
P	P	Postnatal day
	p75^{NTR}	p75 neurotrophin receptor
	PBS	Phosphate Buffered Saline
	PC12	Pheochromocytoma 12
	PCR	Polymerase chain reaction
	PD	Parkinson´s disease
	Pfn1	Profilin I
	PI3K	Phosphoinositide 3-kinase
	PIP_2	Phosphatidylinositol 4,5-bisphosphate
	PKA	Protein kinase A
	PKC	Protein kinase C
	PLCγ	Phospholipase C γ
	PLS3	Plastin 3
	PNS	Peripheral nervous system

	PORN	Poly-D-L-ornithine hydrobromide
	PVDF	Polyvinylidene fluoride
R	RBPs	RNA binding proteins
	RNA	Ribonucleic acid
	ROCK	Rho-associated protein kinase
	RRP	Readily releasable pool
	RT	Room temperature
	RT-PCR	Reverse transcriptase PCR
S	SERF1A	Small EDRK-Rich Factor 1A
	scAAV9	Self-complementary adeno-associated virus 9
	SD	Standard deviation
	SDS	Sodium dodecyl sulfate
	sec.	Seconds
	SEM	Standard error of the mean
	shRNA	Small hairpin RNA
	SIM	Structured Illumination Microscopy
	Sm proteins	snRNP Smith antigen proteins
	SMA	Spinal muscular atrophy
	SMN	Survival Motor Neuron (gene / protein)
	SNK	Serum-inducible kinase
	snRNA	small nuclear RNA
	snRNP	Small nuclear ribonucleoproteins biogenesis
	SV2	Synaptic vesicle protein 2
	SYP	Synaptophysin-1
T	T	Thymine
	TA	Tibialis anterior
	TAE	Tris-acetate-EDTA-buffer
	Taq	Thermus aquaticus
	TBS-T	Tris buffered saline with Tween-20
	TDP-43	Transactive response DNA Binding protein 43 kDa
	Tris	Tris hydroxymethyl aminomethane
	Trk	Tropomyosin kinase receptors
	TVA	Transversus abdominis
	Tyr	Tyrosine
U	U	Units
	UV	Ultraviolet
V	V	Volt
	vg	vector genomes
	VGCC	Voltage-gated calcium channel
W	WASP	Wiskott–Aldrich Syndrome protein
Others	8-CPT-cAMP	8-(4-Chlorophenylthio)adenosine3′,5′-cAMP
	α	Alpha/anti
	β	Beta
	γ	Gamma
	%	Percentage
	°C	Degrees Celcius
	µg	Microgram
	µl	Microliter
	µM	Micromolar
	µm	Micrometer

6.2 List of Figures

6.3 List of Tables

Curriculum vitae

Publication record

Hennlein L, Ghanawi H, Gerstner F, Palominos-Garcia E, Yildirim E, Saal-Bauernschubert L, Moradi M, Deng C, Klein T, Appenzeller S, Sauer M, Briese M, Simon C, Sendtner M, Jablonka S; Plastin 3 rescues cell surface translocation and activation of TrkB in spinal muscular atrophy, *J. Cell Biol.*, 2023. *In press.* DOI: 10.1083/jcb.202204113.

Deng C, Reinhard S, **Hennlein L**, Eilts J, Sachs S, Doose S, Jablonka S, Sauer S, Moradi M, Sendtner M; Impaired dynamic interaction of axonal endoplasmic reticulum and ribosomes contributes to defective stimulus-response in spinal muscular atrophy, *Transl Neurodegener.*, 2022 Jun 2;11(1):31.

Jablonka S, **Hennlein L**, Sendtner M; Therapy development for spinal muscular atrophy: perspectives for muscular dystrophies and neurodegenerative disorders, *Neurol Res Pract.*, 2022 Jan 4;4(1):2.

Ghanawi H, **Hennlein L**, Zare A, Bader J, Salehi S, Hornburg D, Ji C, Sivadasan R, Drepper C, Meissner F, Mann M, Jablonka S, Briese M, Sendtner M; Loss of full-length hnRNP R isoform impairs DNA damage response in motoneurons by inhibiting Yb1 recruitment to chromatin, *Nucleic Acids Res.*, 2021 Dec 2;49(21):12284-12305.

Deng C, Moradi M, Reinhard S, Ji C, Jablonka S, **Hennlein L**, Lüningschrör P, Doose S, Sauer M, Sendtner M; Dynamic remodeling of ribosomes and endoplasmic reticulum in axon terminals of motoneurons, *J Cell Sci.*, 2021 Nov 15;134(22):jcs258785.

Ji C, Bader J, Ramanathan P, **Hennlein L**, Meissner F, Jablonka S, Mann M, Fischer U, Sendtner S, Briese M; Interaction of 7SK with the Smn complex modulates snRNP production, *Nat Commun.*, 2021 Feb 24;12(1):1278.

Tejero R, Balk S, Franco-Espin J, Ojeda J, **Hennlein L**, Drexl H, Dombert B, Clausen JD, Torres-Benito L, Saal-Bauernschubert L, Blum R, Briese M, Appenzeller S, Tabares L, Jablonka S; R-Roscovitine Improves Motoneuron Function in Mouse Models for Spinal Muscular Atrophy, *iScience.*, 2020 Feb 21;23(2):100826.

Academic References

Dr. Sibylle Jablonka   Group leader, Institute of Clinical Neurobiology, University Hospital Würzburg
Versbacherstr. 5, 97076 Würzburg, Germany
Email: Jablonka_S@ukw.de, Phone: +49 931 201-44010

Luisa Hennlein,
Würzburg, September 2022

Affidavit / Eidesstattliche Erklärung

Affidavit

I hereby confirm that my thesis entitled **"Plastin 3 rescues defective cell surface translocation and activation of TrkB in mouse models for spinal muscular atrophy"** is the result of my own work. I did not receive any help or support from commercial consultants. All sources and / or materials applied are listed and specified in the thesis.

Furthermore, I confirm that this thesis has not yet been submitted as part of another examination process neither in identical nor in similar form.

Place, Date   Signature

Eidesstattliche Erklärung

Hiermit erkläre ich an Eides statt, die Dissertation **„Plastin 3 kompensiert die defekte Zelloberflächen-Translokation und Aktivierung von TrkB in Mausmodellen für spinale Muskelatrophie "** eigenständig, d.h. insbesondere selbständig und ohne Hilfe eines kommerziellen Promotionsberaters, angefertigt und keine anderen als die von mir angegebenen Quellen und Hilfsmittel verwendet zu haben.

Ich erkläre außerdem, dass die Dissertation weder in gleicher noch in ähnlicher Form bereits in einem anderen Prüfungsverfahren vorgelegen hat.

Ort, Datum   Unterschrift

Acknowledgements / Danksagung